CRANFIELD UNIVERSITY

Pavlos K Zachos

Gas Turbine Sub-idle Performance Modelling; Altitude Relight and Windmilling

School of Engineering

Ph. D. Thesis

SCHOOL OF ENGINEERING
DEPARTMENT OF POWER AND PROPULSION

Full Time Ph. D.

Academic Year 2009-2010

Pavlos K Zachos

Gas Turbine Sub-idle Performance Modelling; Altitude Relight and Windmilling

Supervisors: Dr. V. Pachidis – Prof. R. Singh
Industrial Advisors: A. Rowe – S. Brown

February 2010

This report is submitted in partial fulfillment of the requirements for the degree of Doctorate of Philosophy

Abstract

Sub-idle is a very challenging operating region, as the performance of a gas turbine engine changes significantly compared to design conditions. In addition, the regulations for new and existing engines are becoming stricter and the prediction of engine's relight capability is essential. In order to calculate the sub-idle performance of an engine, detailed component representation is required. The data obtained from rig tests is usually insufficient at the low speeds. This creates the need for further research about component behavior within the sub-idle regime before any whole engine relight performance prediction is attempted.

Within this research, the sub-idle compressor map generation methodologies are pushed a step forward by the definition of the zero-speed curve, that is the lowest speed line of a compressor map. In this way the sub-idle characteristic can be interpolated between the zero-speed line and the above-idle given speed lines. Consequently, the generation of the characteristic within the whole range of operation is allowed. In addition, the sub-idle and relight combustion modelling is enhanced by a novel combustion model which accounts for fuel evaporation effects. The development of such a model is based on the fact that fuel evaporation effects have a significant impact on the combustion efficiency during the engine relight manoeuvres. Finally, the sub-idle exhaust mixing phenomena are investigated as the relight modelling of a mixed exhaust engine cannot be carried out using the conventional approaches as there is a non-negligible difference between the pressures of the two coaxial jets. The models generated by the component related research are partially integrated within the relight performance simulation solver BD19 in order for whole engine performance simulations to be carried out. More specifically, the windmilling and the groundstarting performance of a modern, civil, high bypass ratio engine is examined.

The current thesis contributes to knowledge both at component as well as at whole engine performance prediction levels. As far as sub-idle compressor performance is concerned, a generic pressure loss model for compressors operating at highly negative incidence angles has been developed. It is validated against experimental

data and is applicable on every compressor with given design parameters. In addition, the new combustion model allows for a more accurate combustion efficiency prediction during the relighting processes while the research on mixed exhaust engine configurations enhances the physical background of the sub-idle mixing process allowing for a more efficient performance modelling. The physics based component related research, in overall, offers significant benefits to the sub-idle and relight performance modelling of gas turbines increasing its predictive capability and therefore the reliability of the current and future aero engines.

Contents

Acknowledgments

This is the outcome of my attempt to investigate a rather unexplored area of the behavior of gas turbine aero-engines, perhaps one of the most wonderful but at the same time most complicated human inventions, since there are still many issues we don't understand about them. We should be feeling the challenge and also be very careful of the quality of our results as the truth in nature is not always that easy to be revealed. However, nothing is as valuable as discovering the truth in ourselves and above all, become, through the research, better people, not only better scientists.

Those few lines shall be the place where only a bit of my gratitude to all those people stood by me during this years will be expressed. Words are sometimes not enough to express what you really feel inside.

First of all I'd like to express my most sincere gratitude to Prof. Riti Singh and Prof. Pericles Pilidis who gave me the chance to work within the Performance Engineering group at Cranfield but also for taking me under their supervision and mentorship. Their contribution in my education and not only, is tremendously recognised and appreciated.

A "*thank you*" is not enough for my supervisor Dr. Vassilios Pachidis for all the effort he made to guide me successfully through this doctoral course during the last three years. His technical, but more importantly, personal support and encouragement, especially during difficult moments was vital, even though at some points I was not able to appreciate it. His friendship without doubt is an honor for me.

I'd like to extend my gratitude to Rolls-Royce plc., the sponsor of this work, and particularly to Stephen Brown, Arthur Rowe, Richard Tunstall, Phil Naylor and Paul Whatley for the really valuable and continuous technical support and advising they offered.

I owe more than a lot to Dr. Jason Howard, who spent many hours with me in the office during the first nine months of my research, to introduce me in the doctoral topic by transferring all his research outcomes.

I would like to show my gratitude also to Bernard Charnley, Derek Brown and Dick Lutley for the collaboration during the experimental part of the project. It was a great experience to work with them in the test area.

I feel also the need to thank Gillian Hargreaves, Rachel Smith, Maria Negus and Sam Broe, our department's postgraduate and UTC administrators, for their excellent contribution, on creating an ideal environment for me to work efficiently.

Dr. Ken Ramsden, Prof. Kostas Mathioudakis and Dr. Timos Kipouros are gratefully acknowledged for their support and advice.

I need to extend my gratitude to Dr. Shahrokh Shahpar, from Rolls-Royce Aerothermal Methods, for his continuous interest in my work and in my progress.

A big "*thank you*" is, undoubtedly, owed to the MSc students I worked with during the last three years. I need to express my deepest gratitude to Matthew Narciewicz, Fabio Pengue, Jad Kozaily, Ruben Garcia, Ioanna Aslanidou, Conny Ruelke, Ahad Mehdi and Fabio Russo not only for their hard work and their technical contribution but also for something more important; their friendship and the continuous personal support they demonstrated. Needless to say that I couldn't have done it without them.

A grateful acknowledgment is expressed also to my UTC groupmates and friends, Erminio Zanenga, Katerina Psarra, Luis Gallar and Martina Mohseni. It was really fun sharing all our good and bad moments but also our concerns in the same office environment.

I had the chance to come across some really valuable people during my first adventure in Rolls-Royce on 2006 thus I cannot miss acknowledging them here for their continuous friendship, support and interest they demonstrate. Dr. Yannis Kyriakoglou, Dimitris Arzoglou, Panayis Synodinos and Maria Katsourou from Rolls-Royce, are people that have added a lot of value in my personal life with their friendship.

I would like to show my deepest gratitude to Dr. Vasileios Kyritsis. After we first met at the end of his doctoral course at Cranfield and until today he is always there for advising and supporting me. His experience and technical knowledge were really valuable and vital for my progress. His friendship is however the greatest honor for me.

The same must be written for Dr. Panos Laskaridis who spent countless hours with me elaborating ideas and sharing his views on various technical (and not only) topics. His critical mind and technical knowledge pushed without doubt forward my doctoral research by motivating me to always look for something more and to improve myself.

I cannot forget the people from Cranfield who proved to be the key persons to make the, not really a lot, free time really enjoyable and relaxing. I'm now convinced that this place creates really strong relationships. A big *"thank you"* is expressed to Petros Gkotsis, Ioanna Tsotsou, Alexandros Sandros, Katerina Moutafi, Leonidas Stavropoulos, Nikos Paterakis, Kostantinos Kyprianidis, Nikos Asproulis, Takis Tsoutsanis, Elias Tsoutsanis, Dr. Frank Noppel, Dr. Greg Ameyugo, Dr. Bobby Sethi, Giannis Goulos, Jan Janikovic, Dimitrios Fouflias and Hariharan Hanumathan.

I owe my most sincere gratitude to my housemates and dearest friends Alekos Terzis, Panos Giannakakis and Marie Lemaitre not only for the lunches, dinners and coffees they have prepared and the countless dishes they did for me during my writing up period but also for the continuous, honest and valuable love and support they demonstrate in every good or difficult moment. Their invasion in my life has proved to be of vital importance for me and I dare to write that they are considered to be my family in England. I would like also to thank them for proof reading this thesis.

A special acknowledgment is owed to Periklis Lolis. A very special friend for more than 20 years now, who decided to start his doctorate at Cranfield a few months ago and joined us at home, contributing significantly in the great atmosphere. I would like to thank him for all the small and big things he has offered me during those years knowingly or not. His friendship is a life gift for me as well. I would like also to thank him for his comments on this thesis.

A can by no means forget the people I missed a lot during the last 4 years that I am abroad; my beloved friends from Greece. I owe them my deepest gratitude for their continuous support, encouragement and the warm welcome they offer me every time I go back home, reminding me where I belong to and how sweet is to have somebody waiting for you back there. Dimitris Mitakos, Tasos Iakovidis, Marina Kousoulidou, Christina Tsiotra, Afroditi Michailidou, Marios Mitrosilis, Fotini Dalakiouridou, Ilias Cheimariotis, Anastasia Dorti, Michalis Mastropavlos, Maria Pappa and Themis Chatzinikolakis are gratefully acknowledged.

I would also like to deeply thank Froso and Stefanos for having offered me, even not knowingly, the most valuable gift in my life.

A very big "*thank you*" is not enough for my beloved family and especially for my parents, Konstantinos and Aristi and my brother Fanis for being always next to me, advising and supporting my life steps, offering their love and understanding. I could not have done anything without them.

Finally, Prof. Anestis Kalfas, my mentor and spiritual father, is gratefully acknowledged for his continuous advising and generally for his enormous contribution in my education as well as in my personal and professional development.

My entire doctoral research effort is sincerely dedicated in the loving memory of my grandfather Theofanis Kiagiadakis and my aunt Kyriaki Kiagiadaki people who set the first bases of my education and I am sure they keep sight of my progress from up there.

P. K. Zachos
January 2010

List of Figures

Nomenclature

A	Area
A_{eff}	Effective area, taking into account flow blockage
A_{ref}	Reference area
c_θ	Circumferential velocity
c_m	Mean axial velocity
C_L	Lift coefficient
C_D	Drag coefficient
C_p	Pressure rise coefficient
C_f	Tangential force coefficient
D	Drag force
D_1	Core dynamic pressure
D_{ref}	Reference diameter
H	Enthalpy (total)
i	Incidence angle to blade
L	Lift force
m	Fuel flow rate exponent
P	Pressure (total)
p	Pressure (static)
PR	Pressure ratio
Q	Flow parameter $\frac{W\sqrt{T}}{AP}$
r	Radius
Re	Reynolds number
r_u	Velocity ratio
T	Temperature (total)
TR	Temperature ratio
t	Temperature (static)
U	Blade speed
V	Velocity
V_{rel}	Relative velocity
V_x or c_x	Axial velocity
W or $\dot{m}$	Mass flow
$\dot{w}_f$ or $\dot{w}_L$	Fuel flow rate
X	Axial force on the blade
Y	Tangential force on the blade

δ^*	Nominal deviation angle
ΔP_L	Pressure loss across injector's nozzle
ΔP	Radial pressure jump P_2-P_1
η_{is}	Isentropic efficiency
ζ	Total pressure loss coefficient
η_{is}	Isentropic efficiency
$\eta_{comb,reac}$	Reaction rate based combustion efficiency
$\eta_{comb,evap}$	Evaporation rate based combustion efficiency
θ	Blade camber angle or Combustion loading
μ_L	dynamic viscosity
ρ	Density
σ	Surface tension coefficient
τ	Torque
ϕ	Flow coefficient $\frac{W\sqrt{T}/P}{N/\sqrt{T}}$
ψ	Work coefficient $\frac{\Delta H/T}{(N/\sqrt{T})^2}$
ψ_{is}	Pressure coefficient $\eta_{is}\frac{\Delta H/T}{(N/\sqrt{T})^2}$
Ω	Rotational speed

Abbreviations

ATF	Altitude test facility
AFR	Air to fuel ratio
BPR	Bypass ratio
DR	Diameter ratio
HPC	High pressure compressor
IPC	Intermediate pressure compressor
LPC	Low pressure compressor
NPR	Nozzle Pressure Ratio
SMD	Sauter mean diameter
SPC	Start power coupling
TMPR	Total mixer pressure ratio

Subscripts

in	Compressor inlet
out	Compressor outlet
1	Blade inlet or core stream
2	Blade outlet or bypass stream
3	Combustor inlet

To her who always stands by me;
To Maria

Chapter 1

Introduction

1.1 Benefits from a successful sub-idle modelling

Sub-idle gas turbine performance covers the operating regimes of groundstarts and in-flight altitude relights. The importance of obtaining knowledge about the sub-idle operating region of an aero-engine is illustrated in the following paragraphs. The benefits of this effort can be compiled into an improvement of the current gas turbine technology, increasing at the same time the manufacturer's confidence on the product.

Engine windmilling performance, relighting and pull-away are mainly matters of safety in aviation [55]. Therefore, they are considered to be major certification issues by the two main certifying bodies FAA and JAA.

Historically, engine performance under windmilling conditions as well as the relight capability have been marginal compared with requirements. However, modern trends in engine manufacturing (smaller engine cores and bigger bypass ratios, 2-engine aircraft rather than 4-engine) have pushed the present situation beyond the limits making it sometimes insufficient to satisfy the regulations. Thus, certification bodies are forced to revise the sub-idle performance requirements pushing the manufacturers to be more concerned about it, taking it seriously under consideration

during the design and testing phases of a new engine. A number of incidents reported during the last decades, proves that engine relight capability is still an issue for the civil aviation (http://www.ntsb.gov):

- **1988**. A large civil aircraft flying among thunderstorms lost both its engines. Unable to relight them, the captain dead-sticked the jet onto a mile-long patch of rain-soaked earth. Fortunately the aircraft and the passengers were unharmed.

- **1987**. Another commercial aircraft suffered from a double flame-out while descending through rain and hail over Thessaloniki, Greece. The crew managed to relight the engines and land without troubles.

- **2002**. An Indonesian Airliner experienced a double flame-out over Java. The aircraft was finally found in a river. One flight attendant was killed and at least 22 passengers received minor injuries.

- **2007**. A civil airframe coming from Tokyo to London Heathrow was forced to fly with one engine in locked-rotor condition for half an hour before the pilot conducted an emergency landing in Helsinki. The problem occurred when due to an overheating the turbine rotors melted and during the emergency cooling process the rotor welded to the casing thus preventing the spool from rotating [101].

A flame-out is thought to occur once every 100,000 non-military flights as mentioned in http://www.airspacemag.com/issues/2006/august-september/flameout.php. Considering that almost 500,000 flights per year depart from Heathrow airport, UK, with a perspective to be increased to 700,000 by 2015 and that dozens of equally busy airports exist globally, it can easily be realised that a non negligible percentage of the flights per year are possible to experience a flame-out with unknown consequences.

The above cases illustrate not only the importance of a robust and reliable sub-idle and relight modeling but also the need of revised and stricter regulations that our new engines have to meet in order to be certified and put in service.

1.2 Sub-idle performance fundamentals

Adapting Walsh and Fletcher's definition, the minimum feasible power level of thrust or power, produced when the requirement of the application is zero is called *idle* [117]. From another point of view, the *idle* point can be defined as the operating point where the engine is rotating with almost no load, producing enough power to undertake only the mechanical losses and maintaining itself on a certain rotational speed.

Every operating point with rotational speed between zero and idle belongs to the *sub-idle* area of the engine. This regime is studied by methodologies quite different than the ones developed for other working areas since this is a far off-design area where the conventional methods for engine performance prediction are not applicable with the desired accuracy.

The sub-idle domain on a compressor map is illustrated in the following picture where, apart from the working line, the speed lines from zero to idle are indicated.

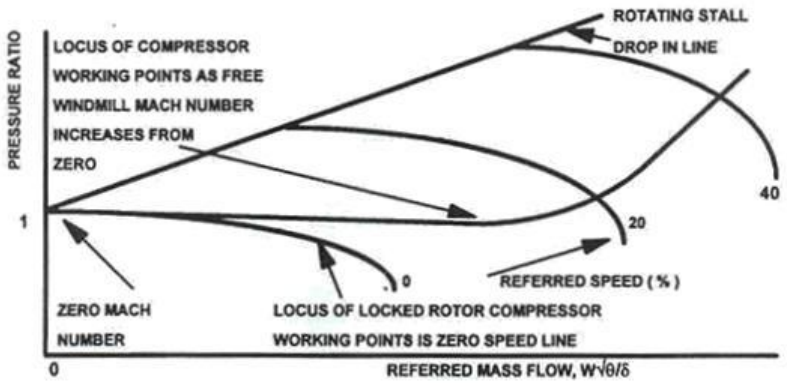

Figure 1.1: Sub-idle regime on a compressor map [117].

1.3 Engine-out performance data necessity

As the safety requirements become stricter, the airframe manufacturers request engine-out as well as engine free windmilling data earlier during the design process than previous years. The most significant for the aircraft design data required are free windmilling drag and mass flow as well as free windmilling rotational speed of the shafts since they strongly affect the aircraft design in terms of the size of the vertical tail, the wing, the pylon and the landing gear system as explained in [6]. Windmill data is also important for the certification of an engine for extended engine-out operation over water which is more specifically influenced by the windmilling performance under icing or even locked rotor conditions.

The same authors also underline the significance of the secondary power extraction capability for accessories design or the estimated pressures and temperatures for combustor or exhaust nozzle detailed design.

1.4 Research scope

The benefits of this research are mainly improving the aero gas turbine technology since industrial plants are very rarely forced to pass through this working area and therefore the interest on their sub-idle performance is very limited.

Since the engine cannot be stabilized at any point within the sub-idle regime, regardless of the running mode (groundstart or relight), there is no doubt that the engine performance parameters are changing with time. Therefore the engine runs transiently, hence transient performance methodologies are required for a successful prediction in this area.

Those methodologies are widely applied for predictions mainly within the above idle area and very often demonstrate a high level of accuracy and robustness. However, the capability of the below idle modelling can still be significantly improved as less resources are invested on it by engine manufacturers up to the moment.

The transient sub-idle engine operation covers the following engine processes which are at the same time the main areas of the current research:

- **Groundstarting** defined as the engine acceleration from a static condition to idle.
- **Relight** or **Altitude relight** which can be distinguished in the following types:
  - *Windmill relight* - engine light up based on the windmilling phenomenon. The engine is in *windmilling* mode when the air stream through the unlit engine causes spool rotation.
  - *Quick windmill relight* - almost identical with the above situation. The only difference is that a quick relight is shorter.
  - *Starter assisted relight* - when a starter motor is employed to assist the relight procedure in case the spool rotation caused by the ram pressure is not able to light-up the engine. Usually occurs at low altitudes and flight Mach numbers.

Generally, the relight performance of the engine is summmarised in the so-called *relight envelope*. This may be considered as the fourth element of the engine's operational envelope along with its environmental envelope, the installation pressure losses and the flight envelope [117]. A typical relight envelope of a gas turbine aero engine is shown in Fig. 1.2, where the different types of relight are clearly distinguished.

1.4.1 Sub-idle engine processes

A brief description of each sub-idle engine process is given in this section for reasons of completeness.

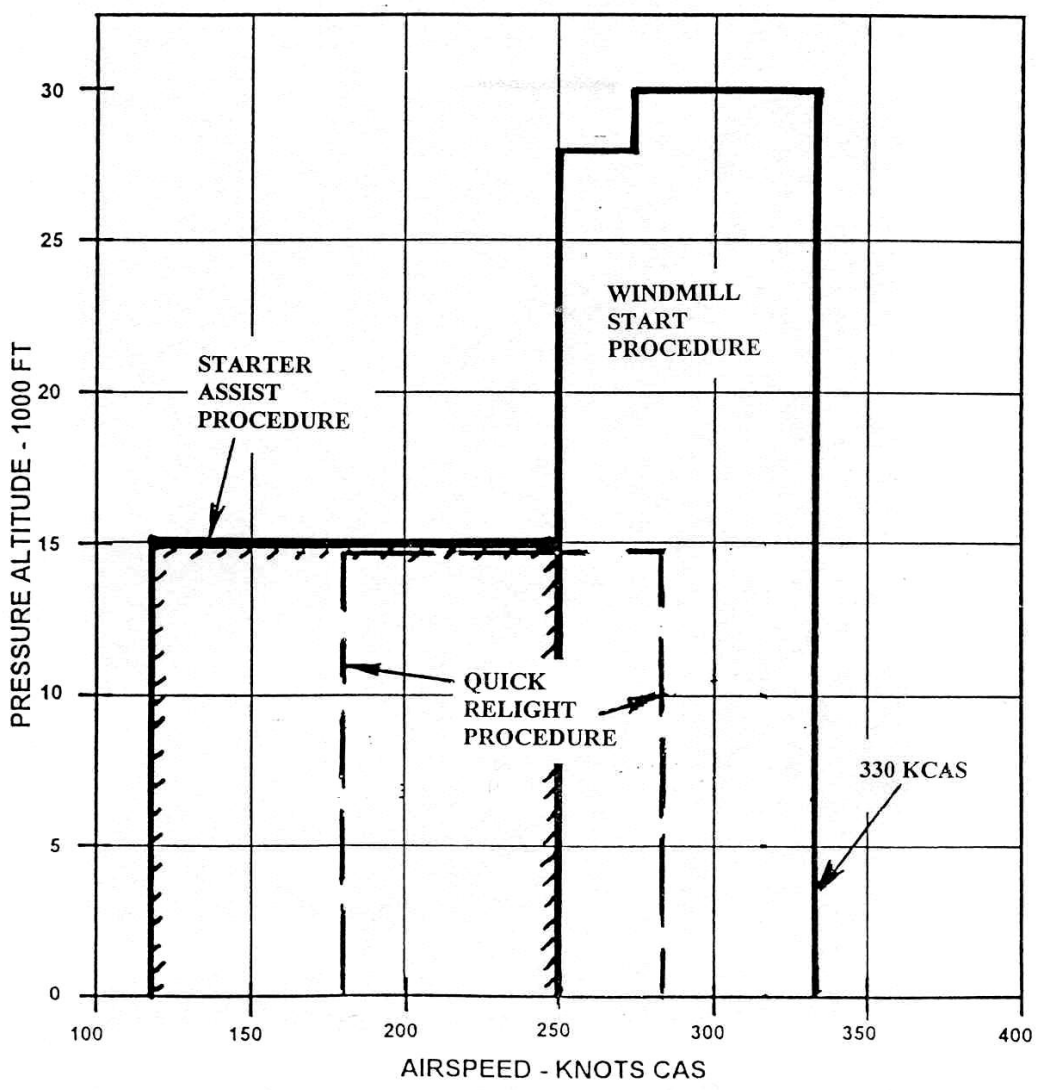

Figure 1.2: Typical large civil engine relight envelope (Rolls-Royce data).

1.4.1.1 Groundstarting

Groundstarting is one of the highest importance every day needs of an aero engine. Technically speaking, groundstarts are transient manoeuvres starting typically from zero rotational speed. Initially the HP spool is accelerated by a starter motor to start the airflow through the engine increasing also the pressure at the inlet of the combustion chamber. At a specific point fuel is injected and the igniters are turned on. From that point the engine has enough energy to continue accelerating up to idle without the motor which is disengaged from the shaft.

1.4.1.2 Windmill relight

This is the relight type initiated by the steady state windmilling of the engine before the acceleration. When an engine flames out during the flight, the spools decelerate to a rotational speed which is maintained by the forward speed of the aircraft which produces a ram pressure at the engine face. This is the so-called *windmilling phenomenon*. According to [51] a windmilling engine is never truly operating at steady state conditions. That is, the free windmilling rotational speed of the engine is not necessarily constant. Nonetheless, the assumption of constant free windmilling rotational speed is generally reasonably done, this way simplifying the modelling .

1.4.1.3 Quick windmill relight

This is a more typical relight situation, where after a flame-out, the engine is required to relight while the spools are still decelerating. Very complex transient phenomena occur during this procedure as for example heat soakage or loss mechanisms throughout the gas path. This engine process has not been tackled by this research activity.

1.4.1.4 Starter assisted relight

Starter assisted relight occurs when the ram conditions are not sufficient for a windmill relight, that is when the engine flames out at low flight Mach numbers or high altitudes. In that case the starter motor provides additional torque, increasing the rotational speed of the HP spool before the re-injection of the fuel.

1.4.2 Performance simulation methods

Several methods for predicting the sub-idle behavior of gas turbine engines have been proposed in the open literature. They are mainly transient techniques, whereas steady state methodologies for predicting free windmill rotational speed or massflow have also been developed. Both types of methods have been applied on turbojet and turbofan engines [18, 61].

Basically, there are two major types of sub-idle models: the complete aero-/thermo- cycle models and the loss coefficient models [6]. The former are similar to the above idle models, based on thermodynamic calculations and component matching techniques and are used to predict the transient operating lines of an engine during start-up processes. The latter are used to estimate the steady state massflow, internal drag or free windmill rotational speed of the entire engine or only the bypass part of it, based on component loss coefficients. Very often, alternative ways to match the components are utilised, based for example on angular momentum or torque equilibrium between the shafts [61, 107] in order to increase the robustness of the performance schemes.

The current research has been conducted using the sub-idle transient performance solver provided by the sponsor. It is called BD-19 and it is a part of the Rolls-Royce Aerothermal Performance (RRAP) suite. A more detailed review of the performance prediction methodologies found within the open literature will be given in a following chapter.

1.4.3 Sub-idle engine characteristics

Whether an engine simulation is successful or not, highly depends upon the quality of the component characteristics introduced into it. Compressor and turbine maps especially are of major importance as they are the bridge connecting our understanding of component performance with overall engine modelling, while knowing the air flow parameters at the inlet of the engine is a very significant condition for the performance prediction of the combustion chamber at windmilling conditions [107]. Consequently, the better the component performance is represented in the maps the bigger the benefit for the whole engine modelling is.

However, in the majority of cases there is no sub-idle area available for most engines due to various reasons. As a first approach, methods for the map generation at low rotational speeds have been developed, mainly based on speed-curve extrapolation from the above idle regimes [51]. A review of those methodologies has been previously presented by Jones [59, 60]. The main drawback of those techniques relies on the fact that they are based on mathematical correlations with poor physical background hence it is highly likely that the flow phenomena at low speeds, such as the loss mechanisms of blade operation at high incidence, are not really captured and therefore represented in the component characteristic. This results in poor predictive capability of the sub-idle performance simulation tools, but it is always a starting point for setting up a sub-idle solver.

In addition, alternative ways of map representation, as for example torque characteristics, may be useful for a more efficient sub-idle performance prediction. Engine's performance representation is perhaps one of the most decisive factors for a successful sub-idle prediction.

Efforts to increase the fidelity of the above mentioned methodologies have been made by the investigation of blade's performance at low speeds which, as will be discussed, is characterised by highly negative incidence angles. In this direction, a definition of the zero rotational speed line of the compressor (mentioned as 'locked

rotor studies' from now on) has been attempted using various tools. This approach allows the transition from map extrapolation to interpolation ensuring at least that there is some physical background in the map generation technique. It also identifies the phenomena that higher fidelity methods need to focus on in order to enhance the low speed compressor performance prediction.

According to the author's views, extrapolating compressor maps in order to adaptively run a performance model is an approach that neither increases the predictive capability of any sub-idle performance solver nor offers a valuable insight on component performance. Therefore running adaptively has no benefit in future engine design while a systematic research on the phenomena dominating the sub-idle performance of the components is much more promising in the sense that identifying their physical background creates predictive methodologies that have much smaller error margin when applied in the design of a new engine.

The latter is the idea throughout the current work; taking advantage of the locked rotor studies carried out and having them as a starting point, an effort to reflect their benefits in a compressor map representation has been made in order to enhance the physical background of the sub-idle map generation.

1.4.4 Component related research

As already mentioned, the quality of the component characteristics relies on how well the physical phenomena occurring in every component are captured. In other words, a better understanding of the physical mechanisms within each component is required. This work covers the sub-idle behavior of major engine components (compressor, combustor and mixer), enhancing the physical background of their operation within the sub-idle regime which is in turn reflected in the performance characteristics of each component as discussed in the previous section.

For this reason, research on component performance has been carried out separately before the whole engine modelling.

In general, the accuracy of a sub-idle performance prediction is strongly dependent on:

- Compressor and turbine performance.
- Successful combustion definition at sub-idle conditions.
- Understanding of sub-idle mixer and nozzle effects.

To be more illustrative, the entire scope of this research can be shown in Fig. 1.3 where all the specific research areas are presented, whereas the interaction between them is underlined.

1.4.4.1 Compressor and turbine performance

The aerodynamic behavior of turbomachinery blading in both components at those extremely far off-design conditions is severely different than their performance within design, or conventional off design regimes. Therefore, it is perhaps the most crucial aspect of the sub-idle research.

At very low shaft rotational speeds the blade operation is dominated by highly negative incidences mainly occurring at the stators while rotors are operating at relatively less negative incidences but still at negative values. The most extreme boundary of compressor or turbine sub-idle operation is the locked-rotor condition which occurs when the ram air has not enough momentum to cause free spool rotation, thus rotor blade rows are locked throughout the engine.

In previous studies, [61], conducted on turbofan engines, the off-design compressor performance models proposed by Howell [53], Griepentrog [116] or Horlock [49] have been used. Other studies, [107], make assumptions in order to define an approximate windmill compressor characteristic, before its use in a theoretical calculation for turbojet engines.

Studies on the performance of compressor blades at highly negative incidence angles have been extensively conducted within the current work and they are the

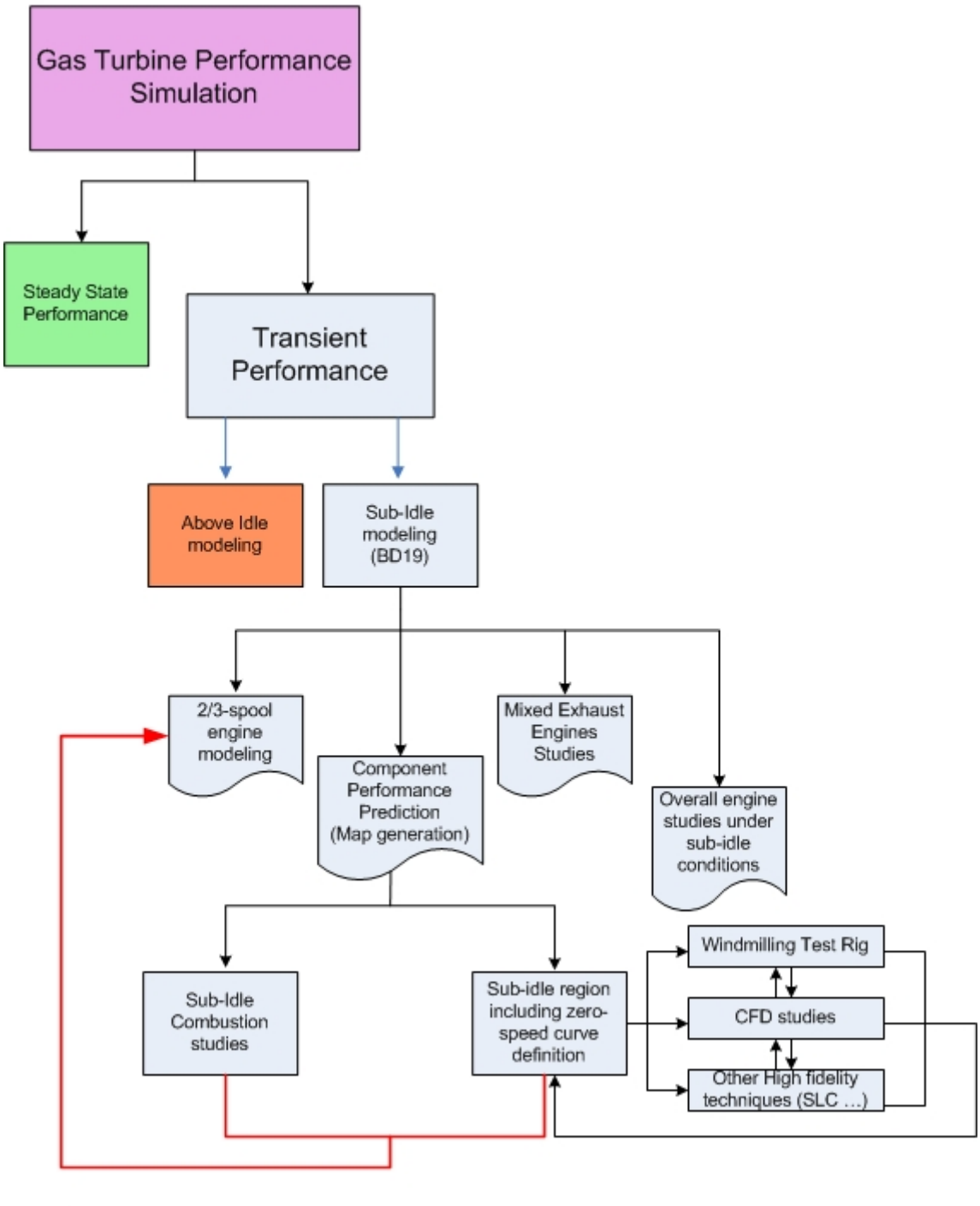

Figure 1.3: Transient sub-idle modeling scope.

starting point for building a more physics-based background as far as the sub-idle compressor performance is concerned.

1.4.4.2 Sub-idle combustion performance

Research on combustion within a relight project cannot be, by any means, of minor significance since combustion related phenomena define the relight capability of the engine and therefore there is a major need to increase the knowledge on this topic. However, combustor performance relies also on the combustor inlet conditions which means that it cannot be studied separately.

Even though the relight performance of a combustor is taken into account during the design phase of an engine, according to which the bigger the combustor the better its relight capability, modern design trends are in favor of the smallest possible chamber volume as in this way the overall engine weight and size is less penalised [55, 51]. Consequently, there is a critical combustor volume compromising the above mentioned issues.

Being so marginal on combustor design implies that the combustor's performance prediction must be accurate and reliable under relight and sub-idle conditions. More specifically, a successfully predicted combustor characteristic combined with the windmill conditions at the inlet must be able to provide the designers with the correct fueling schedule and combustion efficiency for a given required acceleration manoeuvre. Within this work, an effort to identify the factors which define the combustion efficiency before and during the relight transients has been made.

1.4.4.3 Mixed exhaust engine performance

Even though there is some existing work on this topic, the mixing phenomena at low engine power settings have not been fully explored. Considering also the strong influence of the mixer on the overall engine performance [90, 36] it was reasonable to dedicate some effort in this topic focusing on implementing the findings within a

sub-idle performance solver to allow for mixed engine simulations also at low power settings by taking into account the off-design mixing phenomena.

1.5 Research objectives

The sponsor of this research project is Rolls-Royce plc., under the specialization of the Aero Gas Turbine Performance function. Research takes place at Cranfield University whereas placements within Rolls-Royce for the whole engine modelling have performed by the author.

The main aim of this project, not changed compared to previous studies, is to improve the predictive capability within the sub-idle regime of aero gas turbine engines.

With experience from previous studies taken under consideration, the objectives for this project can be summarized as follows, balancing the industrial interests with the academic contribution-to-knowledge perspective.

- Enhance the component performance prediction capability by extending the applicability of already existing techniques towards the sub-idle regime focusing on:

    1. Compressor locked rotor studies.
    2. Fuel injector performance under sub-atmospheric conditions.
    3. Exhaust mixer modelling under sub-atmospheric conditions.

- Utilise the findings of the component specific research within the sponsor's engine performance prediction numerical tool to conduct research on the starting and relight procedure of modern 2 and 3-spool aero gas turbine engines. This research should start from the generation of the engine models for sub-idle simulation as well as the improvement of the actual simulation tool by enhancing the engine matching schemes.

1.6 Deliverables

The outcomes of this research that will finally be delivered to the sponsor can be summarised as follows:

- Experimental results of high incidence cascade tests.
- 2D and 3D blade as well as stage performance studies under highly negative incidence angles. Validation of the numerical tools used for the latter has been conducted against the experimental data obtained from the testing.
- Numerical fuel injection model under sub-atmospheric conditions using a full injector-liner model of a low bypass military engine.
- Numerical model of the mixer of a low bypass engine investigating the mixing processes under sub-atmospheric conditions.
- A fully functional and validated sub-idle map generator including a physics based stage stacking module for the zero speed line calculation of a compressor with given geometry.
- High bypass ratio BD19 engine models for TRENT 500 and TRENT 1000 investigating the effect of starting the engine using the IP shaft.

Chapter 2

Thesis overview

In this chapter a brief overview of the content of the current thesis will be given. In general, since the research fields regarding the component performance are quite different between each other, the literature survey related to each one will be given at the beginning of the relevant chapter, followed by the currently developed methodology, the results, the conclusions and the discussion of the findings. All the methodologies will be integrated to assess the whole engine performance in the last chapters of this thesis, followed by a general discussion and the proposals for future work on the topic. Even though almost all the related literature has been studied, the findings will be very briefly covered hereafter summarising only the most significant aspects.

More specifically, *Chapter 1* introduces the research scope and builds up the concept of sub-idle performance modelling. A list of the project objectives can also be found.

In *Chapter 3* the locked rotor compressor performance findings are presented. Both the experimental and the numerical approach followed for the derivation of the zero speed curve is described. A generic loss model for compressors operating at highly negative incidence angles is also given based on the blade element theory which has been validated under the above mentioned conditions.

The knowledge produced by the locked rotor modelling is used within *Chapter 4* for the generation of sub-idle compressor characteristics. A discussion about alternative map representation approaches at low-speeds is carried out. In addition, the low speed map generation using an interpolation process is being presented while a number of enhancements of the method's physical background is described as well.

Chapter 5 deals with the injection/combustion performance of an airblast atomiser under sub-atmospheric and low power conditions. A mixed reaction-evaporation rate based model for the calculation of the combustion efficiency is proposed based on the observation that the sub-idle combustion process is dominated by fuel evaporation effects.

Mixed exhaust engine performance studies are described in *Chapter 6*. A numerical investigation of the sub-idle and low speed mixing phenomena is presented, highlighting the most important aspects on which a representative exhaust mixer characteristic generation can be relied.

Research regarding the whole engine modelling and more specifically the ground-starting performance of modern civil high bypass turbofan engines is presented in *Chapter 7*. A study regarding the windmilling power offtake capability of the same type of engines is also carried out in order for the BD19 performance prediction solver to be validated for this kind of cases.

The interaction between the doctoral researcher, the industrial sponsor and the MSC students during the project is described in *Chapter 8*. In addition, an approach for the incorporation of the sub-idle modelling within the design phases of a new engine is also proposed.

Finally, a summary of the project findings, the contribution to knowledge as well as recommendations for future work can be found in *Chapter 9*.

The first chapters of the thesis will cover all the fundamental research conducted, related to component issues, aiming to offer a better understanding of the phenomena dominating each component at sub-idle conditions.

In addition, the representation of the findings in such a way that engine performance modelling could take advantage of has been pursued by enhancing the physical background of the map generation methodologies increasing in this way their reliability for overall engine modelling.

A roadmap of the current work is given in Fig. 2.1 where the dependency between the research areas is illustrated. Following the direction from top to the bottom ("How" path), the contribution to each area is made by the area below in other words the answer to the question "How?" is given underneath every topic, describing this way the breakdown of the work. On the other hand, following the direction from bottom to the top, the reason for performing research on each topic is given by the area above ("Why" path).

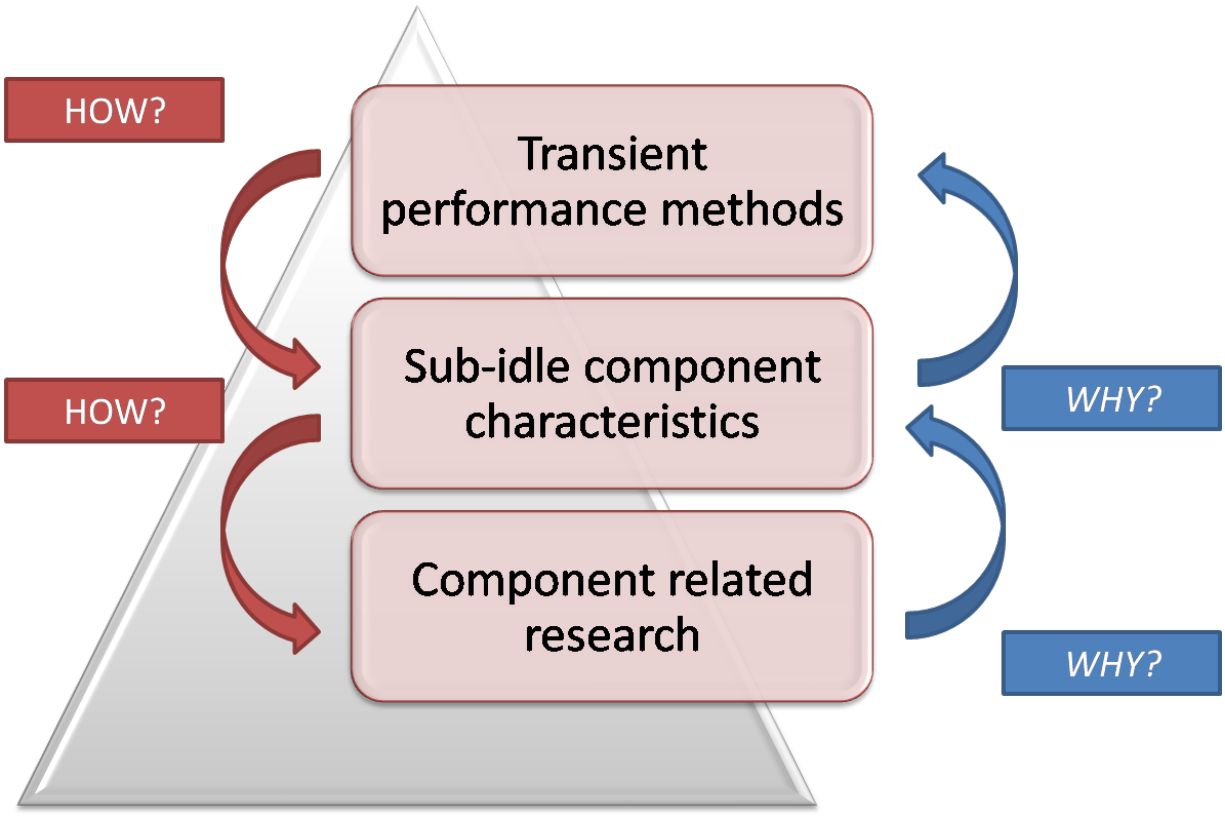

Figure 2.1: Roadmap of the cuurent work.

Chapter 3

Locked rotor compressor performance

3.1 Introduction

As mentioned in the previous chapter, component related research findings are critical for a successful sub-idle performance solver (the basis of Fig. 2.1 pyramid) and therefore are covered within the early chapters of the current thesis.

Compressor characteristics at low speeds and windmilling conditions are fundamental for a successful sub-idle engine simulation. Consequently, the phenomena dominating this component under the above mentioned conditions must be thoroughly investigated before any attempt of sub-idle compressor map generation, using any kind of map extrapolation techniques as mentioned in [51].

A key point regarding low speed compressor performance focuses on the so called "*locked rotor*" studies which mainly examine the compressor behavior when the rotor is frozen but there is still air mass flow through the blades. It has been decided that effort should be put on understanding the locked compressor phenomena, as also stated in [67] and [97], for various reasons:

- In this far off-design point of operation the most severe pressure losses occur,

as both the rotor (which act as stator) as well as the stator blades work under highly negative incidences and fully separated flows, thus the low speed flow structures are very intense and distinguishable from the phenomena at any other rotational speed.

- Identification of the correlation between the inlet mass flow and the total pressure loss allows the derivation of the zero-speed line of the compressor which is the lowest extreme boundary of the compressor characteristic.

- Compressor map generation methods have a significant benefit. Using the zero-speed curve, the lowest boundary of the map is now given allowing this way interpolation instead of extrapolation toward the sub-idle regime. The latter enhances the physical background of those methods by capturing the low speed flow phenomena (Fig. 3.1). In addition, simulation of groundstarts is also allowed.

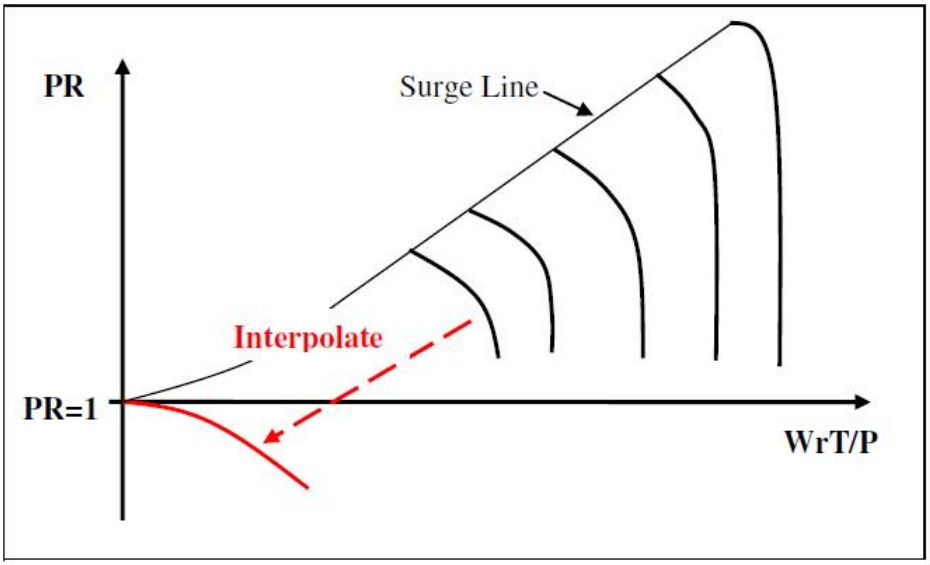

Figure 3.1: Compressor characteristic with the zero-speed line (schematic) [51].

For the above mentioned reasons, one can easily realise that a successful derivation-prediction of the compressor zero-speed line is vital and the entire engine modelling can have significant benefits out of it.

3.2 Literature review

The main literature findings regarding compressor cascade performance are hereafter presented.

3.2.1 Compressor locked rotor definition

Before the description of the flow angles in the various compressor stages under locked rotor conditions, the blade angle terminology used throughout the current thesis from now on must be declared. As illustrated in [52], the properties of interest in a compressor blade row are of two types; related to geometrical and aerodynamic features. Fig. 3.2 describes the cascade nomenclature as used for the current work.

The definition of the flow under locked rotor conditions is given in [51], while further discussion is also done by [67] and [97]. For a compressor without inlet guide vanes (IGV's) the green vectors of Fig. 3.3 represent the relative to the first rotor velocity at design conditions, while the incidence angle becomes more negative at lower rotational speed (red vector). At zero spool speed the flow impinges on the rotor axially as in that case the absolute velocity coincides with the relative and the incidence angle becomes severely negative. Obviously, separation effects occur at the pressure surface of the blade, also characterised by low Reynolds number values. An indicative value for a state-of-the-art HP compressor blade operating at locked rotor conditions is approximately -50 to -60 degrees. Those values remain valid for stator blades operating downstream of steady state windmilling rotors, the incidences in which have slightly reduced values approximately up to -20 degrees but are of course still negative. A representative example of an incidence angle distribution in a modern engine under windmilling conditions can be found in [45]. One can easily realise that such values definitely exceed the existing range of off-design compressor performance studies.

According to [67] the zero-speed line has a horizontal tangent at $W\sqrt{T}/P = 0$

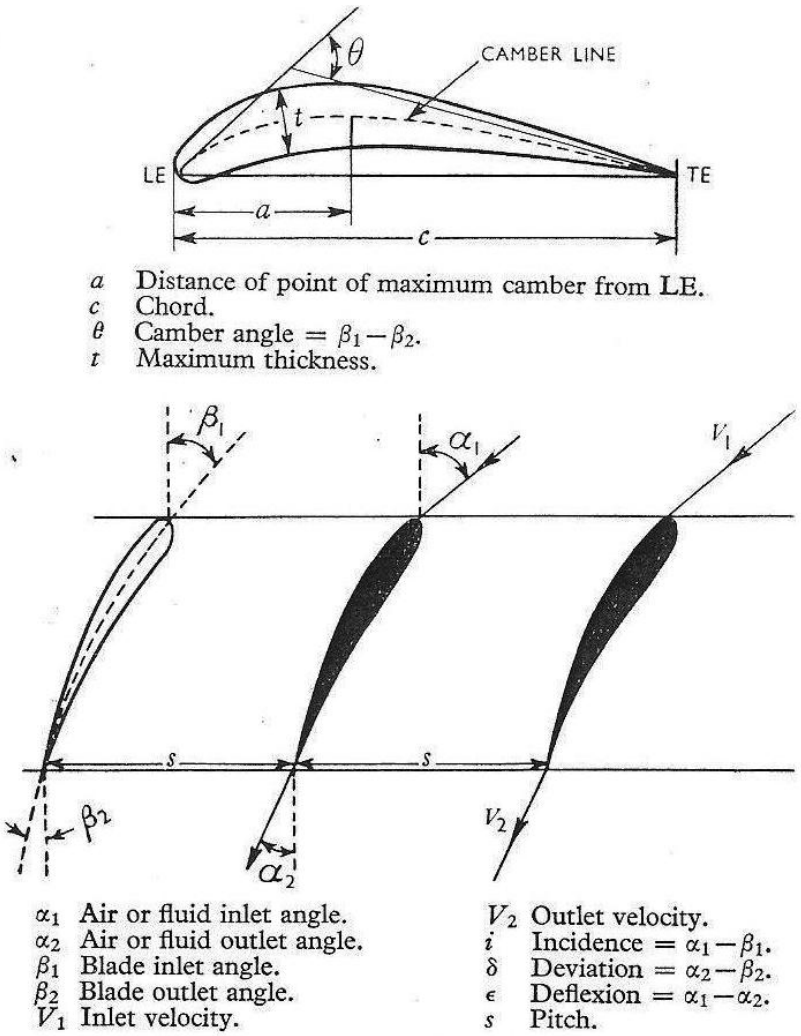

a Distance of point of maximum camber from LE.
c Chord.
θ Camber angle $= \beta_1 - \beta_2$.
t Maximum thickness.

α_1 Air or fluid inlet angle.
α_2 Air or fluid outlet angle.
β_1 Blade inlet angle.
β_2 Blade outlet angle.
V_1 Inlet velocity.
V_2 Outlet velocity.
i Incidence $= \alpha_1 - \beta_1$.
δ Deviation $= \alpha_2 - \beta_2$.
ϵ Deflexion $= \alpha_1 - \alpha_2$.
s Pitch.

Figure 3.2: Compressor cascade nomenclature [52].

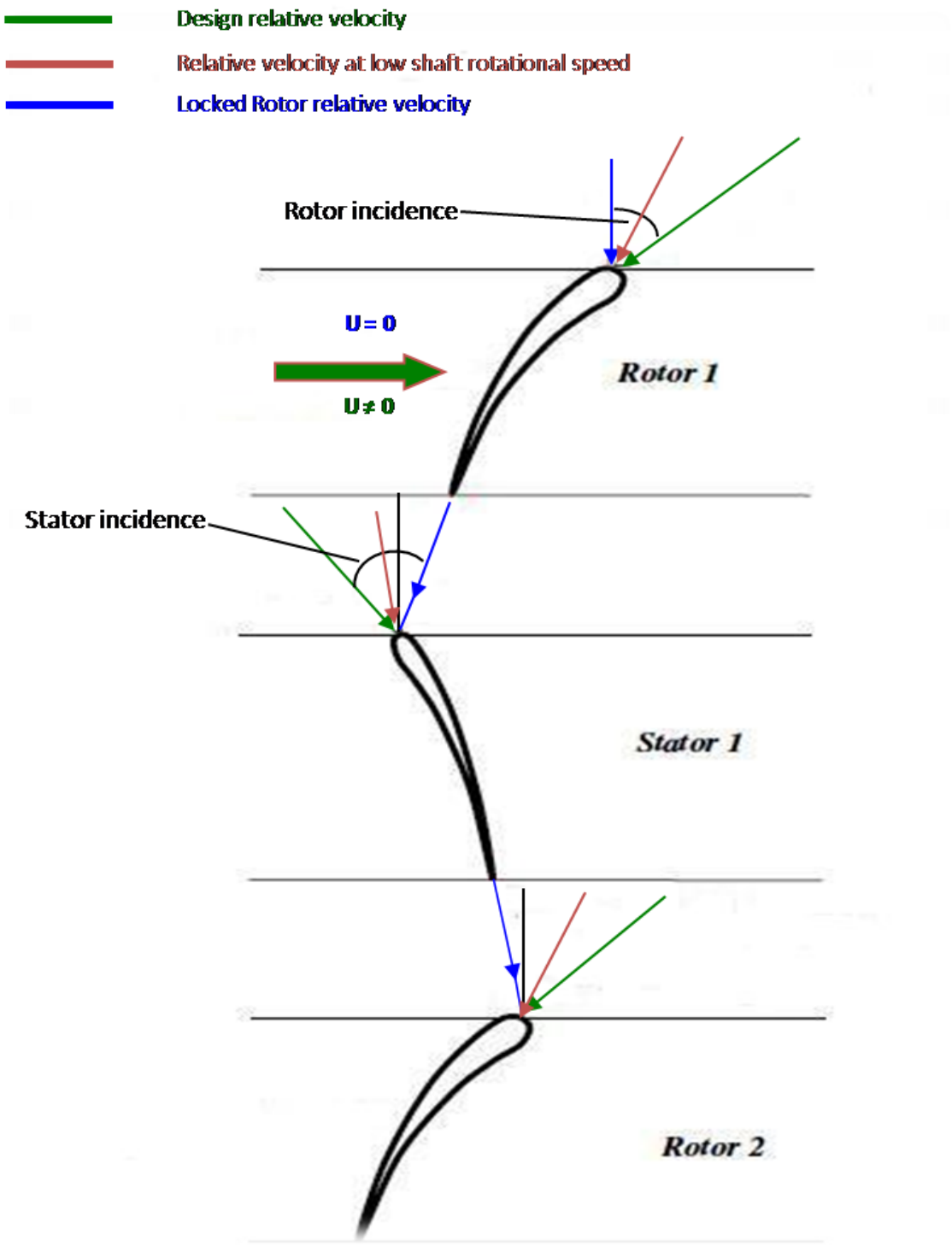

Figure 3.3: Compressor flow angles at design and zero spool speed.

and PR=1, nevertheless test rig data are necessary for a more valid low and zero speed map generation. Thermodynamically speaking, at zero speed there is no energy transfer between the fluid and the rotor therefore there will be no enthalpy (thus total temperature) rise through the compressor stages while the total pressure decreases as the non-rotating blades act purely as obstacles to the flow. However, the torque applied to the blade has non-zero values as the aerodynamic forces due to the separated flows on the blade still exist. Here lays the main advantage regarding the utilisation of torque characteristics for performance simulations as this is the only parameter which stays within finite values throughout the operating regime of a compressor no matter whether it operates at PR<1 (stirrer or turbine mode). The latter allows also for groundstart performance simulations as finite values of performance properties are required at zero-speed, obviously because this is the operating line the transient starts from during this specific engine process.

A deeper analysis about low-speed performance representation and torque parameters is given in Chapter 4. The low speed curves are described and the compressor operating modes are clearly identified.

3.2.2 Findings from previous studies

In this section a brief review of compressor modelling methods at sub-idle conditions is given, emphasizing at the end on the locked rotor studies conducted by Howard in [51].

No systematic zero-speed prediction studies have been conducted up to the moment in the direction briefly described earlier in this thesis. This is mainly due to the fact that no cascade test data exist for the highly negative incidences the compressor blades operate at during locked rotor conditions, as this extreme off-design regime in combination with the high cost of an experimental procedure prevents systematic experimental testing by the manufacturers. Consequently, the latter justifies the lack of predictive capability in sub-idle performance processes. There is only little

knowledge regarding the component and engine phenomena under those conditions and thus the physical background of the modelling methods is relatively poor.

The highest negative incidence angle blade performance data found by the author in the open literature is given by Howell [52], and reproduced in [32], who reports experimentally derived compressor characteristic for a given blade design and cascade configuration within approximately -23 and +10 degrees of incidence. More specifically, pressure loss coefficients, lift coefficients and flow outlet angles are reported for the given blade cascade configuration. Those results are illustrated in Fig. 3.4

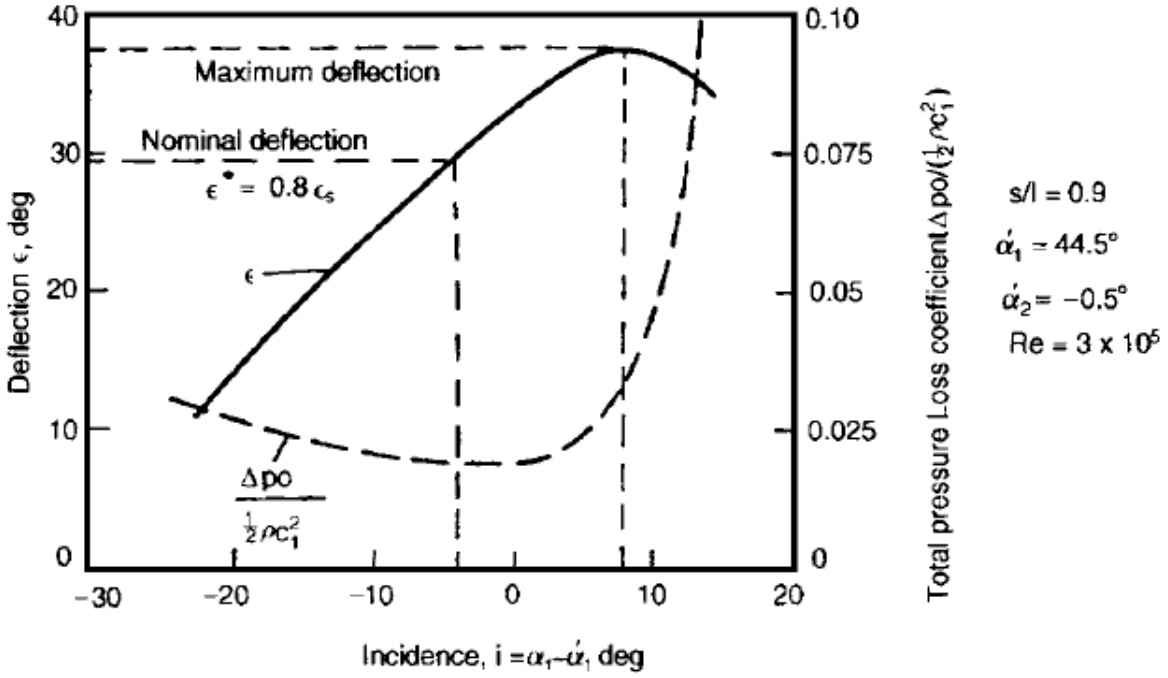

Figure 3.4: Compressor cascade characteristics [52].

The same author has proposed empirical correlations for modelling the different types of losses through axial fans and compressors, which have been used for the practical compressor modelling of turbojet and turbofan engines attempted by Choi et al. in [18] and [61]. However, they are approximate coefficients, not really capable of capturing the correct values of the losses at the extremely negative incidences of the locked rotor conditions. A description and a modelling effort of the compressor

operation at low speeds and windmilling is also reported by Shou in [107] applicable to turbojet engines.

Highly negative incidence data are provided also by Hawthorne in [46] who reproduced Howell's results reported in [54] and presented in Fig. 3.5. As Howard analyses in [51], those studies could not be applied for windmilling and locked rotor studies as the change in the axial velocity through the stage is not taken into account, assumption not valid for the low Reynolds number windmill conditions.

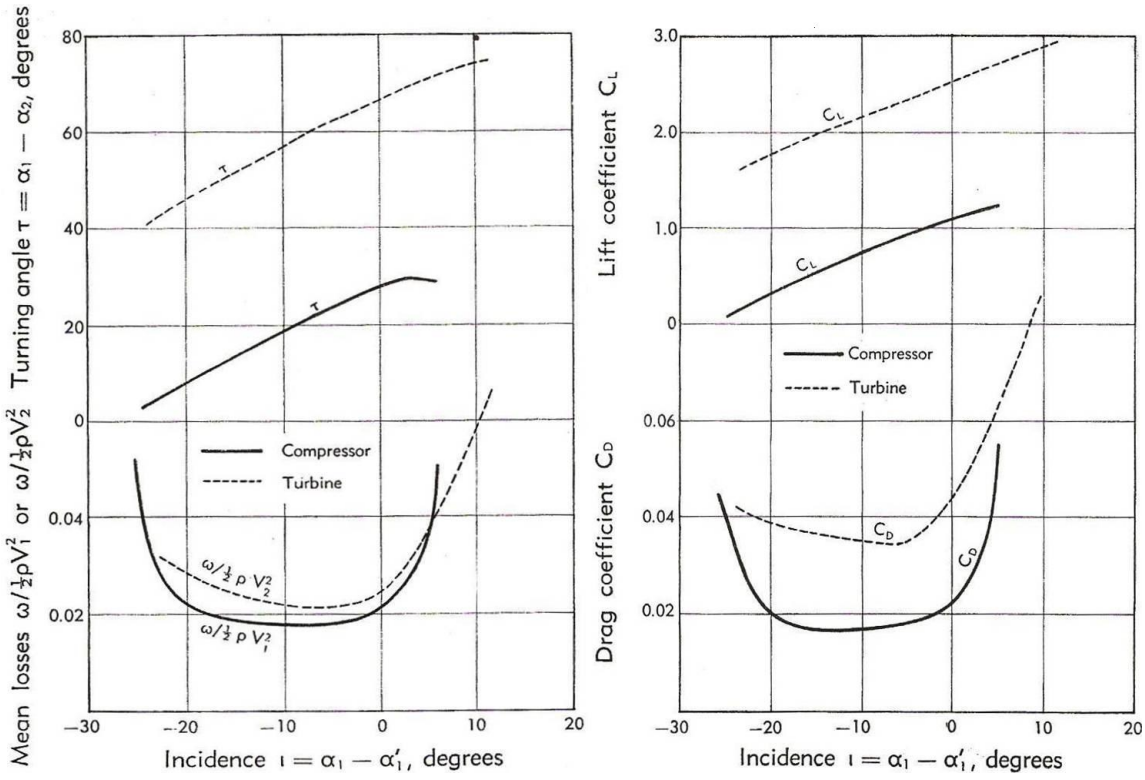

Figure 3.5: Compressor and turbine cascade characteristics [46].

The literature related to compressor cascades and blade performance studies is chaotic as it was (and still is) a vital research topic since the early years of the gas turbine engine. Most of the fundamental text books and papers ([52, 53, 49, 43, 77, 37, 38, 26]) have been studied by the author to enhance his background on compressor performance. However, those are fundamental studies oriented mainly towards compressor design, therefore all the discussion and the test data do not cover a sufficient range of off design operating conditions. Thus they have been used

only for the deeper understanding of the topic and not for obtaining methods and results for highly negative incidence studies under windmilling conditions.

Research related to off design compressor performance has been extensively carried out regarding stall situations [122, 121, 23, 24, 47, 73, 120]. Although separated flows occur also under those conditions due to the highly positive incidences this time, there are major differences in the blade performance therefore the applicability of stall methodologies to model totally separated flows but on the suction side of the blade is still questionable.

A rich source of information regarding fully separated flows is the research related to flat plates under high incidences where loss coefficients can be found obtained either experimentally or by numerical simulations. The reason for performing research related to flat plates at high incidence lies on the fact that their performance must demonstrate similar patterns with compressors at similar incidences. Compressor blades usually consist of low camber airfoils, thus similar to flat plates, especially at high flow angles where the fluid is not guided by the actual profile any more but the flow is dominated by the separation mechanisms. Therefore, as stated in [51] and supported also by the author, there is no significant effect of the compressor blade profile at highly negative incidence flows and consequently as a first approach the blades could be replaced by flat plates in order to take advantage of the rich literature resources.

In general flat plate studies can be categorised into two main groups; external flows around flat plates and internal flows through flat plates in cascade configuration, with more studies carried out for the former. Representative examples of external flows around flat plates where useful conclusions can be taken from, are presented by Sun [112], Taira [113] and Breuer [13]. A parametric analysis in terms of Reynolds number is also carried out to demonstrate its effect on the Lift and Drag coefficients. It is important to assess Reynolds number effects on compressors under sub-idle conditions as it is highly likely to operate below the critical Re = 200000

and therefore the blade performance to be significantly affected [32]. Reynolds number effects were also discussed by Howard [51] and Massey [75]. As highlighted by them, extrapolation of loss characteristics towards windmilling conditions might be far from reality as the error introduced due to the low Reynolds number effects will be significant.

The author believes that Reynolds number effects will be less significant in a windmilling fan, as especially the bypass part, experiences the highest percentage of the windmilling flow which combined with the big characteristic length (fan chord), does not allow for large reduction of the Reynolds number.

Early work on the performance of flat plates in a cascade configuration has been reported by Cornell [19] and Paxson [89, 88], whose work is mainly based on Roelke's pressure loss models for turbine blades [100].

In general flat plate models shall be considered as a starting point for the locked rotor modelling but on the other hand not entirely sufficient. Sub-idle conditions do not allow their unstinting application and require the further development of research methods of higher fidelity.

3.2.3 Comments on previous studies

As mentioned in the previous section, locked rotor studies have been conducted extensively at Cranfield University within the sub-idle project, by Jason Howard [51]. In general three approaches have been used for this research; pure analytical studies, analytical studies combined with pressure loss coefficients derived using CFD and finally experimental testing. All of them aimed at identifying the pressure loss factors and the flow turning at highly negative incidences as defined in a previous section. There was no time for performing any experimental testing. All the related work has been carried out within the current doctoral project and is presented in the current thesis. In this section comments about the validity of the analytical and the CFD approach as performed in [51] will be given.

3.2.3.1 The analytical approach

Effort to produce a theoretical method for the calculation of the torque and the pressure losses within a compressor stage has been put by Howard with the help of an MSC student (J. Bittan). Bittan [11] was based on first principles and incompressible cascade correlations to derive a formula for the circumferential force and torque within a rotor. Nevertheless, his approach assumed *constant axial velocity* through the compressor stage, which is perhaps valid for design point cascade calculations (and very often not even there) but never true for windmilling incidence angles. In addition, it was a totally *inviscous analysis*, which is again a very crude assumption for those fully separated flows dominated exclusively by viscous effects. Finally, the overall torque on the blade was calculated by assuming *constant circumferential force distribution* along the blade span. This may contain an error since the calculation was applied on a 3-dimensional twisted blade therefore with non constant incidence distribution along the span (for axial inlet flow) and consequently with non constant circumferential force distribution as well.

Later during his research, the above mentioned analytical expression was revised to include the axial velocity change while an attempt for a simple *prediction* of the pressure loss across the stage was also made, accounting only for the static pressure drop calculated using the blade drag as derived by Bittan. As expected, this correlation was simply far from reality as the wake, the profile and secondary losses were not included in the calculation thus the estimation of the overall pressure loss coefficient of the stage was wrong because this is a factor that nobody ever knows apart from nature. As mentioned in [51], "*the theoretical method required incorporation of some loss models to determine the pressure loss across the blades*".

3.2.3.2 Locked rotor CFD simulations

In order for the above mentioned idea to be implemented, CFD modelling of locked rotors was carried out aiming at providing a more realistic estimation of the total

pressure loss across the stage by revealing more details about the flow structure. Additionally, a stage stacking technique was applied to generate a whole compressor locked rotor characteristic.

More specifically, HP and fan blades from three different engines (A, C and D) were numerically modelled within a range of highly negative incidence angles representative of locked rotor conditions. The results were plotted in terms of the total pressure loss coefficient and in terms of the aerodynamic coefficients of the blades as illustrated in Figs. 3.6 and 3.7 while a representative flow structure is presented in Fig. 3.8.

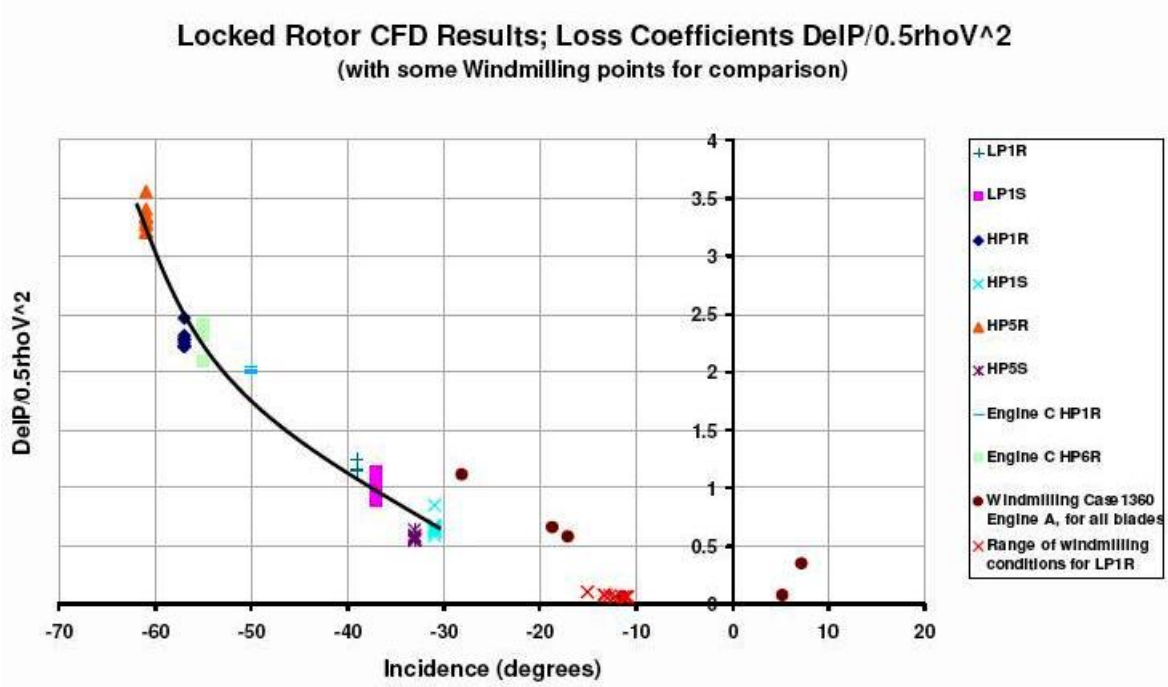

Figure 3.6: Compressor blade total pressure loss coefficients derived from CFD [51].

Even though the attempted simulations on stators were not of any success because the actual incidences (larger than in the rotors, see Fig. 3.3) could not be achieved with the solver, these studies revealed that the loss and blade aerodynamic coefficients are a polynomial function of the incidence angle. Flow exit angles were found to be approximately equal to blade exit angle in every case, outcome which will be put in doubt later on within the current thesis, while it was also confirmed

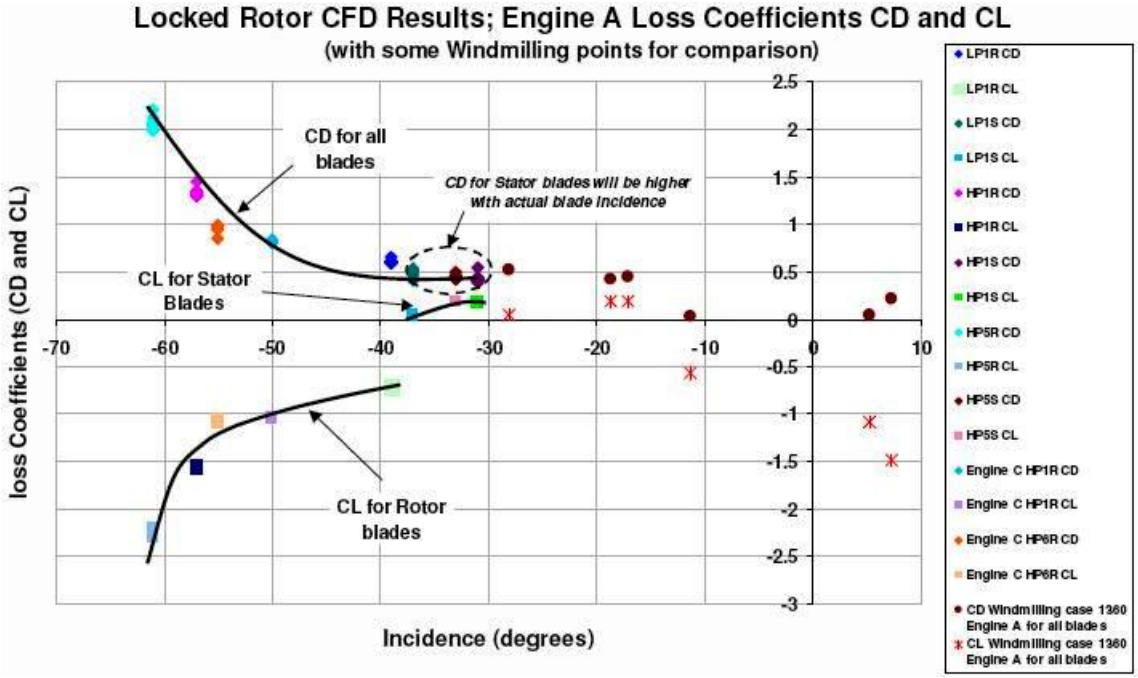

Figure 3.7: Compressor blade aerodynamic coefficients derived from CFD [51].

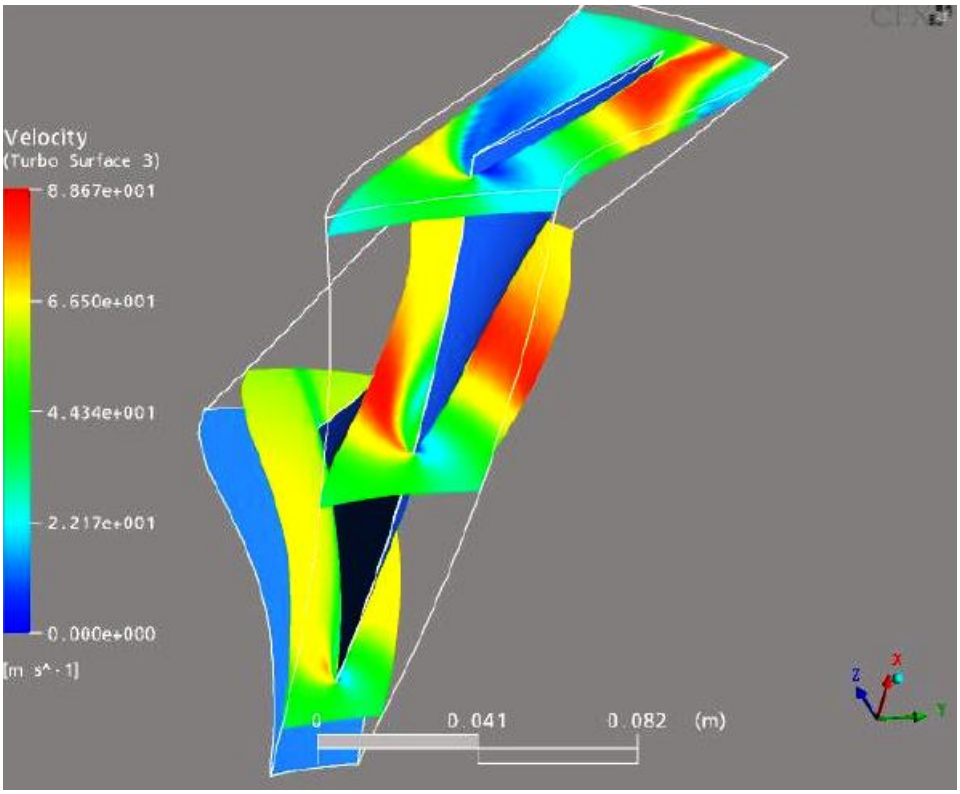

Figure 3.8: CFD locked rotor results [51].

that the static pressure drop can be reasonably well predicted by the solver. On the other hand, the loss mechanisms which translate the total pressure drop into velocity and then into loss (entropy increase across the channel) can not be well predicted and this is a known problem of the CFD's capability in simulating fully separated flows [3]. Finally, the significance of the secondary loss mechanisms has been revealed as the the graphical representation of the simulations has indicated strong tip leakage vortices which occupy a big percentage of the blade span especially at low aspect ratio blades. In addition, flows in the radial direction are also a big challenge for the numerical tool. Therefore, the weakness also of the theoretical loss prediction mentioned above was verified.

A significant outcome of the above described research is the proof that the low cambered compressor blades at highly negative incidences behave like flat plates. In other words the actual blade profile has little effect on the losses which are in turn dominated by the totally separated flows.

What should be also kept from this investigation is the fact that "*those CFD results can be used as qualitative rather than quantitative information*", as Howard points out in [51]. In other words there is a lot of space for improvements regarding the accuracy of the numerical results.

3.2.3.3 Conclusions and iniatives for further research

In general, the studies conducted by Howard can be considered as a very good starting point for the locked rotor (and stator) negative incidence modelling, underlining the methodology that should be followed.

According to the author of this thesis there are three main points where further research must be based on:

- The experimental testing of compressor blades at negative incidence to create a validation platform for the numerical results
- The improvement of the CFD capability by conducting numerical studies of

higher fidelity and finally

- Enhancing the generality of the pressure loss models.

The existence of an experimental facility for high incidence blade testing at Cranfield, contributes significantly on the deeper understanding of the topic. It offers a first class validation platform for the improvement of the numerical studies which can be even more enhanced by exploring the solver's capabilities trying to take the most out of it or identifying and take into account its weaknesses. Additionally, and more importantly, the existing loss at negative incidences have been generated by Howard using in every case highly twisted 3-dimensional blades which means that there is no constant incidence along the span for axial inlet flow. In every case the mentioned incidence is the mid-span incidence angle but in most cases there is a ± 12 degrees of variation in its value between the hub and the tip. This implies that, having a fixed variable incidence (given blade models) makes the study less generic as different incidence distributions for different blade designs will result in different aerodynamic behavior and therefore the existing plots cannot be considered as generic. Further parametric analysis on 2-dimensional blade performance at negative incidences, different solidities and stagger angles is required. It must be also combined with the validation of a methodology of radial profile stacking in order any 3-dimensional blade to be generated, therefore the loss model to be more generic. Work in this direction is presented in a later section of the current chapter.

3.3 Locked rotor research methods

The experimental as well as the numerical work carried out in order for the locked rotor compressor performance issue to be tackled are presented in the current section.

3.3.1 Experimental testing of compressor blades

As mentioned above, the first step forward on locked rotor research is the experimental testing of a compressor cascade at highly negative incidence in order to generate a set of test data against which any numerical study can be validated against. The test facility was initially designed by Howard [51] between 2006-2007 and finilised by the author who also assembled the rig and performed the experiments during 2008-2009. A schematic of the experimental facility is given in Fig. 3.9, while the final assembly including the instrumentation modules is illustrated in Fig. 3.10. In addition a description of the blade geometry as defined in Fig. 3.2 is given in Fig. 3.11

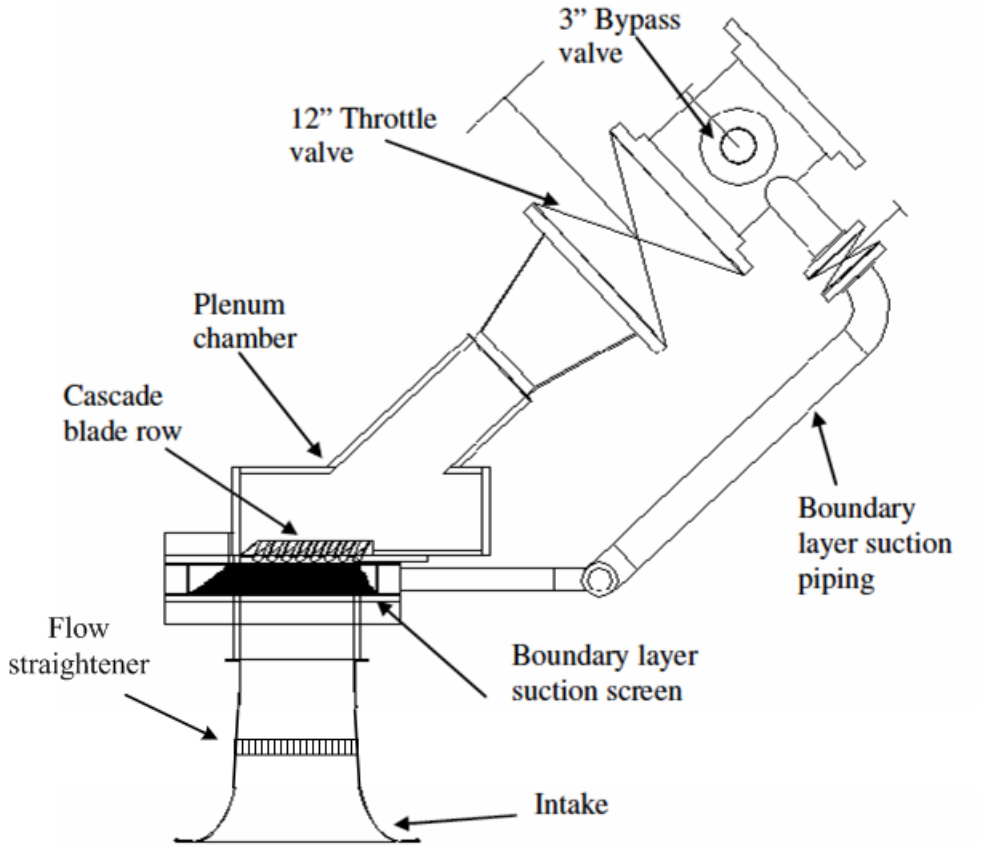

Figure 3.9: Locked rotor test rig layout (schematic).

The blades are staggered in their design stagger angle value. A detailed description of the facility as well as of the experimental procedure followed has been published in [123]. As the aim of this section is not to describe in detail the experimental techniques, these can be found in [123], the main conclusions of this study

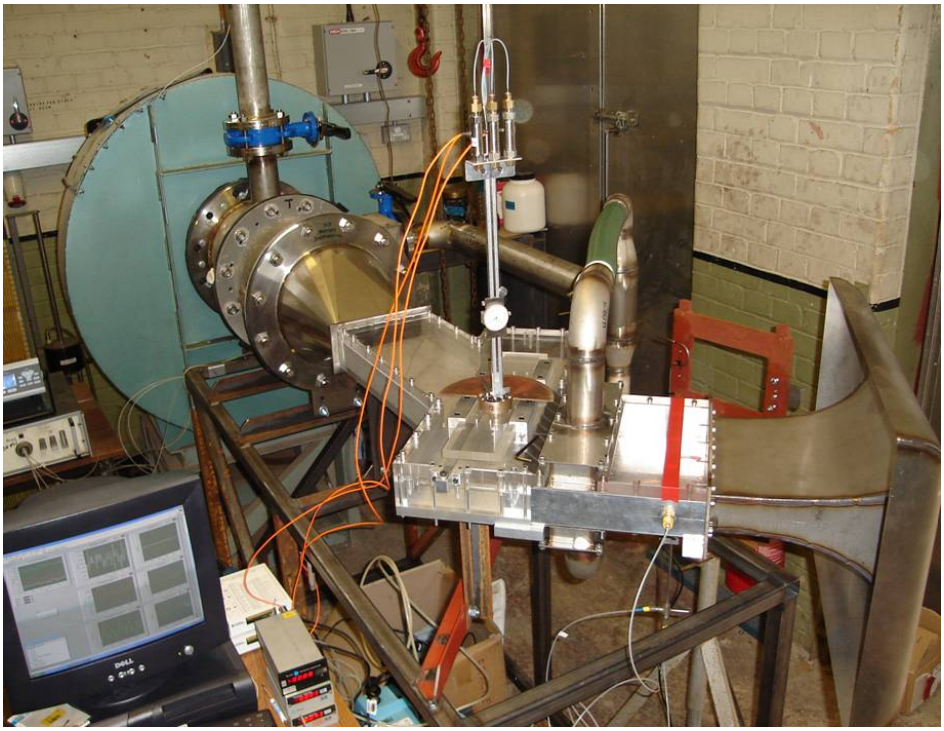

Figure 3.10: The experimental facility.

can be summarised as follows:

- Highly 3-dimensional, state-of-the-art HP compressor blades at -58 deg incidence angle have been used for the tests.

- Pressure measurements at two positions downstream with controlled upstream conditions have been conducted in order for the total pressure loss and the steady state velocity field downstream (exit flow angles) to be evaluated.

- The measurements have been conducted using a 3-hole pneumatic pressure probe at a preliminary stage and a 5-hole probe for the final tests in order for the 3-dimensional effects to be captured adequately. Both instruments were in-house manufactured and calibrated, while the data acquisition system was in-house designed and assembled as well.

- The total pressure loss coefficient and the spanwise flowfields for every inlet Mach number tested have been measured, revealing the main and the secondary flow structures. The spanwise pressure loss and flow outlet angle dis-

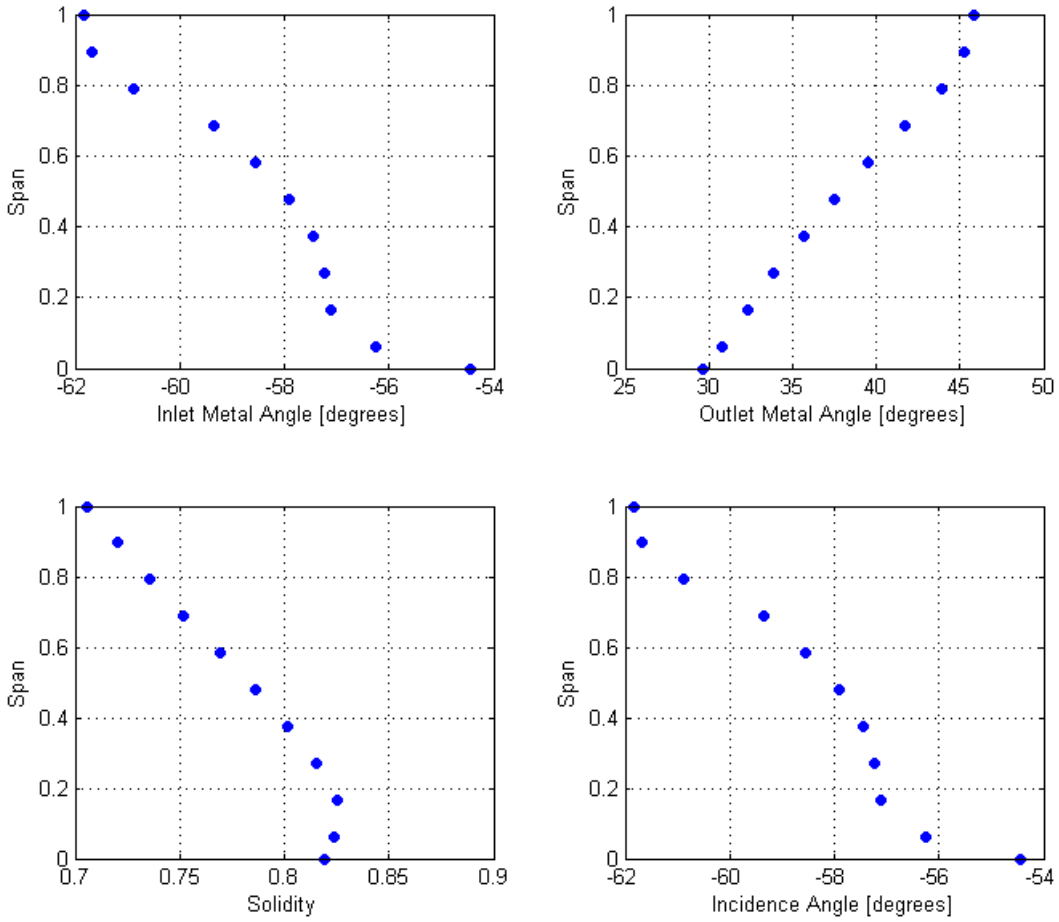

Figure 3.11: Spanwise distribution of the blade profile geometry.

tribution as obtained by the two instruments employed is illustrated in Figs. 3.13, 3.14, 3.15 for all the inlet Mach numbers tested.

- A detailed uncertainty analysis of the measured properties has been also carried out and the high level of confidence on the measured data has been justified.

- In general, the experimental procedure provided with data which can be reliably used as a calibration-validation platform for further numerical studies aiming to investigate highly separated flowfields, as will be shown in the following section.

3.3.2 Numerical studies on locked rotor performance

Having obtained the experimental validation platform as described previously, the confidence on the numerical tools can be significantly enhanced. At a first approach the chosen CFD solver has been validated against the experimental data. A numerical model of the experimental facility was created and after a parametric analysis with respect to the solver capabilities, the most appropriate CFD technique able to capture as accurately as possible the flow phenomena, was identified.

This work was carried out by Fabio Pengue, an MSc researcher during academic year 2007-08, supervised by the author of this thesis and Dr. V. Pachidis. Again, all the analysis can be found in [91], while it was also published in [124], therefore only the main conclusions will be mentioned hereafter.

The software used for the simulations was CFX, a commercial CFD solver oriented mostly for turbomachinery and internal flow applications, while ICEM was used for all the required geometry and mesh generation.

3.3.2.1 Evaluation of the CFD capability

Before any simulation of the examined cascade, the solver's capabilities were initially explored. Simulations on a test case available and extensively investigated in the public domain have been conducted for which both numerical as well as experimental data exist; that is the Zierke and Deutsch cascade.

Simulations on this case showed that off-design cascade simulations can be adequately approximated by the chosen numerical tool after a careful selection of the turbulence closure and its settings as described in [124]. Additionally, a study regarding the effect of the boundary conditions as well as of the mesh size on the quality of the final solution identified the most appropriate boundary sets and the required mesh size.

3.3.2.2 Validation of the numerical solver

The Zierke and Deutsch validation runs revealed the flexibility and capability of the CFD solver before the actual validation against the experimental data of the locked rotor cascade was conducted.

The geometry built for this purpose with its various blocks is shown in Fig. 3.12. An assessment regarding the need of running unsteady simulations was also conducted. As shown in [124], even though there are significant unsteady effects in the flow due to the separation regions, the phenomena are highly periodic and consequently can be captured by the less time expensive steady simulations. In addition, the main interest of this study is the evaluation of the mean loss coefficient at high incidence angle while the zooming into the unsteady flow structure and their analysis is an issue of secondary significance and outside the scope of the research.

The comparison between the two sets of experimental results and the numerical simulations is illustrated in Figs. 3.13- 3.15.

As seen from the spanwise distributions of the pressure loss:

- The CFD model looks capable enough to capture the flow phenomena leading

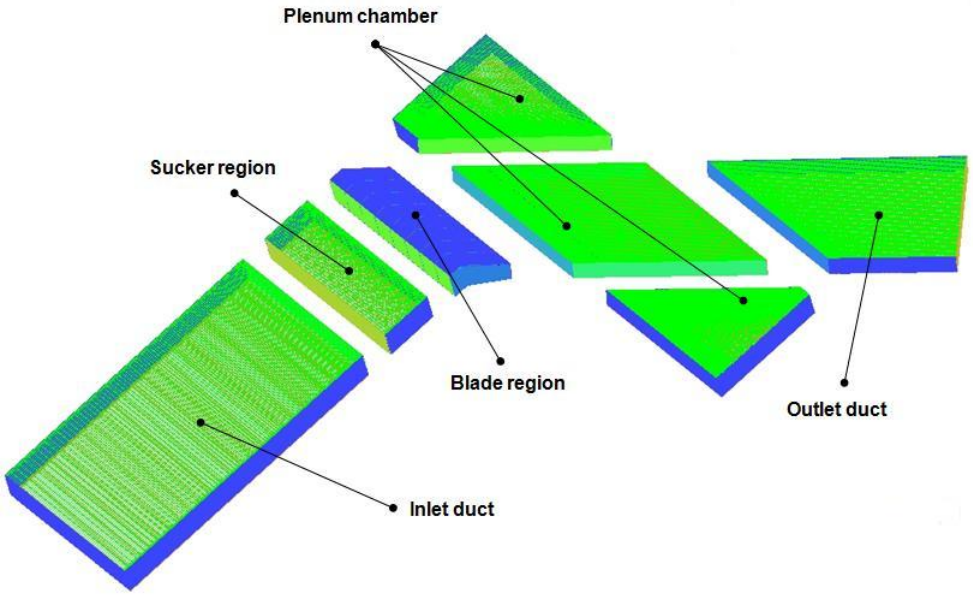

Figure 3.12: Domains of the computational model.

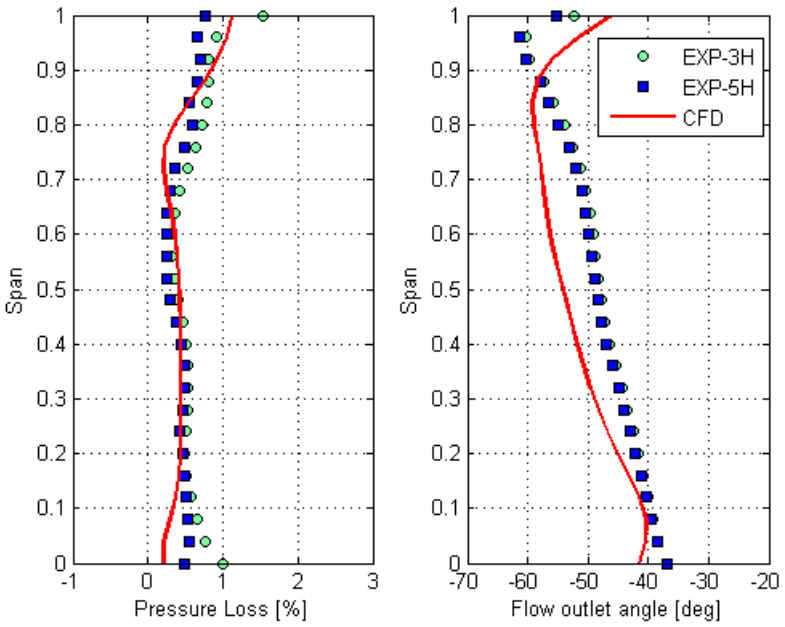

Figure 3.13: Pressure loss and flow outlet angle at M = 0.07.

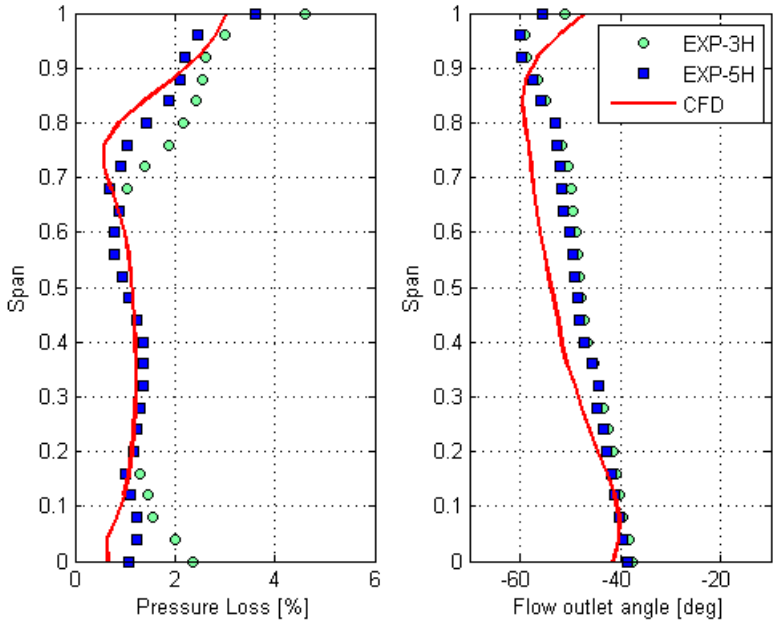

Figure 3.14: Pressure loss and flow outlet angle at M = 0.1.

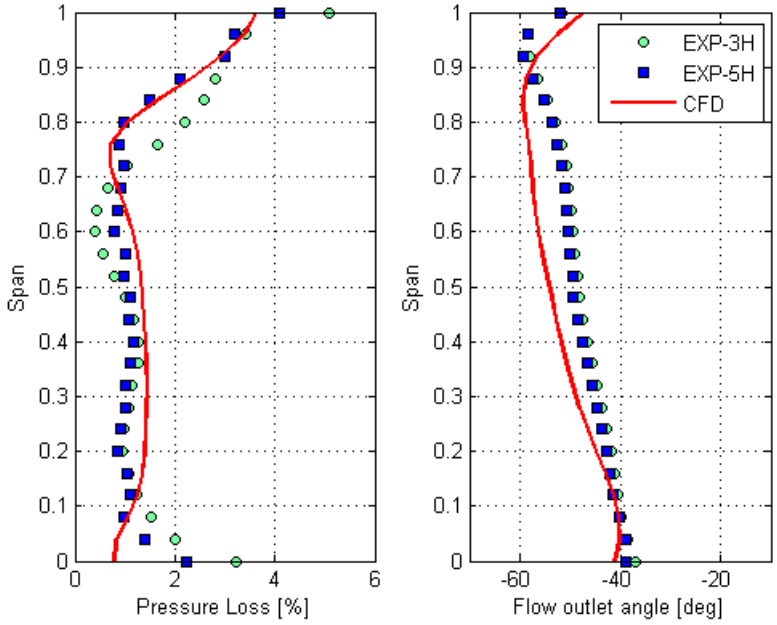

Figure 3.15: Pressure loss and flow outlet angle at M = 0.12.

to increased pressure losses through the high incidence compressor blades.

- The validation against the 3-hole probe experimental data has shown that the pressure loss is predicted with less than 8% error, while this deviation is reduced when compared against the 5 hole probe data.

- Comparison against the 5 hole probe test data is more appropriate as in this case more 3-dimensional flow effects are captured whereas loss of this information by the 3-hole instrument results in less overall dynamic head measurement which in turn gives a lower value for the total pressure and thus a higher loss.

- The above is mostly emphasized in highly 3-dimensional flow regions such as the hub and the tip, as shown in the previous figures.

As far as the overall cascade performance is concerned, the measured as well as the calculated values are illustrated in Fig. 3.16 in a non-dimensional way which covers all the low speed area of cascade operation (that is for M $<$ 0.3).

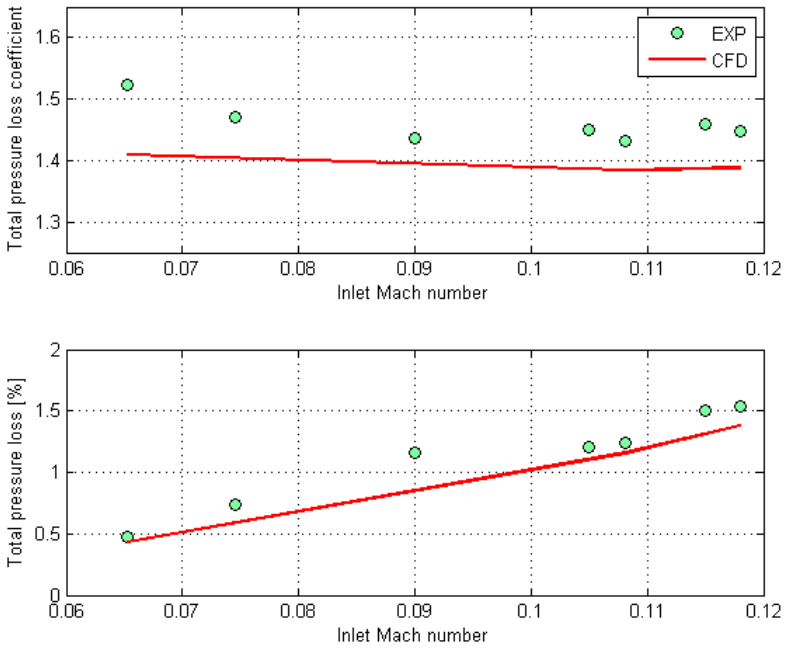

Figure 3.16: Pressure loss for the locked rotor cascade.

As can be seen from Fig. 3.16 the very low speed region of operation is dominated by Reynolds number effects as an increased total pressure loss coefficient value is

observed. Nevertheless, this is expected, as the very low speed experimental tests were carried out at inlet Mach number value, at which such a phenomena are likely to appear. As already mentioned, more extensive studies on the low speed Reynolds number effects are required in order for a more complete view of the locked rotor performance to be obtained.

Regarding the flow exit angle distribution, (see Fig. 3.17), even though the general trend between the numerical and the experimental data is in good agreement, there is a constant deviation observed which is mainly due to the swirl introduced by the centrifugal fan driving the air through the wind tunnel facility. Considering the capability of the CFD solver, it was believed that the exit flow angle prediction would not be that far from the measured one (thus within a reasonable range of error) since even with the distortion from the wind tunnel fan the trend of the test data is perfectly captured by the CFD. Besides, as already mentioned, the main weakness of the numerical prediction lies on the total pressure loss, while the outlet velocity is usually better predicted. The latter enhances the reliability of the numerical tool and encourages further research on totally separated flows.

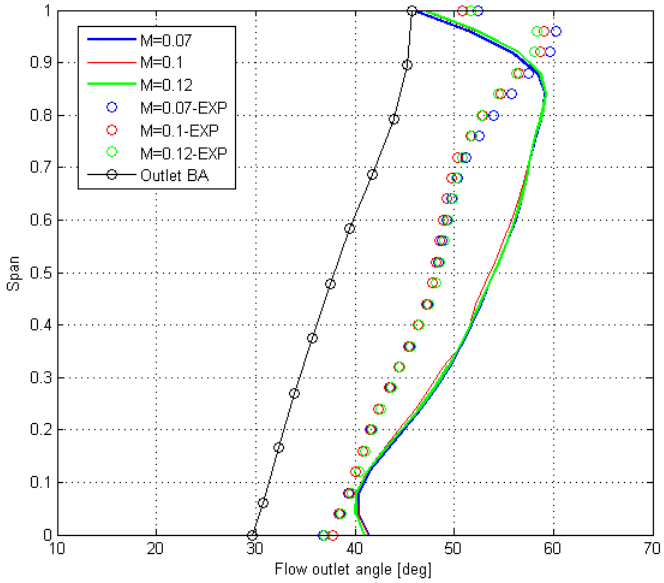

Figure 3.17: Exit flow angle for the locked rotor cascade.

However, as expected, there is no dependency of the flow exit upon the inlet

Mach number.

3.3.2.3 Concluding remarks

The objective of this comparative research using both experimental and computational tools was to increase the confidence in the numerical solver for conducting research in highly separated flowfields such as those occurring in compressor blades at highly negative incidence angles.

In order to say whether the effort is successful or not awareness of the limitations of both approaches is necessary. By having a closer look at the quality of the numerical model generated, it is worthy to mention that the poor definition of the hub and tip boundary layer regions as well as the weakness of the solver to sufficiently predict its thickness implies that the numerical loss prediction should be under-estimated [91, 123]. This argument is also enhanced by the widely known weakness of most numerical tools to predict correctly the massive entropy generation in case of extreme off-design turbomachinery flows.

On the other hand and as far as the experimental capability is concerned, instrumentation's uncertainties but more significantly the highly 3-dimensional flows which cannot be fully captured by the probes imply that in that case the overall measured pressure loss through the blades must be over-estimated.

The above mentioned remarks act in favor of the overall outcome as it is suggested that a rather bigger deviation between the numerical and the experimental results is obtained due to the weaknesses of both techniques which is amplified with the velocity. However, this is a systematic error which can be eliminated by increasing the fidelity of both approaches giving extra care to their weak aspects as they are described above.

As became apparent from the previous analysis, a rather macroscopic validation of the numerical solver was carried out in the sense that only the total pressure loss and flow deflection have been studied in a steady state approach, while a deeper

investigation also of other flow properties and even inside the channel could have also been carried out. However, one should always keep in mind the aim of the study which at this stage is nothing more than an evaluation of the available numerical capability to approximate the overall performance of a locked rotor stage with respect to the loss it imposes to the inlet flow. At the end of the day, the overall compressor performance is of major interest. Nevertheless, and contrary to the above statement, the more physical phenomena captured by the map the higher its quality is. However, considering the challenges that such an off-design case is tackled numerically and experimentally, starting from a more general study is a very good first step, while work on obtaining confidence on the tools is in progress. At a later stage, deeper understanding of the flow phenomena will be required in order for the quality of the locked rotor performance studies to be even more improved and completed.

The bottom line from this investigation is that a systematic and multidisciplinary study of the locked rotor phenomena such as the one described above, enhances the numerical capability while offering valuable momentum regarding the understanding of the dominant physical mechanisms at those conditions.

3.4 Pressure loss modelling for compressors at highly negative incidence

As already mentioned in section 3.2.3.3, not only an improvement of the CFD simulations quality but also a more generic approach to predict compressor performance at highly negative incidences was required in order for the physical understanding to be enhanced. The former is greatly ensured by the validation-calibration approach of the numerical solver described previously. The latter, nevertheless, is not captured by the previous analysis since, as already mentioned, highly 3-dimensional blade simulations make the analysis more geometry blade specific than generic.

In this direction, the blade element theory has been employed in order to further scrutinise the 3D analyses conducted up to now. The benefit out of this approach is a significantly more generic method for the compressor blading performance prediction, as will be shown in the following paragraphs.

3.4.1 Blade element theory

What is mainly suggested by the blade element concept is that each 3D blade consists of infinite 2D cross sections along its span. For the blade designers it is assumed, at a preliminary stage, that each such element operates as a 2D aerofoil without any interaction with the rest and thus the 3D blade can be designed by stacking radially a certain number of 2D blade elements of known performance [32] as shown in Fig. 3.18. Deep mathematical analyses based on that concept can be found in [85] and [98] and will not be reproduced in the current thesis. A very enriched list of references can be also found in [32].

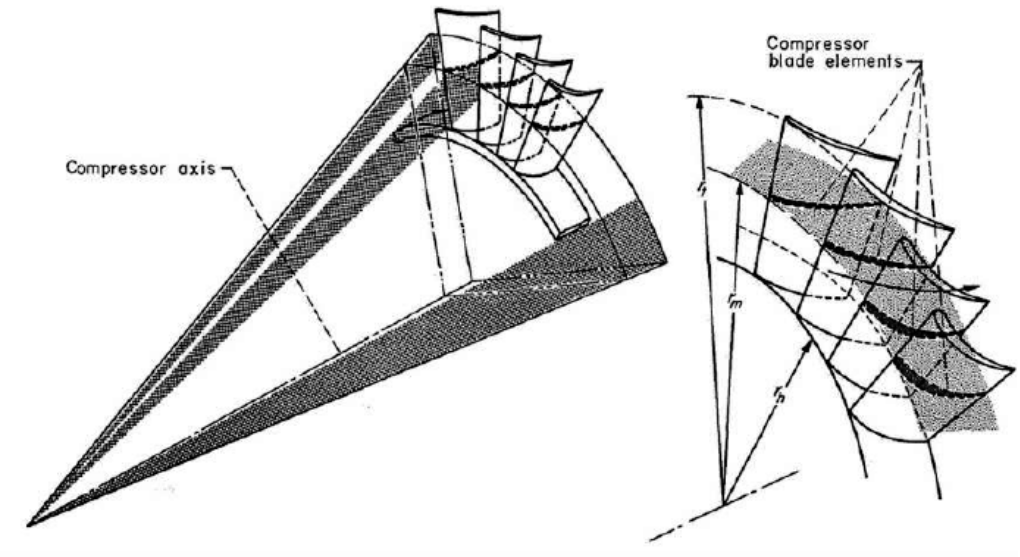

Figure 3.18: Blade Elements in a annular Compressor Cascade Row [98].

The question is whether such an analysis could be valid for off-design conditions such as the ones studied here. In that case any kind of 3D compressor blade design could be approximated by a number of 2D sections also at off-design conditions.

Therefore, having a number of systematic, 2D cascade data for different incidences, solidities, stagger and camber angles, will allow the performance prediction of any 3D blade design by just putting together the 2D profiles.

This simplification must be done with awareness though, as all the 3-dimensional effects caused by secondary radial flows are not taken into account.

3.4.2 Application on blades at negative incidence

In order to prove the applicability of the above explained concept on compressor cascades at highly negative incidence, a comparative study to verify whether a 3D blade performance can be approximated by a number of 2D sections was undertaken.

The following work was performed by Cornelia Ruelke, an MSc researcher who worked within the UTC during 2008-09 and supervised by Dr. V. Pachidis and the author of this thesis [102].

During this work, the flowfields obtained with a 3D annular cascade CFD simulation approach have been compared against 2D simulations at the same span-wise positions of the geometry also with exactly the same solidity, incidence and stagger angle at the correspondent radial position of the 3D blade. The locations have been chosen at three positions: at 10% and 90% in the span-wise direction, in order to minimize the wall effects, and at mid-span position (50%). The followed procedure is illustrated in Fig. 3.19.

The 3D model is a high fidelity HPC1 rotor of engine C (see Figs. 3.20 and 3.21) and all the CFD set up is described in great detail in [102]. Regarding the 2D simulations, the required number of computational domains similar to the one illustrated in Fig. 3.22 has been generated. The comparison was carried out on the basis of the total pressure loss and flow exit angle as defined in [32]. Those coefficients are reproduced hereafter based on Fig. 3.23.

The non-dimensional pressure rise (or drop in this case) coefficient and the tan-

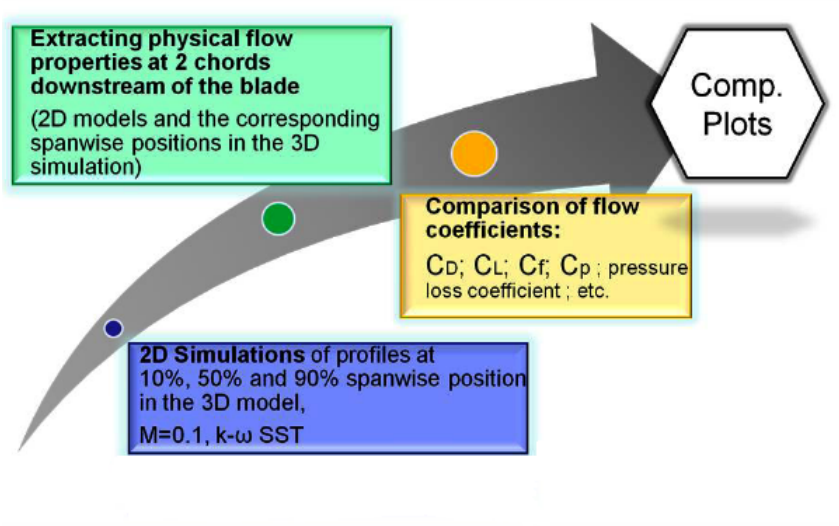

Figure 3.19: Process validation.

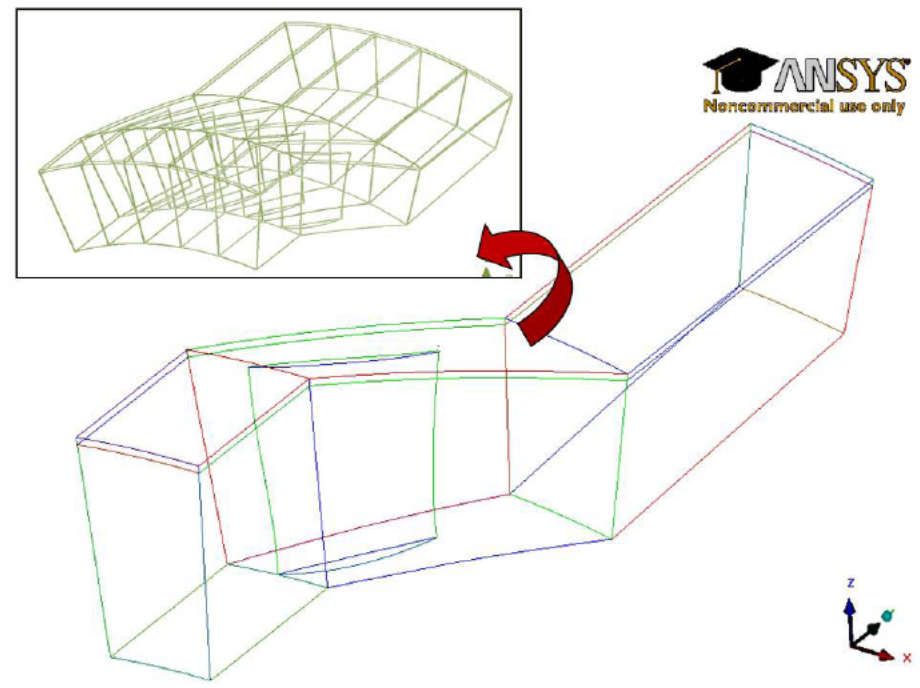

Figure 3.20: Single passage model.

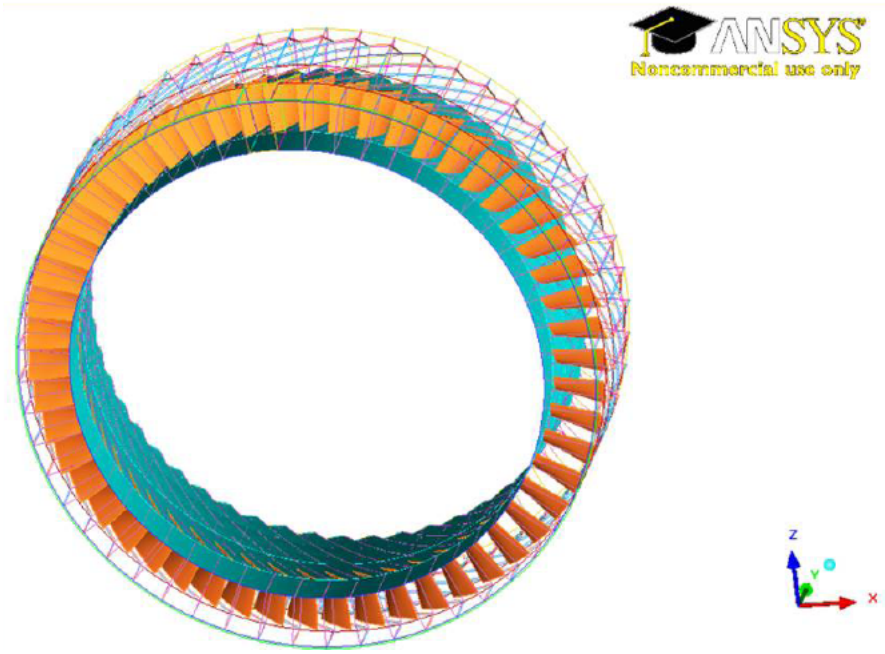

Figure 3.21: Entire HPC1R annulus.

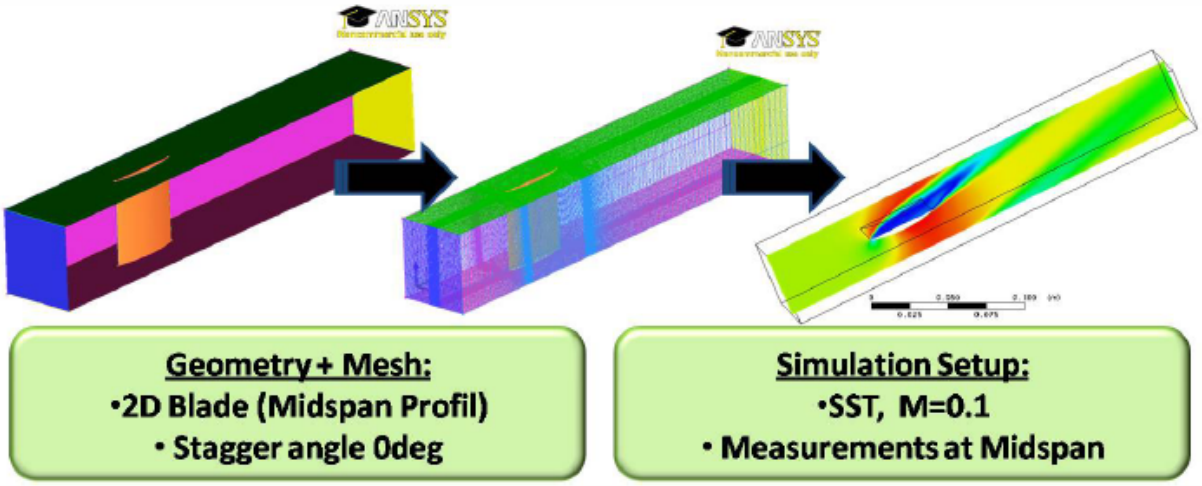

Figure 3.22: 2D simulation process.

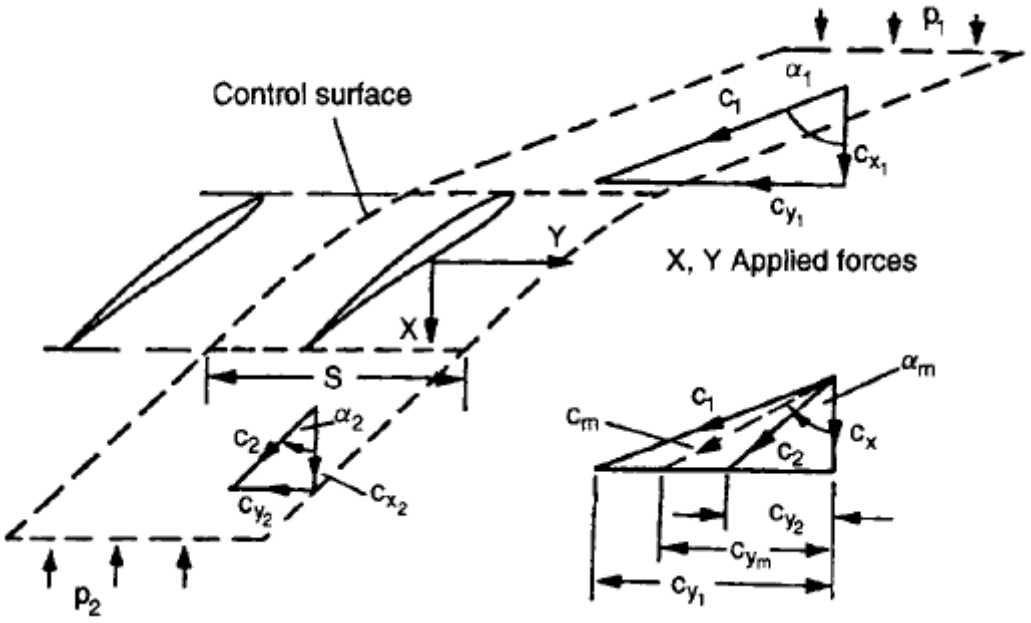

Figure 3.23: Forces and velocities in a compressor cascade with the assumption of constant axial velocity [32].

gential force coefficient shall be defined as:

$$C_p = \frac{X}{\frac{1}{2}\rho c_x^2} \tag{3.1}$$

$$C_f = \frac{Y}{\frac{1}{2}\rho c_x^2} = 2(\tan\alpha_1 - \tan\alpha_2) \tag{3.2}$$

and can be correlated as:

$$C_p = C_f \tan\alpha_m - \zeta \tag{3.3}$$

where

$$tan\alpha_m = 0.5(\tan\alpha_1 + \tan\alpha_2) \tag{3.4}$$

and ζ the total pressure loss coefficient defined as

$$\zeta = \frac{\Delta P}{\frac{1}{2}\rho c_x^2} \tag{3.5}$$

On a different basis, the lift and drag coefficients may also be used for comparative studies defined as:

$$C_L = \frac{L}{\frac{1}{2}\rho c_m^2 l} = 2\frac{s}{c}\cos\alpha_m(\tan\alpha_1 - \tan\alpha_2) - C_D\tan\alpha_m \tag{3.6}$$

$$C_D = \frac{D}{\frac{1}{2}\rho c_m^2 l} = \zeta\frac{s}{c}\cos^3\alpha_m \tag{3.7}$$

based on the lift and drag forces as represented in Fig. 3.24

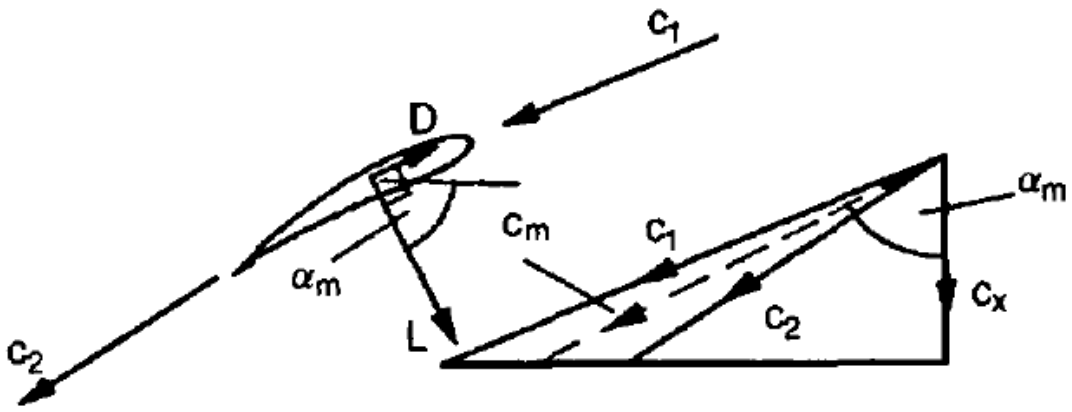

Figure 3.24: Lift and drag forces on a blade [32].

The simulations were conducted for inlet Mach number 0.1 in all cases which implies that both the total pressure loss coefficient as well as the flow exit angle (deviation) angle are dependent only upon the inlet flow angle and not upon the Reynolds or the inlet Mach number. The measurements of the properties of interest have been taken 2 blade chords downstream for two reasons; firstly to allow for better flow mixing and thus a more realistic value of total pressure loss and secondly in order to avoid the highly fluctuating separated wake. However, downstream measurements on compressor cascades can be taken in several different positions, providing with slighly different values for the total pressure coefficients. This has been a topic of discussion and various analyses can be found in the literature [22, 95], concering also the averaging of mixed-out turbomachinery flows. Mainly, it has to do with the entropy generation rate as we go further downstream of the blade trailing edge. In

other words, the more space is given to the flow to expand a higher percentage of its dynamic head is transformed into pressure loss, until all the losses of the system will be developed, theoretically in infinite distance downstream. However, such a process does not occur in gas turbines as in a very short distance downstream of each blade row, the next one is located, keeping the losses in a lower value but already "reserved" by the flow dynamic head in the form of increased flow entropy, that is energy that sooner or later will be dissipated being apparently not of any benefit. Therefore, it is of major importance to define the position where the loss measurements are to be taken in the most representative way according to the application under study [25]. Finally, more CFD settings regarding the current testcase are described in [102].

Starting from the comparison of the outlet flow angle (α_2) which primarily defines the tangential force coefficient (C_f), it can be seen that the maximum difference between the full 3D and the stand-alone 2D profile simulations at the corresponding positions (referred to as "*quasi-3D blade*" from now on), is in the order of 11% at the hub with the fully 3D simulation to predict slightly reduced value. The latter has an impact on the calculation of the tangential force coefficient (see Fig. 3.26) where the maximum difference between the two approaches (3D and quasi-3D) is of an order of 12% for the mid-span position and not at the hub as expected. This simply happens because the percentage error of the tangent of the exit flow angle obtains its maximum value at the mid-span (19.1%). It is reminded that the inlet flow angle is always zero and constant for all the cases.

In addition, the static pressure drop across the passage defines the static pressure drop coefficient (C_p) and the comparison between the 2D and 3D cases is even more encouraging as the maximum error is not more than 7% for the hub position, as illustrated in Fig. 3.27. It needs to be underlined herein that the average axial velocity between the upstream and downstream position has been used instead of the conventional definition of the parameter as given in Eq. 3.8.

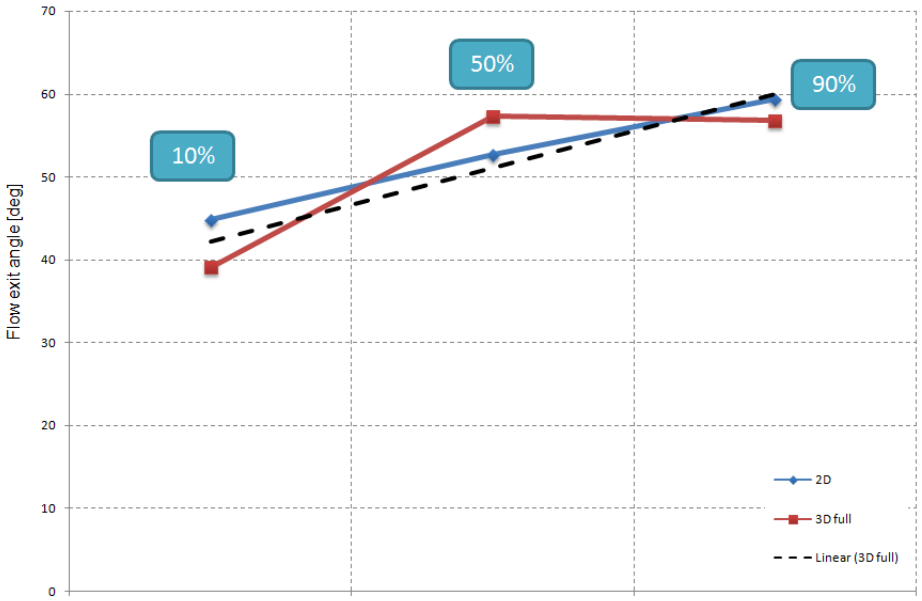

Figure 3.25: Outlet flow angle comparison.

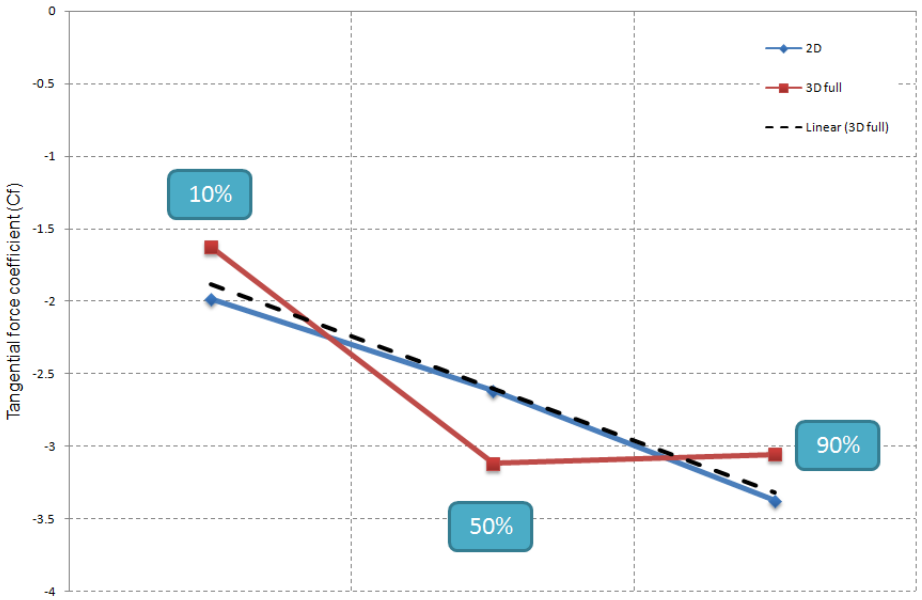

Figure 3.26: Tangential force coefficient comparison as calculated by the CFD predicted outlet flow angle.

$$C_p = \frac{X}{\frac{1}{2}\rho(0.5(c_{x1} + c_{x2}))^2} \tag{3.8}$$

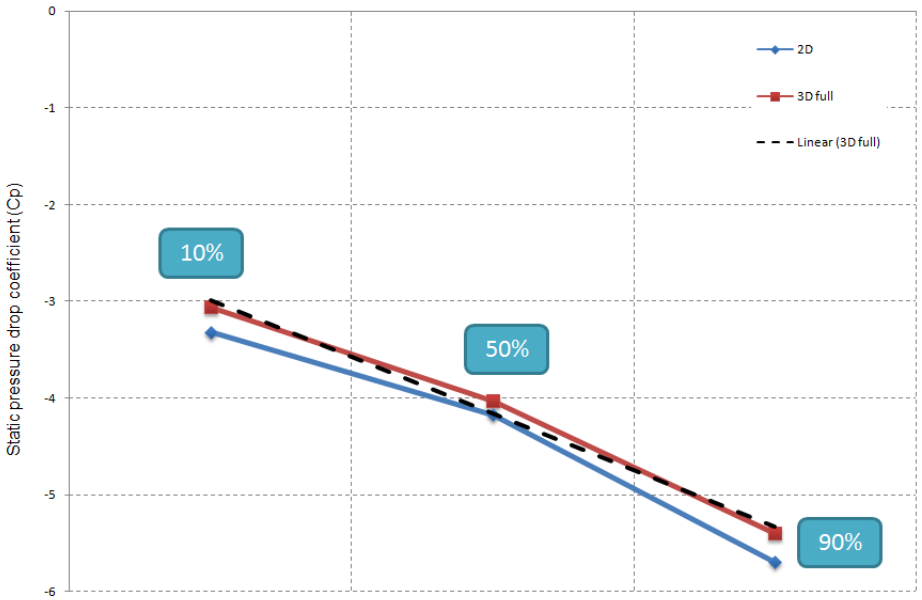

Figure 3.27: Static pressure drop coefficient based on the CFD predicted static pressure drop across the channel.

Having obtained those non-dimensional coefficients the total pressure loss coefficient can be calculated by Eq. 3.3. The calculated values at every position are illustrated in Fig. 3.28.

This comparison reveals the maximum error at the mid-span position in the order of 35% mainly due to the error coming from the tangential force coefficient calculation. The observed error at the two other positions (hub and tip) is not more than 7%.

In addition, if the 3D data are approximated with an R^2 line, it can easily be seen that the latter collapses almost perfectly on top of the 2D simulation results (quasi-3D blade). Therefore, it can safely be concluded that *if a fully 3D blade is approximated by a number of radially stacked 2D blade profiles operating at exactly the same conditions as the correspondent 3D sections (stagger, solidity, incidence),*

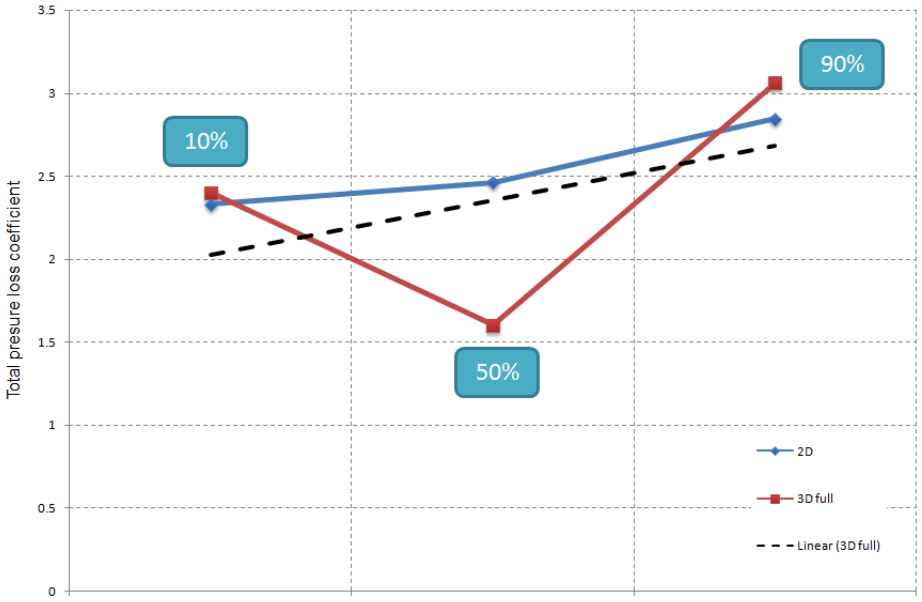

Figure 3.28: Total pressure loss coefficient as calculated by the tangential force and static pressure drop coefficient.

the average performance of the blade can be predicted, without any significant error, by averaging the performance of the 2D blade sections.

The above statement proves that a highly negative incidence pressure loss model generated with the proposed philosophy can be generic enough to predict the off-design performance characteristics of any 3-dimensional blade design.

On the other hand, if the total pressure loss (as directly predicted by the solver - see Fig. 3.29) and flow deviation are used for the derivation of the C_D and C_L coefficients, the plots in Figs. 3.30 and 3.31 are obtained.

A first comparison between Figs. 3.28 and 3.29 reveals that for the 3D blade simulation the solver predicted values are lower than the calculated by the C_p and C_f coefficients by maximum 28%, confirming that the numerical tool tends to under-estimate the total pressure loss [1]. However, there is no significant error between the calculated and predicted values regarding the quasi-3D simulations as apparently the flow structures are simpler.

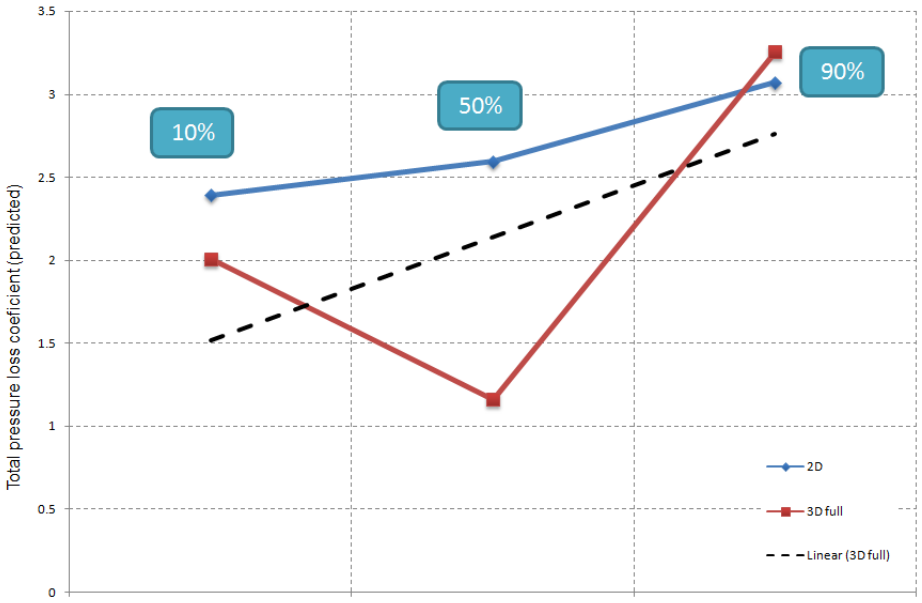

Figure 3.29: Total pressure loss coefficient directly predicted by the CFD solver.

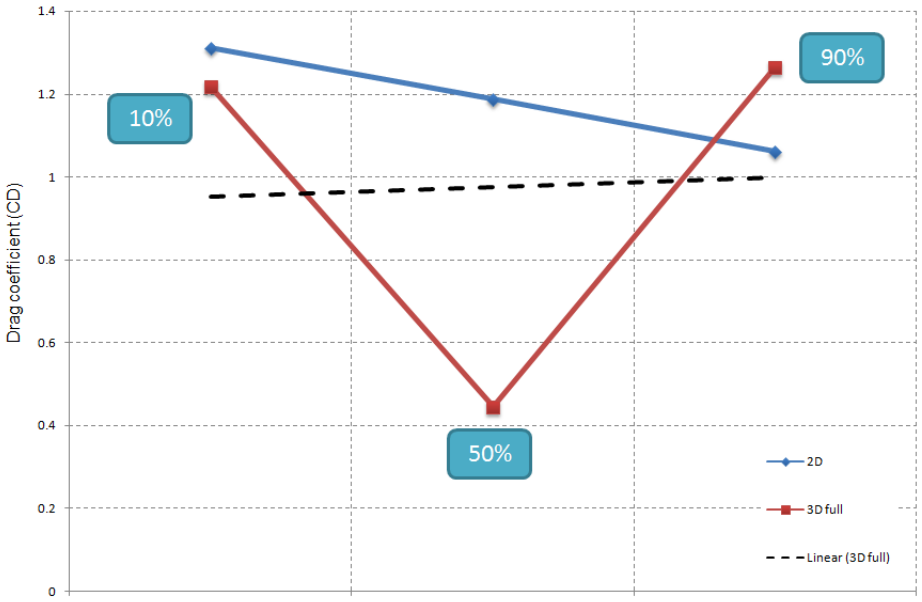

Figure 3.30: Drag coefficient calculated by the CFD predicted total pressure loss.

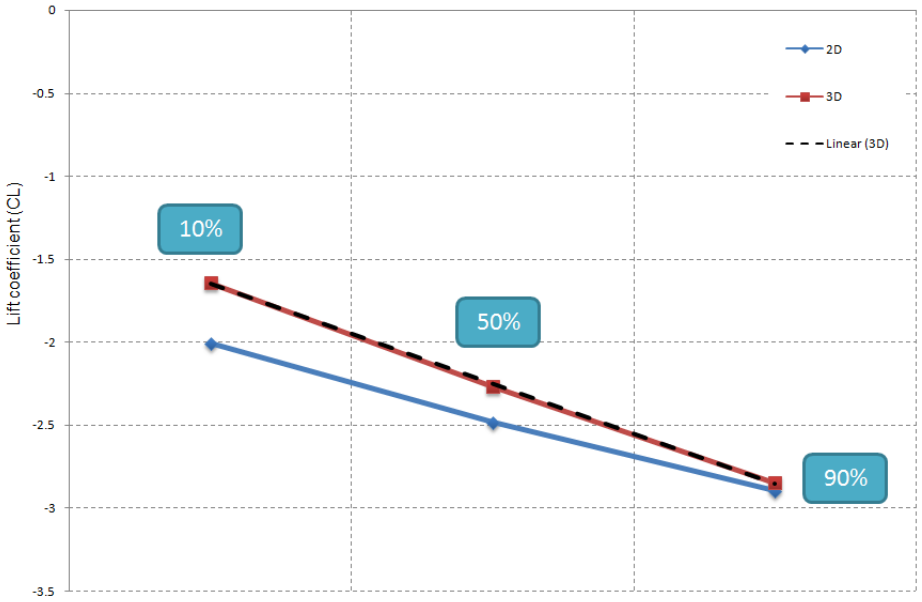

Figure 3.31: Lift coefficient based on outlet flow angle and the CFD predicted total pressure loss.

By looking at Figs. 3.30 and 3.31 and comparing the 3D with the quasi-3D case, it can easily be observed that the big deviation at the predicted total pressure loss coefficient is directly reflected on the drag coefficient. The maximum error appears at the mid-span position and it is of the order of 63%. A significant amount of error (18%) appears also in the lift coefficient calculation.

This comparison reveals that relying on the solver for an accurate total pressure loss prediction is not wise as also the C_D and C_L coefficients deviate significantly between the 3D and the quasi-3D simulations. This happens because, first of all, the solver has poor capability to predict correctly the total pressure loss in such an off-design system and also because the mathematical calculation of C_D and C_L is more complicated and more dependent on the total pressure loss than the simpler definition of C_p and C_f coefficients. Therefore the errors in the prediction of all the properties have a stronger impact on the first set of coefficients.

Consequently the approximation (R^2 line) and averaging of the 3D data is not

as close to the quasi-3D as it was before. Therefore, it can be concluded that in case the predicted total pressure loss coefficient value and the C_D, C_L aerodynamic coefficients are used, the average performance of the 3D blade is significantly less accurately approximated by the quasi-3D case.

The outcome from the above analysis is that a simplified blade element theory looks to be valid also for far off-design cases as long as a suitable definition of the aerodynamic blade coefficients is employed. This finding allows the approximate performance estimation of every 3D blade operating under such off-design conditions using a radially stacked number of 2D profiles. It can be argued here that no certain comparison can be done between the 2D and 3D cases as far as the total pressure loss is concerned due to the radial flows occurring in the 3D case increasing significantly the overall amount of energy loss. However, as can be seen from the above results it does not look that 3D flows have a strong impact in the average loss. 3D flow structures might rearrange radially the flow layers (and this justifies the difference between the 2D and 3D property distribution) but no significant increase in the overall loss occurs as an large percentage of the total pressure loss (and probably of a bigger order of magnitude than the radial losses) comes from the separated regions along the span.

Hence, the performance of the individual 2D profiles can easily be taken from a database as described in section 3.4.4, thus no complicated 3D model generation and simulations are required at a first approximation.

3.4.3 Comments on the locked rotor deviation angle

An important aspect, which disagreement looks to exist on within literature findings on totally separated flows is the flow deviation angle under locked rotor and windmilling conditions. It is reminded that the deviation angle along with the total pressure loss define the overall cascade performance as they are the two unknowns in the system of viscous equations mentioned in section 3.4.2.

Howard in [51] having performed numerical studies on a highly twisted fan blade at locked rotor and windmilling conditions, argues that *"the CFD results confirm that the flow leaves the trailing edge with approximately the blade exit angle"*. However, no numbers of this "approximation" are presented, thus the statement needs to be re-examined.

Additionally, the same statement is made by Cornell in [19] based on very early flat plate cascade studies. Nevertheless, it is worthy to examine closer the accuracy of the above conclusions as the deviation angle value, as will be shown, has a very strong impact on the overall cascade performance for high values of the total pressure loss coefficient (which is the case for the examined case).

The total pressure loss coefficient is plotted for a typical cascade geometry in Fig. 3.32, for a range of negative incidence angles as derived by the previously described CFD studies. On the same plot, the drag coefficient C_D is also shown for three different values of flow exit angle (37.5 -b2-, 43.5 and 50 deg. respectively). It is reminded that the drag coefficient is dependent upon the flow exit angle, as suggested by Eq. 3.7. As shown, the effect of the flow exit angle on the drag coefficient is not very large for high values of total pressure loss coefficient.

In addition, the blade lift coefficient is plotted in Fig. 3.33 for different flow exit angles, as calculated by Eq. 3.6 taking into account the drag term (which is usually neglected at low incidence studies).

As can be seen from Fig. 3.33, for the same change in flow exit angle the change in the lift coefficient increases as we go to higher negative incidences. The latter implies that at high loss conditions the flow exit angle has more impact on the blade performance for negative incidences, therefore even relatively low values of flow deviation can by no means be neglected.

In Figs. 3.34 and 3.35, the pitchwise distribution of the flow deviation angle is illustrated for design conditions as well as at -58 deg incidence (mid-span incidence angle for the HPC1R 3-dimensional blade under examination in annular configura-

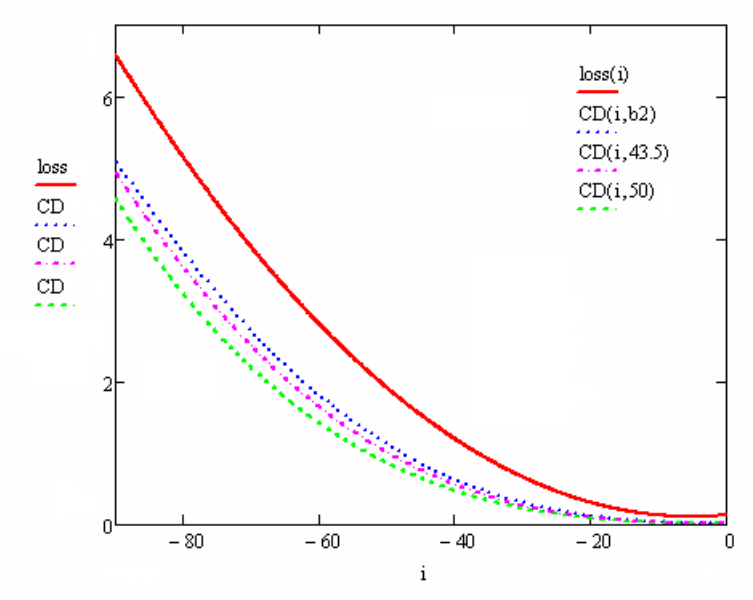

Figure 3.32: Total pressure loss and drag coefficient for different values of exit flow angle as a function of incidence.

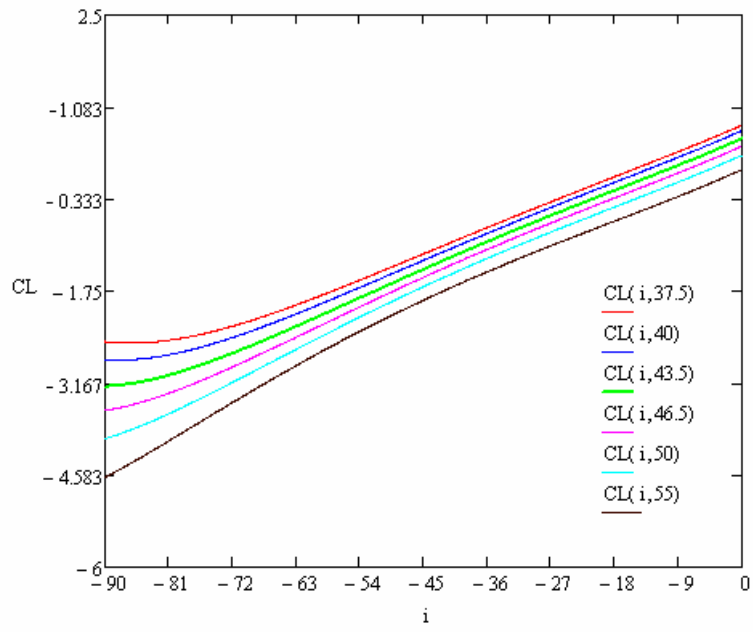

Figure 3.33: Lift coefficient for different values of exit flow angle as a function of incidence.

tion) at the trailing edge and 1 chord downstream of the cascade.

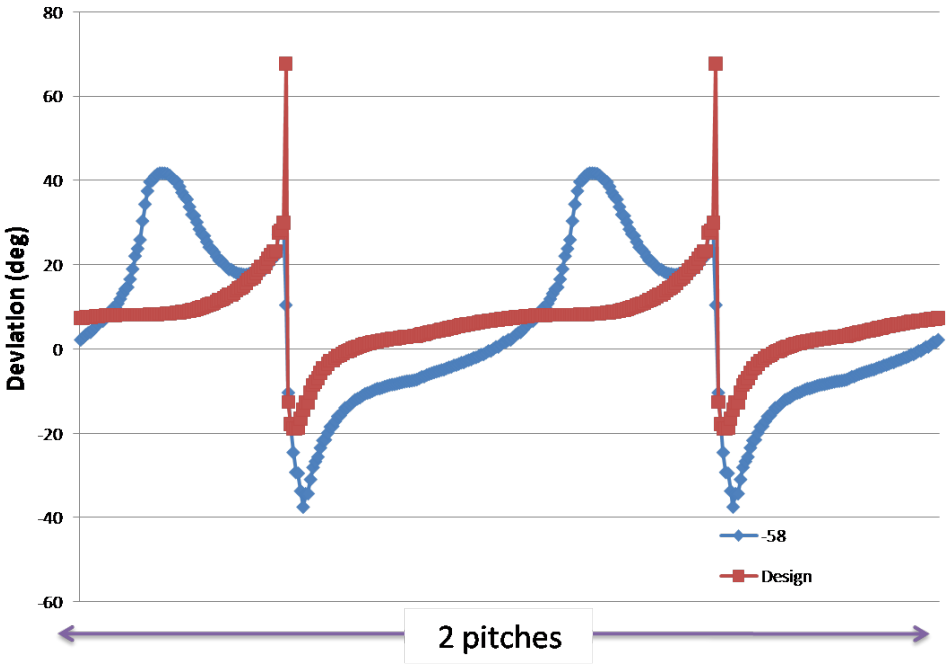

Figure 3.34: Deviation angle for design point and -58 deg incidence at the mid-span trailing edge plane.

As can be seen, especially from the second plot which is more indicative of the blade performance as it accounts for mixing losses, flow deviation angle has a small but not negligible value at design conditions while it is even higher at off-design in the order of 10 deg. (see also Fig. 3.17) and therefore the flow exit angle (blade exit angle increased by the deviation angle) becomes approximately 50 deg. for this case. As shown above this affects significantly the blade performance, therefore it is obviously not recommended to ignore it for theoretical off-design cascade calculations. The overall deviation results for the entire range of simulated conditions reflect also the above statements and are presented in the following section.

3.4.4 Loss model composition

As mentioned in an earlier paragraph pressure loss models are generally used for the prediction of the blade performance in terms of pressure loss and flow deviation for a specified range of operating conditions. Several examples can be found within

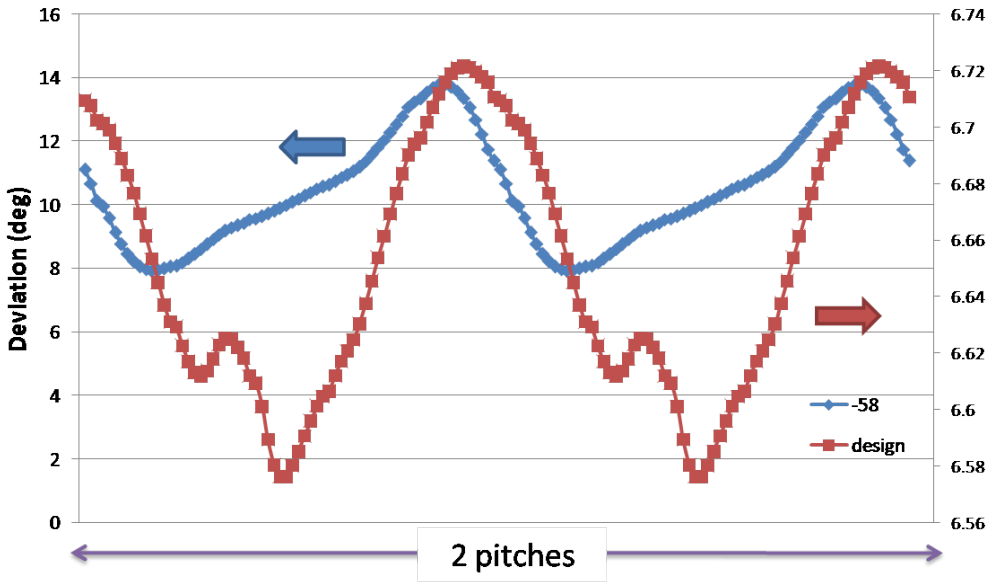

Figure 3.35: Deviation angle for design point and -58 deg incidence at the mid-span 1 chord downstream.

the literature and can be used as a guideline also for off-design models generation such as those described in the current thesis [106]. Having proved that a simplified blade element concept is also valid for sub-idle off-design conditions, a generic model to describe the performance of a blade operating under such conditions must be generated.

A parametric investigation in terms of incidence, solidity and blade stagger angle has been conducted at a first stage using the *mid-span profile* of the given blade. Blade camber has not been taken into account as its impact plays a secondary role in the overall performance of the cascade and has little effect on the losses as mentioned in [51]. More specifically, it has been found and also confirmed by the current study, that low cambered compressor blades behave like flat plates at such high incidences. This is quite reasonable because the low blade camber does not drive the flow any more as it is totally separated from the profile without any position of reattachment, as can be seen from Fig. 3.36. This cannot be argued for lower incidences where the blade camber needs to be taken into account as a parameter which affects the cascade performance. The range the parameters of interest have been studied within

are illustrated in Fig. 3.37.

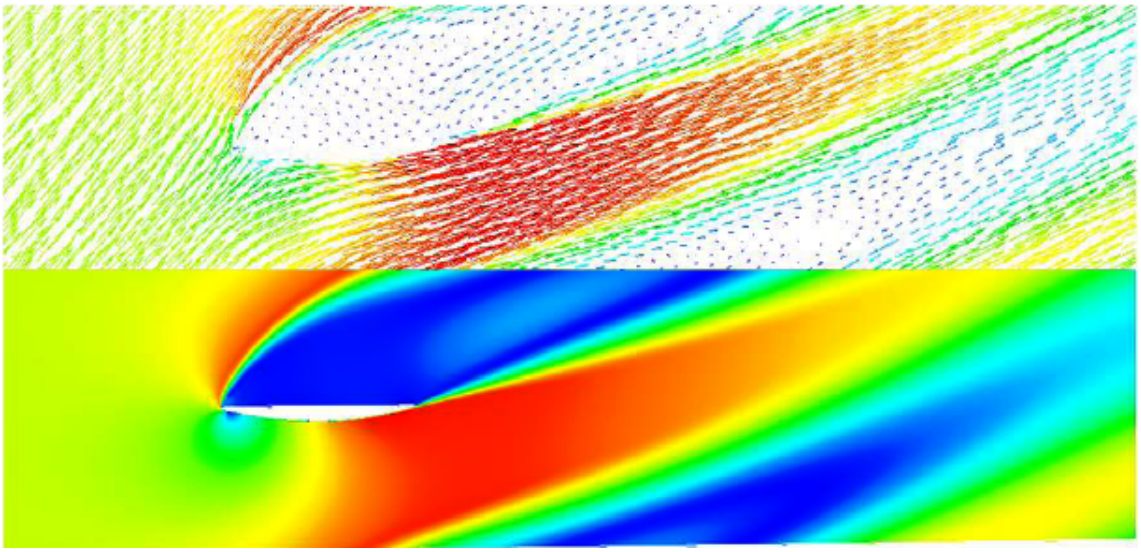

Figure 3.36: Mid-span Blade Profle at α = -60 incidence and zero blade staggering [102].

The non-dimensional coefficients that describe the blade performance are presented in Figs. 3.38 to 3.40. Having this information, the total pressure loss as well as the flow exit angle can also be calculated by the correlations given earlier in this chapter.

As can be seen from the above plots there is still a number of testcases to be run in order for the specified parameter range to be fully covered. The existing data however is generic enough and can readily be used for far off-design blade performance predictions.

3.5 General comments - concluding remarks

At this stage, a number of comments on the above described methodology can be made:

- First of all, the fact that for all the numerical studies a **commercial CFD solver** has been employed, limits significantly the depth in which the investigation can be done, in the sense that unavoidably such a tool is treated as a

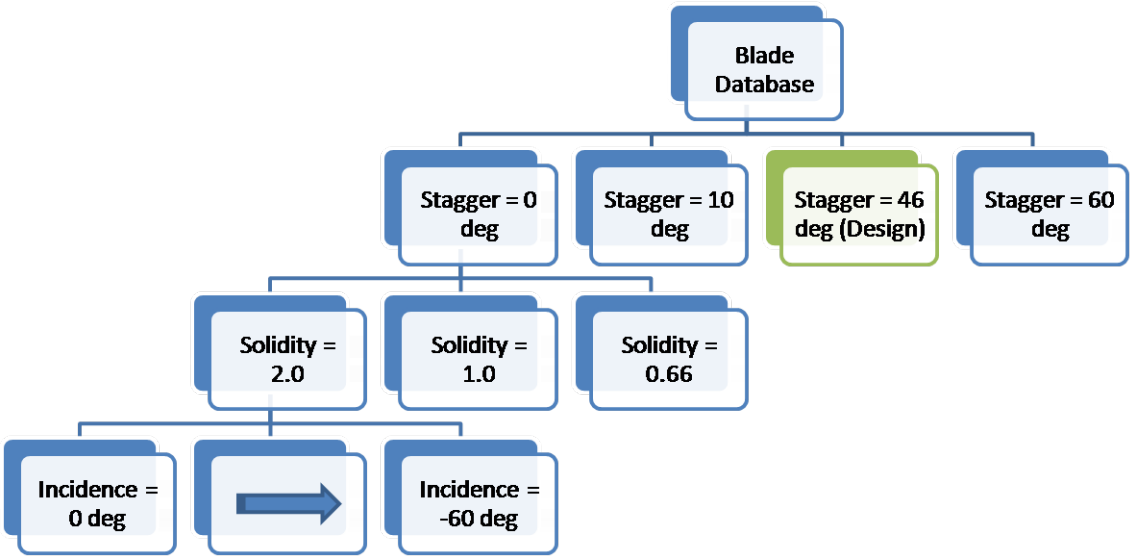

Figure 3.37: Range of parameters of interest for off-design generic pressure loss generation.

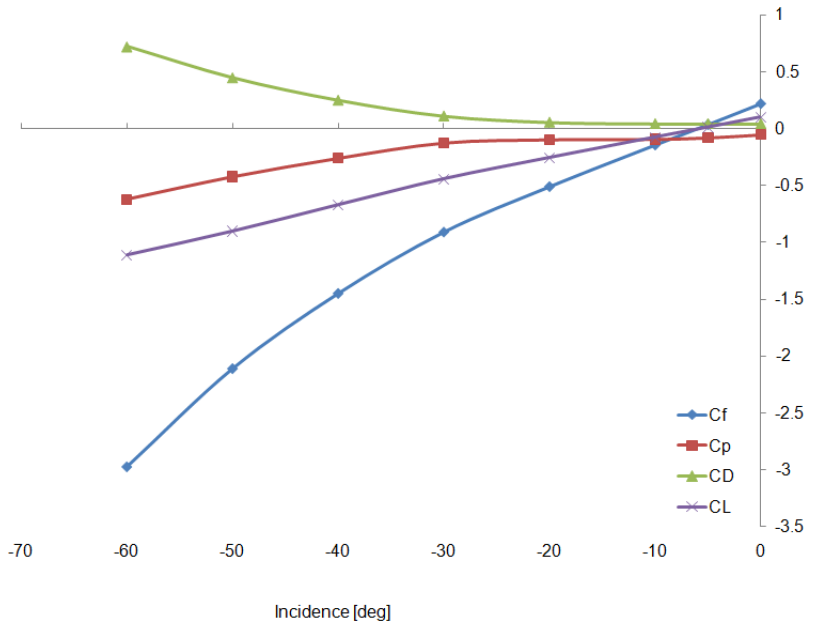

Figure 3.38: Aerodynamic blade coefficients for zero staggered blade at solidity = 2 and negative incidence angles.

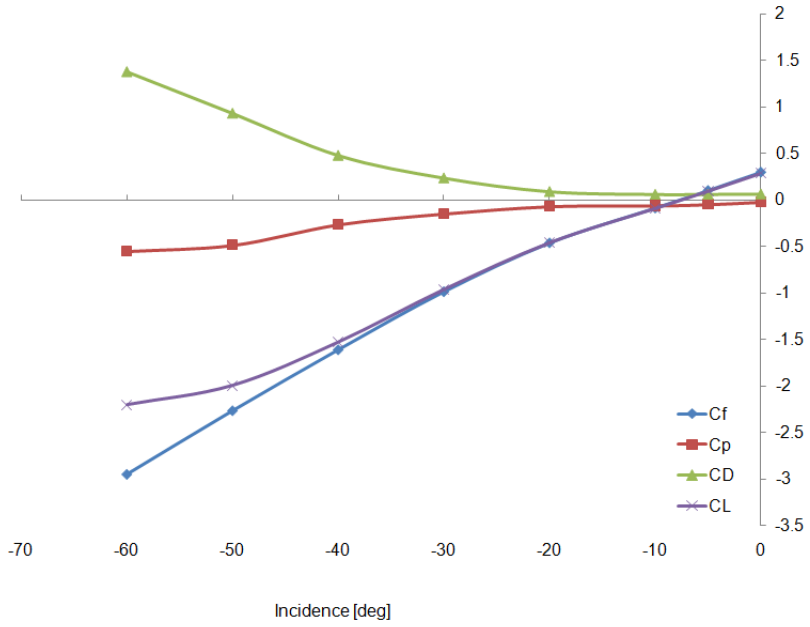

Figure 3.39: Aerodynamic blade coefficients for zero staggered blade at solidity = 1 and negative incidence angles.

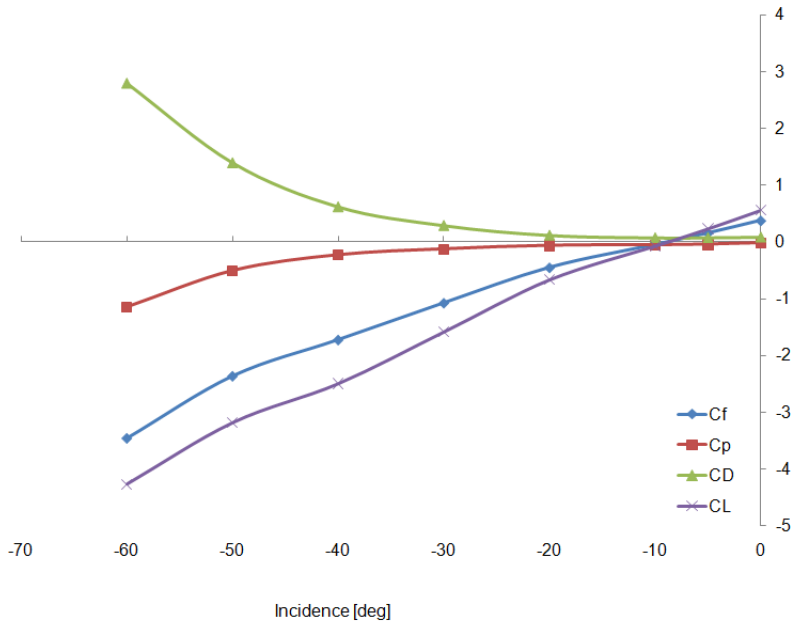

Figure 3.40: Aerodynamic blade coefficients for zero staggered blade at solidity = 0.66 and negative incidence angles.

black-box. According to the author's opinion an open code of known capability would have improved the quality of the final results.

- In such a case, secondary effects, as the Reynolds number effects, should be investigated since even the experimental testing has shown that the performance is influenced by them.

- In addition, the significance of the 3-dimensional effects that are lost or neglected within the transition from the 3D to the 2D flow, needs to be assessed.

- This study pushes forward the previously developed methodology by Howard and as recommended by him a generic pressure loss model for the specific conditions has been developed. Nevertheless this does not mean that the current analysis has no drawbacks. A more sophisticated pressure loss model could be generated based on the above described ideas by increasing also the fidelity of the numerical studies with top quality CFD simulations.

- The findings of this investigation will significantly contribute in the generation of the compressor characteristics as demonstrated in Chapter 4, while the locked rotor results can easily be used also for the modelling of the fan outlet guide vanes (OGV's) at windmilling conditions which produce almost all the engine drag and can easily be approximated as locked rotors. Finally, methods that rely on pressure loss modelling, such as streamline curvature solvers, can be enhanced as well.

Chapter 4

Compressor sub-idle characteristic generation

4.1 Introduction

All the component related research and its findings must be captured in the component characteristic, as mentioned in [117], in order to allow for a whole engine performance prediction of higher fidelity.

Usually, component characteristics are derived by rig tests for the expected range of operation. In standard engine design however, there are no component tests at low speeds and especially within the sub-idle regime as their cost in time and other resources is significantly high. Hence, for the relight modelling and performance predictions to be carried out, the original above-idle component characteristics need to be extrapolated towards the sub-idle area as mentioned in an earlier chapter.

Up to the moment, only mathematical techniques with poor physical background have been used for such map generation, hence, not surprisingly, there is no significant predictive capability at sub-idle performance simulations. The first step to improve this situation is the introduction of the locked rotor studies, which allow the transition from map extrapolation to interpolation as the very first rotational

speed line of the characteristic can be better predicted.

In this chapter the map generation techniques described in [51] will be further developed by enhancing their physical background mainly taking advantage of the locked rotor studies. More emphasis is given into compressor characteristics as this is the most challenging component with respect to its sub-idle performance. Work on turbines, previously carried out by Howard [51], showed that the applied extrapolation techniques are sufficient to generate accurate characteristics. Finally, the work done on combustor characteristics extrapolation proved that it is not sufficient to capture combustion related phenomena at low speeds, hence more component specific work needs to be done to enhance the physics of its operation before any attempt to generate a more accurate map for it.

Before developing the methodology for the physically enhanced compressor characteristic generation, aspects regarding alternative map representation approaches will be mentioned. This part of the work will be developed with respect to:

- Alternative map representation techniques.
- Map generation methodologies and
- Description of an automatic map generation tool using first principles for producing compressor characteristics of higher fidelity.

4.2 Map representation approaches at low speeds

In this section the usefulness and the benefits that can be taken out of alternative map representation approaches will be explained.

4.2.1 Euler's equation at low speeds

Before analyzing the different approaches that can be used for map representation at low speeds, it is worthy to recall a few fundamental formulations about thermo-

dynamics of turbomachinery and build up the main concepts required for the more detailed studies of the following sections.

As explained by Dixon in [32], the work done on the fluid per unit mass or the specific work is defined as:

$$\Delta H = \frac{\tau\Omega}{\dot{m}} = U_2 c_{\theta 2} - U_1 c_{\theta 1} \tag{4.1}$$

as a function of the moments of all external forces acting on the system, the shaft rotational speed and the change in swirl velocity between the inlet and the outlet of the control volume. This equation is widely known as the *Euler's equation* and it is derived simply by the law of moment of momentum.

The torque on the shaft can easily be derived by rearranging the terms as a function of the change in the internal energy of the fluid and is defined as:

$$\tau = F \times R \tag{4.2}$$

In addition, the isentropic efficiency of a thermodynamic compression process is the ratio of the isentropic specific work upon the effective specific work required to bring the gas from its initial state to the final.

$$\eta_{is} = \frac{\Delta H_{is}}{\Delta H_{effective}} \tag{4.3}$$

or

$$\eta_{is} = \frac{\left(\frac{P_{out}}{P_{in}}\right)^{\left(\frac{\gamma-1}{\gamma}\right)} - 1}{\frac{T_{out}}{T_{in}} - 1} \tag{4.4}$$

An engine operating under sub-idle conditions and especially during groundstarts and windmill relights is forced to pass through points where the mass flow, rotational speed and pressure ratio are significantly low. Especially the latter very often obtains values less than unity, which means that the compressor is falling into an undesired

condition operating as *stirrer* or even as a *turbine* depending on the sign of the specific work.

Walsh and Fletcher have described schematically the compressor operation at this regime.

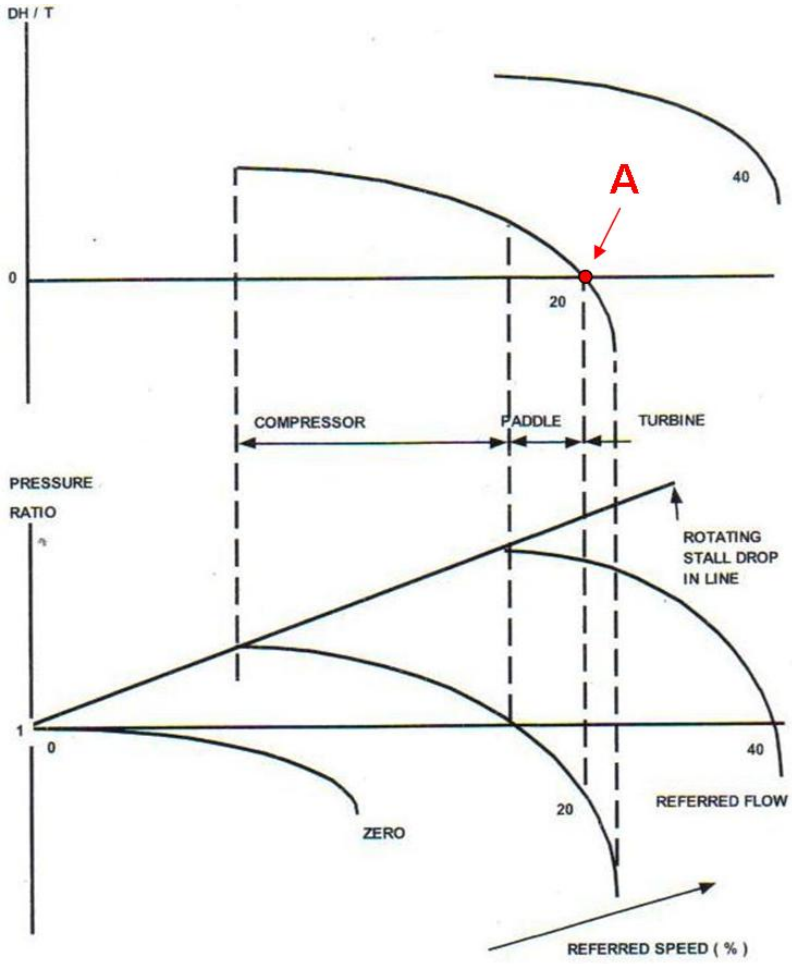

Figure 4.1: Compressor operating modes for PR $<$ 1 indicating zero specific work point [117].

As can be easily seen from the above, there is no value for efficiency at zero engine rotational speed (no enthalpy rise at all), when at the same time the efficiency definition is not continuous at the point of zero specific work (point A on Fig 4.1 and see also Fig. 4.2).

A more clear explanation of the different operating modes that a compressor can work within is given in the following schematic (Fig. 4.2). As it can be seen, for

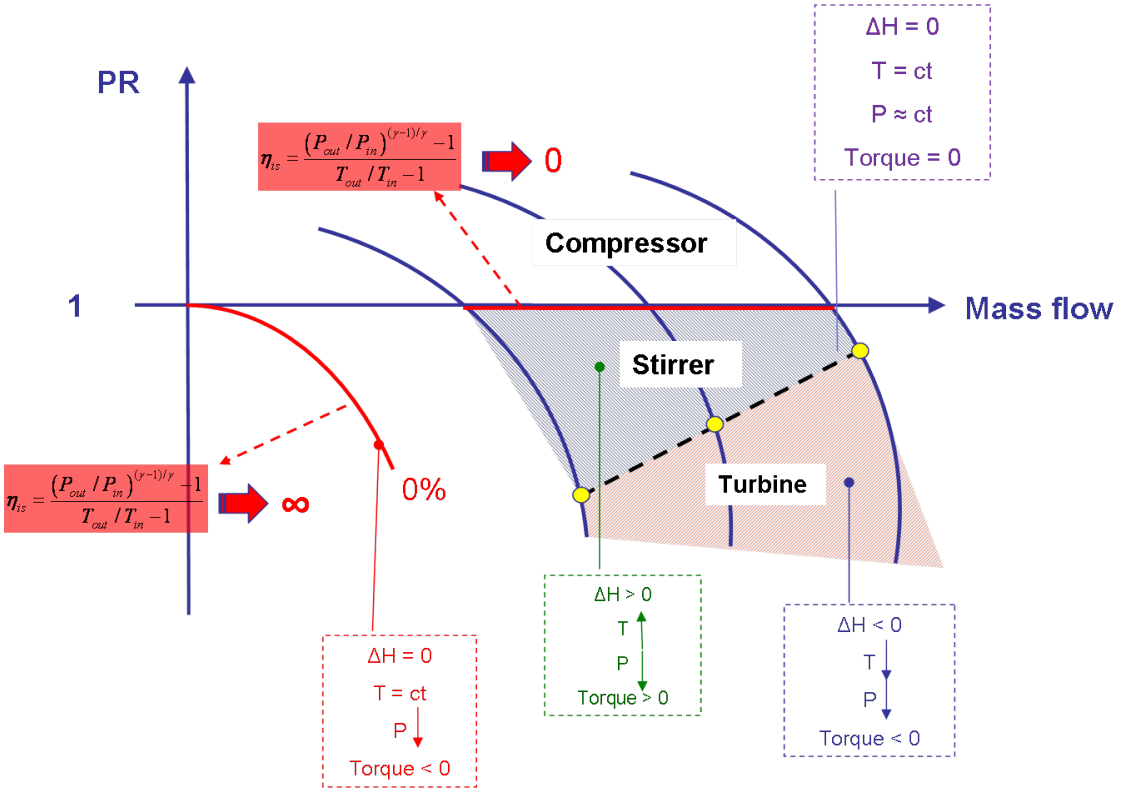

Figure 4.2: Compressor low speed operating modes with definition of the corresponding thermodynamic properties.

a locked rotor compressor there is obviously no enthalpy rise in the rotor thus the total temperature remains constant. However, the flow experiences a significantly increased amount of pressure loss as, apart from the stators, that operate at highly negative incidence, the rotor also imposes a similar amount of pressure loss since it operates exactly as a stator. Therefore -see the efficiency definition- the efficiency obtains an infinite value allowing by no means its use for performance calculations and especially engine groundstarts (it is reminded that groundstarting simulation requires the zero speed curve). Nevertheless, the zero speed line torque has a finite value as there are still aerodynamic forces exerted by the air onto the blades. The torque definition is convenient, consequently, for an alternative definition of the locked rotor compressor operation.

Another drawback of the efficiency definition within the low speed region is the locus of the points where its value is zero. As shown in Fig. 4.2 those points are all

the points of PR = 1, implying that the only work given by the rotor is consumed to overcome the pressure losses through the engine.

Finally, regarding the two other compressor operating regions, in the stirrer case, there is some enthalpy (thus total temperature) rise by the rotor however the extremely off-design incidences on the blades do not allow any part of this work to be transformed into total pressure rise. In that case this work is used to stir the air into the engine reducing its total pressure and forcing the efficiency parameter to obtain negative values.

The opposite happens when the compressor operates as a turbine. Within this region the air produces work on the rotor experiencing a total enthalpy (thus temperature) and total pressure drop. In the two last cases, however, there is always a finite value for the torque parameter positive or negative correspondingly.

Regarding the interface between the two previously mentioned operating regions, it is unavoidably a locus of points where the transition between the two regimes takes place. Therefore, on that locus there is no total enthalpy (thus total temperature) rise and since the rotational speed is not zero, the torque necessarily obtains a zero value, while the total pressure remains approximately constant in the rotor and all the pressure loss that the flow experiences is due to the stators of the OGV's.

Consequently, as shown above, if the *torque* is known, the specific work (total enthalpy rise or drop) can easily be calculated in the entire operating range including the regions where efficiency is discontinuous. This is because the discontinuities in efficiency are expressed as sign changes in torque, while at zero rotational speed, even though there is no rotation of the shaft, thus no efficiency value, the torque still has a definite non zero value as there are still aerodynamic forces on the blade, no matter whether the shaft rotates or not. The torque can generically be calculated by cascade analysis as shown in Chapter 3.

Therefore, there is a need to modify the map parameters for the sub-idle performance simulations and replace the definition of isentropic efficiency with the

definition of torque to enhance the low speed performance simulation.

4.2.2 The use of torque for low speed map representation

As mentioned by Kurzke in [67] the representation used for the map is of secondary importance as long as the physical content of the data remains the same. Kurzke was also the first to underline that the definition of isentropic efficiency is unsuitable for sub-idle engine studies, as it becomes zero at zero rotational speed (hence no groundstart simulation is possible) and also it presents a discontinuity for the windmill operating points of the compressor. The analysis which can also be found in [58, 59, 60, 51] will not be reproduced hereafter. Therefore an alternative property must be found to replace the isentropic efficiency contours for the sub-idle regime of the map.

The property, as mentioned in the previous section, which allows no discontinuities in the representation of component performance is the *torque* applied on the engine shaft. Riegler in [97] and Jones in [58] suggest a couple of torque definitions but neither an application of their expressions has been attempted so far on engine simulations nor even a map generation using this approach.

Only Howard [51] has produced torque characteristics based on CFD studies and cascade analytical expressions without attempting any engine simulation using them though. In addition, he further analysed the benefits on the performance modelling if torque is utilised as far as the multi-match points at power off-take characteristics are concerned, based on Braig [12] and Rodgers [99].

4.3 Map generation techniques

The methodologies developed for low-speed compressor map generation are presented in this section.

4.3.1 Literature review

The majority of literature pieces related to map generation methodologies at sub-idle, focus on the *extrapolation* of the above idle map towards the sub-idle region till a lowest rotational speed other than the zero one.

As it can easily be realised they are all mathematical techniques of limited predictive capability, as no deep knowledge of the low speed phenomena was available. Therefore, only an approximation of the map can be done. Only a reference of the published methods will be given hereafter as a very detailed description of each one can be found in [58, 59, 60, 51]. The very first method related to map extrapolation was published by Agrawal and Yunis [4] and it was the basis for all the studies followed by Gaudet [40] or Choi [18], to mention the most important ones.

As explained in an earlier section, switching from extrapolation to interpolation, enhancing at the same time the physical background of those techniques, can be achieved using the zero-speed studies to define the very first line of the map in order to bring the methods closer to the real low speed phenomena.

This philosophy was suggested and partially implemented by Howard [51], who proposed a methodology for zero-speed generation and used it to generate more accurate compressor characteristics. His studies employed the linearised parameters (ϕ, ψ, ψ_{is}) to avoid the discontinuity in efficiency and conduct the extrapolation. However, they were engine specific and no generic method was proposed for torque map generation. As shown finally, the maps generated with this approach cannot be used for performance predictions without any adjustment using rig experimental data when available, or adaptive running of engine models in order to find the best map settings to match the transient running lines of the simulated engines.

4.3.2 Low speed map generation

Within this work a map generation platform has been created, incorporating a modified Howard methodology as well as a torque based map generation technique.

This work was mainly carried out by Ioanna Aslanidou a Thermal Power MSc student supervised by Dr. V. Pachidis and the author of this thesis [7, 8].

The objective was to create a robust, interactive and user friendly map generator platform having available a range of different techniques and user defined options regarding the map parameterisation. In this way, further development of the tool is allowed whilst compressor maps can be obtained without any modification in the main methodology avoiding formulation or other type of errors. In general, it was decided that such an approach enhances the performance modelling in the sense that it accelerates and increases the quality of the map generation pre-processing phase.

4.3.2.1 Fundamentals of map generation methodology

The main philosophy of map generation is illustrated in Fig. 4.3. Once the map is in the desired format and the beta lines are used to define the map points, the values of the three parameters used are a function of beta and quasi-dimensionless speed (referred to as "*speed*" from now on). In order to expand the map, both the speed and the beta lines have to be extrapolated for all parameters.

The first step is the extrapolation of speed lines. In order to do that, a final speed curve has to be defined. The minimum and maximum beta points are guessed and the final speed curve is calculated based on the lowest speed line of the above idle region. Once this curve is known, the beta lines can be expanded, matching each point of the lowest speed curve to its corresponding one of the minimum speed curve. The speed curves in between are then calculated and the speed extrapolation is completed.

The equations used for speed and beta line extrapolation is a user defined option and can be either linear or polynomial. The order of the equation affects the resulting compressor map, and its influence is investigated in a later chapter.

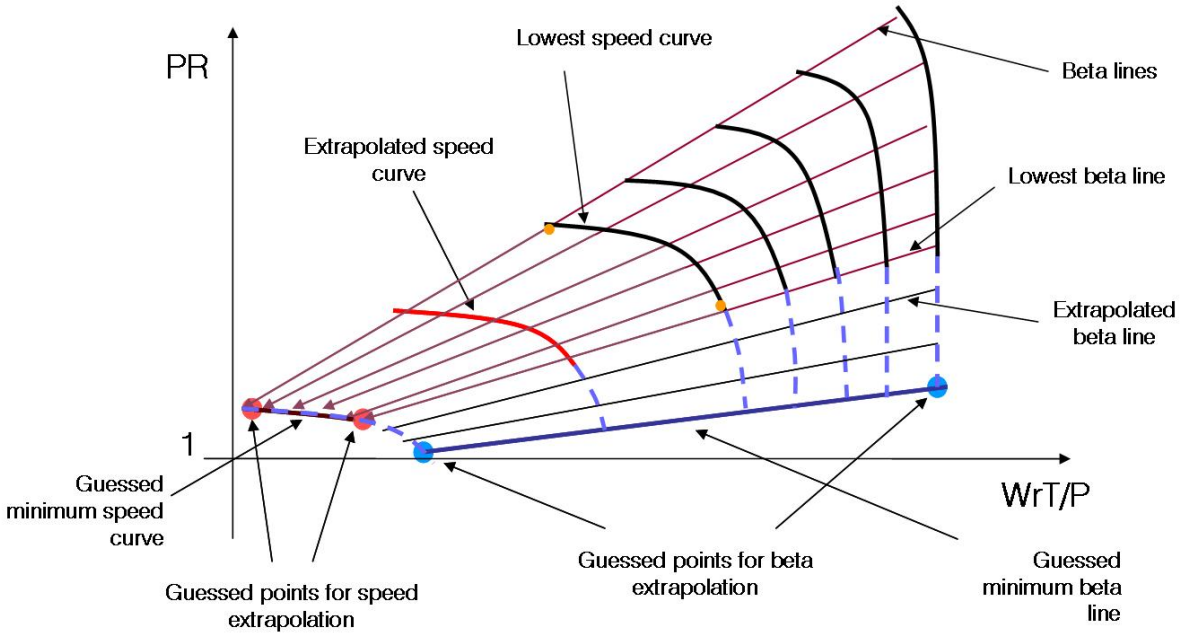

Figure 4.3: Overview of the map generation methodology on a conventional map.

4.3.2.2 Map generation using linearised parameters

As indicated in [51], ϕ, ψ and ψ_{is} are used for map generation (either extrapolation or interpolation) in order for the discontinuities in efficiency to be avoided. This process is carried out three times, for each one of the compressor performance parameters before switching back to the conventional map format at the end. The format of the three matrices is illustrated in Fig. 4.4.

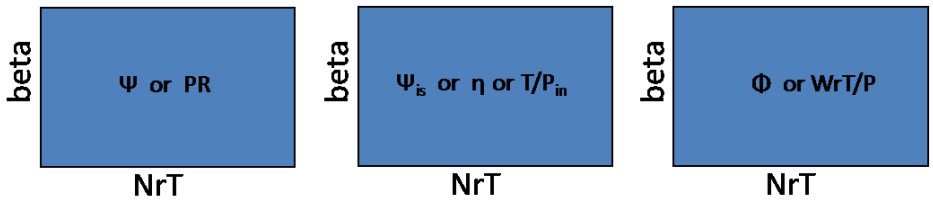

Figure 4.4: Overview of the map generation methodology on a conventional map

The definition of those parameters is reminded:

$$\phi = \frac{V_x}{U} \propto \frac{W\sqrt{T}/P}{N/\sqrt{T}} \tag{4.5}$$

$$\psi = \frac{\Delta H}{U^2} \propto \frac{\Delta H/T}{(N/\sqrt{T})^2} \tag{4.6}$$

$$\psi_{is} = \eta_{is}\frac{\Delta H}{U^2} \propto \eta_{is}\frac{\Delta H/T}{(N/\sqrt{T})^2} \tag{4.7}$$

From the definition of ϕ, it can be seen that when the rotational speed approaches zero, the values of the parameter are very high. This is because there is still a significant amount of mass flow going through the engine and therefore the numerator is much higher than the denominator. This means that the extrapolation of speed lines using the flow coefficient is not possible, because this increase in the values cannot be predicted in a reliable way. This problem is solved with the use of quasi-dimensionless mass flow parameter $W\sqrt{T}/P$ as shown in the left part of Fig. 4.5.

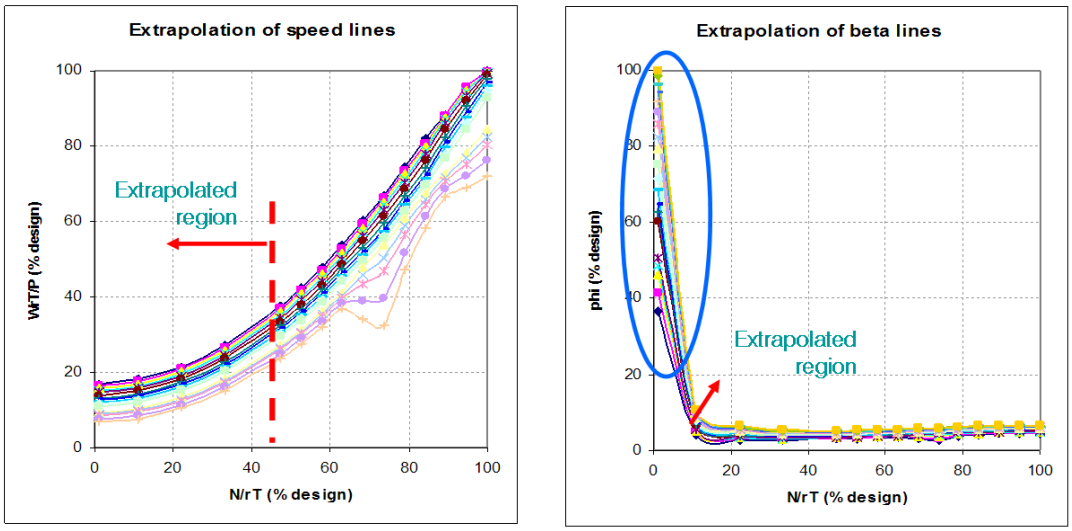

Figure 4.5: Low speed ϕ extrapolation [51].

In the cases of work and pressure coefficient, this problem is not encountered, because the increase in enthalpy, which is the numerator, is also very low and counterbalances the squared rotational speed.

4.3.2.3 Map generation using torque

Using Euler's equation and the linearised parameters as defined in the previous section the quasi-dimensional torque group can be derived:

$$\frac{\tau}{P_{in}} = \phi \cdot \psi \cdot (\frac{N}{\sqrt{T}})^2 \cdot \frac{60}{2\pi} \tag{4.8}$$

When using the torque parameter group for extrapolation, problems as the one described previously are not encountered, because all the variables used are continuous in the entire compressor map. The pressure ratio is always positive, as is the mass flow. Torque has negative values at zero rotational speed and at the turbine mode of the compressor, but does not have any discontinuities. Therefore, with the use of these parameters, the extrapolation can be carried out without any obstructions and it is more consistent. In addition, as the parameters used are more connected with the physical phenomena in the compressor, since they describe torque and pressure losses on the blades, the methodology becomes more robust. The guess of the lowest speed values and of the lowest beta line points in terms of mass flow, pressure ratio and torque adds to that as well.

4.3.2.4 Definition of lowest speed line

At a first approximation, the requirement for a lowest rotational speed line is fulfilled by guessing it. This procedure is illustrated in Fig. 4.6

The difference between the values of the variable at the minimum and maximum beta points is calculated for both the lowest speed curve, ΔY_{max}, and the guessed end points of the minimum beta line, ΔY_{min}. The ratio of the two and the difference between the points at adjacent beta lines, Δi_{max} is then used to calculate each Δi_{min} for the variable at the minimum speed line according to the similarity law [4]:

$$\Delta i_{min} = \Delta i_{max} \cdot \frac{\Delta Y_{min}}{\Delta Y_{max}} \tag{4.9}$$

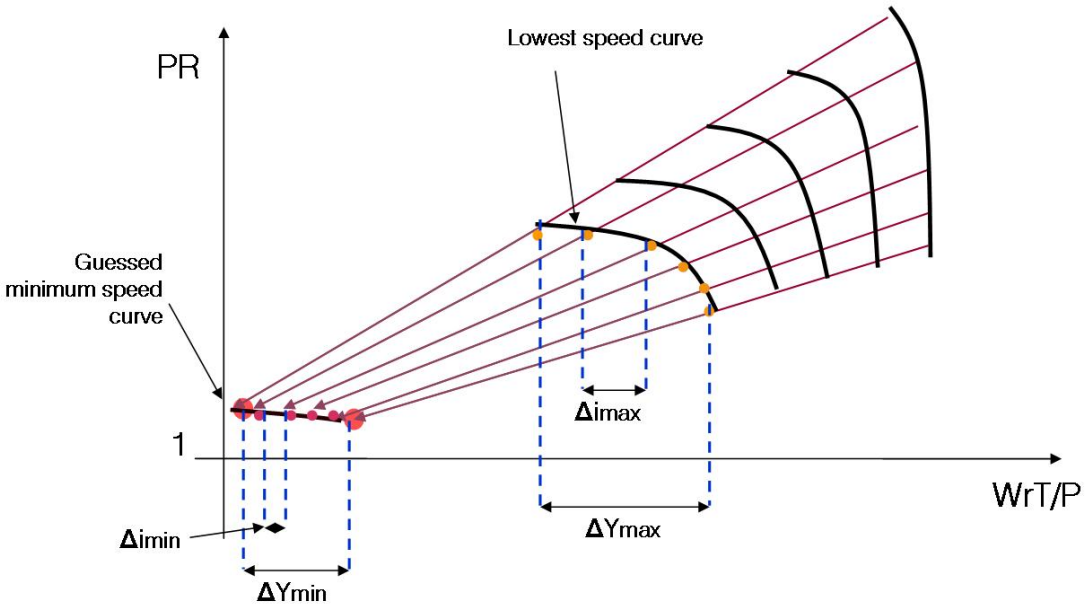

Figure 4.6: Lowest speed line generation.

This process is repeated for all three variables in order to calculate the entire line for each variable from the guessed points.

When calculating the minimum speed line using guessed values for the parameters, there are two main assumptions made. The first is that the minimum speed line is similar in shape to the above idle one and also that the guessed values of the parameters represent with an acceptable accuracy the performance of the compressor at that rotational speed. The former does not influence the calculated line that much, because it implies that the distance between the points on the curve is proportional to that of the lowest speed line, with a proportionality factor that is defined by the guessed end points of the curve. The second assumption, however, is the one that mostly influences the resulting map. If there is no data about the compressor behaviour at that speed it is arbitrary to assume that its performance parameters have these specific values and the resulting compressor map is not reliable.

The lowest speed line can also be calculated with significantly higher accuracy from locked rotor studies, enabling the generation of the map with a pure interpolation process, which is analyzed in the following section.

4.3.2.5 Whole compressor zero speed line calculation and map interpolation

The compressor speed lines that are calculated using the procedure described above are not accurate enough and have to be compared and aligned with data from engine tests. This is due to the fact that extrapolation itself is a purely mathematical process, therefore the results may have no physical meaning. This is exactly what creates the need for a better definition of the extreme sub-idle region of the map. In order to do that, the zero speed line, at locked rotor conditions has to be defined. The zero-speed line calculation is based on the locked rotor studies described in Chapter 3 and will be analysed in a following section of the current chapter as well.

Once the zero speed curve is known, the map can be produced using an interpolation technique, thus providing a much better definition of the low speed curves.

In Chapter 3 a generic technique for the generation of the zero-speed line of a single blade row has been described. In order for the overall compressor characteristic at locked rotor condition to be generated, a stage stacking method has been applied as firstly introduced in [51]. The applied methodology is developed originally in [77].

The calculation of the zero speed curve of the compressor is based on two main assumptions. The first is that the total temperature of the gas remains unchanged. This is because there is no work and therefore no increase in the enthalpy of the gas, as the rotors are locked. The second is that the density remains constant throughout the compressor. This is not entirely accurate, but the change in pressure and temperature of the gas stream is too small to cause significant changes in the density.

Flow angle definition within the stages. When air flows through a compressor cascade, it does not follow exactly the path defined by the blades, but it deviates from the blade exit angle. This deviation is almost always in a direction that reduces

the deflection of the fluid, as the deflection of the flow causes an increase in pressure and the flow always wants to avoid that.

Deviation models for normal flow conditions can be found in [52] based on experimental cascade testing. *Carter's rule* has been proved the most popular and accurate formulation to predict the deviation angle for a wide range of operating conditions based only on the blade geometry and not on the flow conditions. An insight on deviation prediction methods is given by Cumpsty in [21].

This model can be applied for a preliminary modelling at locked rotor conditions while the generic deviation loss model as described in Chapter 3 can increase the accuracy of the results.

Flow parameters. The conditions at the inlet to the compressor are given in the form of Mach number, total pressure and total temperature. From this data, the static pressure and temperature can be calculated, as well as the velocity at the inlet. Based on the assumption of constant density and constant mass flow, the axial velocities throughout the compressor can be calculated from the continuity equation, taking into account the change in area. Once the axial velocities have been calculated, the tangential and the circumferential velocities can also be calculated from the known flow angles.

Inlet flow range. The procedure described in the previous section has to be repeated for a range of Mach numbers to calculate the entire zero speed curve of the compressor. The first point of the zero speed curve is at Mach=0. The last point can be defined as the point at which the compressor begins to choke. The Mach number of that point can be calculated as follows.

The area of the compressor is decreasing in order to compensate for the increase in density under normal operating conditions and maintain constant mass flow, depending on the design axial velocity. Therefore the compressor will choke at the last stator if the inlet Mach number reaches its critical value. The value of the outlet

flow function, Q, for Mach=1 is obtained from Q curves. This value can be used to calculate the inlet quasi-dimensionless mass flow from equation 4.10

$$\frac{W\sqrt{T_1}}{P_1} = \frac{W\sqrt{T_2}}{A_{2,eff}P_2} \cdot \sqrt{\frac{T_1}{T_2}} \cdot \frac{P_2}{P_1} \cdot A_{2,eff} = Q_2 \cdot \frac{PR}{TR} \cdot A_{2,eff} \tag{4.10}$$

$A_{2,eff}$ is the effective area of the last stator. PR and TR are obtained from the stage stacking calculation carried out for the derivation of the zero speed curve. The choking quasi-dimensionless mass flow of the locked compressor can be calculated iteratively.

$A_{2,eff}$ is estimated using the geometric area of the last stator and taking into account a blockage factor due to the boundary layer and the flow separation as shown in Fig. 4.7

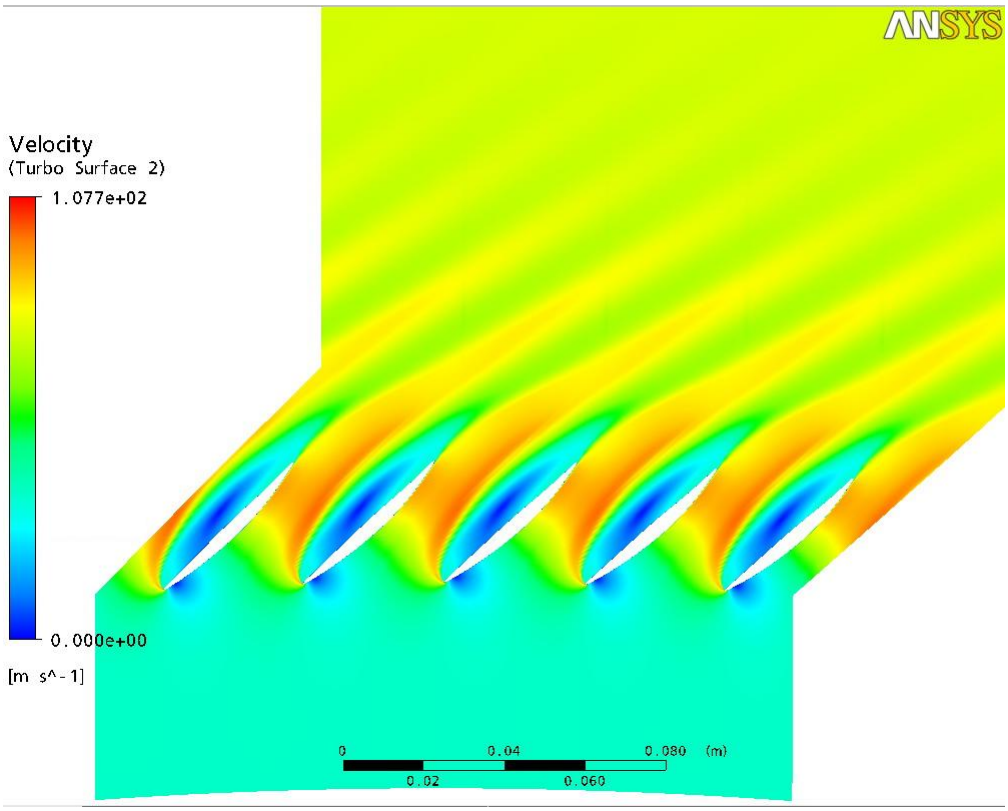

Figure 4.7: Channel blockage due to flow separation [102].

Even though further research on blockage factors is required, a very reasonable value would be of the order of 30-40% in that case. Once the range of inlet Mach

number is determined, it can be used for the calculation of the PR for the locked rotor conditions.

Pressure loss coefficients. As already mentioned the loss modelling for every stage, is based on the generic pressure loss models described in Chapter 3. As the forces on each blade are calculated, using the non-dimensional coefficients, the zero-speed torque can easily be calculated based on Eq. 4.2.

Stacking of stage characteristics. Once the torque and the total pressure losses on the blade are known, they can be summed up to give the characteristic of the entire compressor. The total torque exerted on the blades is the sum of the torque exerted on the rotor blades and the total pressure loss is calculated from the static pressure loss and the velocities at inlet and outlet.

4.3.2.6 Fan map generation

The most challenging component of the turbofan engine when it comes to performance modelling is the fan itself. When the engine is operating at off-design conditions, with reduced thrust, the bypass ratio increases. In addition, the fan blades are more twisted than the compressor ones and the flow pattern changes significantly from hub to tip. There is also a large difference in the blade speed. This creates the need for different maps for the hub and tip. As highlighted in [115], the difference in the characteristics would not be a problem for a compressor, as in that case the flow enters a single component downstream. The airflow downstream of the fan, however, is divided between the bypass duct and the core. The two streams have been subjected to compression processes with different characteristics, so these two processes should be described separately, with different maps for the root and the tip.

Furthermore, as the bypass ratio is changing, it is also a variable for fan operation, and this has to be taken into account for map representation. A single map

is used for referred flow as a function of speed and beta and this is then split between root and tip using the bypass ratio. Pressure ratio and efficiency also change between root and tip. For initial modelling, they can be assumed equal. A first improvement is to use a different map for the tip and evaluate the pressure ratio and efficiency of the root by applying factors. For rigorous off-design modelling, a series of fan root and tip maps are required as a function of bypass ratio.

The maps used and their level of detail depend on the data availability and the requirements of the performance model. Howard in [51], uses a total fan characteristic in order to be compatible with BD19's requirements. The total fan map is the one produced from original testing but it is hard to find as it is immediately split to root and tip characteristics. For the engines studied, as there is no total map available, the above idle root and tip maps can be combined using the bypass ratio. A simple linear relationship for the bypass ratio as a function of speed can be derived from the above idle model simulations, using the rotational speed at design and idle. Once this has been defined, the total characteristics can be calculated from equations 4.11 and 4.12 by mass averaging the pressure ratio and efficiency of root and tip [51].

$$TotalFanPR = \frac{BPR}{BPR+1} PR_{tip} + \frac{1}{BPR+1} PR_{root} \tag{4.11}$$

$$TotalFanEfficiency = \frac{BPR}{BPR+1} \eta_{is,tip} + \frac{1}{BPR+1} \eta_{is,root} \tag{4.12}$$

Once the root and tip maps have been combined, the total fan map can be converted to the parameters selected and the extrapolation process is carried out in the same way as in the case of the compressor.

4.3.3 Physical enhancements on the map generation process

Map extrapolation, as mentioned before, is a purely mathematical technique and, as such, its results may not have any physical meaning. Therefore, first principles must be employed to enhance the physical background of the method. Without any form of alignment and validation, the compressor map cannot be considered as an accurate (or at least sufficiently accurate) representation of the compressor performance. There are several checks and techniques that can be employed in order to better define the map points and the shape of the resulting low speed curves.

4.3.3.1 Alignment against ATF data

The Altitude Test Facility (ATF) reproduces the inlet conditions in altitude and flight Mach number and therefore allows the simulation of the engine operation at inlet pressures and temperatures other than those at sea level. This data can be used to check the agreement between the points measured from engine tests and the ones predicted from the map extrapolation process. The mass flow, pressure ratio and torque is calculated from the experimental data and these points are then plotted on the extrapolated compressor map. The agreement can be checked by calculating the deviation of the actual point from the predicted curve in terms of mass flow, pressure ratio, torque and rotational speed. In order to facilitate that check, extrapolated speed lines with the same rotational speed as the ATF data points can be calculated. If the agreement between the extrapolated speed lines and the data points is not satisfactory, the extrapolation process has to be repeated with different parameters.

4.3.3.2 Adaptive running of performance calculations

Performance calculations can provide valuable feedback to the map generation process. The calculation of steady state windmilling or power offtake points can provide some more check points that can be used to verify that the calculated points do lie

on the map. In addition, the calculated operating lines for different maps can be compared with any experimental data available and be used to assess the accuracy of the chosen map generation process.

4.3.3.3 Steady state windmilling points

As mentioned in Chapter 1, a gas turbine engine cannot operate at steady state windmilling. However this theoretical condition is very useful for sub-idle performance calculations as it is the locus of the points that all the transient windmill relights start from.

During steady state windmilling, the torque acting on the compressor blades is zero. The temperature ratio is unity and the pressure ratio is below one. When looking at the conventional compressor map of pressure ratio versus mass flow, the steady state windmilling line is the border between the stirrer and the turbine operating regions. Therefore, when plotting it in form of pressure ratio the line should be below PR=1 whereas in the torque map it should be on the line of zero torque. If the steady state windmilling line can be predicted it can provide more check points for the map generation process.

4.3.3.4 Zero speed curve calculation

The definition of the zero speed curve should also be mentioned, as it represents the physical enhancement of the map generation process very well. It is derived from physics-related studies and assists in the definition of the low speed curves on the map.

4.3.3.5 Choking mass flow on every speed line

The end points of the last extrapolated beta line have to be guessed for the expansion of the map. Physical check points can also be introduced for beta extrapolation, decreasing the resulting error. The maximum speed line of the compressor map is

usually choked, so the mass flow of the guessed beta point should be the same as that of the last point on the original speed line. The pressure ratio should be below 1 and the torque should be negative in order to make sure that the operating region represented in the map covers all the operating modes of the compressor.

The choking mass flow of the compressor when operating at locked conditions can also be calculated if the geometry is known. This is done through an iterative process, combined with the calculation of the zero speed curve. Therefore the other end point for beta extrapolation can be defined as the point where the compressor starts to choke and the mass flow passing through it is maximum.

The same idea can be used to check the maximum mass flow of the other speed curves. Since, however the pressure losses at non-zero rotational speeds are not known, this can only be used as one more physical check point for the matching of the pressure ratio, temperature ratio and mass flow of the choking point of that speed curve.

4.3.3.6 Speed line alignment

Howard [51] proposes a few checks that can be used to ensure that the generated map does not violate any physical laws when extrapolated at linearised parameters.

Speed line collapsing on ϕ-ψ plot. A first check is to plot the above and below idle speed lines in terms of ϕ-ψ. As this is a non-dimensional representation, the speed lines should come close together.

Speed line collapsing on ψ-ψ_{is} plot. The next step is to plot the original and extrapolated speed lines in the form of ψ-ψ_{is} plot. The slope of this line represents the efficiency. This does not vary significantly along a constant speed curve when the compressor is operating normally, so all the speed curves should be represented as lines roughly parallel to each other. When the compressor operates as a stirrer or as a turbine, the efficiency is not defined properly in terms of physical meaning;

it can be negative or approach infinity. Therefore the speed lines may extrapolate out linearly, to match the spread in the data points.

4.3.4 General comments

As it will be presented in the following section, all the above mentioned techniques have been implemented within the map generation platform. Undoubtedly, there is always room for further improvements in every single enhancement method which may lead to an even more accurate compressor performance representation by the generated characteristic. It is up to the future researchers to test and validate the fidelity of the generated characteristics and then to also refine the physical enhancement approaches as described herein.

4.4 Map generation platform overview

As mentioned in the beginning of this chapter, one of the aims of the current work was to create a robust tool for sub-idle engine map generation, incorporating all the available techniques on a single module, allowing the map parameterisation and definition using a number of input files. Hence, a flexible platform is created keeping the potential of further future development by enhancing of the current map generation techniques or the incorporation of new ones without having to start every time from scratch. In addition, it offers convenience to the user of any sub-idle performance simulation tool, as the characteristics can be provided in a few sequential steps after setting up the user defined parameters of the generation algorithms.

4.4.1 Main code modules

The main code is written in FORTRAN and is divided in five parts (Fig. 4.8) which are described in the following sections.

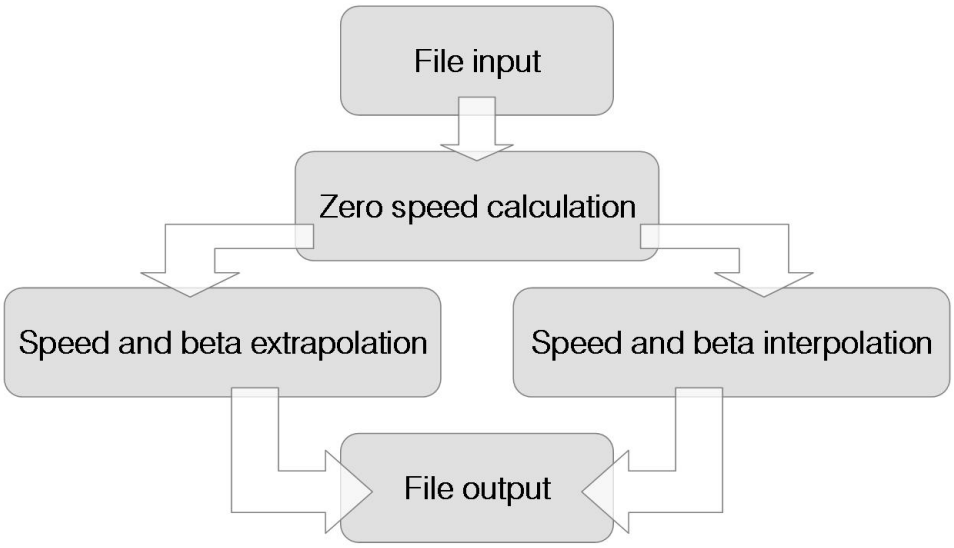

Figure 4.8: Main modules of map generation platform [7]

4.4.1.1 Initial set up

In the beginning of the program, after variable declaration and table allocation, the extrapolation settings are defined. These include the selection of component type - compressor or fan -, the number of initial speed and beta curves and the desired number of extrapolated curves.

4.4.1.2 Input files and data manipulation

The first step is the input of all the data required for the calculations. In the beginning of the code, the compressor map is input along with some more data. Data that is only required by certain subroutines is read in the respective subroutine in order to keep the structure of the code as simple as possible and to be able to use each subroutine independently.

A detailed description of the subroutines of this part is given in [7] and will not be reproduced hereafter.

4.4.1.3 Zero speed line prediction

The second step is the calculation of the zero speed curve. This can be done by guessing the end points of the curve and calculating it based on the above idle data. The most accurate way, however, is to calculate it following the generic methodology described in section 4.3.2.4. The torque and pressure loss on the blade are calculated based on the forces on the blade and then stacking the half stage characteristics.

A number of subroutines is also developed for this purpose and described in great detail in [7].

4.4.1.4 Speed and beta extrapolation or interpolation

Once the lowest or zero speed curve is calculated, the extrapolation or interpolation process can be carried out. There are two main possibilities: the curve is either *guessed* or *calculated* from the blade forces. In the first case, the map is generated with an extrapolation process, whereas in the second through interpolation. However, as highlighted in Fig. 4.9 the guessed speed curve may also be for zero rotational speed, in which case the torque parameter has to be used for map interpolation.

In order to perform the procedure itself, two subroutines are used, one for speed and one for beta lines. The equation used for extrapolation (or interpolation) is either linear or polynomial for both cases, with the option to choose between the two. These subroutines are called for each of the three variables used for map representation. The extrapolation of speed lines is carried out first, followed by beta.

The methodology used in the interpolation case is the same; the only difference is that it is carried out using torque parameters, zero rotational speed as the lowest speed line and the calculated speed curve. The subroutines used are the same. The extrapolation (or interpolation) procedure described in this section is summarized in Fig. 4.10.

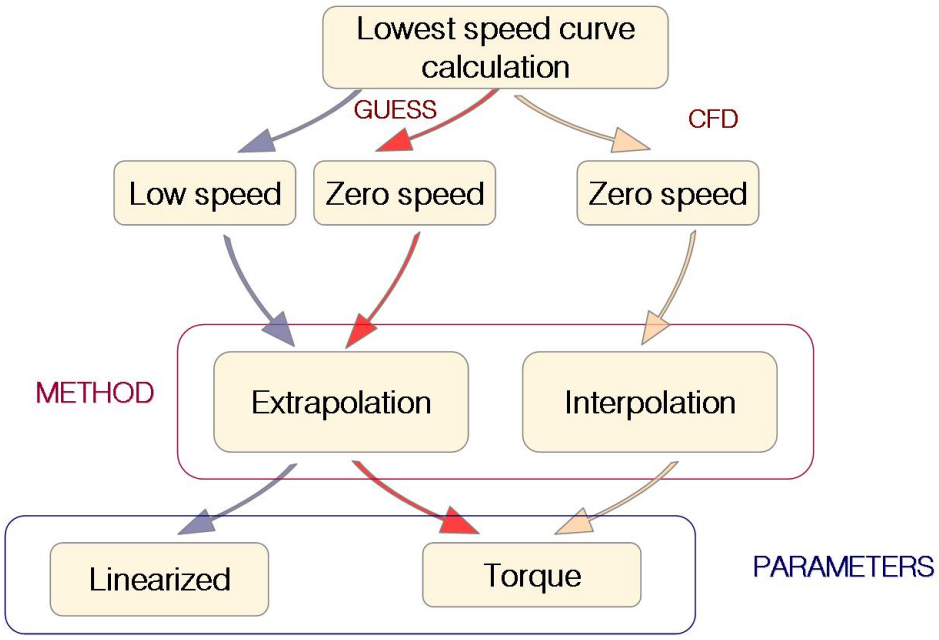

Figure 4.9: Different strategies for whole map generation depending on the input data [7].

4.4.1.5 Output files

The overall map is then transformed to the desired format, exported and plotted in Matlab using a graphical interface developed within the project for this purpose. The tool is capable of generating output files compatible with the format required by BD19. In this way generating, loading and using the maps for relight performance simulations is a matter of minutes.

4.4.2 Code overview

The main parts and all the subroutines described above are combined to a single program for map generation. A more detailed overview of the entire code is given in Fig. 4.11

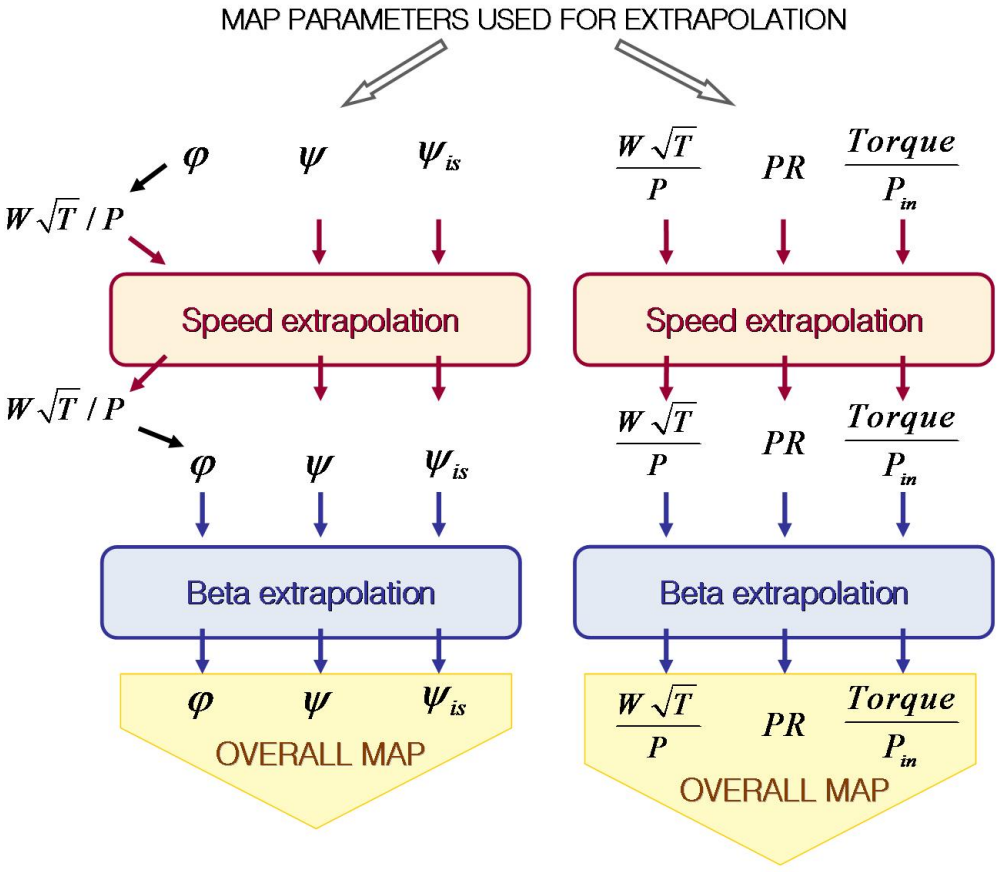

Figure 4.10: Map generation overall process [7]

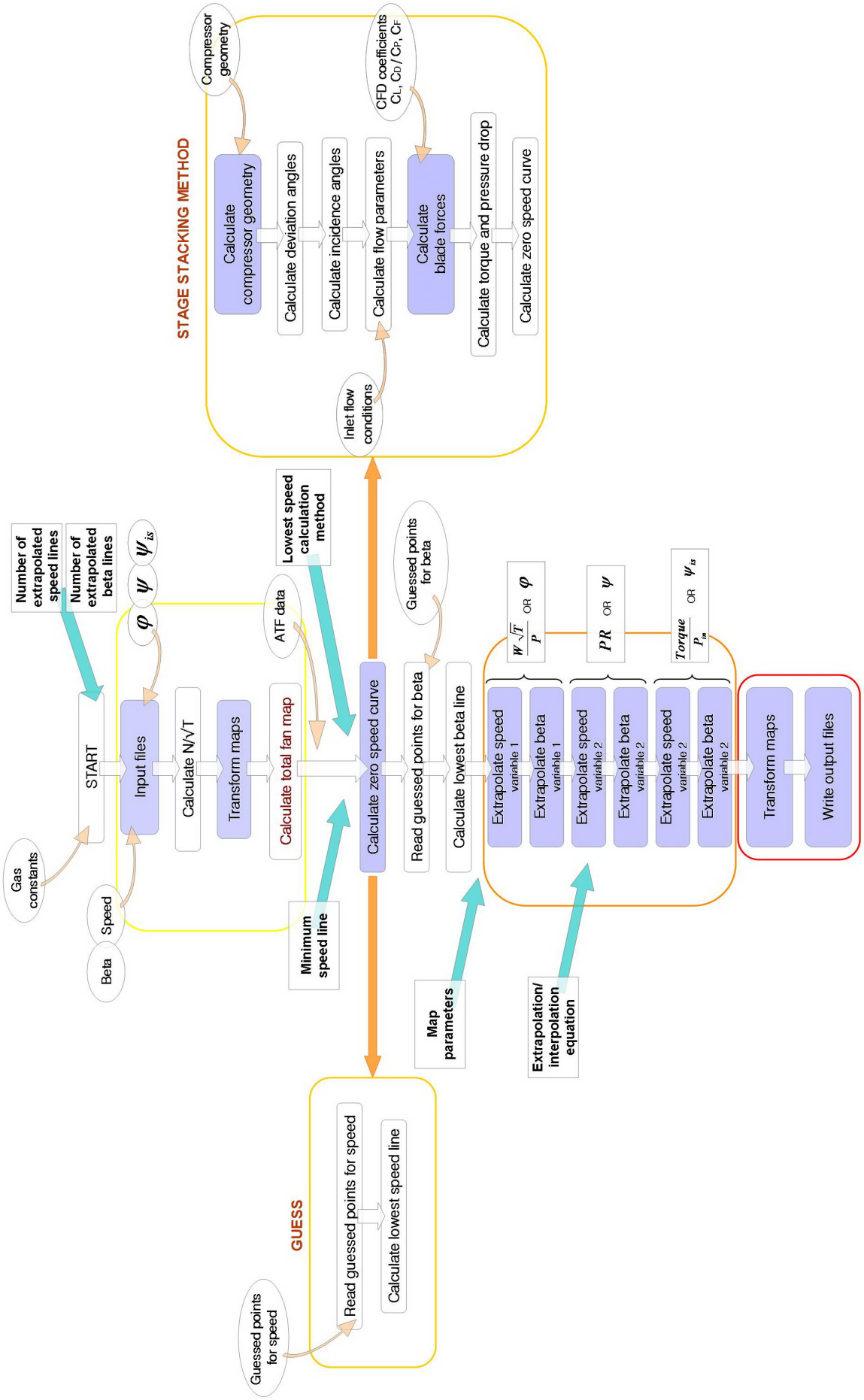

Figure 4.11: Overview of the map generation tool including all the separate modules [7].

4.4.2.1 Summary of user defined parameters

A single code was written for all applications, therefore the choice of the various procedures is done inside the code and so is the definition of the extrapolation settings.

The parameters used to switch between the different parts of the code are:

- Component type

  This is used to select whether the code is run for a compressor or a fan with split maps. In the case of the fan, the root and tip maps have to be combined to a total map before the map generation is carried out.

- Zero speed curve

  This is used to define the way the zero speed curve is calculated. It can be either by guessing the end points or with the use of CFD derived loss coefficients.

- Aerodynamic coefficient type for zero speed prediction based on the generic pressure loss model.

- Map generation technique allowing to chose between the linearised parameters method and the torque based technique as previously described.

- Number of generated speed lines

- Speed values of generated speed lines

- Number of generated beta lines

- Mathematical model used for extrapolation or interpolation

- Minimum speed line value

4.5 Results and discussion

In this section a number of representative characteristics derived using the above described tools will be presented. The main test case is the HP compressor of a low BPR military engine (Engine A), while the method has been also successfully applied on the characteristics of high BPR civil turbofan engine.

4.5.1 Engine A characteristics extrapolation

Two different map extrapolation techniques are presented hereafter; the first is the traditional method based on the linearised parameters while a second approach based on torque map extrapolation is also shown.

4.5.1.1 Extrapolation using linearised parameters

As already explained the map extrapolation using linearised parameters was firstly applied by Howard [51] for his sub-idle studies. The method has been implemented in the current map generation tool and applied in order for the code to be validated against the already existing maps. The original engine A characteristic as provided by the sponsoring company is shown in Fig. 4.12.

As it can be seen, the lowest speed line is only the 63.2% speed with respect to design. The extrapolation of the map using the linearized parameters imposed a constraint on the value of speed at the last speed line. This was selected to be 1% of the design value. After the transformation into linearised parameters the extrapolated map is illustrated in Fig. 4.13. As can be seen, the lowest speed curve is quite far away from the rest without collapsing on top of them as expected by a ϕ - ψ representation. However, this speed curve shifting happens unavoidably for such a low rotational speed since both the flow and the work parameters experience a significant increase in their actual values. In addition, as it was established later on, this curve shifting is necessary for the successful generation of the characteristic

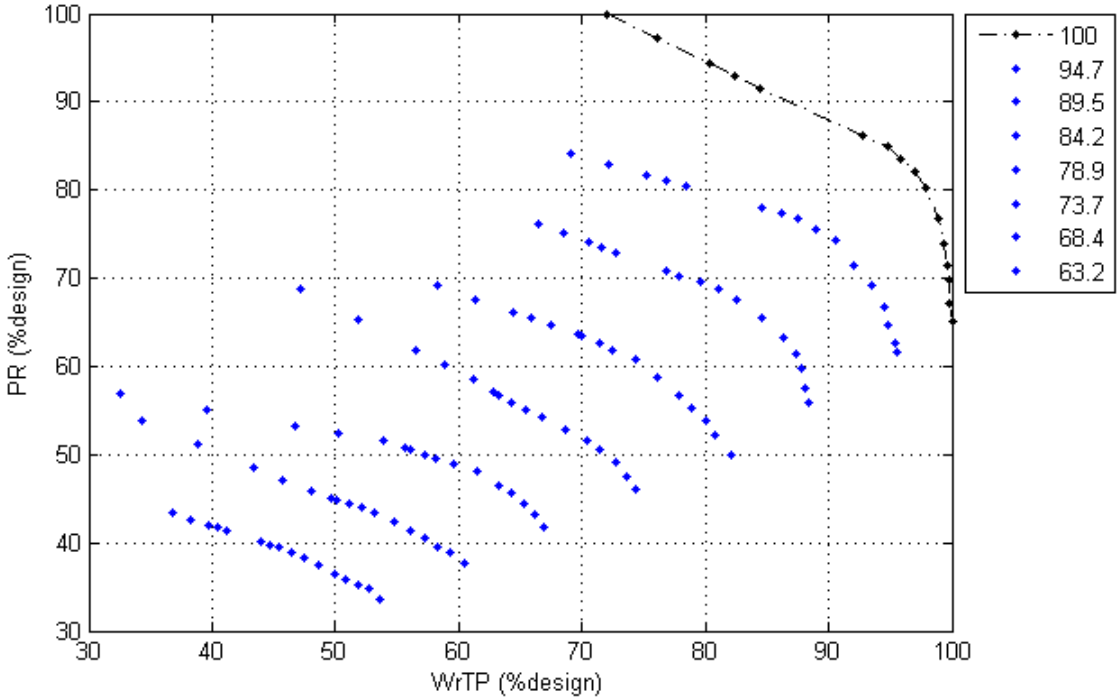

Figure 4.12: Above idle characteristic for Engine A.

using the conventional parameters and is a process also performed by Howard in [51]. Fig. 4.14 shows the generated map in terms of ψ - ψ_{is}.

In the normal operating region of the compressor, all the speed lines are roughly parallel, and expand in the region where the compressor is operating as a stirrer ($\psi > 0$, $\psi_{is} < 0$) or as a turbine ($\psi < 0$, $\psi_{is} < 0$). The slope of the lines represent the isentropic efficiency. For the normally operating compressor within the design range of operation, the efficiency changes are not that significant and that is why the slopes of the above idle given speed lines are not so different one from each other. Efficiency drops start to happen as the speed lines are extended towards the stirrer or turbine regions. The latter becomes obvious by the noticeable reduction of the speed line slope in the extrapolated regions. It must not be omitted that the pressure coefficient has to reflect the fact that the isentropic efficiency cannot be defined properly in the low speed region, especially when the pressure ratio is close to or below unity.

Fig. 4.15 shows the extrapolated map in conventional parameters.

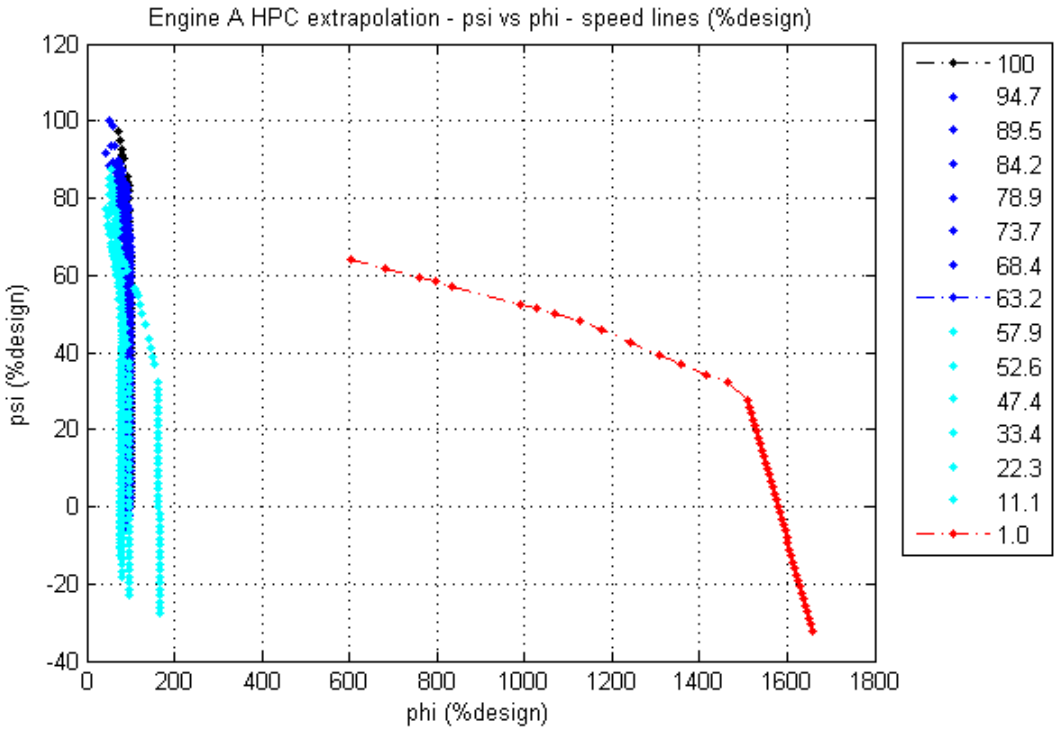

Figure 4.13: Extrapolated engine A map in linearised format.

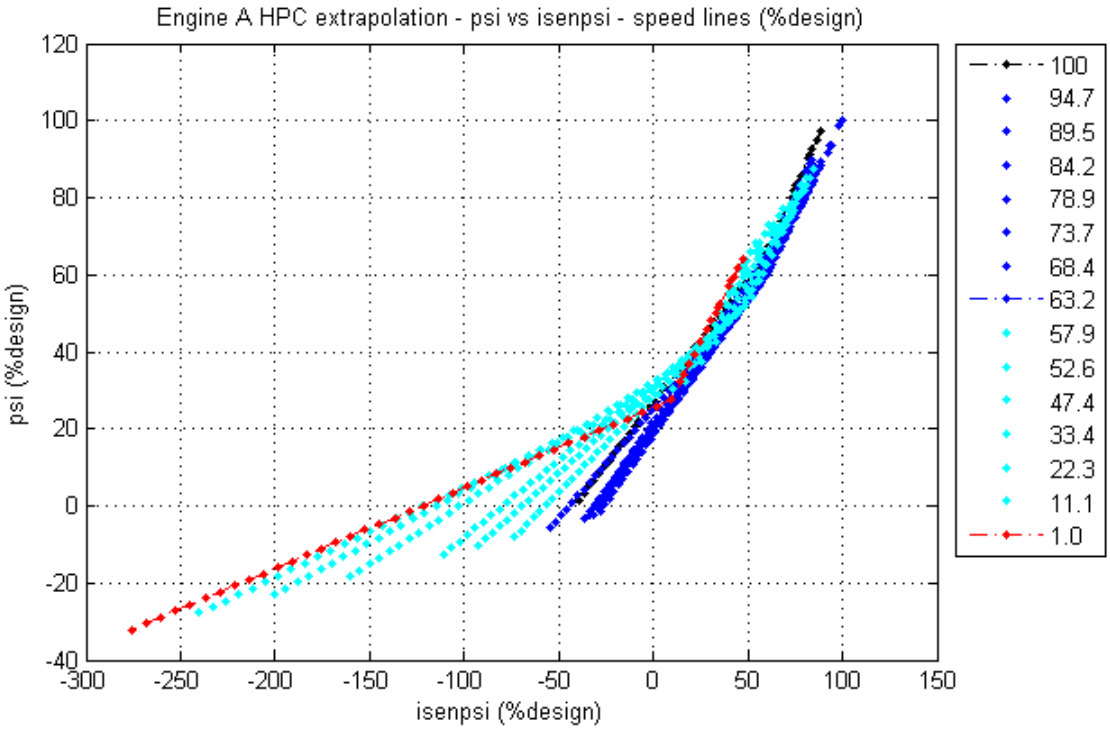

Figure 4.14: Speed line alignment in respect to the isentropic efficiency for map extrapolation using the linearised parameters [7].

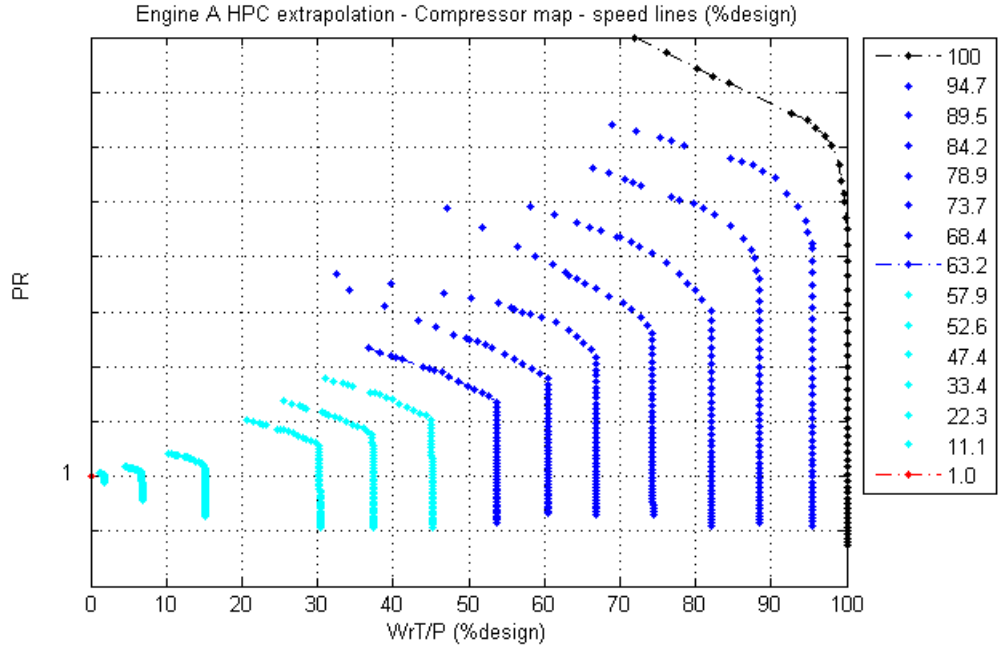

Figure 4.15: Extrapolated engine A map in conventional format [7].

The extrapolated map can also be transformed into torque characteristic, after the extrapolation process, as shown in Fig. 4.16.

4.5.1.2 Extrapolation using the torque parameter

As shown in the previous section, the use of linearized parameters results in strange values for ϕ, ψ and ψ_{is} when performing the extrapolation. The main advantage of the torque parameter group is that all the variables have values that are close to the above-idle ones, without facing discontinuities, even in very low rotational speeds.

The extrapolated maps in terms of PR and torque parameter against non-dimensional mass flow is shown in Figs. 4.17 and 4.18 respectively.

4.5.2 Engine A characteristics interpolation

The main contribution of the current work, as mentioned in a previous section, is the switching of the map generation techniques from extrapolation to interpolation using a known zero-speed chic as described in Chapter 3.

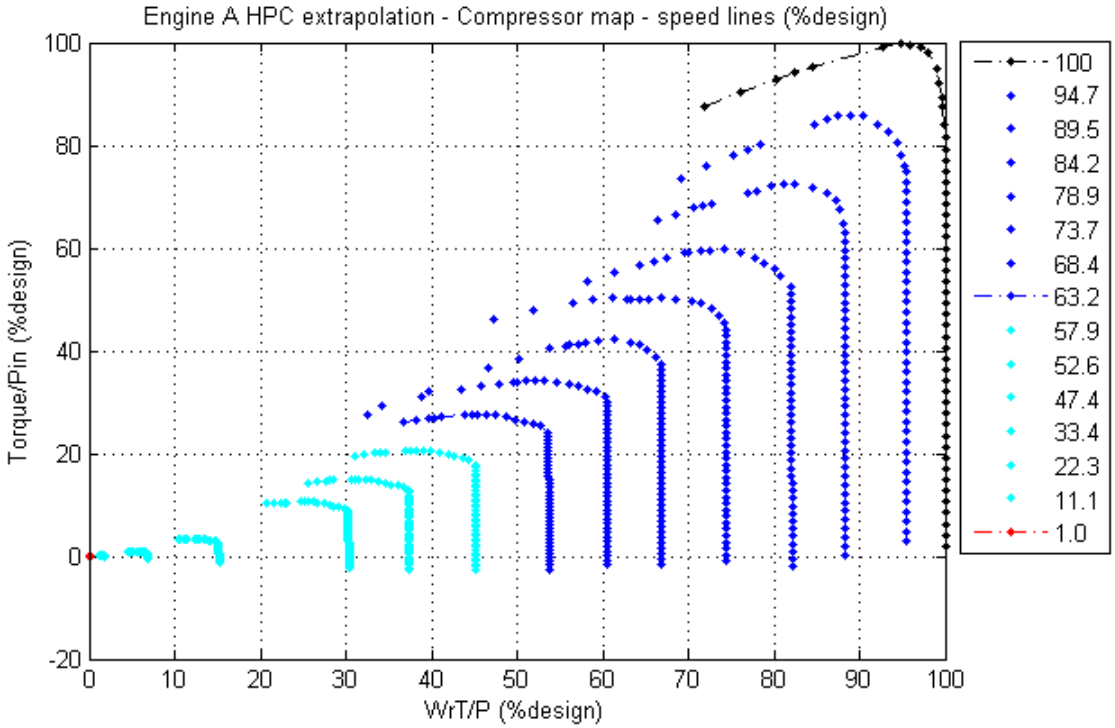

Figure 4.16: Extrapolated engine A map in torque format [7].

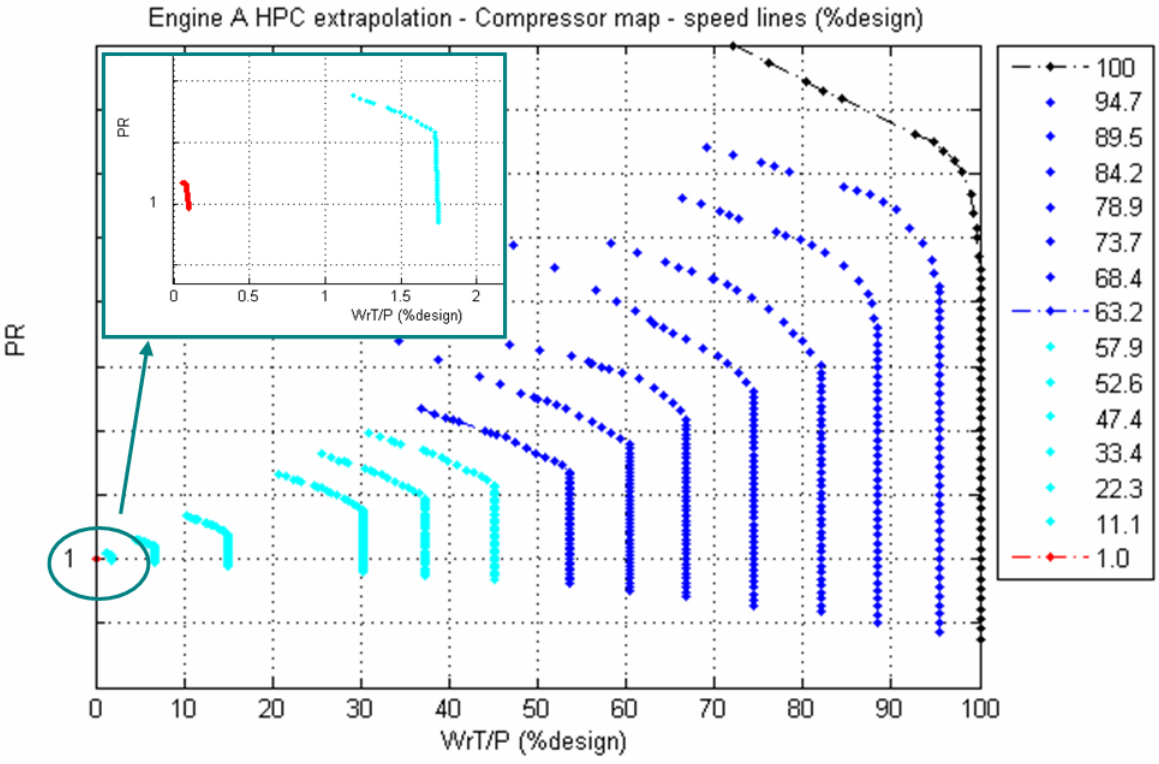

Figure 4.17: Plot of PR versus $W\sqrt{T}/P$ for the extrapolation of the HPC of engine A using torque [7].

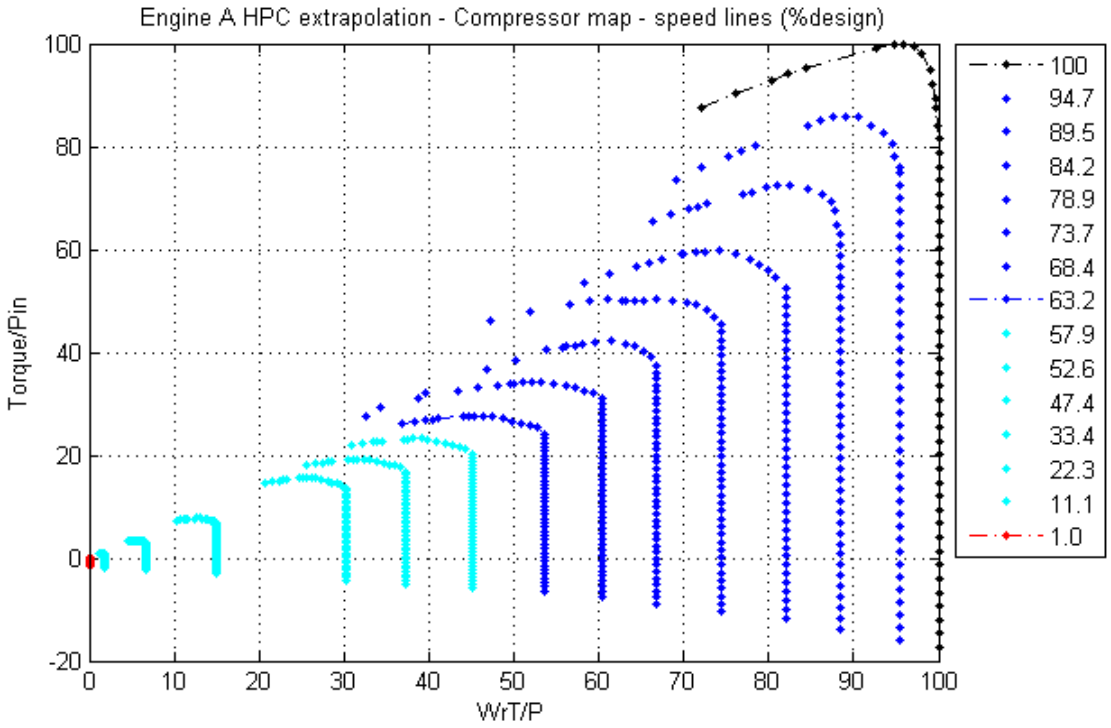

Figure 4.18: Plot of $Torque/P$ versus $W\sqrt{T}/P$ for the extrapolation of the HPC of engine A using torque [7].

In this section the results of this effort will be presented starting from the derivation of Engine's A zero speed curve. The stage stacking technique is employed and the derivation of its characteristics is performed using exclusively the torque parameters, as the existence of the zero speed curve does not allow the use of linearised parameters.

4.5.2.1 Zero speed line derivation

The calculation of the zero speed line requires detailed information regarding the geometry of the blade, the inlet and outlet angles and the radii for all the blade rows of the compressor.

The derivation of the zero speed curve by stacking the individual stage characteristics is shown in Fig. 4.19, where the torque parameter is plotted.

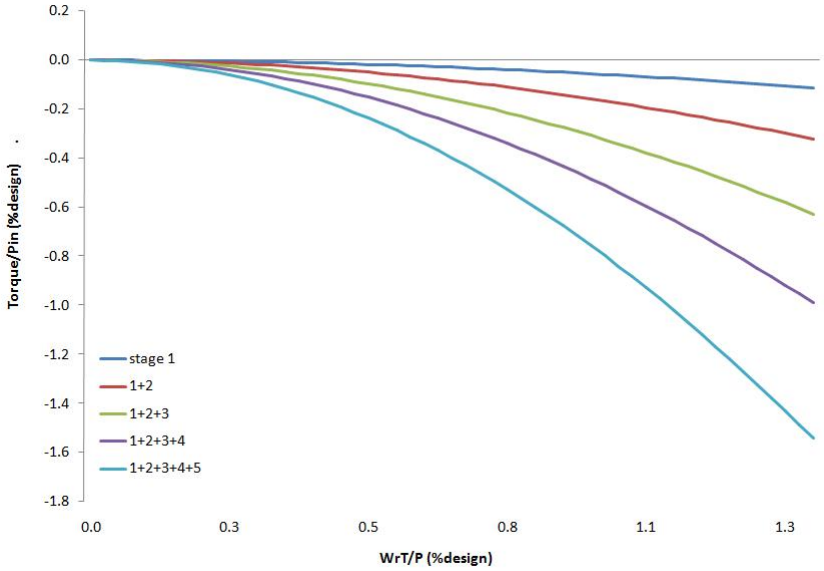

Figure 4.19: Torque zero speed line prediction for engine A HPC using locked rotor studies and a stage stacking technique [7].

4.5.2.2 Map interpolation

The calculated zero speed line is used for the interpolation of the compressor map between this line and the above idle data. The generated characteristic in conventional form is shown in Fig. 4.20. The zero speed line is smoother and more accurate, and this defines the shape of the below-idle speed lines better, as shown in Fig. 4.21. The interpolated map is presented in figure 4.22 in terms of $Torque/P$ and $W\sqrt{T}/P$. The low speed region is shown in figure 4.23.

4.5.3 Discussion and general comments

Engine A is considered to be a very good test case as apart from the above idle map of the HP compressor, detailed data of the compressor and blade geometry was available. This enabled the generation of the map in the sub-idle region using all three methodologies; extrapolation using linearized parameters, extrapolation using torque parameters and interpolation.

As explained above, it was observed that the extrapolation of flow cannot be

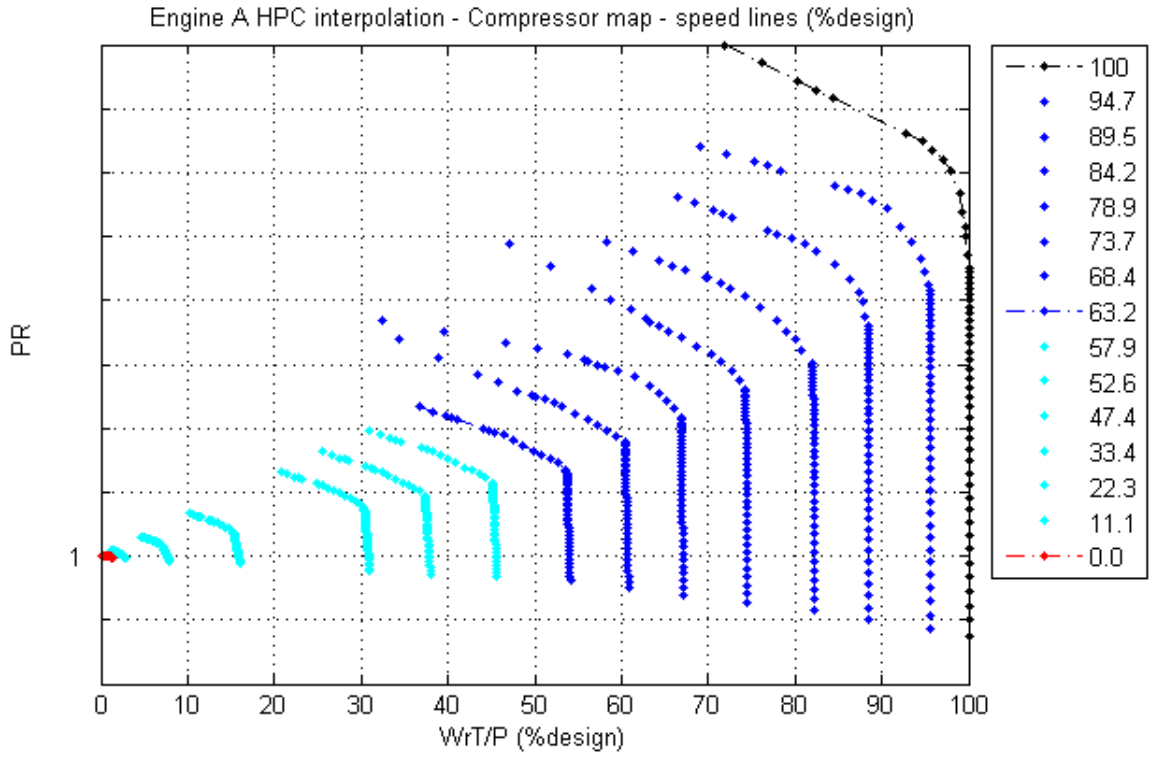

Figure 4.20: Engine A characteristic in conventional parameters after map interpolation [7].

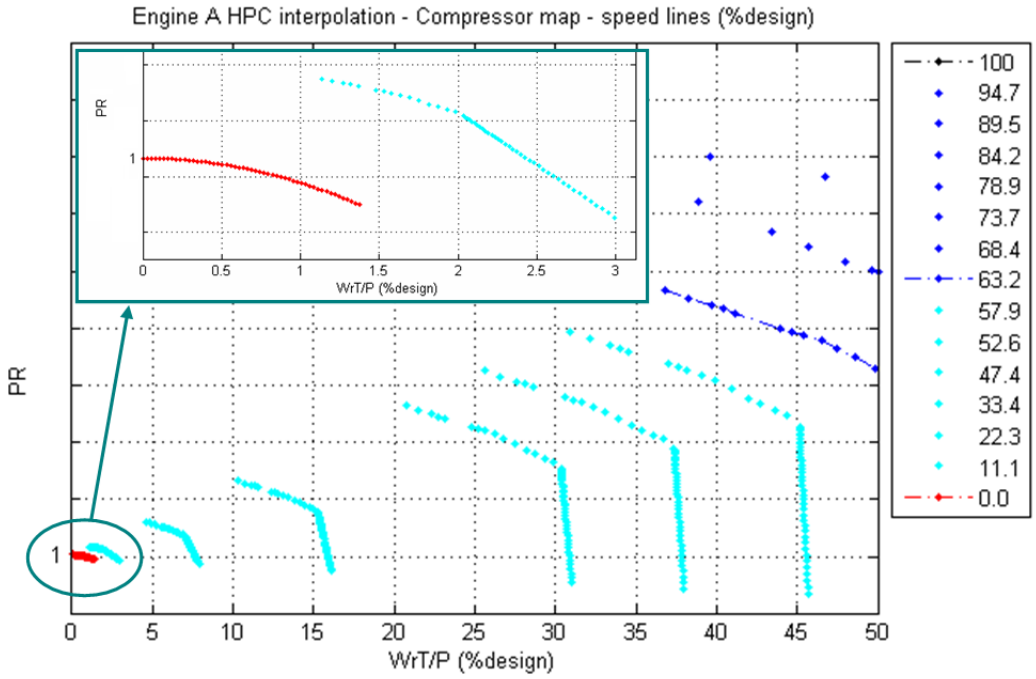

Figure 4.21: PR versus $W\sqrt{T}/P$ for the interpolation of the HPC map of engine A in the low speed region [7].

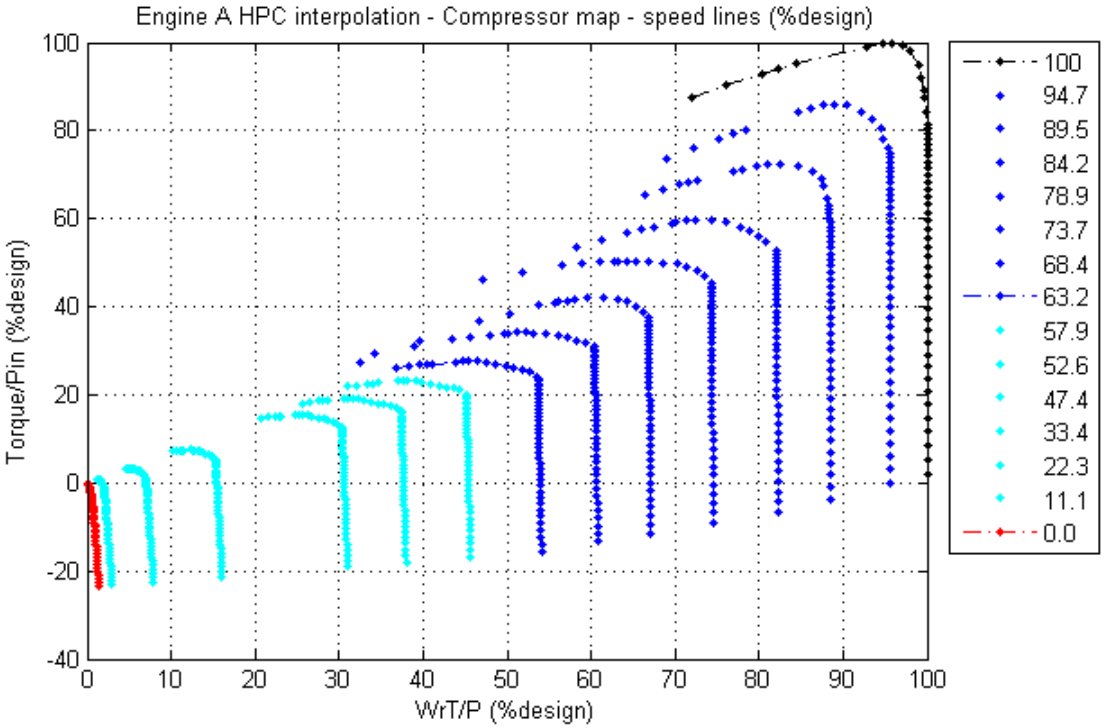

Figure 4.22: $Torque/P$ versus $W\sqrt{T}/P$ for the interpolation of the HPC map of engine A [7].

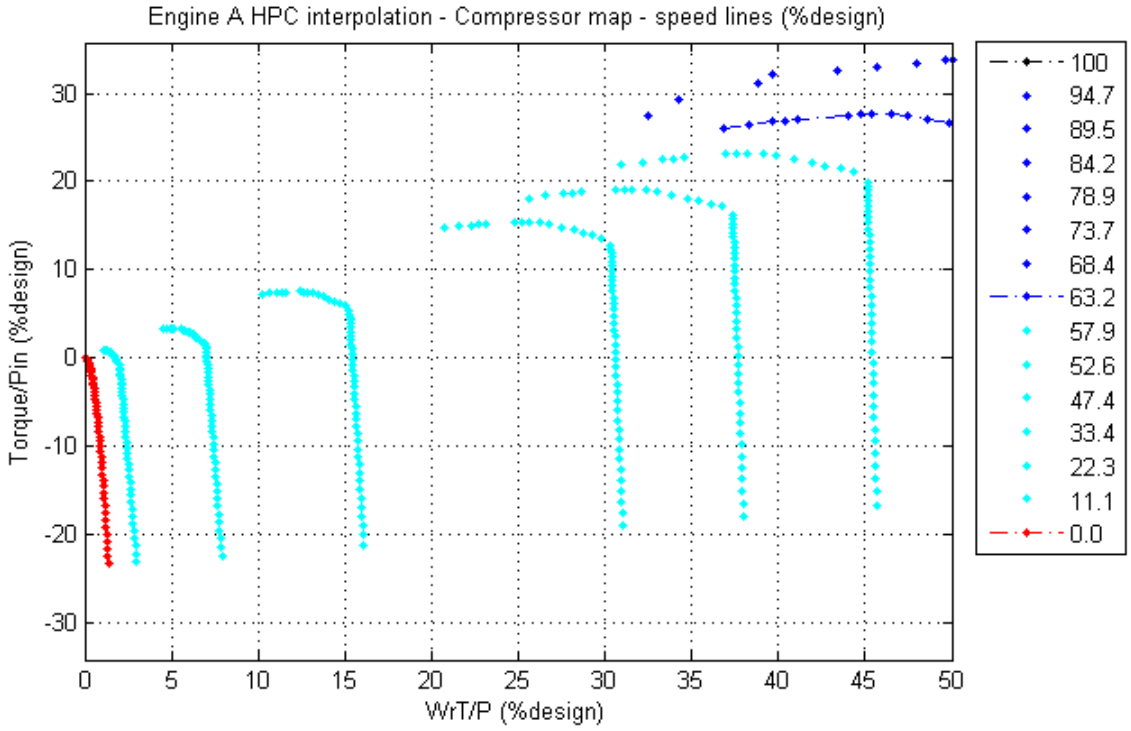

Figure 4.23: $Torque/P$ versus $W\sqrt{T}/P$ for the interpolation of the HPC map of engine A focused in the low speed region [7].

performed using ϕ, because that would result in non-realistic values of mass flow in the low speed region and this was the reason that the extrapolation of mass flow was always performed using $W\sqrt{T}/P$. There were no problems with the extrapolation of work and pressure coefficients, as long as the rotational speed at the last speed line was higher than zero.

On the contrary, the use of the torque parameter eliminates these problems and enables the generation of the map down to zero rotational speed through either extrapolation or interpolation. In addition, torque is a physical parameter and can represent the phenomena determining the operation of the compressor in the sub-idle region better than isentropic efficiency or the linearized coefficients.

The use of torque provides a more generic and robust methodology, as the map can be generated up to zero rotational speed and is recommended.

It should be noted that the differences in the approach used, especially in the case of extrapolation, are not reflected on the resulting map but mainly on the capabilities and the ease of use of the software.

The quality of the resulting map depends on the quality of the above-idle data, as it is generated through a mathematical process, even if it is enhanced with first-principles based checks. The calculation of the zero speed curve of the compressor assists significantly to a better definition of the low speed region of the map, resulting in smoother and more accurate curves.

The issue of speed curve alignment against ATF data should be looked into more thoroughly, as the ATF data points do not align well with the speed curves even in the original region of the map. Finally, as seen from the maps presented above, there is a kink in the speed curves, which results from beta extrapolation. Therefore, the speed lines require smoothing before they can be inserted in a performance calculation program. Software SmoothC can be used for that, as it is a good tool for smoothing of compressor maps, noted in [67].

4.6 Concluding remarks

In this chapter a methodology for the sub-idle map generation was described. As illustrated above, a map generation tool was implemented in FORTRAN in order to provide a robust platform for low speed compressor characteristic generation that can easily be used as a pre-processor of the BD19 performance prediction code. The methods proposed and initially applied by Howard have been incorporated into the solver while new methodologies regarding map interpolation and the use of the torque parameter have been also introduced enhancing the physical background of the sub-idle map generation.

With such an approach, further research on map generation methods is straight forward as the main basis is already built. The parameterisation of the map can also accelerate the engine performance studies providing the user with a reliable and quick tool for rapid sub-idle map generation.

Undoubtedly, lots of improvements can be incorporated into the tool starting from more physical checks or more flexible (or even alternative) interpolation options. A summary of the recommended future tasks is given in the last chapter of this thesis.

Chapter 5

Sub-idle combustion performance

5.1 Introduction

One of the most crucial topics of research within the project is to investigate the combustion mechanics during the transient relight engine processes (windmill relights, groundstarts etc.). Enhancing the knowledge on the combustion mechanisms implies that more sophisticated models can be derived to describe the sub-idle combustion and therefore increasing also our predictability on the relight capability of an engine.

In the current chapter after the definition of the sub-idle combustion problem, a number of parametric studies attempting to investigate the sub-idle performance of an atomiser is presented and discussed. This research shall be the basis for further tasks aiming to identify and quantify the factors that dominate the low efficiency sub-idle combustion.

5.2 Literature Review

Within this section the major literature findings are presented. However, references to useful pieces of work are made throughout the chapter.

5.2.1 The process of combustion

When introducing the field of combustion it is important to understand the role the combustor plays. The combustion chamber is used to supply heat to the working fluid before expansion occurs at the turbine. The geometry of the combustion chamber is defined by the requirements for a low pressure loss, wide stability limits and high combustion efficiencies and other geometrical constraints relating to the cross sectional area and length of the engine.

The stability limits are an important way of defining the boundaries of an environment upon which normal or effective operation can exist. These limits may represent a boundary where any further deviation past this boundary will result in a break down in the performance of the combustion chamber or extinction of the flame. To define what the term "*stability limits*" describes it is important to understand the delicate balance that must be maintained between the burning velocity of the flame, and the velocity of the mixture flow stream.

The balance that is referred to as "*flame stabilisation*" in a flowing gas stream operates upon simple principles. The fresh air and fuel mixture are forced to flow downstream of the compressor. This flow velocity may change with engine operational speed as the engine transitions between its idle and design point speed. The combustion wave propagates at an almost constant rate, this however can change with environmental effects such as pressure within the combustion chamber. The combustion wave however propagates in the opposite direction to that of the fuel and air mixture. The requirement for stabilisation is generated as the flame must be kept within the combustion chamber and also within a specific region of the combustion chamber to maintain flame stability and to avoid over heating of critical components such as the inlet nozzle guide vanes. If the burning velocity of the combustion wave or flame is higher than that of the flow velocity then the flame will move upstream at a velocity (Flame speed - Velocity Flow). If the flow velocity is higher than that of the combustion wave the flame will move downstream at a

velocity that is equivalent to (Velocity flow - Flame speed).

It can be concluded that to maintain flame stability the flow velocity must be equal to that of the flame speed, and that no movement of the flame will occur. This relationship has been defined by Beer and Chigier in [10]: "*The condition for flame stabilisation in a flow field of non uniform velocity is that there is a point in the flow field where the flow velocity is equal and opposite to the velocity of the combustion wave*". This quotation summarises well the discussions raised in this chapter. Because of these issues that have been discussed the combustion chamber and combustion systems must be designed to produce good stability performance.

The most frequently used method of representing a combustion system performance graphically is to produce what is commonly termed a stability loop diagram. The stability loop relates fuel and air ratios with flow velocity to produce an operational envelope for the combustor. A typical stability loop is shown in Fig. 5.1.

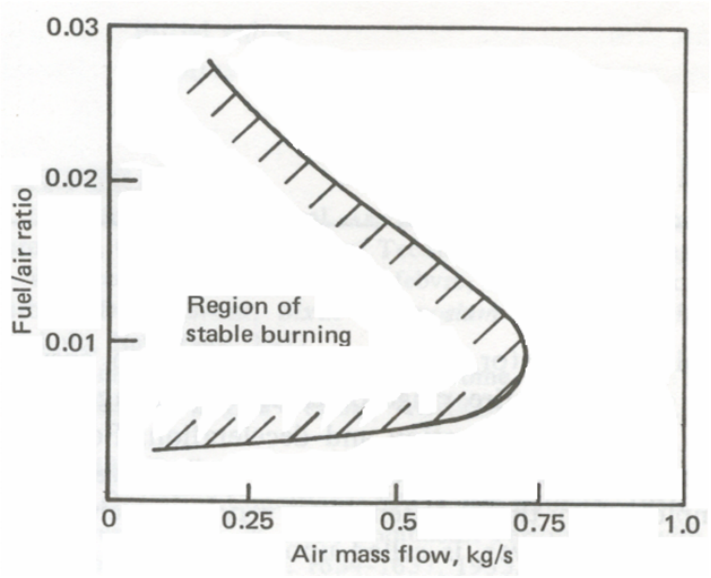

Figure 5.1: Typical combustor operational envelope [68].

From Fig. 5.1, the flow speed at which the combustion chamber will either blow out or be extinguished may be determined. As the limits of operation are expressed in terms of fuel and air ratio as well as flow velocity, they may be directly related to engine running conditions. A further advantage, if this arrangement of data is

that the performance may be obtained for a combustion loading value at a given AFR (Air Fuel Ratio), which can be used as part of the design or development process as a tool. This correlation of data is obtained from testing the combustion chamber on test beds and from correlations of previous experience. Much of the estimation of combustion performance is done, based upon past experience and relating previous designs with geometrical constraints. This allows the design of these combustion systems to be produced with a good estimation of its predicted operational performance before testing. This is an example of a process where the relationship between both combustion and performance predictions is necessary in the completion of a valid engine design.

Apart from that, knowledge on fuel atomisation along with the performance of different types of atomisers is required for a complete picture of the combustion system to be obtained. The theory of evaporation and the different forms of fuel dispersal are complex but yet important to understand, when considering the performance of the combustion system. An in depth review of fuel atomisation methods can be found in [84] while a detailed description of different atomiser configurations is given in [68] and [69].

5.2.1.1 Combustion efficiency definition

Combustion efficiency is a measure, in percentage terms, of the engines ability to burn the fuel entered into the combustion zone. The combustion efficiency also can be considered as a measure, in percentage, of energy released from the fuel in comparison to the maximum fuel energy.

The modern gas turbine engine combustion system has been developed to a very high level. The combustion system is so efficient that at specific operational conditions combustion efficiencies of over 90% may be obtained.

The combustion efficiency can be expressed in **four general formats** based upon the condition of combustion. The derivation of each expression is dependent

upon the factors that are known to be influencing the process of combustion.

$$\eta_{comb,reac} = f(\theta) = f(\frac{P_3^{1.75} \cdot A_{ref} \cdot D_{ref} \cdot exp(T_3/300)}{\dot{m}_{air}}) \tag{5.1}$$

One of the most common combustion efficiency models is represented by Eq. 5.1. Under this model the process of combustion is only limited by the *speed of chemical reaction* (reaction based model).

The combustion efficiency can be defined also upon different combustion models. A. H. Lefebvre suggests that the process of combustion may be considered in terms of a simplified model. This basic model states that the process of combustion is dependent upon the time required for fuel evaporation, chemical reaction and mixing of the fuel and air. Based upon this simple assumption, different combustion models that represent the process of combustion under each of these limiting conditions may be derived.

A rate limiting condition is an environmental or physical condition that restricts the rate that combustion occurs. An example is the evaporation rate, where many factors may slow down the speed of evaporation. Under a case where evaporation is the only rate limiting process a model that describes the process of combustion may be defined with the following equation [68].

$$\eta_{comb,evap} = \frac{8 \cdot (\frac{k}{Cp})_g \cdot ln(1+B) \cdot (1 + 0.25 \cdot Re_{SMD}^{0.5}) \cdot t_{res}}{\rho \cdot SMD^2} \tag{5.2}$$

A further condition, described as a combined condition, can also be present, where two rate limiting conditions may exist, both limiting the rate of combustion. More details about different combustion models can be found in [68] and will not be reproduced hereafter.

5.2.1.2 Combustion loading definition

The term combustion loading is important as it describes an analytical design tool that is used in the design and comparison of combustion chambers and their performance. The term combustion loading refers to a means of considering the performance of a combustion system in terms of its volume. Combustion chamber design is a complicated process and is highly dependent upon the use of previous information. When designing a new combustion system it is important to ascertain whether the combustor will meet its required performance goals. However, the performance of combustion chamber is extremely difficult to be predicted without the design and construction of complex and expensive test rigs. Thus, the design of combustion systems is mostly based upon previous design knowledge. The combustion loading, or otherwise termed theta parameter, is an important tool for reducing the requirement for extensive testing and performance analysis.

An example of how combustion loading is used in the design of combustion chambers can be seen by considering a short example. The operation of an engine's combustion chamber from the windmill condition up to its design speed in terms of combustion efficiency plotted against combustion loading can be illustrated in a graphical format.

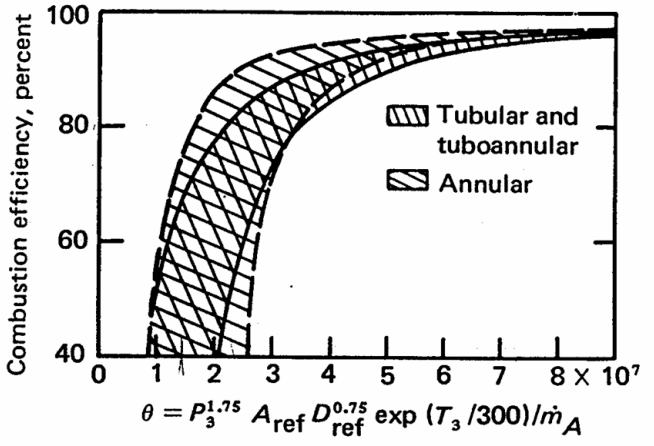

Figure 5.2: Combustion loading for different combustion systems [68].

From Fig. 5.2 it can be seen that the various differing combustion chambers form

a series of trends. Taking the example now that a new design is required to meet a series of conditions in terms of its combustion efficiency at various operational conditions, it is possible to look at the existing trends and determine an approximate volume that would be required to meet these conditions based upon existing knowledge. By using the combustion loading equation there is the ability to relate design performance to geometrical configurations and volumes.

Analytically, combustion loading can be expressed as:

$$\theta = \frac{P_3^{1.75} \cdot A_{ref} \cdot D_{ref} \cdot exp(T_3/300)}{\dot{m}_{air}} \tag{5.3}$$

It can be seen from the expression above that the loading parameter includes geometrical relationships. Therefore, this can be used as a means of estimating the performance capabilities of a new design with some basic dimensional knowledge.

The more relevant application of the loading equation is as quoted by A. H. Lefebvre [68] that "*it's possible to predict with reasonable accuracy, combustion efficiencies at flow conditions out of the range of test facilities*". This is quite important in the discussion about the implications of the loading equation upon the windmill relight condition and in terms of its definition during sub idle conditions. Such use of this expression is a very useful tool in the design of modern combustion systems and its use has significant advantages in the windmill relight modelling. This is because it is very difficult to test combustion at the windmill relight conditions in a test bed.

5.2.1.3 Other parameters definition

In this section a few useful properties for the following analysis will be defined.

- **Droplet Sauter Mean Diameter (SMD or D_{32})**. This is the diameter of a drop within the spray whose ratio of volume to surface area is the same as that of the whole spray. It is dependent, among other parameters, on the type

of the atomiser and different models for various atomisers are proposed in the literature [68].

- **Critical Drop Diameter.** This is the diameter corresponding to the transition to a mode where the process of evaporation starts to degrade combustion efficiency. It is defined as:

$$D_{crit} = \sqrt{8 \cdot \frac{k}{C_{p_g}} \cdot \frac{1}{\rho_f} \cdot ln(1+B) \cdot t_{res}} \tag{5.4}$$

- **Mass-transfer number, B**:

$$B = \frac{c_{pg} \cdot (T_0 - T_e)}{L + c_{pL} \cdot (T_e - T_L)} \tag{5.5}$$

which is a constant for conventional kerosene and gets a value of 3.75 [68].

- **Thermal conductivity of fuel vapor, k.** As defined diagrammatically in [69].

- **Residence time.** This is the time available for a single fuel drop to be burnt as it passes through the combustion zone. It can be defined as:

$$t_{res} = \frac{\rho_{air} \cdot Vol_{comb}}{\dot{m}_{air}} \tag{5.6}$$

5.2.2 Sub-idle combustion issues

The ability of an engine to light at sub-idle windmilling and starting conditions is obviously very important, and the combustor design sizing is therefore based on providing a sufficient volume and on decreasing the flow velocity enough for propagation of the ignition flame.

Many factors effect the combustor at windmilling conditions; ignition, stability limits, fuel temperature, heat soakage, fuel scheduling, and the inlet flow conditions

depending upon the engine operating conditions and flight environment.

The majority of literature in the public domain suggests that the process of combustion under windmill relight conditions is a poorly understood field, due to the expense issues regarding low pressure testing facilities. A further problem with performing ground tests, simulating combustion performance during windmill relights is that the process of combustion can be unstable and produce large quantities of emissions and noise which are required to be contained. These factors result in very little windmill relight test data being available in the public domain thus it is also very difficult to obtain windmill relight combustion data even in the private sector. The theories that surround such operational conditions are also limited, this hence makes the importance of research into such operational conditions vital.

A fully aligned and predictive sub-idle performance model would have the ability to provide the windmilling conditions at the combustor entry prior to light-up. With a preliminary predicted combustor characteristic, the performance model would be able to devise the fueling, combustor inlet conditions, combustion efficiency and combustor volume, required for a given acceleration schedule.

5.2.3 Previous work at Cranfield UTC

A lot of work was conducted within the UTC on sub-idle combustion issues by Howard [51]. Two main objectives set for that research mainly oriented to directly improve the performance solver before enhancing the physical background of the process. Hence, out of necessity, methods were developed to extrapolate the common combustion characteristics (loading - efficiency) towards the sub-idle regime.

Additionally, empirical derivation of the combustion efficiencies during the transient paths has been also attempted by running adaptively the performance model. The backed-out efficiencies were then analysed in respect to the engine conditions.

5.2.3.1 Drawbacks of the previous studies

As described by Howard [51], commenting on the objectives of his research, these are set in the previous paragraph, are based on the assumption that the performance model characteristics are thermodynamically and aerodynamically correct also within the sub-idle and low speed regime. That means that similar flow phenomena are assumed to occur within the entire range of the engine operation allowing the application of the above idle knowledge to the sub-idle region as well.

However, it has been found that the performance extrapolation method is not sufficient to capture the low speed phenomena imposing a significant error in the simulation process. In other words, extrapolating the combustor map leads to insecure conclusions about its performance as the physics are not captured.

As this technique proved erroneous, an adaptive approach involving running the performance model and factoring the combustion efficiency was used in order the second objective to be fulfilled.

5.2.3.2 Feasibility study of evaporation based efficiency modelling

Given that the above mentioned approach is not predictive, some research on the physical mechanisms for sub-idle combustion was carried out in the direction to identify whether the combustion loading approach and the reaction-based modelling were suitable for relight performance simulations.

In this direction, the critical droplet diameter (Eq. 5.4) was investigated in comparison to the SMD for a representative altitude relight condition of Engine A. As found from this analysis and shown in Fig. 5.3, the SMD is significantly larger that the Critical Drop Diameter which indicates that droplet evaporation at these conditions (low pressures and high altitudes), may be limiting the combustion process as mentioned in [51] as well.

Therefore, more research was required to identify other definitions for deriving the combustion efficiency, applying the evaporation rather than the reaction based

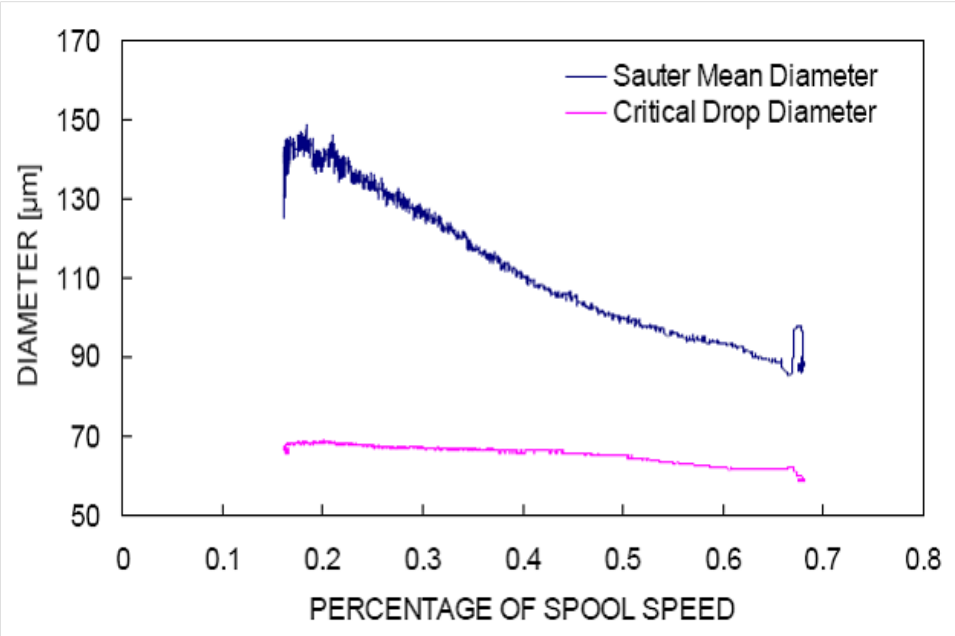

Figure 5.3: Comparison between critical drop diameter and SMD for very low pressure conditions [51].

models. In order the research in this direction to be initiated and given that the fuel evaporation is dependent upon the type of the atomiser, apart from the operating conditions, a better knowledge of the high SMD values around windmilling and sub-idle conditions would be useful. An open literature investigation presenting typical SMD values for sub-atmospheric conditions are discussed by Caines [14]. Additionally, a detailed literature review on this topic is given by Howard in [51], highlighting the direction towards such a research must be oriented without implementing, though, any kind of model to assess its applicability. A detailed definition of current work's aims and objectives can be found in the following section.

5.3 Aims and objectives

Based on the above mentioned observations, as primary aim of this research can be set the development and the feasibility study of the applicability of an evaporation rate based model for sub-idle combustion efficiency calculations. In order to do so, a feeling of the spray characteristics (mainly droplet diameters which affect the

efficiency) must be obtained at low pressure conditions.

At the same time, the range of operation (expressed as percentage of spool speed) within which the reaction rate based and the evaporation rate based models are applicable needs to be determined. This definition is required in order a generic mixed combustion efficiency model to be introduced to be used for the simulation of any transient engine relighting process.

The main objective of this work is to create a CFD model for a two-phase liquid spray in order to conduct an investigation on the behavior of a typical airblast (after sponsor's request) atomizer during altitude relight conditions and the effect of such conditions on its performance regarding the atomization quality as well as combustion efficiency. At these conditions, the low air density results in a lower mass flow going through the atomizer hence, a decreased energy that is used to break-up the liquid sheet. The effect of the liner wall is also taken into account in order to offer a better understanding of the whole combustion system's sub-idle performance. This work was initially carried out by Jad Kozaily [65], [66] and continued by Ahad Mehdi [79], Thermal Power MSc students, closely supervised by Dr. V. Pachidis and the author of this thesis.

5.4 Sub-atmospheric fuel injector performance

The performance of an airblast atomiser under sub-atmospheric conditions is examined in the current section.

5.4.1 Introduction and model description

For the purposes of this study, a high fidelity numerical model of a modern, typical airblast atomiser in service was created according to the specifications of the sponsoring company. The atomizer configuration used in this study is a swirled airblast atomizer. It has three air swirlers, all co-swirling and concentric. The fuel is also

swirled and introduced between the innermost and middle air swirler.

Air swirlers consist basically of several flat or curved vanes mounted either axially or radially at each airflow inlet of the atomizer. They are to generate swirl components to produce strong shear stresses for a better atomization while the main role of the outer swirler, also called dome swirler, is to cause recirculation in the primary zone of the combustor. The full geometry of the airblast atomizer can be seen in Fig. 5.4.

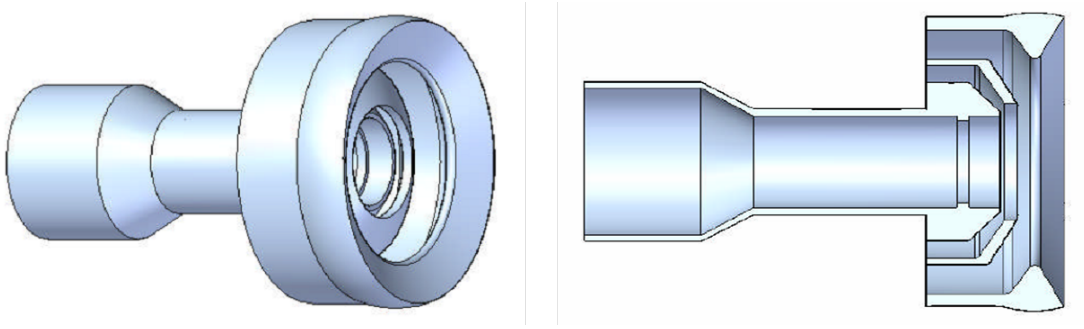

Figure 5.4: CAD design of the swirl airblast atomiser [65].

A close description of the numerical atomiser model is given in Fig. 5.5, while the generated computational domain is presented in Fig. 5.6.

The domain consists of seven main boundaries listed as follows: Three swirling air inlets for the injector, one co-flow air inlet, a pressure outlet, an outer wall and the rotational periodic boundary.

The **co-flow air** describes the gas surrounding the injector [68]. In order to keep droplets recirculation to a minimum, a low co-flow air velocity of 1 m/s was supplied parallel to the direction of injection in all cases.

Even though this is a cruel assumption, the initial simulations were performed at this conditions in order the pressure effects to be isolated. In addition, a use of a realistic co-flow velocity value without any liner walls modelled would be unjustified. In that respect, it was decided to keep the co-flow velocity to a minimum and to examine its effect in a second approach where also the combustor chamber would be included in the modelling (see following section).

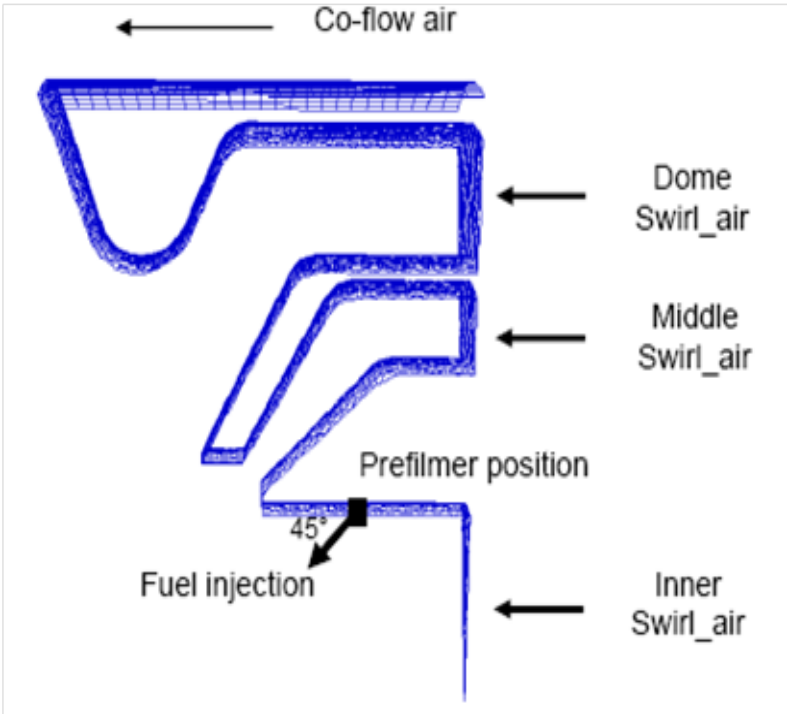

Figure 5.5: The airblast atomiser model [65].

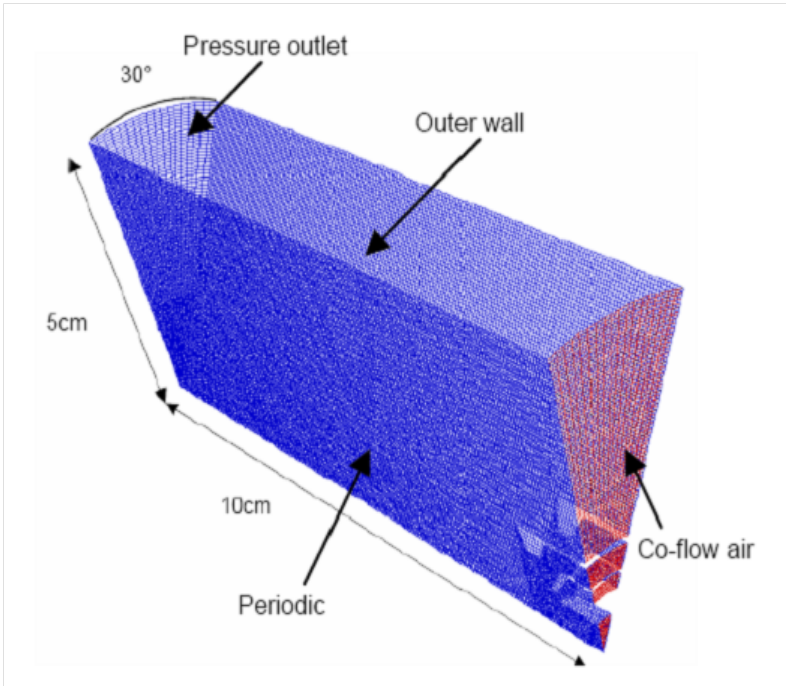

Figure 5.6: The computational domain and the boundaries [65].

More details about the simulation strategy (mesh sensitivity study, coupling between the discrete and the continuous phase etc.) and the assumptions done within this work can be found in [65].

5.4.2 Case studies

In general, the work was divided into three main case studies as shown in Fig. 5.7. The objective of the first one was to investigate the effect of sub-atmospheric pressures upon the spray structure while keeping all the other parameters constant. The second and third cases aimed respectively at highlighting the difference in the effect of fuel flow and relative velocity upon the SMD, between atmospheric and sub-atmospheric conditions.

P [KPa]	:	101	41	31			
Vrel [m/s]	:	28					
AFR	:	1.4					
$\dot{w}_f$ [g/s]	:	12					
P [KPa]	:	101	80	62	41		
Vrel [m/s]	:	28					
AFR	:	2	1.8	1.6	1.4	1.2	
$\dot{w}_f$ [g/s]	:	8.4	9.24	10.5	12	14	
P [KPa]	:	101	41				
Vrel [m/s]	:	10	15	20	28	40	50
AFR	:	2	1.6	1.2			
$\dot{w}_f$ [g/s]	:	8.4	10.5	14			

Figure 5.7: Case studies [65].

5.4.3 Results and discussion

The results of this study and discussion is carried out in the current section.

5.4.3.1 Effect of sub-atmospheric conditions

Droplet distribution. The spray quality was examined at the atmospheric and the two sub-atmospheric conditions. The first feature to notice is the increase in mean diameters at altitude relight conditions compared to atmospheric. The overall mean diameter increased by 50 to 100% at sub-atmospheric conditions. However, the impact on the Sauter Mean Diameter was greater where SMD values degraded from 100 μm at atmospheric conditions up to 200 and 300 μm at 41 and 31 kPa respectively. Droplet distributions are presented hereafter for the three considered conditions. In order to keep the same scale for all the distributions, the droplet diameters data for the sub-atmospheric cases were truncated at the value corresponding to the maximum diameter found at the atmospheric case. However, the detailed spray composition will be discussed in the next section.

The data presented in Fig. 5.8 through 5.10 show the widening in droplet sizes at altitude relight conditions compared to the atmospheric case. The range of droplet diameters broaden from [0 - 200] μm at atmospheric to [0 - 500] μm at sub-atmospheric conditions. The widest size distribution was found at 31 kPa.

Furthermore, the Weber number calculated for the droplets near the atomizer prefilmer at each condition indicated a transition from the shear breakup mechanism to the multimode break-up ($We_{101} = 107$, $We_{41} = 42$, $We_{31} = 33$). This was reflected by the maximum diameter profiles that were recorded at the three conditions. In fact, the maximum droplet diameter for the two sub-atmospheric cases was found to exceed the liquid sheet thickness ($D_{max,41} = 1.8mm$, $D_{max,31} = 2.4mm$). This indicates that the primary breakup at these conditions is indeed poor.

This confirms what one might expect intuitively that a decrease in air density would result in lower shear stresses that are unable to provide complete atomization of the liquid sheet. However, more comments can be made here. First, a decreased air density would be expected to increase the Liquid / Gas relative velocity; hence, providing a better atomization. However, since the Liquid / Gas relative velocity in

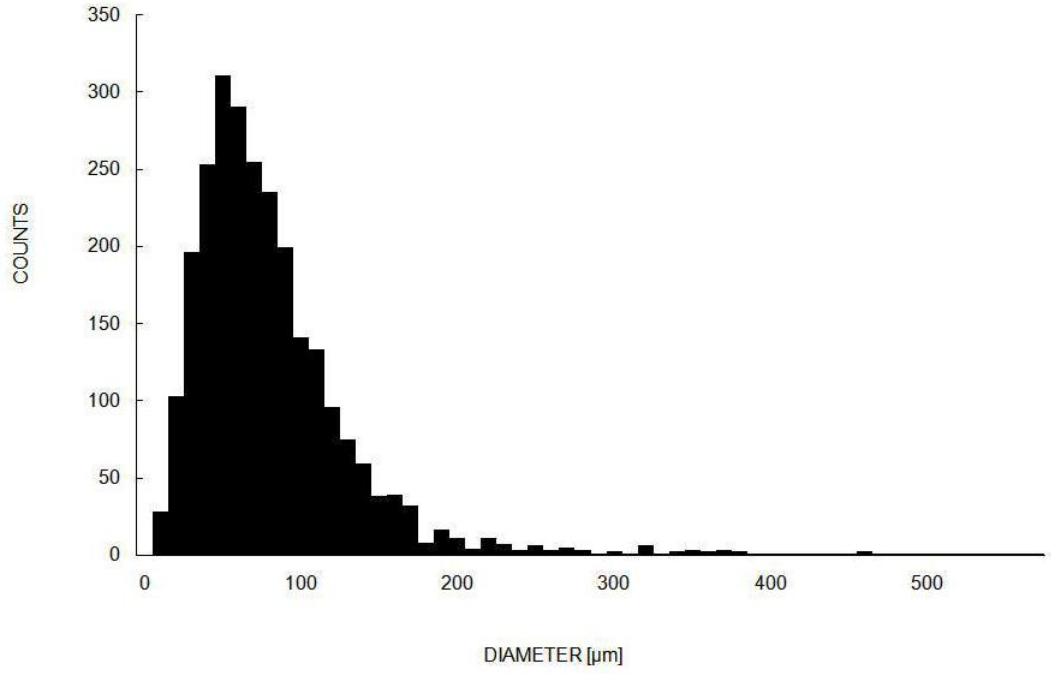

Figure 5.8: Droplet distribution at atmospheric conditions [65].

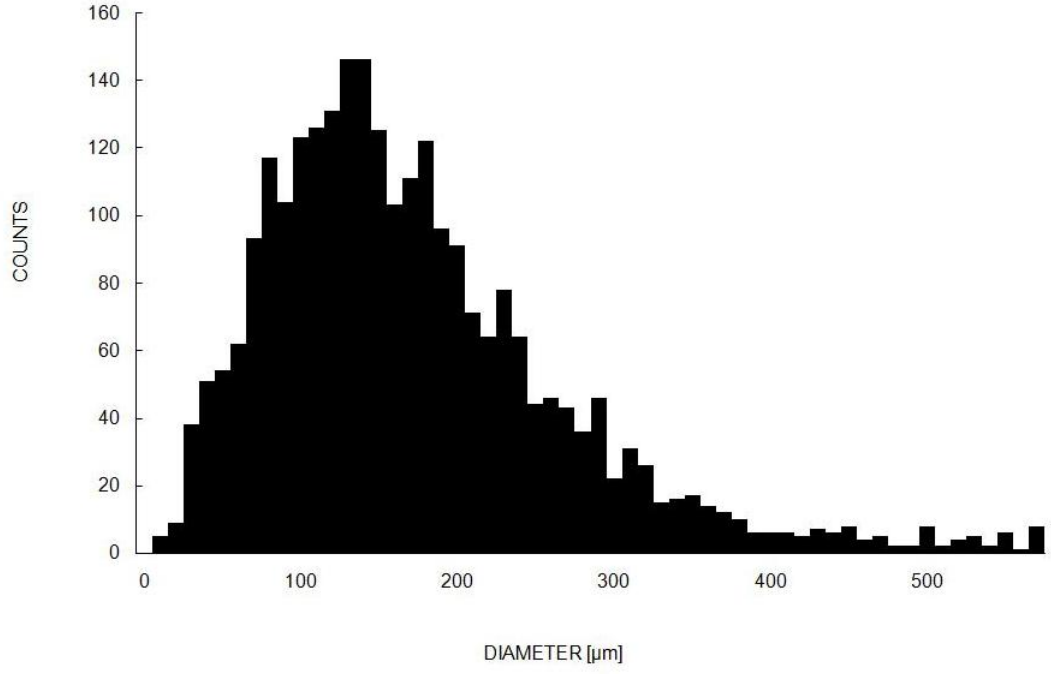

Figure 5.9: Droplet distribution at 41kPa [65].

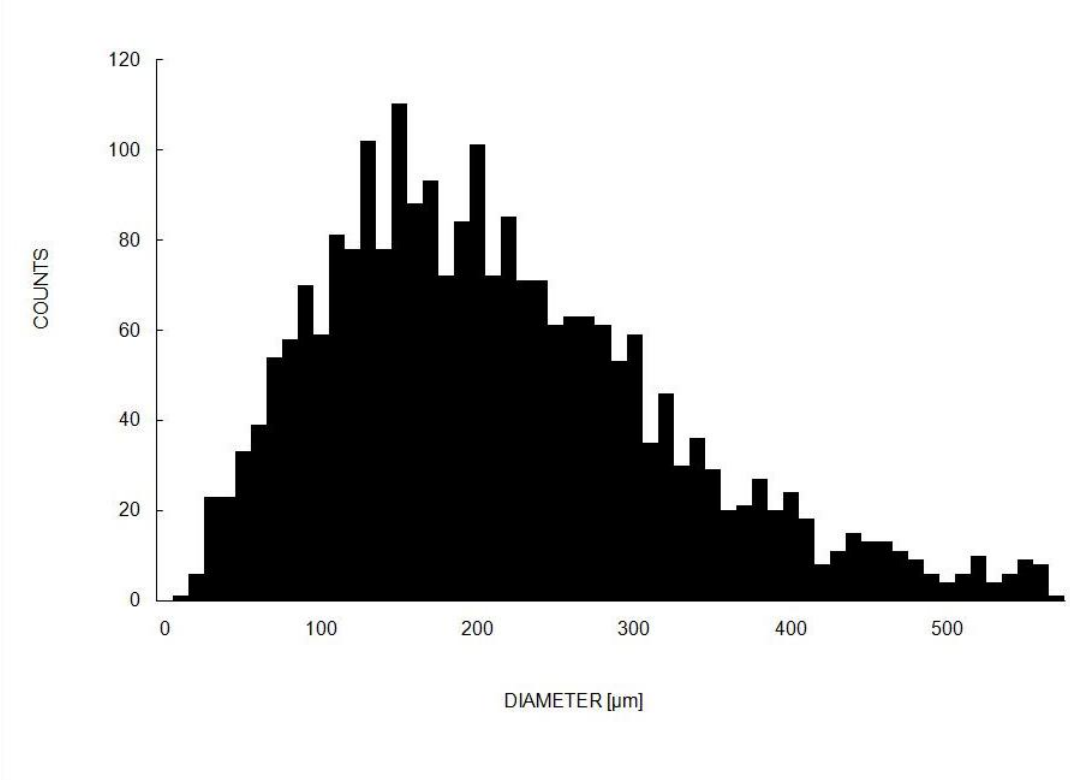

Figure 5.10: Droplet distribution at 31kPa [65].

this study was kept constant, an attempt to explicit the reasons for such increase in droplets' size would therefore conform more to the reality. Suggestions for the possible explanations are:

- The decreased air density yielded a lower mass flow passing through the atomizer resulting in a lower energy to shatter the liquid sheet.
- The influence of low air pressure resulted in smaller aerodynamic forces acting on the droplets.
- Despite that low density air penetrates better between the liquid droplets, the low ambient pressure provided a thin atmosphere that was unable to prevent droplets coalescence. This effect made the situation worse as the droplets inertia became bigger and vise versa.

Second, no single cause can completely explain the total degradation of the spray under windmilling altitude relight conditions. Other factors like the combustor

aerodynamics and geometry would highly affect the spray dynamics in terms of droplets recirculation, penetration etc.

Spray structure. In order to shed more light on the different spray structures, it was decided to quantify the composition of the sprays at various positions downstream the injector. Shown in Fig. 5.11 is the Rosin-Rammler distribution plotted for the three conditions. It can be seen that 95% of the droplets diameter at atmospheric conditions are below 150 μm whereas for the two sub-atmospheric cases, 40% and 20% of the droplets are of diameter greater than 200 μm and 400 μm respectively. The degree of axial and circumferential uniformity was examined by looking at the percentage of liquid volume at different positions along the injector center line. The data obtained are illustrated in Fig. 5.12 and Fig. 5.13.

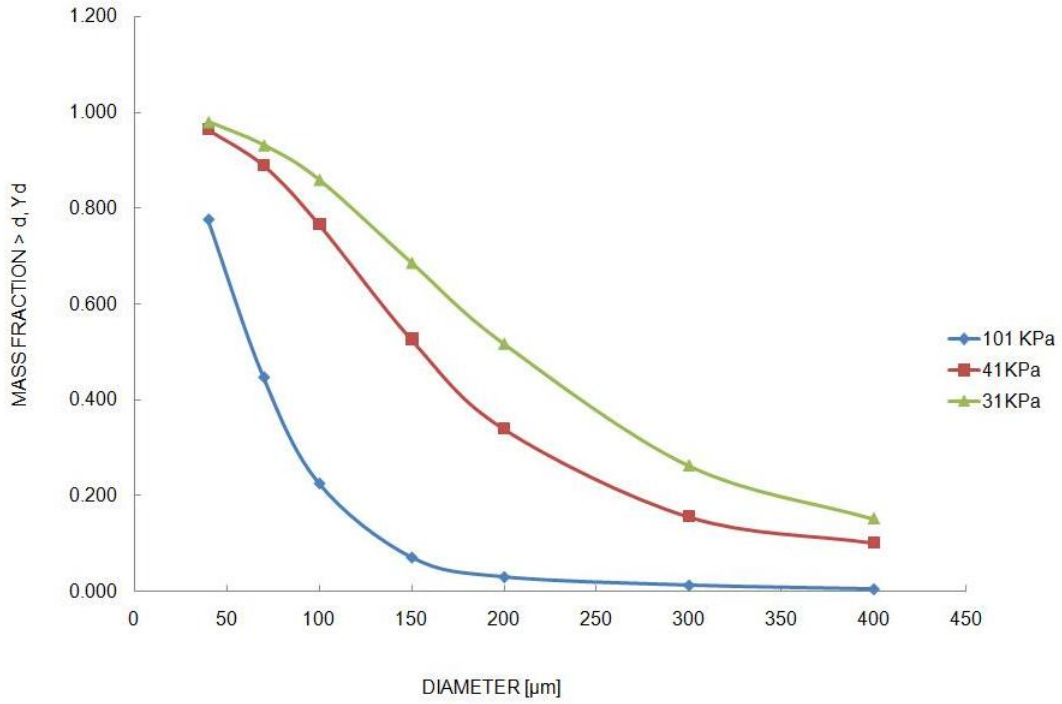

Figure 5.11: Rosin-Rammler distributions for the considered cases [65].

Spray dynamics. The particle velocity is illustrated in Figs. 5.14 through 5.16 for the atmospheric and sub-atmospheric conditions (101, 41 and 31 kPa respec-

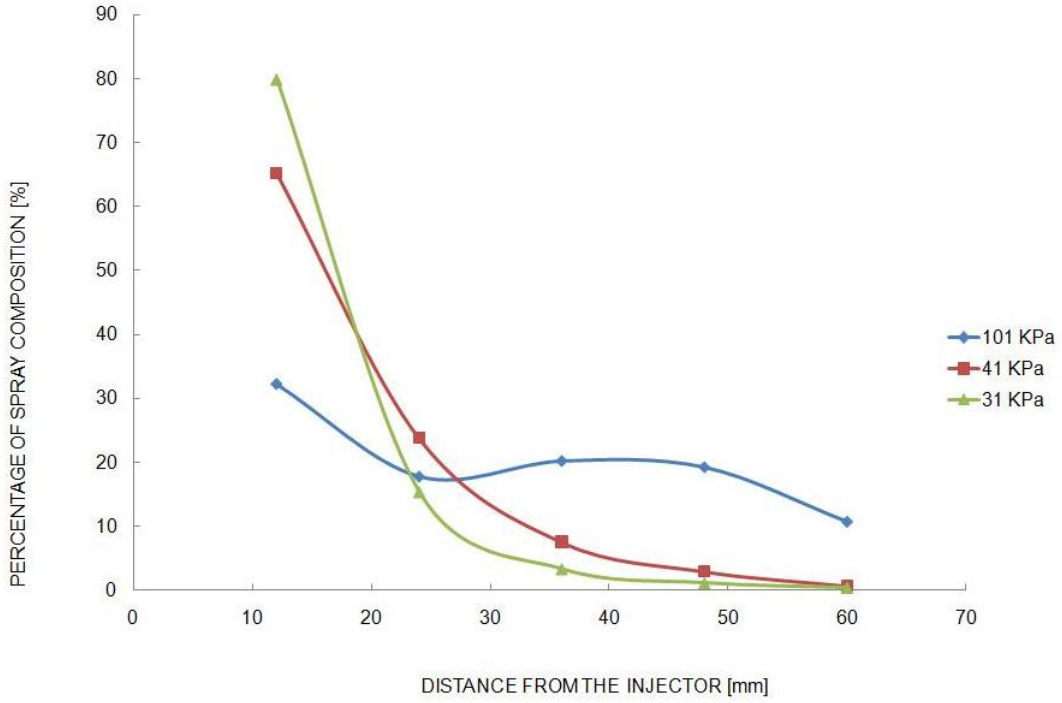

Figure 5.12: Spray composition along the injector center line [65].

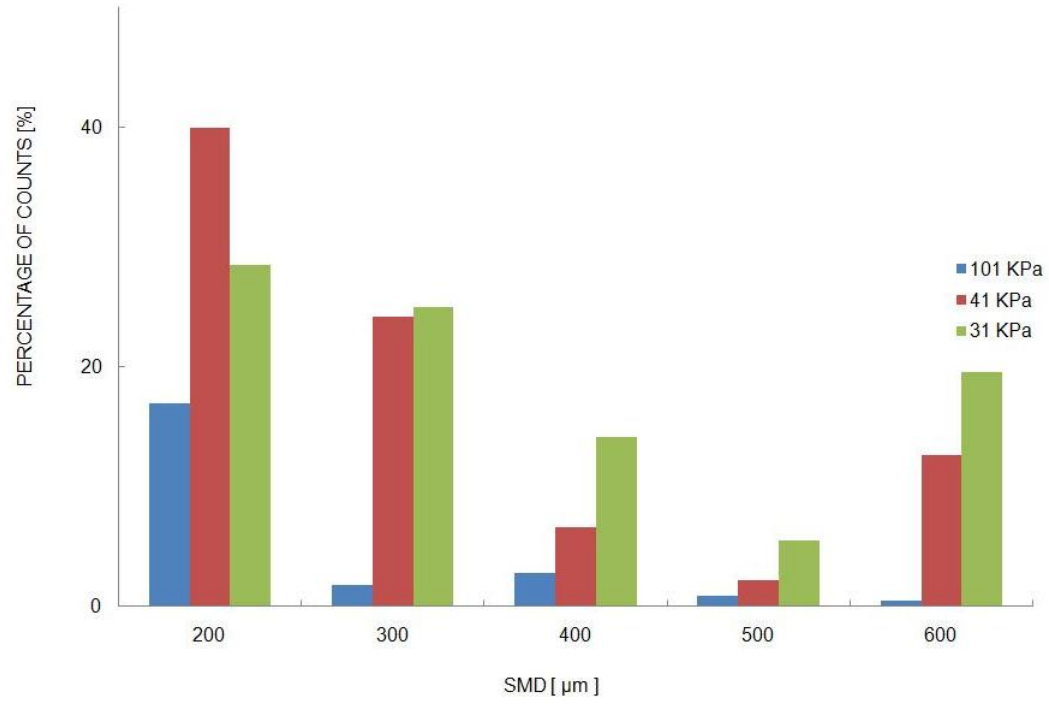

Figure 5.13: Spray composition 12mm downstream of the injector [65].

tively). From this comparison can be observed that for the first case, a high velocity magnitude is maintained by the particles for a longer distance from the injector than in the latter case. In addition, the maximum velocities observed at 101 kPa are significantly higher than the maximum velocities in the 41 kPa case by at least 50%. For the atmospheric case, droplet velocities increase as the spray radius increases. The maximum velocities are observed at the mid-radius of the spray while further downstream, the values are gradually decreasing to become minimum at the boundaries. It is also worth to be mentioned that the maximum velocities are reached by the droplets located in the inner layer of the spray which is the part of the discrete phase interacting with the highest velocity air (it is reminded that the external swirl air streams are decelerated due to the interaction with the low speed surrounding air). A similar trend in the velocity distribution is not observed in the sub-atmospheric cases. The particle velocity increases gradually until it reaches a maximum at the spray penetration limit. This is due to the low concentration of droplets that are dispersed in the gas phase in that region which provided a high Air / Liquid proportion.

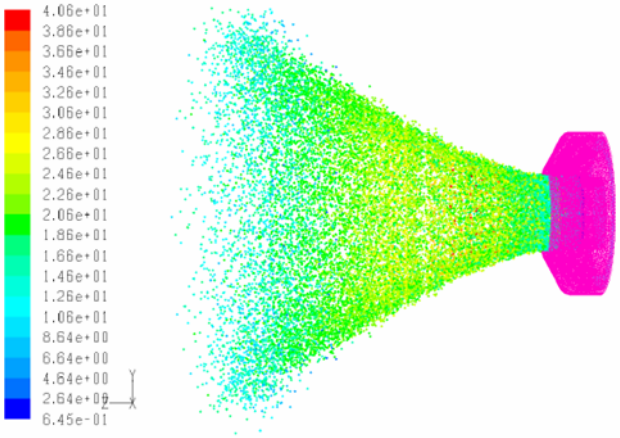

Figure 5.14: Droplets - velocity magnitude - 101kPa [65].

In addition, jet penetration at the three conditions was examined. Considering the same injection time, a contraction in the spray at sub-atmospheric conditions is observed compared to atmospheric. The resulting spray structure could therefore

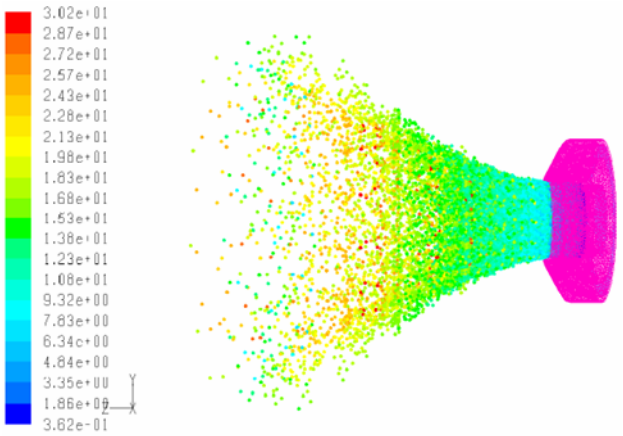

Figure 5.15: Droplets - velocity magnitude - 41kPa [65].

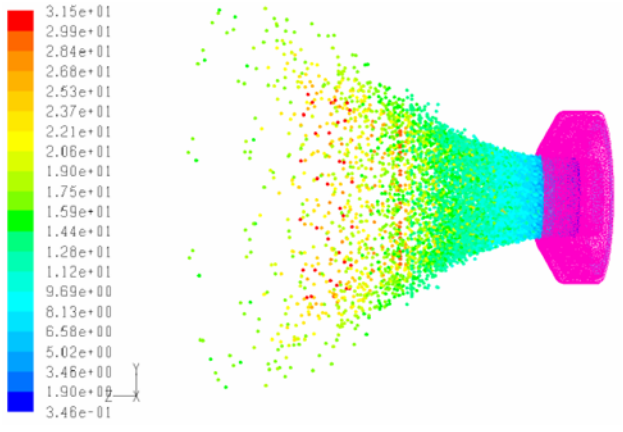

Figure 5.16: Droplets - velocity magnitude - 31kPa [65].

be looked at as being composed of two sub regions: a dense area that lies from the injector to the mid radius and a well dispersed region after that. Considering the mass averaged droplet penetration, it can be observed in Fig. 5.17 through 5.20 that the axial and radial penetration at 41 kPa is 40 to 45% decreased in comparison to the 101 kPa case, resulting in a poor fuel-air mixing. Since the geometry of the combustion chamber also affects the homogeneity of the fuel-air mixture, it can be said that taking this aspect into consideration during the design phases of the engine combustor, the overall combustion performance can be significantly improved.

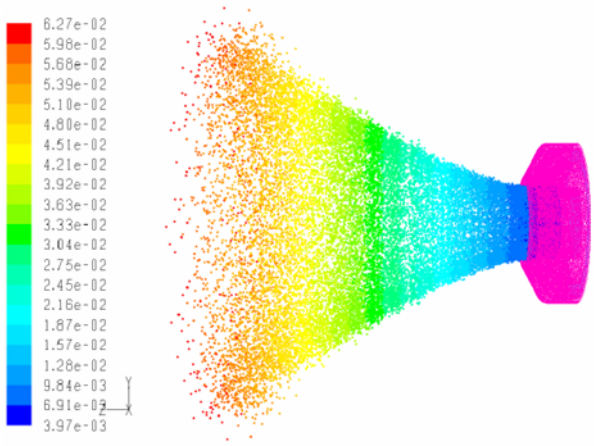

Figure 5.17: Droplets - penetration - 101kPa [65].

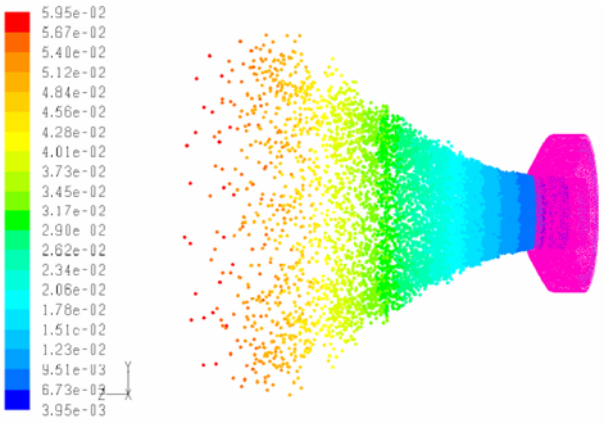

Figure 5.18: Droplets - penetration - 41kPa [65].

Regarding finally the particle residence time presented in Fig. 5.21 and Fig. 5.22 for the 101 kPa and the 41 kPa cases respectively, it can be seen that the injection

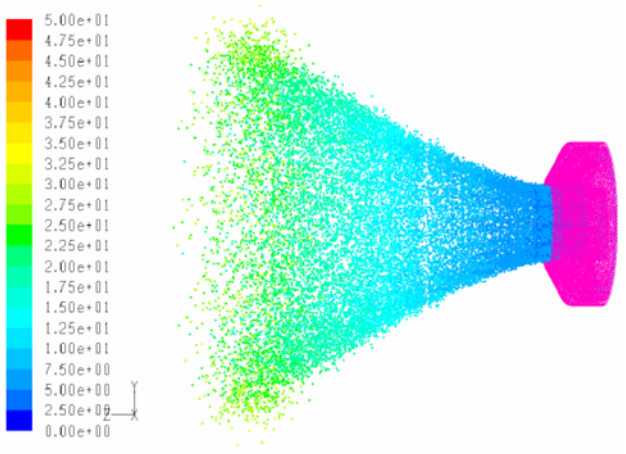

Figure 5.19: Droplets - radial coordinate - 101kPa [65].

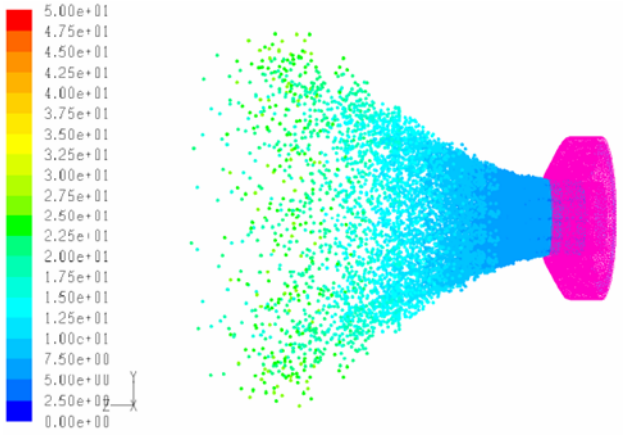

Figure 5.20: Droplets - radial coordinate - 41kPa [65].

at atmospheric conditions creates a downstream propagating jet since the particles with the highest residence time are exclusively located at the spray penetration limit. On the other hand, at sub-atmospheric conditions quite big recirculation areas can be observed which results in a non uniform distribution of the particles within the spray structure, since as shown also in the picture, droplets of high residence time are almost everywhere inside the jet.

This is also obvious from the pathlines and velocity contour plots, Fig. 5.23 and 5.24, for the continuous phase which reveals the flow recirculation in the regions surrounding the fuel jet.

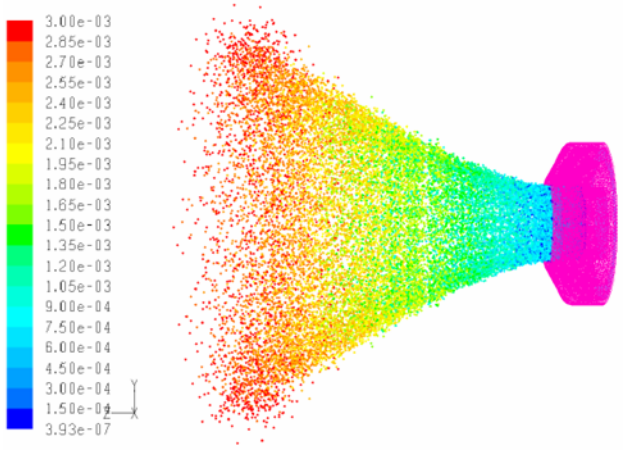

Figure 5.21: Droplets - residence time - 101 kPa [65].

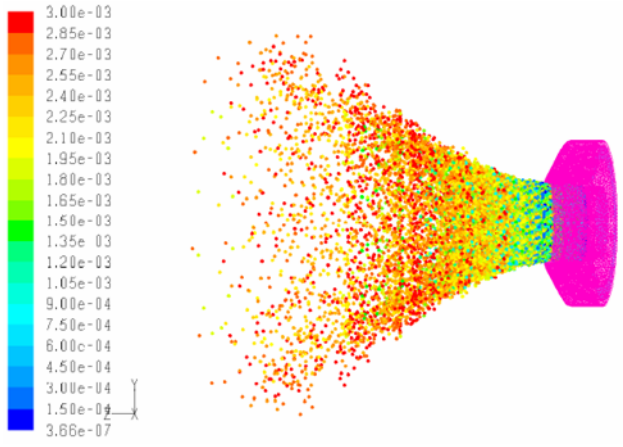

Figure 5.22: Droplets - residence time - 41 kPa [65].

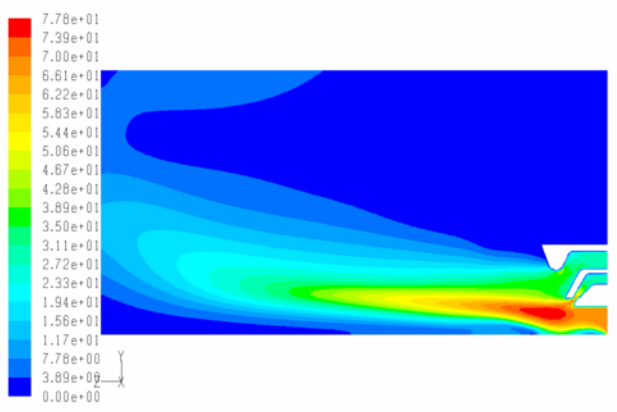

Figure 5.23: Continuous phase - velocity magnitude - 101 kPa [65].

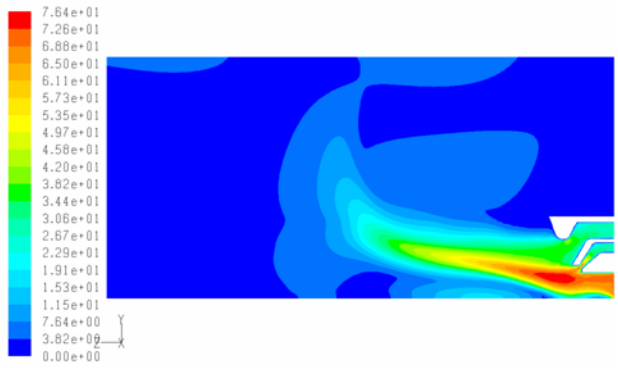

Figure 5.24: Continuous phase - velocity magnitude - 41 kPa [65].

5.4.3.2 Effect of fuel flow rate

This section presents the effect of different fuel flow rates on the SMD. SMD values as a function of pressure are presented in the following plot for a range of liquid flow rates. The results show that for atmospheric conditions, the SMD is less dependent upon the fuel mass flow than at lower pressures. In addition, the SMD values are rapidly increasing as the pressure decreases. However, a stabilization seems to appear for the lowest sub-atmospheric pressures simulated (left side of the curve), which indicates a threshold of pressure where SMD values stop to increase.

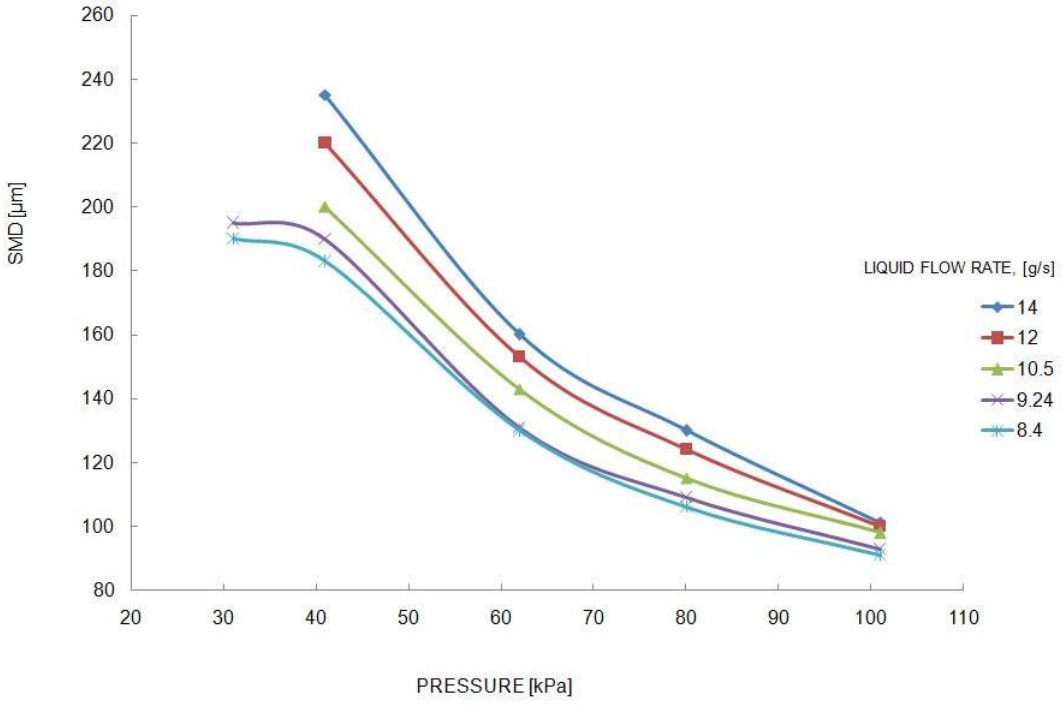

Figure 5.25: SMD as a function of operating pressure at different fuel flow rates [65].

In an attempt to explicitly express the SMD dependency upon fuel flow, a different representation of the above data is presented in Fig. 5.26. The SMD values have been plotted as a function of fuel mass flow for the different pressure conditions simulated. At atmospheric pressure, the results show an increase of 11% in the Sauter Mean Diameter between the lowest and highest fuel flow rate simulated. This

is because, for the same air mass flow, the AFR is reduced. Therefore, the amount of air momentum per unit mass of liquid is decreased and the total energy of the air is no longer sufficient to provoke the same degree of atomization. However, at 41kPa, the increase in SMD reached 28.5%. This indicates that at sub-atmospheric pressure, the SMD becomes more dependent upon the fuel flow rate.

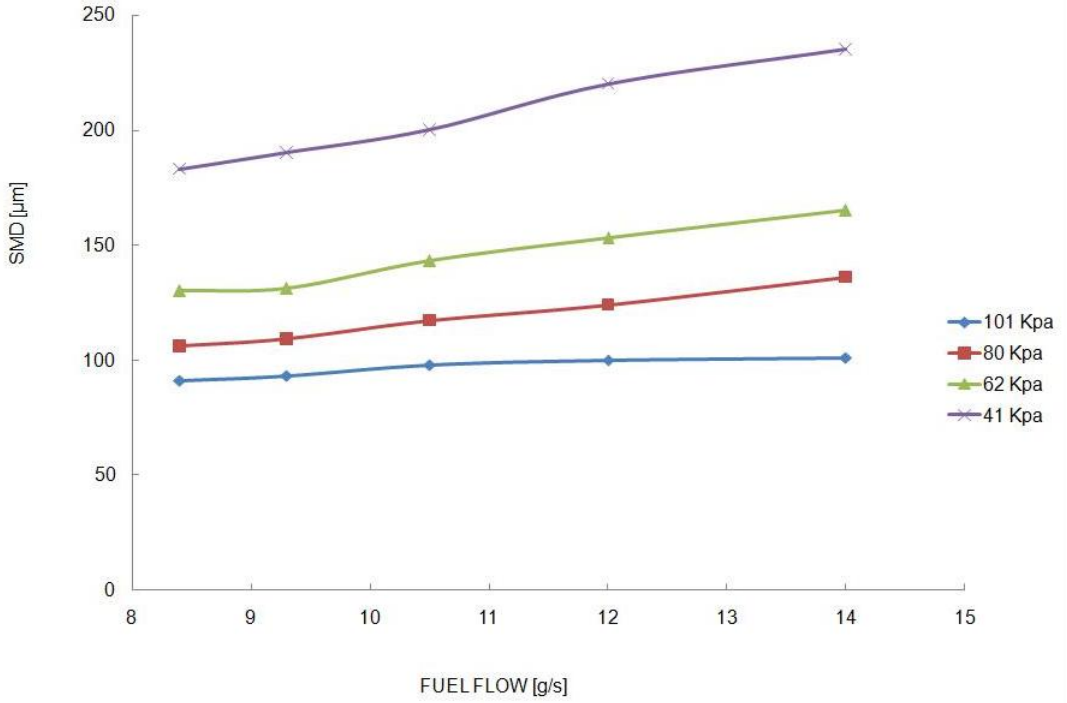

Figure 5.26: SMD as a function of fuel flow at different sub-atmospheric conditions [65].

Generally, the dependency on fuel flow including many other factors is used to define the performance of the atomizer, trying to predict the SMD values by a logical combination of these parameters.

The correlation of the present data as also illustrated in Fig. 5.26 above. It shows that at atmospheric pressure, the predicted exponent of the fuel mass flow is fairly close to the one in the analytical expression for the SMD of a *pressure swirl* atomizer (and not of an airblast atomiser) provided by [68] and [69] as follows:

$$SMD = 4.4 \cdot \sigma^{0.6} \cdot \mu_L^{0.16} \cdot \rho_L^{0.16} \cdot \dot{m}_L^{0.22} \cdot \Delta P_L^{0.43} \tag{5.7}$$

However, at sub-atmospheric conditions, a shifting of the curves can be observed. This can be better described by an exponent value of 0.5 as far as Eq.5.53 is concerned. This value appears to be constant for the various sub-atmospheric pressures simulated. This can be seen as, at conditions of low air velocity, the airblast atomizer might be behaving like a pressure swirl which relies only on the fuel pressure drop to create the Liquid / Gas relative velocity for break-up. This raises the interest in investigating the performance of the airblast atomizer at these conditions using pressure swirl correlations.

Nevertheless, the numerical solver employed, considers the liquid sheet thickness identical to the prefilmer gap. This assumption could only be considered valid at conditions of full power where the fuel pressure is at its maximum. This will be far from the windmilling relight case where the fuel pressure is at its minimum and cavitation phenomena are to occur very frequently.

5.4.3.3 Effect of relative velocity

The effect of low relative velocity case was studied in an attempt to highlight the difference in the spray deterioration between atmospheric and sub-atmospheric conditions. Attention is given to the threshold of relative velocity where atomization is no longer possible [9].

SMD values as a function of relative velocity are plotted in Fig. 5.27 for 101 kPa and 41 kPa absolute pressures. Fuel flow was kept constant (8.4g/s). For the two test conditions, it could be seen that as the relative velocity decreases, the SMD increases. This is due to the decreased low aerodynamic shear stresses. However, at sub-atmospheric conditions, the SMD sensitivity to increase could be easily revealed while it is not the case at atmospheric condition. At 15 m/s relative velocity, the increase in SMD at 41 kPa is 40% higher than at 101 kPa, both compared to the

initial drop sizes at the highest relative velocity.

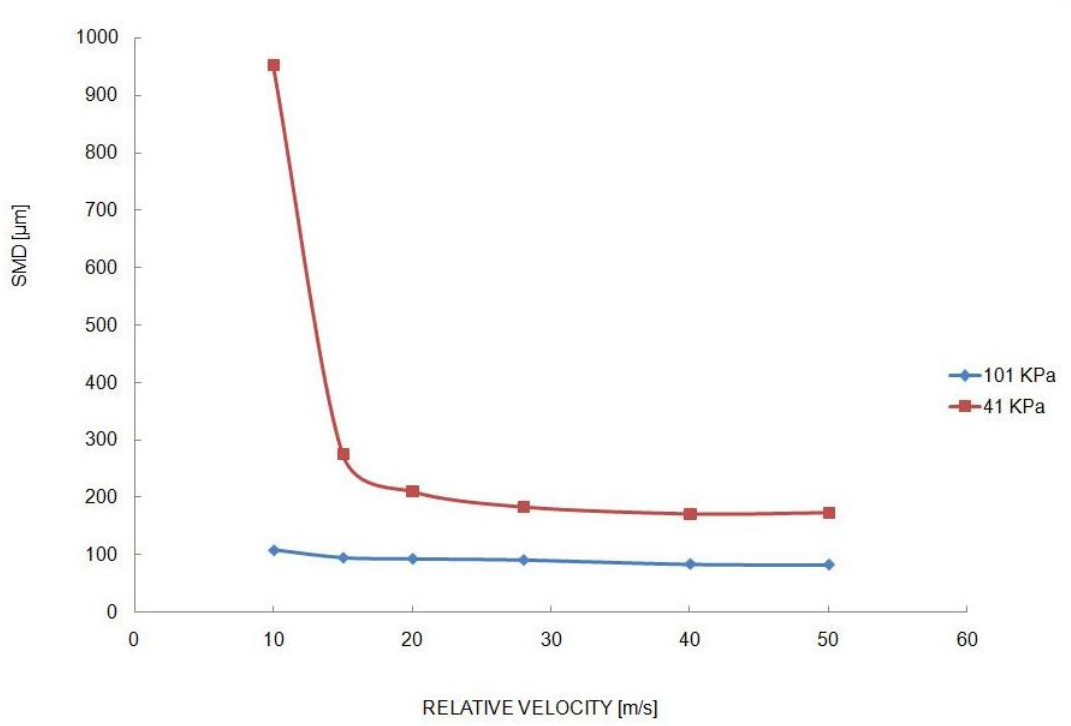

Figure 5.27: Influence of relative velocity upon SMD [65].

The most interesting feature concerns the observed quality of the spray at the lowest two relative velocities. At 15 m/s, both sprays maintained a minimum level of atomization, however, at 10 m/s, a loss of the spray at sub-atmospheric conditions is observed (Fig. 5.31) while the spray maintained a good structure at the atmospheric case (Fig. 5.30). This total degradation in atomization is also reflected by the high value of SMD which is close to the prefilmer gap size.

This could also be interpreted as, in order to prevent the loss of the spray that occurred at sub-atmospheric condition, an additional 5 m/s of relative velocity for the present test case could compensate the adverse effect of low air density compared to atmospheric. This sounds a plausible explanation since the atomization process in airblast atomizers could be improved either by increasing the air velocity, air density or AFR if the liquid properties were kept the same.

In order to reveal if the above trend in SMD augmentation would be influenced by

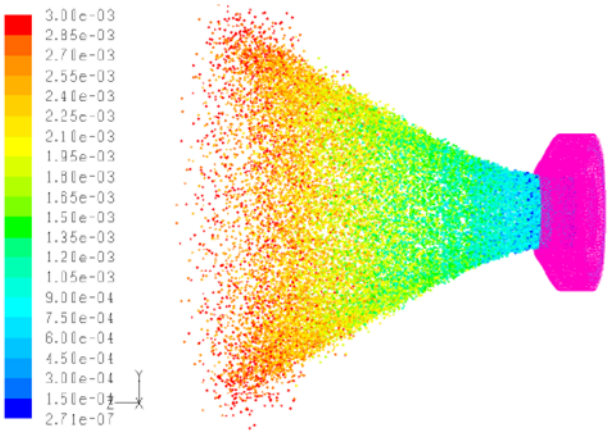

Figure 5.28: Spray structure - Relative Velocity = 15 m/sec - 101 kPa [65].

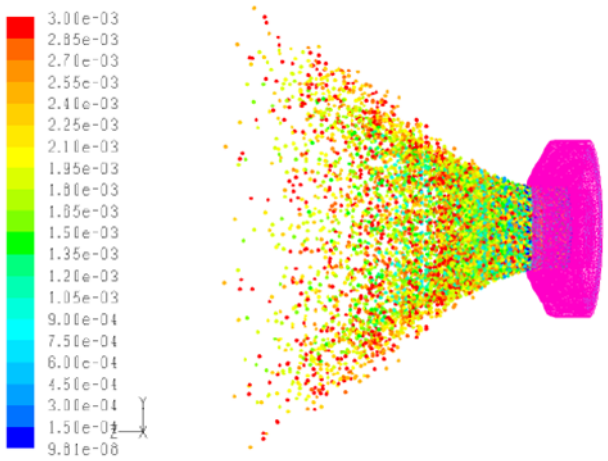

Figure 5.29: Spray structure - Relative Velocity = 15 m/sec - 41 kPa [65].

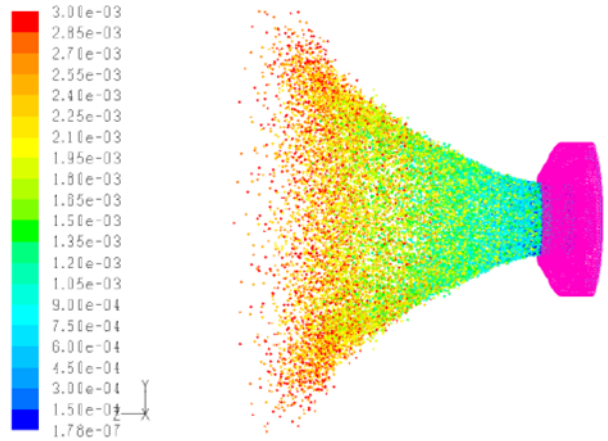

Figure 5.30: Spray structure - Relative Velocity = 10 m/sec - 101 kPa [65].

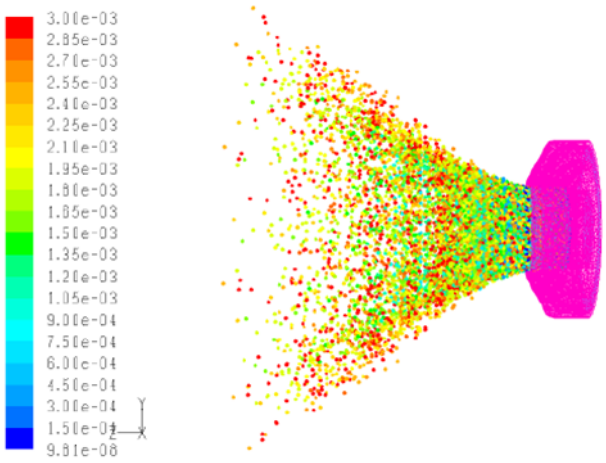

Figure 5.31: Spray structure - Relative Velocity = 10 m/sec - 41 kPa [65].

the quantity of fuel flow injected, three different liquid flow rates were also simulated for the 41 kPa case. Inspection of the results as summarized in Fig. 5.32 shows that for a fixed sub-atmospheric pressure, when the relative velocity decreases, the trend of the increment in SMD for various fuel flows keeps approximately the same aspect.

5.4.4 General comments - Concluding remarks

In this section a preliminary numerical assessment of the performance of a fuel injector at low power conditions was presented. The liner wall was not taken into account in this study in order its effect to be studied separately having first assessed the performance of the stand alone atomiser, isolating this way the influence of every parameter that affects the problem. Three case studies were performed to investigate the effect of sub-atmospheric pressures, Air Fuel Ratio and Liquid / Gas relative velocity upon the quality of the fuel spray under sub-atmospheric conditions. The results showed:

- Droplet size distribution expressed a significant broadening at sub-atmospheric conditions [0 - 500] μm compared to atmospheric [0 - 200] μm. SMD was found to increase by a factor of 2 and 3 at 41 and 31 kPa respectively.

- At sub-atmospheric conditions, a high concentration of larger droplets was lo-

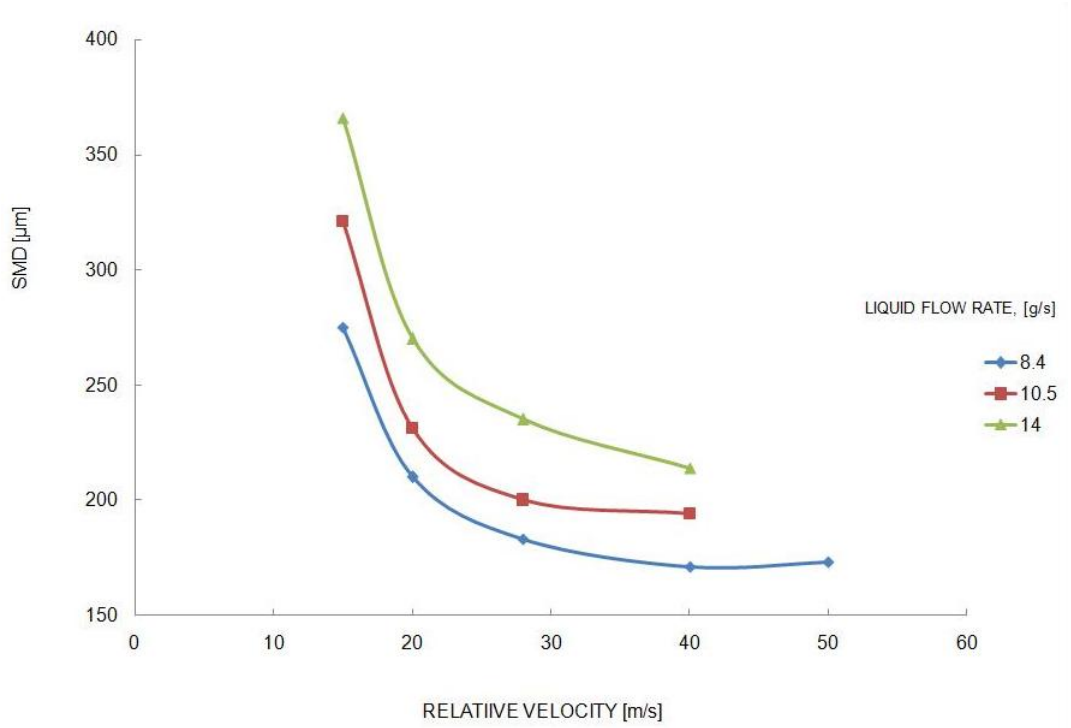

Figure 5.32: Influence of relative velocity upon SMD at 41 kPa for different fuel flows [65].

cated near the injector doubling the volume of liquid at the mentioned position compared to atmospheric conditions.

- Low air density yielded in lower aerodynamic forces that were unable to drive the droplets at a velocity close to the atomising air stream.

- The spray penetration at relight conditions was found decreased by 40 to 45% in comparison to the atmospheric case resulting in a poor Fuel-Air mixing.

- SMD revealed high sensitivity to increase with fuel flow rate at altitude relight conditions. As a preliminary performance investigation, the prefilming airblast at conditions of low air velocity is believed to act like a pressure swirl atomizer at low air pressures.

- The existence of a threshold for minimum relative velocity before the loss of spray was observed higher at altitude relight compared to idle. This was

perceived to diminish the operability range of the atomizer under altitude relight conditions.

Having made the above mentioned observations the effect of the liner wall in the injection procedure will be presented in the following section.

5.5 Effect of liner wall on atomiser's performance

The geometry of the airblast injector is maintained as described previously, while the liner wall of Engine A is now added. Its effect on the performance of the atomiser, as well as spray dynamics studies will be presented in section 5.5.1. Furthermore, a parametric study in terms of combustor size is discussed in section 5.5.4. The cases under investigation are the same as before (see section 5.4.2) for compatibility purposes.

5.5.1 Model definition

The liner of engine A is included in the basic injector model as illustrated in Fig. 5.33.

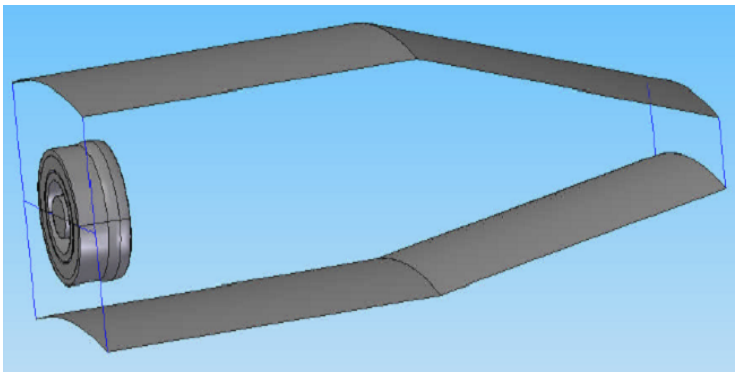

Figure 5.33: 3D view of injector model including liner wall [79].

The entire domain consists of eight main boundaries as shown in the Figs. 5.34 and 5.35:

The CFD simulation strategy followed is described in great detail in [79] and will not be included in the current thesis. It is only to be emphasized that the value of

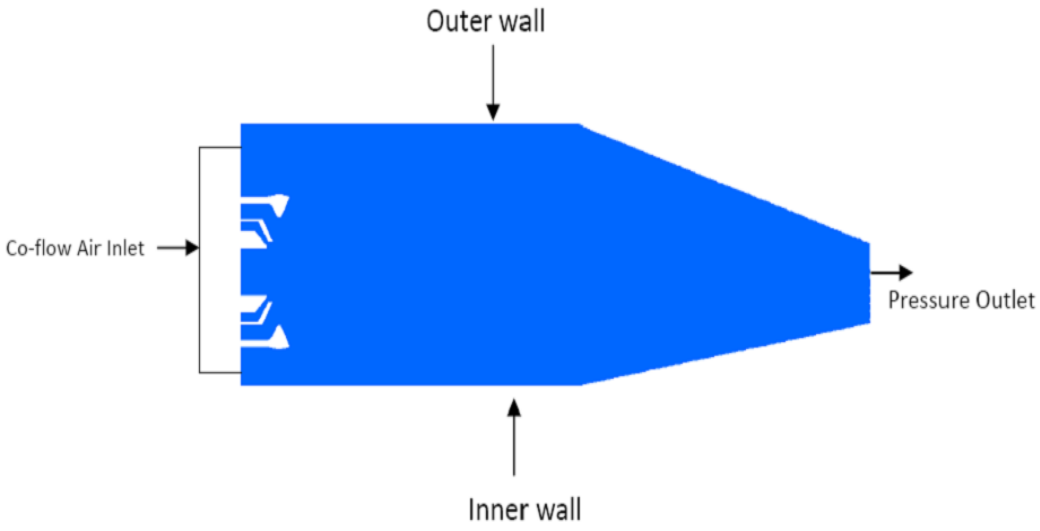

Figure 5.34: Cut section of the injector-combustor model [79].

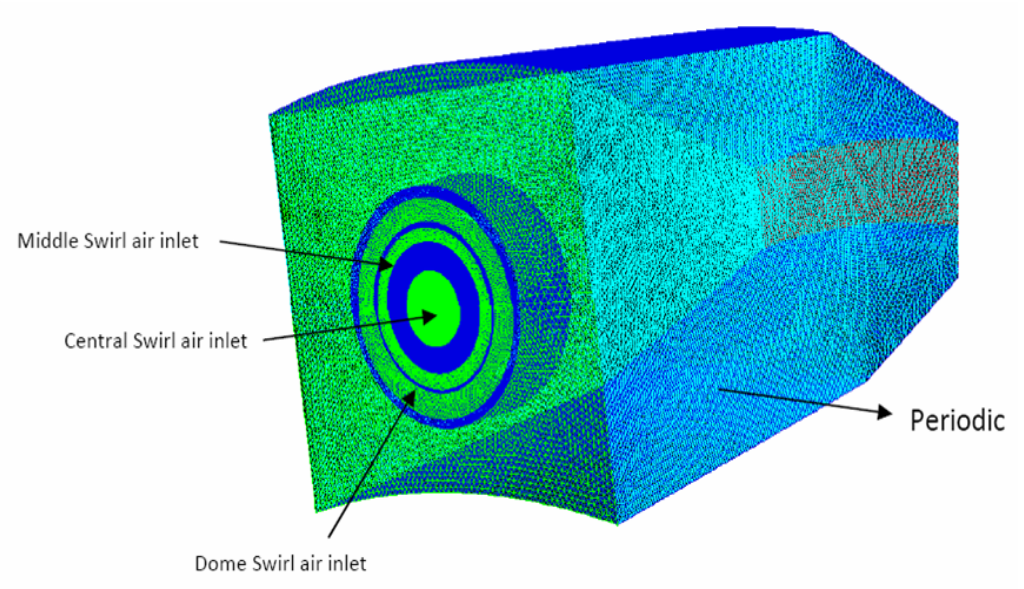

Figure 5.35: Boundary types of the injector-combustor model [79].

the co-flow velocity has now been set to a more realistic value (18 m/s), dropping this way the assumption of the almost non existing co-flow velocity used in the stand alone atomiser model. This way the interaction between the co-flow stream and the fuel-air mixture injected into the combustor can be also taken into account.

5.5.2 Solver's validation

The model has been compared against experimental data provided by the sponsor. The objective of the validation was to identify the error within which the numerical tool is capable of predicting the SMD of the fuel droplets under the specified conditions.

The outcome of this comparative study was a deviation within 10% over-prediction of the SMD value at the given conditions of pressure, temperature and fuel flow rate.

5.5.3 Results and discussion

As done in a previous section, the effect of various conditions in the performance of the injector is herein presented.

5.5.3.1 Effect of sub-atmospheric conditions

Droplet distribution. The fuel spray structures at different sub-atmospheric conditions were analyzed in terms of droplet diameter distribution. A wide broadening of droplet diameter was observed for two sub-atmospheric pressures (corresponding to different altitude relight cases).

At atmospheric conditions (101 kPa) it varied from 0 to 120 μm and having Sauter Mean Diameter (SMD) of only 65 μm. However, the droplet size showed an extensive broadening at the sub-atmospheric cases at 41 kPa and 31 kPa, ranging from [0 - 300] μm and [0 - 400] μm respectively as shown in the following figures.

It should be noted that the number of particle counts in the stand-alone injector model is less, as only a 30 deg section was modelled and represents only the number

of fuel particles in that region. Therefore, in the comparative plots the counts of the early model are reflected by the right hand side vertical axis.

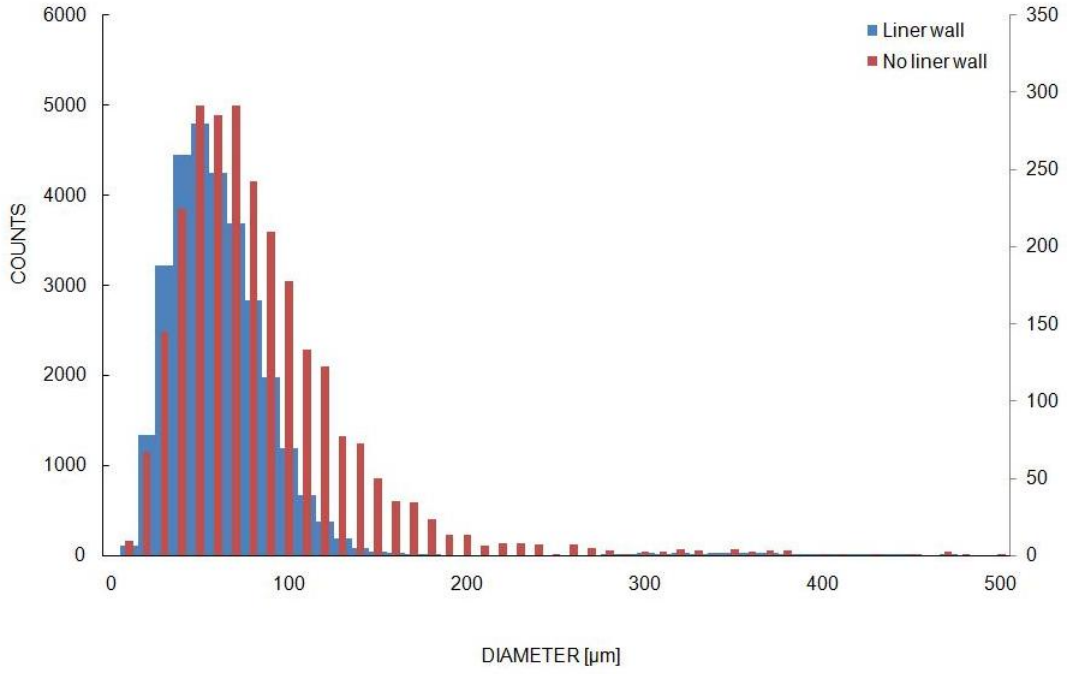

Figure 5.36: Droplet distribution at atmospheric conditions with and without liner [79].

The following schematic summarises the effect of sub-atmospheric conditions on the two configurations.

A wide broadening of droplet diameter was observed when the liner wall geometry was included to the simulation from atmospheric to sub-atmospheric conditions. This was expected as for sub-atmospheric conditions, air density decreases thus reducing the shear stresses, which results in poor atomisation of the fuel liquid sheet. However, a decrease in air density should increase the fuel / air relative velocity near the injection point, which should provide a better atomisation environment. But as stated in the last chapter, the fuel / air relative velocity was kept constant at 28 m/s for all the simulations, which is a typical velocity at these sub-idle conditions. As a consequence, the effect of low atmospheric pressure results in low aerodynamic

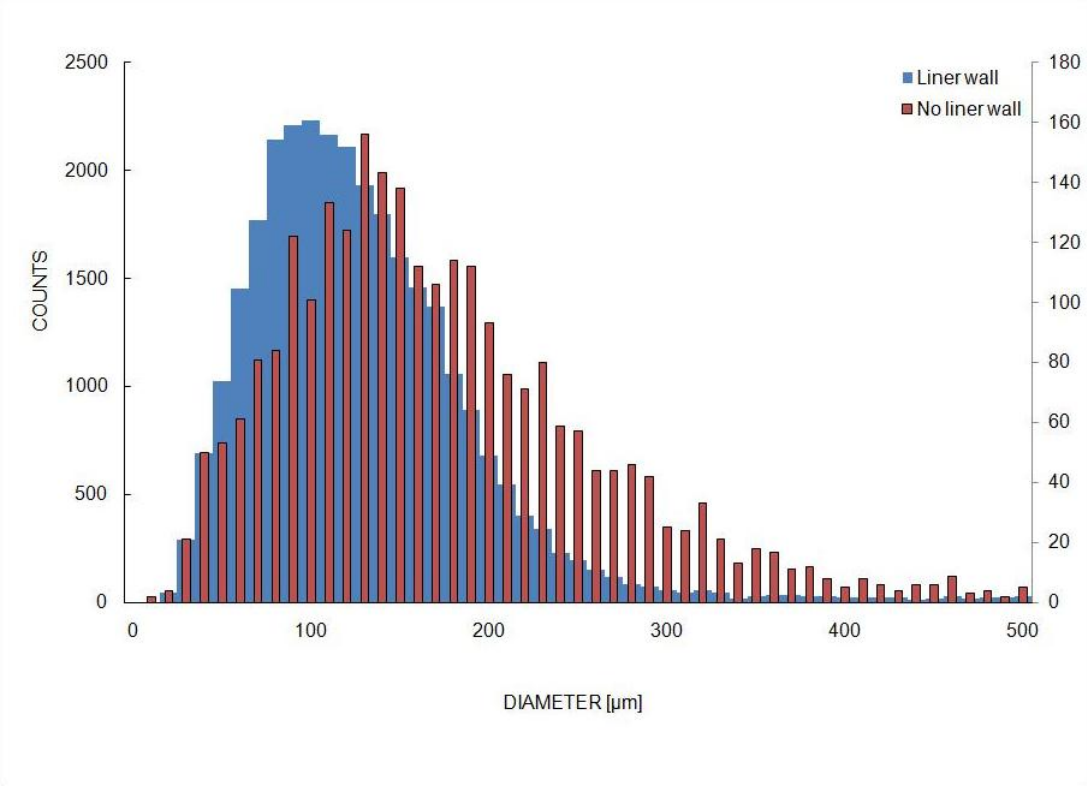

Figure 5.37: Droplet distribution at 41 kPa with and without liner [79].

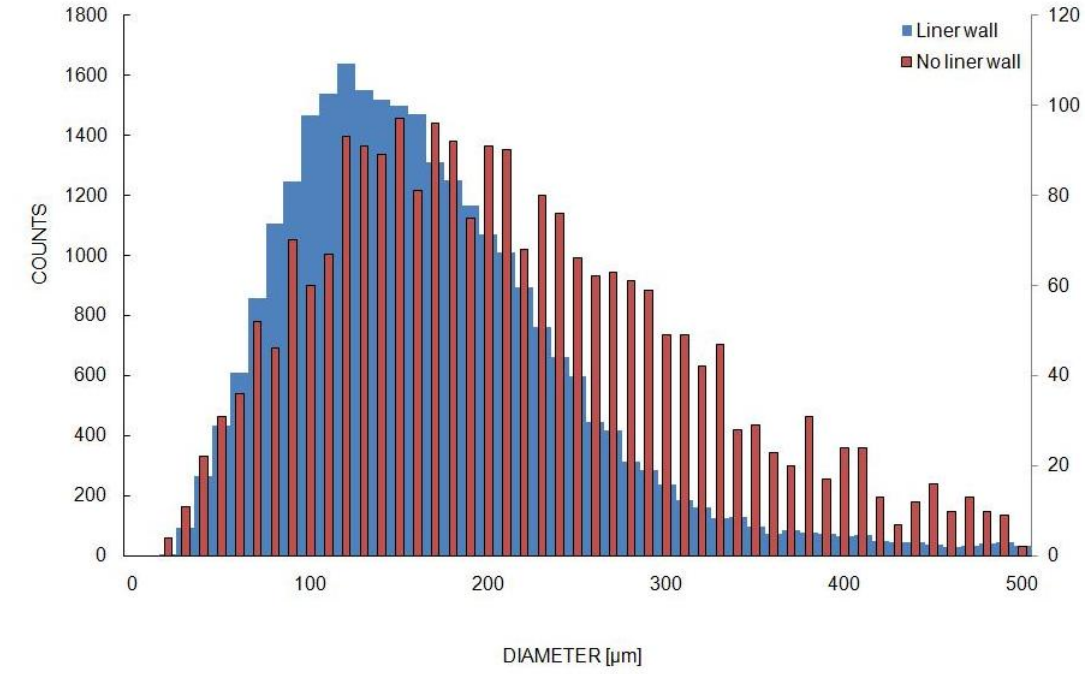

Figure 5.38: Droplet distribution at 31 kPa with and without liner [79].

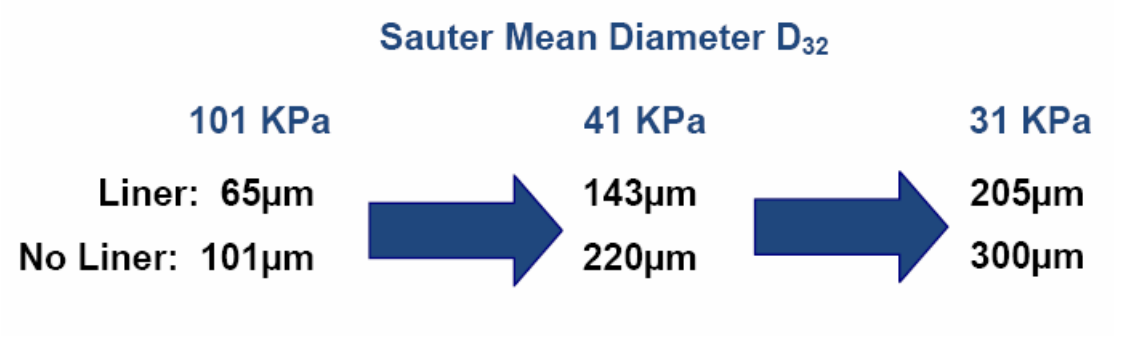

Figure 5.39: Effect of sub-atmospheric conditions on SMD for the injector and the injector-combustor wall model [79].

forces on the fuel droplets and a wider droplet size distribution.

Furthermore, the comparison of the airblast model with and without liner wall showed a wide variation in terms of droplet size distribution. As can be seen from the above figures, the atomiser-only model showed a wider distribution of droplet diameter both at atmospheric and sub-atmospheric pressures. It varied from [0 - 200] μm at atmospheric to about [0 - 500] μm at 31 kPa. Whereas, the base line model (Geometry 1) of the current study varied from [0 - 120] μm at atmospheric to about [0 - 400] at 31 kPa. SMD values also showed similar variations between the models as previously illustrated.

This difference is mainly caused because of two reasons. First, the co-flow air velocity was assumed to be 1 m/s in order to neglect the effect of surrounding air, as the main focus and objective was to analyze only the fuel spray of the airblast atomizer. Also no proper liner wall was included in the model, thus not confining the air and fuel in the real combustor environment. The co-flow air was increased and kept constant at 18.5 m/s, which considerably raised the shear stress forces on the fuel liquid sheet. By including the liner wall, the fuel / air mixture was confined in a defined volume thus also increasing the stresses between fuel and air streams, which results in lower droplet sizes.

5.5.3.2 Effect of fuel flow rate

The effect of fuel flow rate upon SMD is illustrated in Fig. 5.40 at atmospheric and sub-atmospheric conditions.

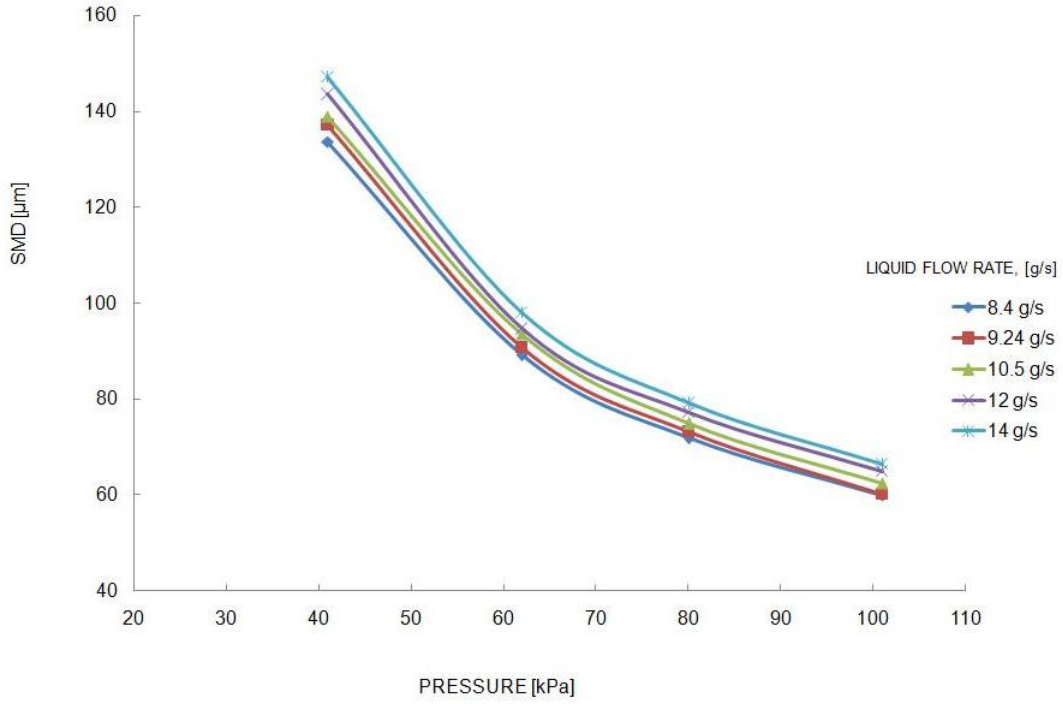

Figure 5.40: Effect of fuel flow rate upon SMD at different sub-atmospheric conditions [79].

As it can be observed from the above diagram at atmospheric conditions, SMD of Geometry 1 showed less dependency on the fuel flow rates. For example at 101 kPa and 80 kPa, the change in fuel flow rate slightly affects the SMD of the fuel droplets unlike at low pressures. In addition, the decrease in operating pressure rapidly increases the SMD due to poor atomization of the droplets. The increase in fuel flow rates at these conditions further deteriorates the atomization and mixing processes.

In order to explicitly express the dependency of SMD on the fuel flow, a different representation of the same result is shown in Figs. 5.41 and 5.42 compared with the results of the stand alone injector model. Each diagram illustrates a different

operating pressure simulated.

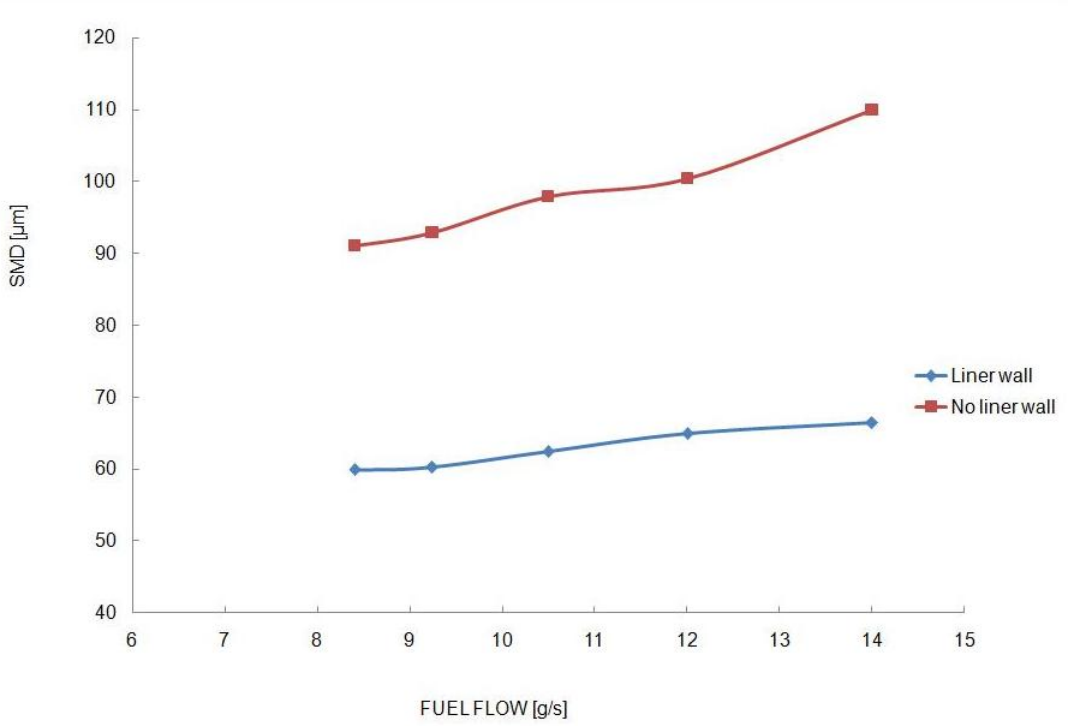

Figure 5.41: Effect of fuel flow rate upon SMD at atmospheric conditions for the stand alone injector and injector-liner wall model [79].

It can evidently be observed that the effect of liner wall and co-flow velocity immensely reduces the SMD of fuel droplets at both atmospheric and sub-atmospheric conditions. This is mainly due to the co-flow air velocity, which enhances the atomization and mixing process. On the other hand, an increase in fuel flow rate still results in high SMD, because for the same air mass flow rate, AFR is reduced. This reduction of air momentum per unit of mass fuel is attributed to loss of energy of air, preventing it from delivering a same degree of atomization.

5.5.4 Effect of combustor's sizing on fuel spray characteristics

One of the objectives of this study was also to model the three liner walls having different diameters. The variation of diameters was defined by the spacing between the liner wall and atomizer. Apart from the baseline geometry, two more models were

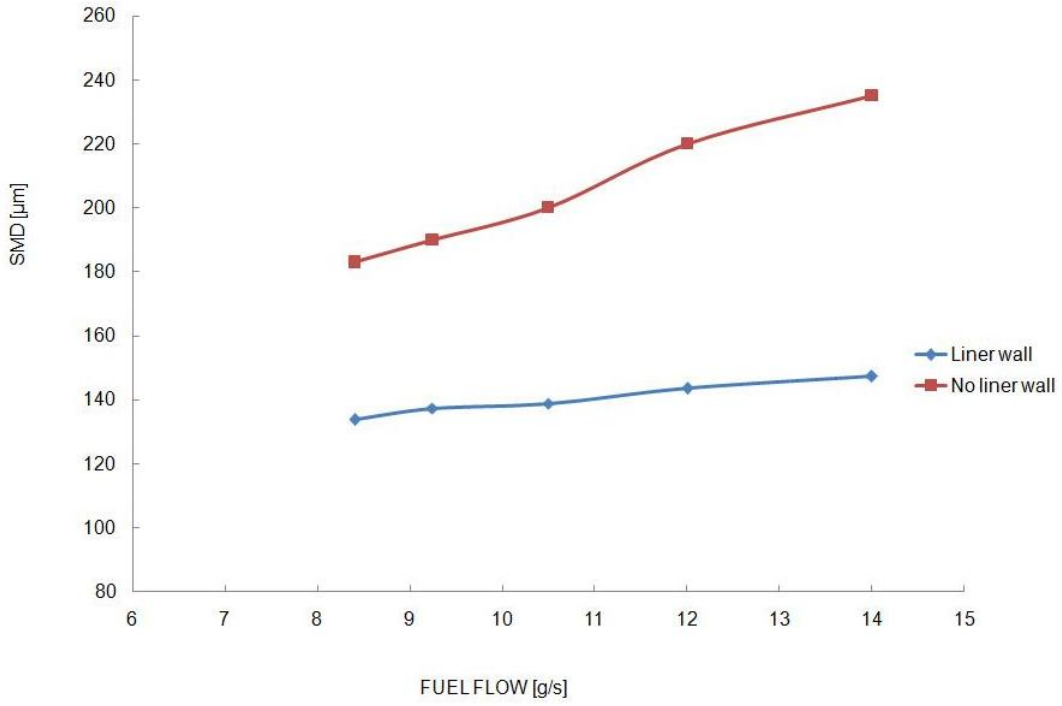

Figure 5.42: Effect of fuel flow rate upon SMD at 41 kPa for the stand alone injector and injector-liner wall model [79].

generated; a 50% (Geometry 2) and a 200% (Geometry 3) liner wall-atomiser spacing in respect to the baseline geometry. The two additional models are illustrated in Figs. 5.43 and 5.44.

The three models were analyzed at different sub-atmospheric conditions, as the first case study, at constant fuel flow rate of 12 g/s. The baseline model has already been shown in previous section. However, Figs. 5.45 to 5.47 illustrate the droplet diameter distribution that was recorded for all the three geometries including the baseline geometry, as well as the no liner model, in order to provide a better understanding of the effect of different sized liner walls on spray structure at sub-idle conditions.

SMD values at the three operating conditions for all the geometries were also recorded and it was found that the SMD of fuel droplets was slightly affected by the change in the spacing of the liner walls, as illustrated in schematic 5.48:

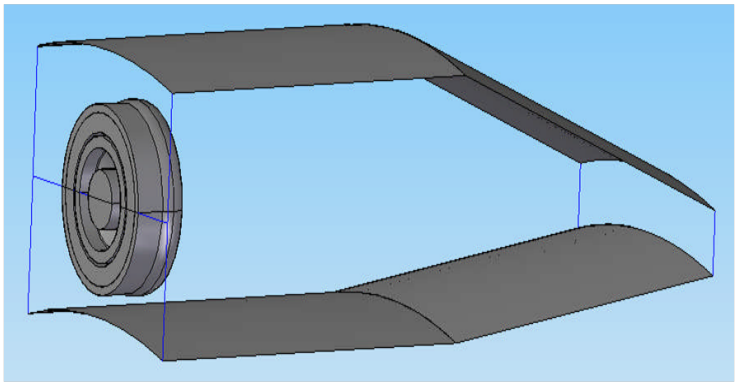

Figure 5.43: 3D view of injector model including liner wall for 50% spacing [79].

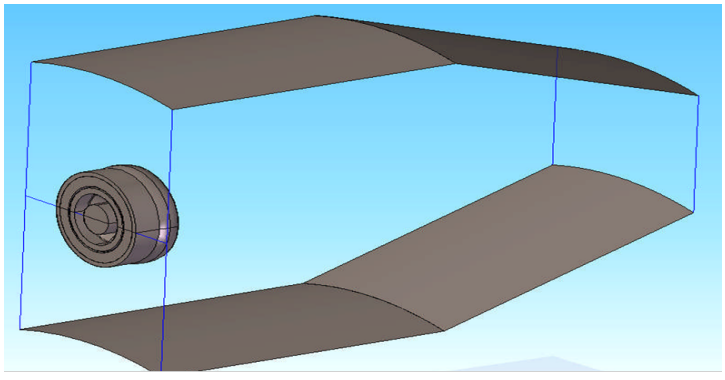

Figure 5.44: 3D view of injector model including liner wall for 200% spacing [79].

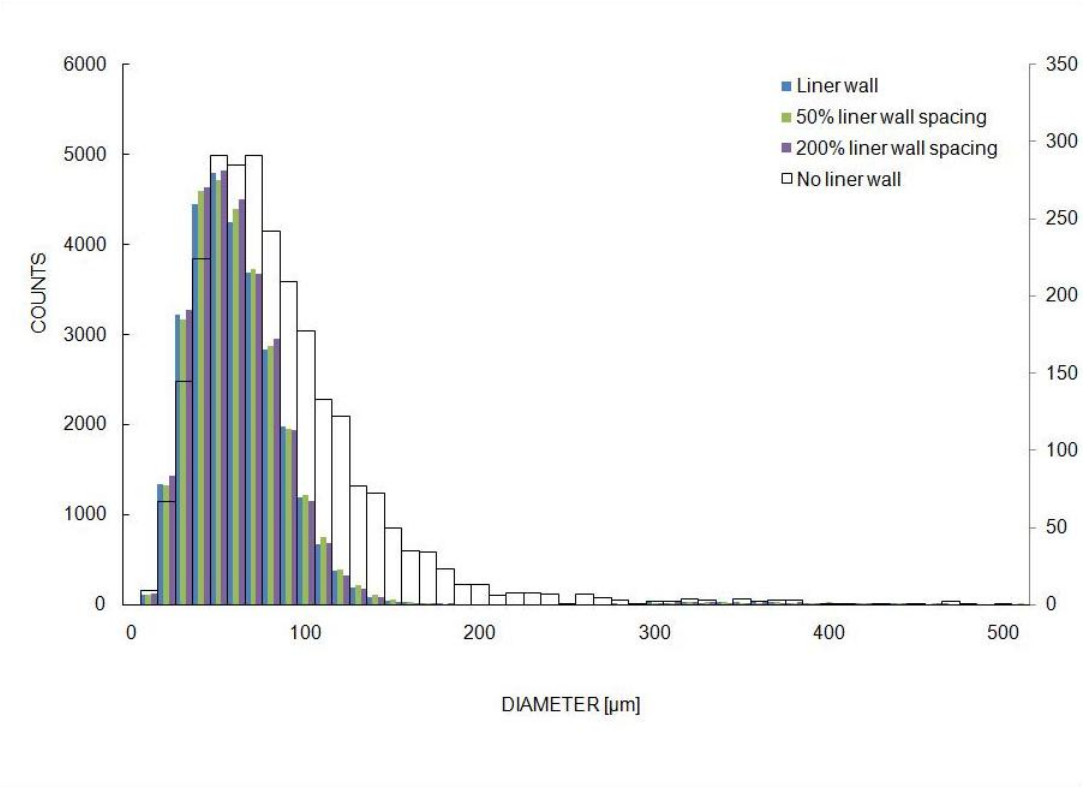

Figure 5.45: Droplet distribution at atmospheric conditions for different combustor diameters (no liner model included for comparison) [79].

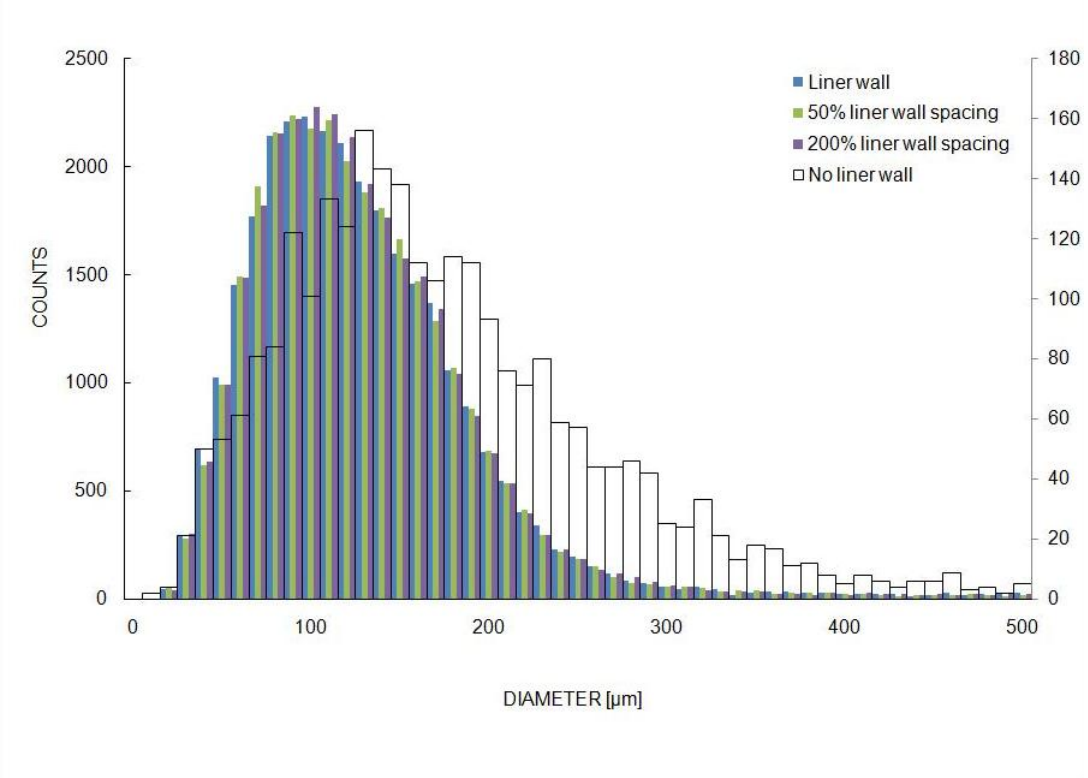

Figure 5.46: Droplet distribution at 41 kPa for different combustor diameters (no liner model included for comparison) [79].

The main observation made out of this analysis was the variation of the SMD in respect to the liner wall diameter. As it can be seen from Figs. 5.45 to 5.47, the droplet diameter distribution is very similar for all the three liner wall geometries and at both atmospheric and sub-atmospheric conditions. As a consequence the diameter distributions show a wide broadening at sub-atmospheric cases; from about [0 - 100] μm at 101 kPa to about [0 - 400] at 31 kPa. A detailed analysis regarding the effect of every combustor design upon the injector's spray dynamics can be found in [79].

Finally, the effect of fuel flow rate upon the SMD at different sub-atmospheric conditions was investigated for the three combustor designs. Comparative results are presented in Figs. 5.49 to 5.52 where also the no liner model results are included for reference.

As can be seen, there is a significant change in the SMD when the liner wall is included. However, it looks that the sizing of the combustor does not affect the

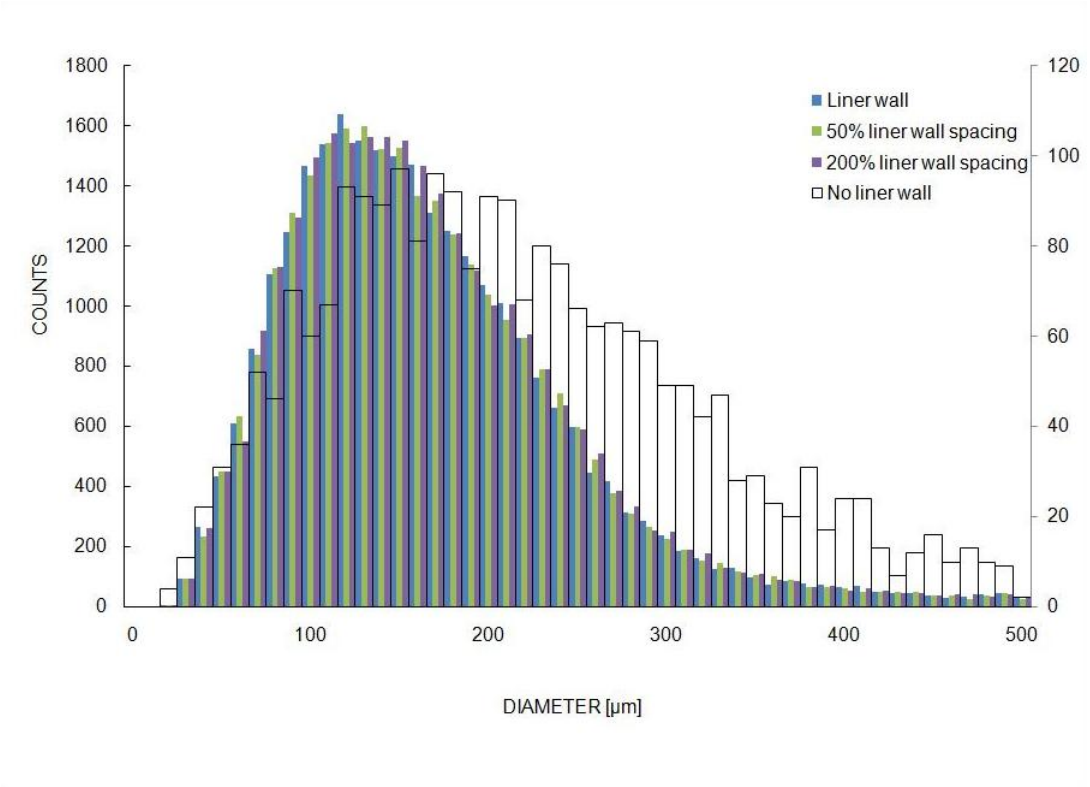

Figure 5.47: Droplet distribution at 31 kPa for different combustor diameters (no liner model included for comparison) [79].

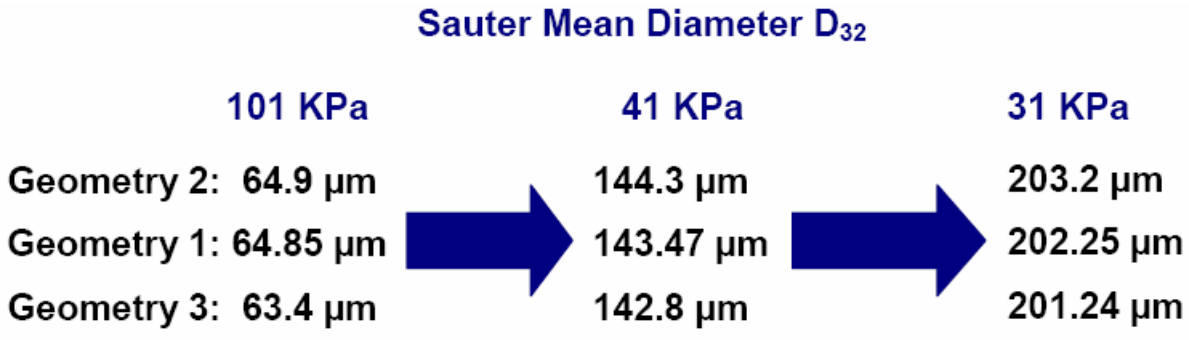

Figure 5.48: Effect of sub-atmospheric conditions on SMD for different combustor diameters [79].

SMD of the spray as the lines for the different combustor configurations collapse one on top of the other while the fuel flow rate influences the SMD as explained in a previous section.

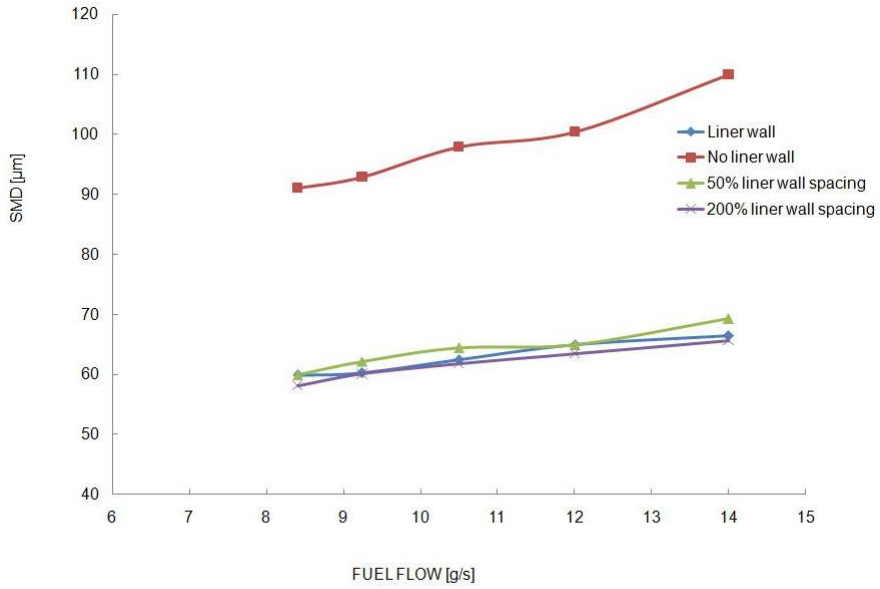

Figure 5.49: Effect of fuel flow rate on SMD for different combustor diameters at atmospheric conditions (no liner model included for comparison) [79]

5.6 Performance modelling approach

In this section the layout of a new combustion model that accounts for evaporation rate effects is presented.

5.6.1 Mixed reaction-evaporation rate based model layout

In respect to the SMD expression as given in section 5.4.3.2, originally derived by Jasuja [56] and reproduced in [68], a few more comments can now be made.

As seen from Eq. 5.53 a constant exponent of 0.22 is given to the fuel flow rate. This expression does not account for different pressures and consequently for sub-atmospheric pressures, as the experimental tests had been carried out at constant

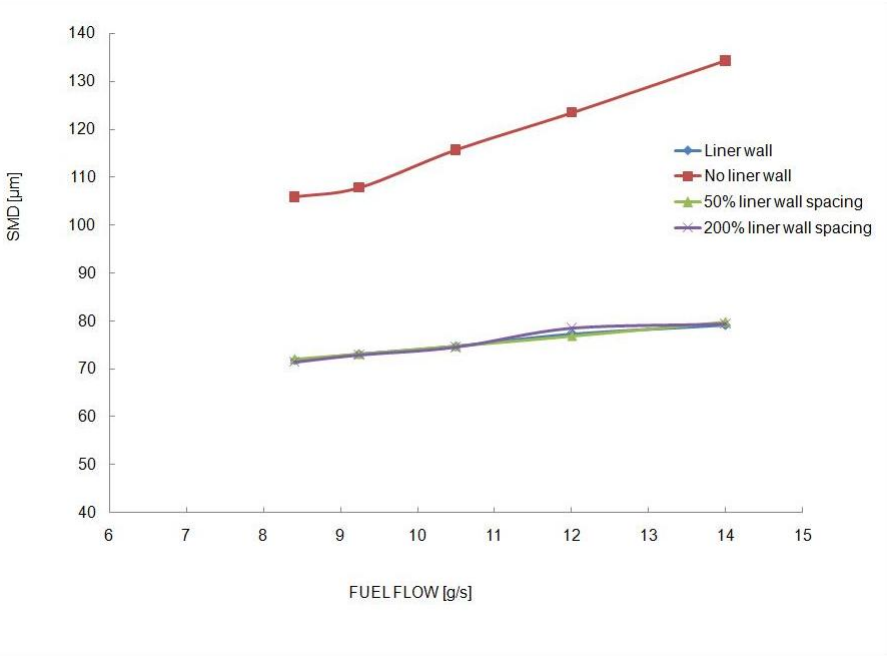

Figure 5.50: Effect of fuel flow rate on SMD for different combustor diameters at 80 kPa (no liner model included for comparison) [79].

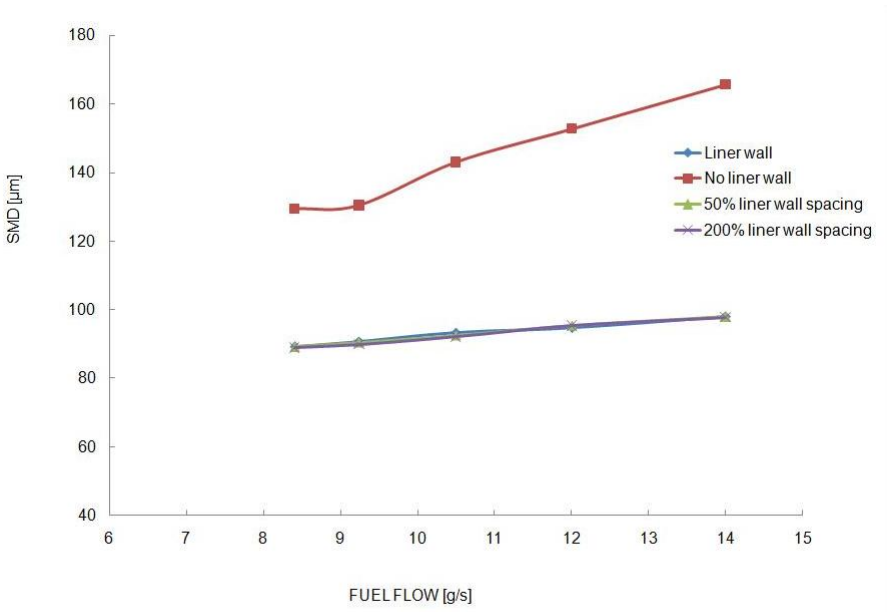

Figure 5.51: Effect of fuel flow rate on SMD for different combustor diameters at 62 kPa (no liner model included for comparison) [79].

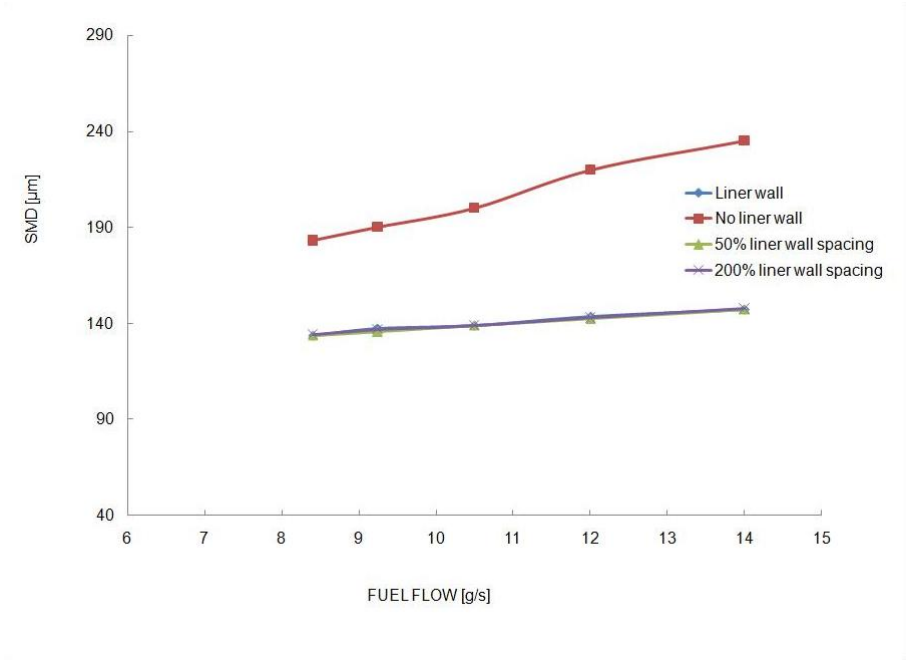

Figure 5.52: Effect of fuel flow rate on SMD for different combustor diameters at 41 kPa (no liner model included for comparison) [79].

pressure conditions.

The above described investigation, however, showed that the sub-atmospheric pressure has, indeed, an impact on the SMD for a range of different fuel flow rates. This effect must be included in the model for more accurate prediction of the evaporation based combustion efficiency for the airblast atomiser. On the other hand, the combustor diameter has apparently no effect on the spray SMD ,therefore no action should be taken in this direction as far as the model expression is concerned.

The impact of the pressure on the SMD for different fuel flow rates can be included in the expression 5.7 by correcting the exponent of that property as shown in [65]. However, the quantitative derivation of the exponent as carried out in [65] is based on the cruel assumption of co-flow velocity of 1 m/s, while there is no liner wall included in the modelling. Therefore, the derivation of the exponent function must be based on the complete model, that is on the results shown in Figs. 5.49 to 5.52.

Thus, for a given value of sub-atmospheric pressure, p, the value of the fuel

flow rate exponent, m, which applies better on the SMD distribution at the given pressure may be derived by the above mentioned plots and the formula:

$$m = \frac{0.22 \cdot \log \dot{m}_{L,101} - \log(\frac{SMD_{101}}{SMD_p})}{\log \dot{m}_{L,p}} \tag{5.8}$$

With this approach, the impact of the sub-atmospheric pressure can be included in the SMD expression, which in turn is required for the explicit calculation of the evaporation rate based combustion efficiency as described by Eq. 5.2. This generic expression can be used in any case the Sauter Mean Diameter is found to excess the Critical Drop Diameter value during a relight process. For the cases where the reaction based combustion efficiency is needed, the calculation can be based on the generic efficiency characteristic as given in [68] or on the engine's combustor characteristic. The latter can be done as long as rig tests are available, keeping in mind that there might always be a need for a low speed extrapolation. However, this extrapolation process is not required for extremely low speeds as previously, since the evaporation rate based modelling provides more accuracy in this regime.

To conclude with, a more generic, corrected combustion efficiency model is introduced, both reaction and evaporation rate based, depending on the SMD value of the droplets:

$$\eta_{comb} = \begin{cases} f(\frac{P_3^{1.75} \cdot A_{ref} \cdot D_{ref} \cdot exp(T_3/300)}{\dot{m}_{air}}) & : SMD < D_{crit} \\ \\ \frac{8 \cdot (\frac{k}{Cp})_g \cdot ln(1+B) \cdot (1+0.25 \cdot Re_{SMD}^{0.5}) \cdot t_{res}}{\rho \cdot SMD^2} & : SMD > D_{crit} \end{cases} \tag{5.9}$$

where the SMD for the evaporation rate based expression can be derived from Eq. 5.7 taking into account the sub-atmospheric pressure effect by modifying fuel flow rate's exponent as derived by Eq. 5.8.

5.6.2 Impact on combustion efficiency

If a summarizing plot of the SMD evaporation rate based expression is generated accounting for the sub-atmospheric conditions, the result looks like Fig. 5.53.

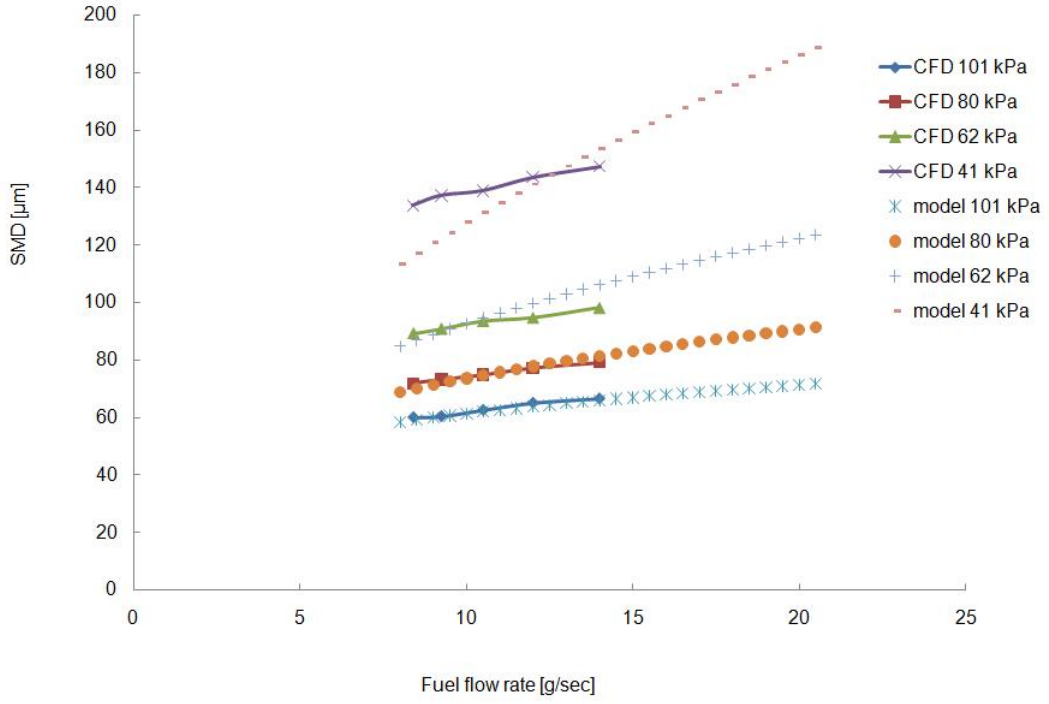

Figure 5.53: SMD as a function of fuel flow rate at different sub-atmospheric conditions as predicted by the CFD and as calculated by the analytical model with the corrected exponent.

In this plot the CFD results are compared with the SMD value calculation by applying the previously described analytical model, using the exponent correction as well. If this expression is used, in turn, for the derivation of the evaporation rate based efficiency, the result is illustrated in Fig. 5.54.

This plot reflects the effect of the sub-atmospheric pressure in the calculation of the evaporation rate based combustion efficiency through the correction in the SMD representation to account for low pressures. As can be seen, there is a quite significant impact on the combustion efficiency, which also enhances the variations in combustion efficiency assumed for different altitude relight cases as confirmed by

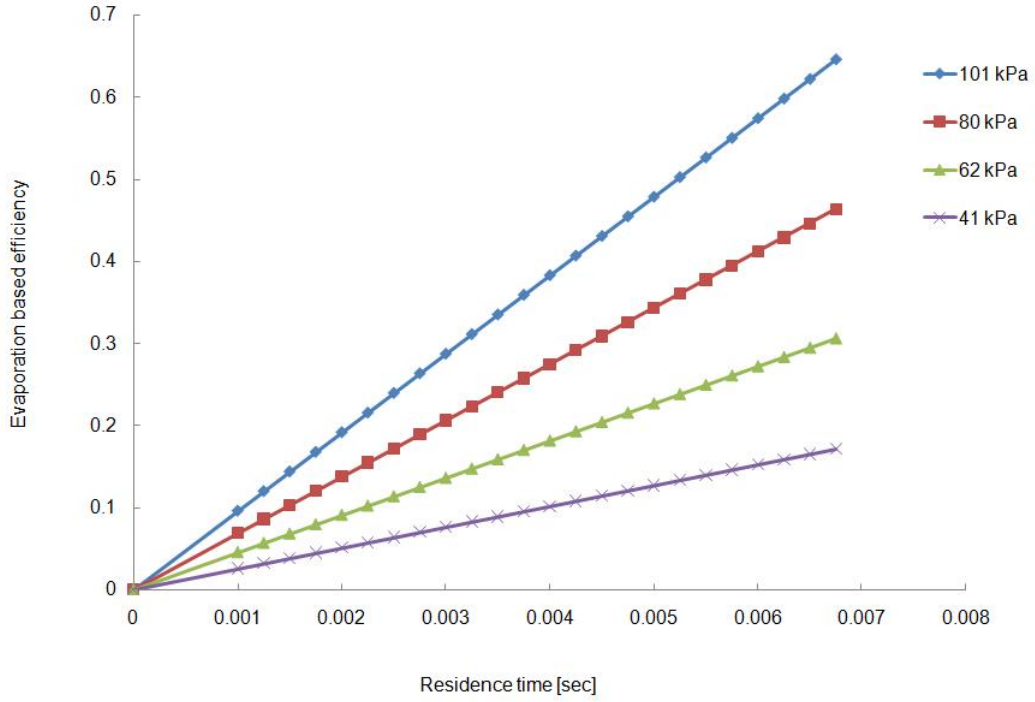

Figure 5.54: The effect of the corrected SMD analytical equation onto the evaporation rate based combustion efficiency.

the sponsor [101].

5.6.3 Integration approach within a performance solver

Having a model like the one described herein, its integration within a performance solver is an issue of vital importance. Unfortunately, not such integration was possible to be carried out within the given timeframe of this doctoral project, nevertheless a few things can be mentioned for future reference.

As demonstrated from the model's layout, the property that defines whether the reaction rate based or the evaporation rate based part of the model is to be applied for the efficiency calculation is the spray SMD in comparison to the Critical Drop Diameter. This information, that is required in every time step of the transient simulation, implyies that at every time step an estimation of the SMD needs to be done based on the previously mentioned correlations. Consequently, a more sophisticated combustion performance module is required. The concept of the "*advanced engine performance simulation*" as described in [86] can be applied here. In few words, a more advanced component simulation module can be plugged into the conventional performance solver to enhance its performance simulation capability. In this case, the combustion efficiency model as well as its interaction with the rest of the engine can be incorporated into the solver with an SMD against Critical Drop Diameter flag which defines the active efficiency calculation model. In case the reaction rate based model is required, the combustor characteristic can be used as usual. When the evaporation rate based model is needed the calculation can be done analytically as demonstrated.

Alternatively, an investigation using engine data can be carried out in order to identify any threshold of relighting time that the evaporation rate based model needs to be replaced by the reaction rate based one. In other words to see if there is any specific time step during the relight process, confirmed by engine data, that the evaporation is not limiting any more the combustion efficiency. Besides, it might be

also possible to define that point analytically.

5.7 Concluding remarks

The work presented in this chapter describes a new approach for the modelling of the combustion process during relight engine manoeuvres, especially at high altitudes where the low air pressure changes significantly the performance of the atomiser by affecting the fuel spray characteristics and consequently the efficiency of the combustion process.

The derivation of the model relies on computational research as there was limited availability of experimental data. Therefore, further investigation regarding the accuracy of the results needs to be carried out before its application on any performance solver, while very useful conclusions can be made out of the application of the model for engine performance predictions. A calibration process might be required in respect to any engine data available or its validation against experimental data that may be derived by future tests.

To conclude with, the application of such a model might improve the predictive capability regarding the overall engine relight performance by enhancing the physical background of the component performance prediction, according to the concept introduced in the first chapter of this thesis.

Chapter 6

Exhaust mixer sub-idle performance

6.1 Introduction

The mixer is one of the least explored components of a turbofan engine. The complexity of the fluid dynamics phenomena occurring in the mixing of two fluids with different density has limited the knowledge achieved so far, especially under sub-idle conditions. The mixer is modeled in a performance code as a device that equalizes the static pressure of the two streams under any condition. This is, of course, an assumption and leads to significant errors when the engine is operating at off-design conditions. Another aspect that needs to be addressed is the influence of the mixer on the mass flow that is going through the gas generator. The understanding of the phenomena leading to lower mass flows in the core is of crucial importance.

Previous research at Cranfield [51] has roughly highlighted the methods that should be used within this research topic. In this chapter, an analysis of the physical mechanisms dominating the sub-idle mixing in gas turbine engines is carried out, pushing the previously proposed methodologies a step forward.

6.2 Literature Review

6.2.1 Design point mixer performance

The mixer is the device between the propelling nozzle and the LP turbine exit which equalizes the temperature of the the two exhaust streams (cold and hot). An injection mixer is presented in the following figure from Frost's work [36].

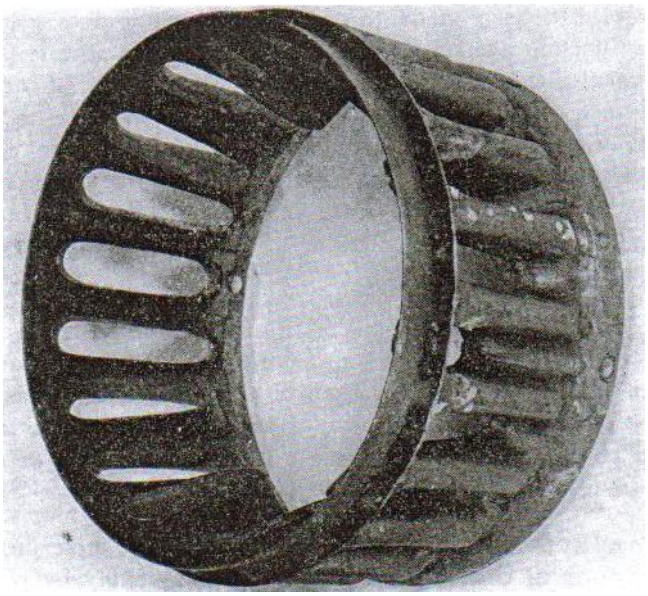

Figure 6.1: Injection chute mixer [36].

Pearson [90] has shown that as long as the two streams have the same temperature, without pressure loss, the fuel consumption of the engine is improved by 5-7%. This is applicable for turbofan engines with by-pass ratio equal to unity. In addition, by conducting comparative studies between mixed and unmixed turbofans, he has managed to show that for the same thrust a mixed engine needs much less fan work, increasing the cycle efficiency.

The same conclusion can be also expressed in a different way as Fig. 6.2 illustrates. For the same fan pressure ratio, the mixed engine produces more thrust. The reason is that in the case of an unmixed engine the maximum thrust can be achieved by equalizing the velocities of the two jets, whereas in a mixed engine the maximum thrust is achieved by equalizing the total and eventually the static pres-

sure of the two jets. For the latter to be done, a lower fan pressure ratio (=fan work) is required.

As shown, there is also a dependence on the by-pass ratio of the engine.

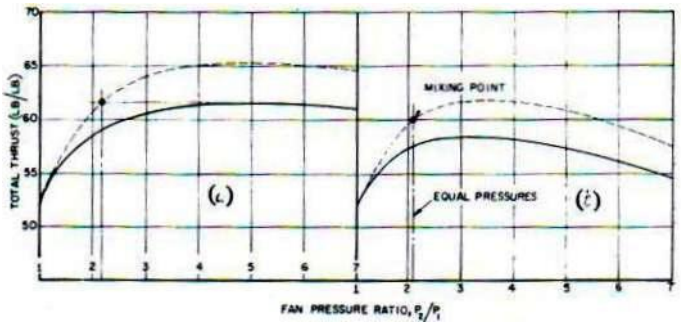

Figure 6.2: 0.75 BPR engine. Left: 100% efficient compressor and turbine. Right: 87% compressor polytropic efficiency, 90% turbine polytropic efficiency. Broken line: mixed jets. Solid line: unmixed jets [90].

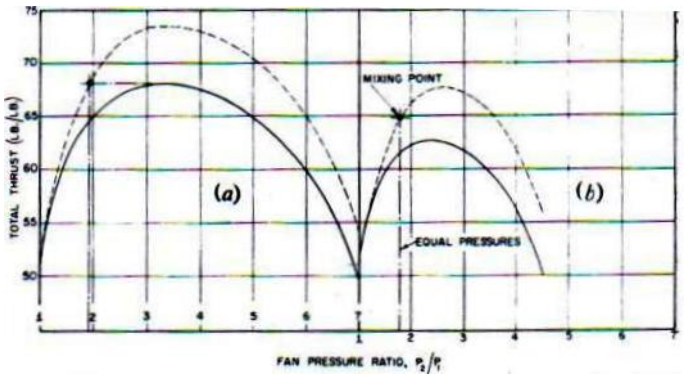

Figure 6.3: 1.5 BPR engine. Left: 100% efficient compressor and turbine. Right: 87% compressor polytropic efficiency, 90% turbine polytropic efficiency. Broken line: mixed jets. Solid line: unmixed jets [90].

The same conclusion has been reached also by Frost [36] a few years later. In his more extensive studies he combined theoretical as well as experimental methods in an effort to understand the mixing mechanisms and the benefits from them in a turbofan configuration. Correlations for the losses during the mixing are also proposed in this work.

6.2.2 Off-design mixer performance modelling approach

All the above mentioned issues regard *design point considerations*. The current status for mixer modeling at off-design performance simulations is to equalize the static pressures of the hot and cold streams and use simple correlations to simulate the mixing process [105, 76, 117].

No reference is given, not only by the above mentioned authors but also generally in the literature, about the mixer performance in far off-design conditions and especially under sub-idle conditions. The reason for this is that during the mixing process, some very complicated physical phenomena take place, which are not totally understood and thus a quite poor and simplistic modeling is applied for performance simulations. Literature related with the process of turbulent mixing is quite helpful in understanding some of the phenomena occuring also during a sub-idle mixing process.

Regarding previous off-design studies at Cranfield University, Howard [51] has shown that the traditional mixer modelling assumptions affect significantly the prediction of the engine performance during windmill relights. Therefore, a *mixer performance characteristic* has been proposed to replace the simplistic assumption of equal static pressures. A preliminary map for Engine's A mixer has been generated using only ATF data and interpolating among them. The map represents the correlation between the static and the total mixer pressure ratio having engine bypass ratio as a parameter. Engine's A mixer map is presented in Fig. 6.4. This approach works quite well for engine simulations throughout the relight envelope and especially for extreme cases, which was almost impossible to simulate with the previous modeling approach. Fig. 6.5 illustrates the Engine's A transient running line from steady-state windmilling up to idle conditions for flight Mach=0.9 on 25,000 ft. altitude.

The matching between the simulation and the ATF data for this windmill relight case is almost perfect. In addition, it looks that there is a pattern behind this be-

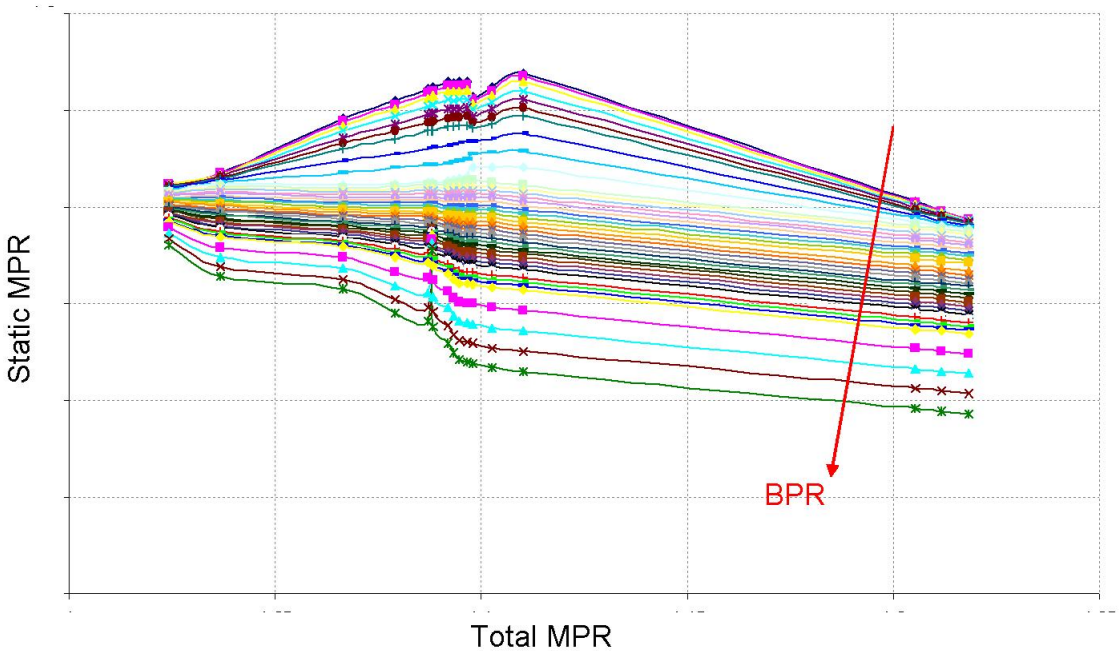

Figure 6.4: Preliminary mixer performance map for Engine A [51].

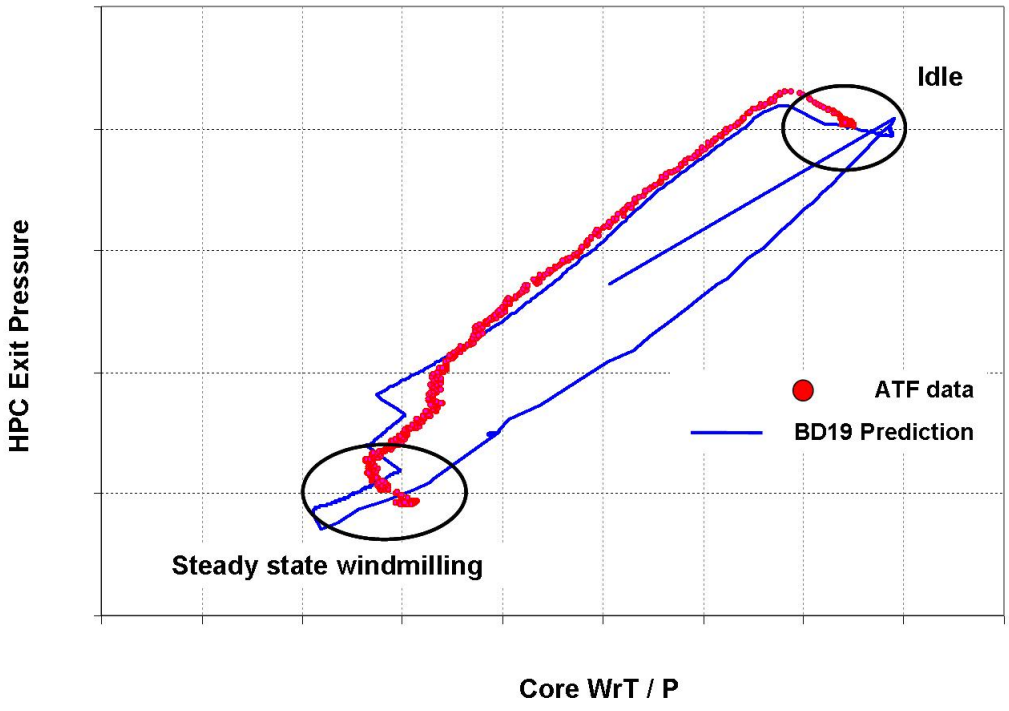

Figure 6.5: Egine's A measured and simulated running lines at M=0.9 on 25,000 ft. using the new approach for the mixer modelling.

havior, whose understanding, as well as the definition of the most suitable approach to describe it for the benefit of a performance solver, is the aim of this research.

The work presented in this chapter has been carried out initially by Ruben Garcia [39] and at a second stage by Fabio Russo [103], Thermal Power MSC students, closely supervised by the author of this thesis and Dr. V. Pachidis.

6.3 Sub-idle mixed engine modelling

In order to understand the physics of the problem, it was decided to take a step back and before the implementation of the preliminary model within the performance solver, to conduct a numerical analysis in order to identify any kind of general rules that dominate the problem.

For that reason, a series of mixer models have been generated and run for a range of operating conditions as described later within the current section. The engines used for these studies are Engine A (geometry provided by the sponsor) and the available in the public domain Engine B [48].

6.3.1 Engine A modelling

A preliminary 2D CFD model of engine was generated by Garcia [39] and was refined by Russo [103] who also switched in 3D. The high fidelity model as well as the computational mesh is illustrated in Fig. 6.6. A detailed analysis about the chosen CFD simulation strategy is given in the third chapter of [103] and will not be reproduced hereafter.

The availability of a few experimental data regarding the sub-idle performance of this mixer configuration allowed their initial comparison against the numerical results. In order to compare the results on the same basis, the test cases of Table 6.1 were simulated.

Thanks to the availability of the engine data, an assessment of the most efficient

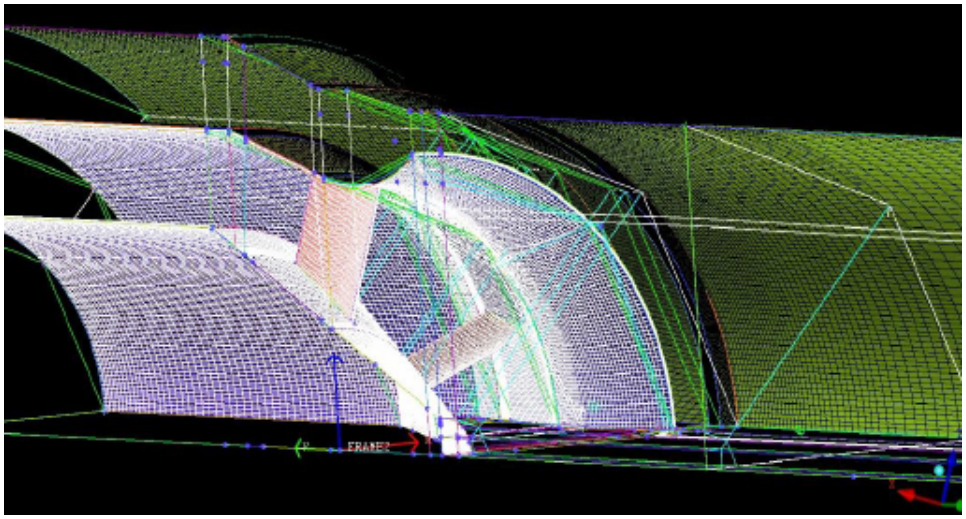

Figure 6.6: 3D engine A mixer model [103].

Table 6.1: Engine A test cases

FLIGHT CASE	ALT [ft]	MACH
6620	25000	0.9
1360	15000	0.59
3380	0	0.4
3270	25000	0.54

simulation set up has been conducted by analysing the effect of different types of boundary conditions (mass flow inlet or pressure inlet). In addition, the deviation between the experimental and the numerical results due to the uncertainties in the core temperature have been evaluated, motivated by the fact that such uncertainties have been identified throughout the available engine data. As shown in [103], the effect of the temperature ratio on mixing is very significant and needs to be known in order to achieve a reliable enough simulation result.

Nevertheless, no safe conclusion can be derived by this first comparison between the numerical and the ATF data because of the low level of reliability the latter proved to have after closer examination. In addition, the efficient calibration of the CFD solver is not allowed for the same reason; therefore the validation of the solver against an open literature mixing case was necessary. The idea is then to validate properly a new, simpler 2D axisymmetric model at full power conditions and lower

down the level of pressures to understand more the physics related to the low speed mixing process.

6.3.2 Engine B modelling

An open literature case with plenty of experimental results available [48] was used to validate the numerical solver. On that basis, extra care was given to the generation of the model, the meshing strategy and the set up of the CFD simulations as far as the boundary conditions, the turbulence closure, the convergence criteria and inlet / outlet sensitivity study are concerned.

A sensitivity analysis was carried out and the results were compared against the experimental information provided, in order to enhance the reliability of the solver before proceeding in a flowfield analysis.

The previously mentioned studies, which indeed increase the trustworthiness of the numerical tool, are described in great detail in the fourth chapter of [103] and will not be reproduced hereafter.

6.3.3 Flowfield analysis and generic modelling approach

Having validated the solver, an insight in the performance of the exhaust mixer is attempted hereafer for off-design conditions. In order for the off-design conditions to be better quantified the Nozzle Pressure Ratio (NPR) and the Total Mixer Pressure Ratio (TMPR) are defined as follows:

$$NPR = \frac{P_{cold}}{P_{AMB}} \tag{6.1}$$

$$TMPR = \frac{P_{cold}}{P_{hot}} \tag{6.2}$$

while it is reminded that the bypass ratio is defined as:

$$BPR = \frac{A_2 \cdot \rho_2 \cdot V_2}{A_1 \cdot \rho_1 \cdot V_1} \tag{6.3}$$

For the sub-idle conditions, NPR is significantly lower than at full power conditions, while TMPR's value is far from unity.

After careful analysis of windmilling test data it can be easily concluded that windmilling conditions are characterized by the following feature:

$$TMPR \longrightarrow NPR$$

In this section, the Engine B flowfield analysis is presented while later on, a comparative study among Engine A, B and C (the latter is a variation of Engine B) is also carried out in an effort to evaluate the common features of different mixer configurations (mainly in terms of bypass ratio) and to propose a more generic approach for the successful modelling of such a component.

6.3.3.1 Engine B flowfield analysis

Despite the fact that the two mixing streams in gas turbine engines have significantly different temperatures and densities, for obvious reasons, within this study it has been decided to keep the streams at equal total temperatures in order to be closer to the sub-idle conditions. Actually, this is not a far from reality assumption, as for a non lit combustor, the core and the bypass streams can be assumed to be at equal total temperature.

At these conditions the *velocity ratio* becomes the driving parameter [42]. The imposition of equal temperatures should not be seen as a restriction, and the effects of differences in density can be analyzed in a second moment. It is instead becoming a big advantage when the boundary conditions are going towards typical windmilling ones and the two streams have comparable temperatures and densities. If the ratio of the two densities is constant, the paramount importance of the velocity ratio can

be easily transferred to another parameter, which is the *mass flow ratio*, or in other words, the bypass ratio of the engine. Therefore, assuming that the density ratio is exactly unity, the BPR is essentially proportional to the velocity ratio r_u only, as confirmed by the simulation results presented in Fig. 6.7. The non-linear dependency of the BPR upon the TMPR is illustrated in Fig. 6.8. The non-linearity relies on the fact that the TMPR has a second order dependency upon the Mach number (which in turn is a linear function of the velocity ratio for nearly incompressible flow).

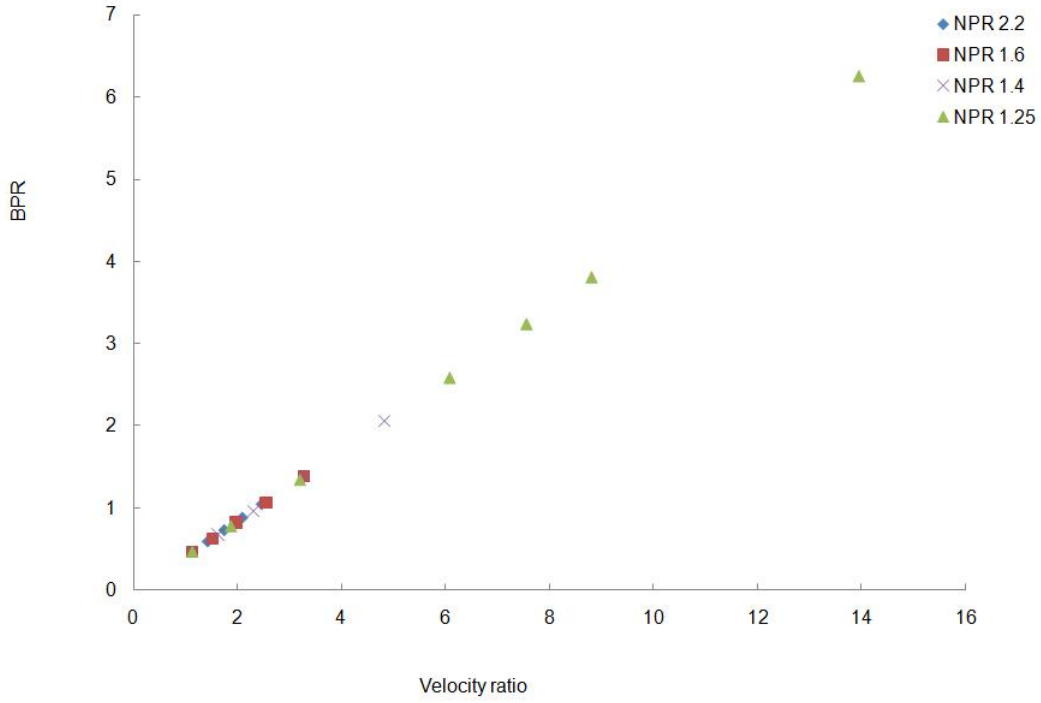

Figure 6.7: Dependency between bypass ratio and velocity ratio at different nozzle pressure ratios and total mixer pressure ratios [103].

However, as seen from Fig. 6.8, there is a significantly stronger interaction between the BPR and TMPR for low NPR's that is closer to windmilling conditions, which is related with the steep increase in the velocity ratio at higher TMPR's. In other words, it needs to be identified how the high values of velocity ratio obtained for high TMPR's and low NPR's affect its dependency with the BPR.

In order this effect to be explained, the following can be written:

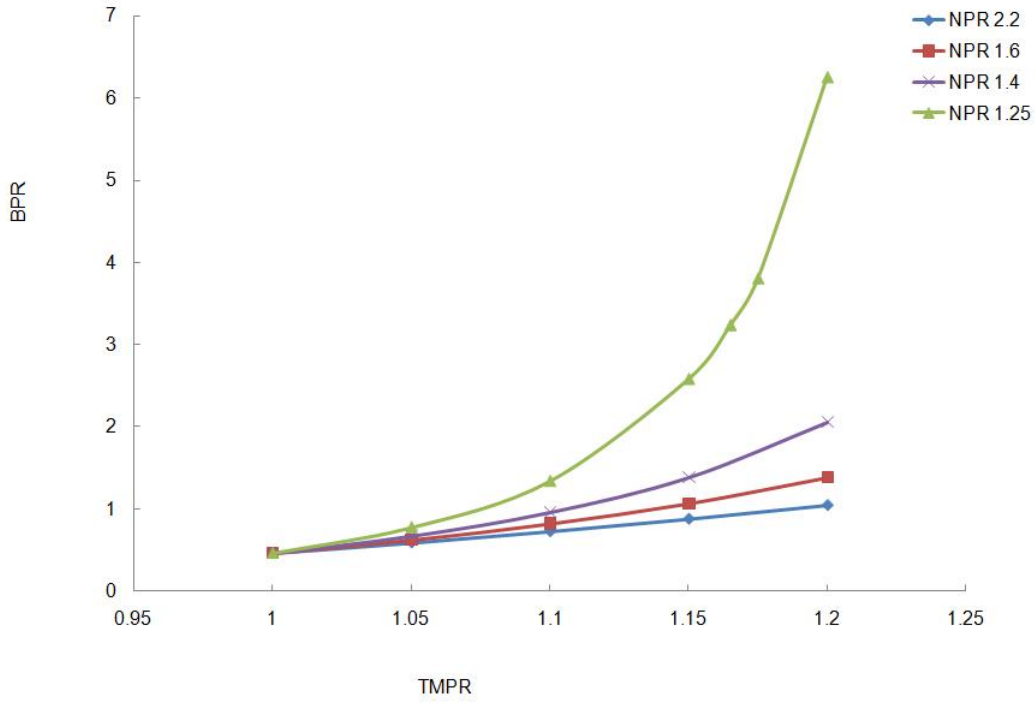

Figure 6.8: Dependency between bypass ratio and total mixer pressure ratio at different nozzle pressure ratios [103].

$$TMPR = \frac{P_2}{P_1} = \frac{p_2}{p_1} \cdot \frac{(1 + \frac{\gamma-1}{2} M_2^2)^{\frac{\gamma}{\gamma-1}}}{(1 + \frac{\gamma-1}{2} M_1^2)^{\frac{\gamma}{\gamma-1}}} \tag{6.4}$$

or

$$TMPR \cong \frac{(1 + \frac{\gamma-1}{2} M_2^2)^{\frac{\gamma}{\gamma-1}}}{(1 + \frac{\gamma-1}{2} M_1^2)^{\frac{\gamma}{\gamma-1}}} \tag{6.5}$$

which can also be written as:

$$TMPR \cong \frac{(\frac{1}{M_1^2} + \frac{\gamma-1}{2} \cdot \frac{M_2^2}{M_1^2})^{\frac{\gamma}{\gamma-1}}}{(\frac{1}{M_1^2} + \frac{\gamma-1}{2})^{\frac{\gamma}{\gamma-1}}} \tag{6.6}$$

From this expression it can be seen that TMPR is not a function of the velocity ratio only, but also of the absolute value of the velocities or Mach numbers. In other words, the steep increase in velocity ratio, is not caused by the difference in total pressure between the two streams only, but also by the small level of velocities in the core, which in turn are caused by the small NPR of the system at windmilling. That means that for a small NPR, a difference in total pressure between the two streams becomes of increasing importance in determining the velocity ratio between the two flows and for high TMPR, in turn, the core flow becomes less and less important, until the total mixer pressure ratio becomes a function of the bypass stream Mach number (M_2) only.

Therefore, as we approach windmilling conditions, the velocity ratio loses gradually its significance and the driving parameter becomes the bypass Mach number only. Further analysis regarding the behavior of the mathematical formulations can be found in [103].

$$TMPR \cong (1 + \frac{\gamma - 1}{2} M_2^2)^{\frac{\gamma}{\gamma-1}} \tag{6.7}$$

Seen in another way, the bypass Mach number at the mixing plane can be written as a function of the total mixer pressure ratio only. This means that knowing the

total pressure and mass flow in the bypass duct (i.e. knowing the flow function) it is easy to calculate within a small error the core total pressure.

An important flow pattern that appears under off-design operating conditions and is worthy to be further examined is the recirculation within the exhaust mixer.As suggested in [96] this will happen for a velocity ratio between 5 and 8. As found in the literature, the physical reason behind the reverse flow region is that the "*radial pressure jump*" ΔP, which is proportional to the velocity difference between the two streams, becomes bigger than the dynamic pressure of the core stream D_1. If a plot of BPR against $\Delta P/D_1$ is generated, as in Fig. 6.9, it is expected that when this ratio is close to 1 the CFD should predict the starting of the recirculation.

The above statement seems to be valid as the beginning of recirculating test cases is at NPR = 1.25 and TMPR = 1.2 according to the CFD simulation.

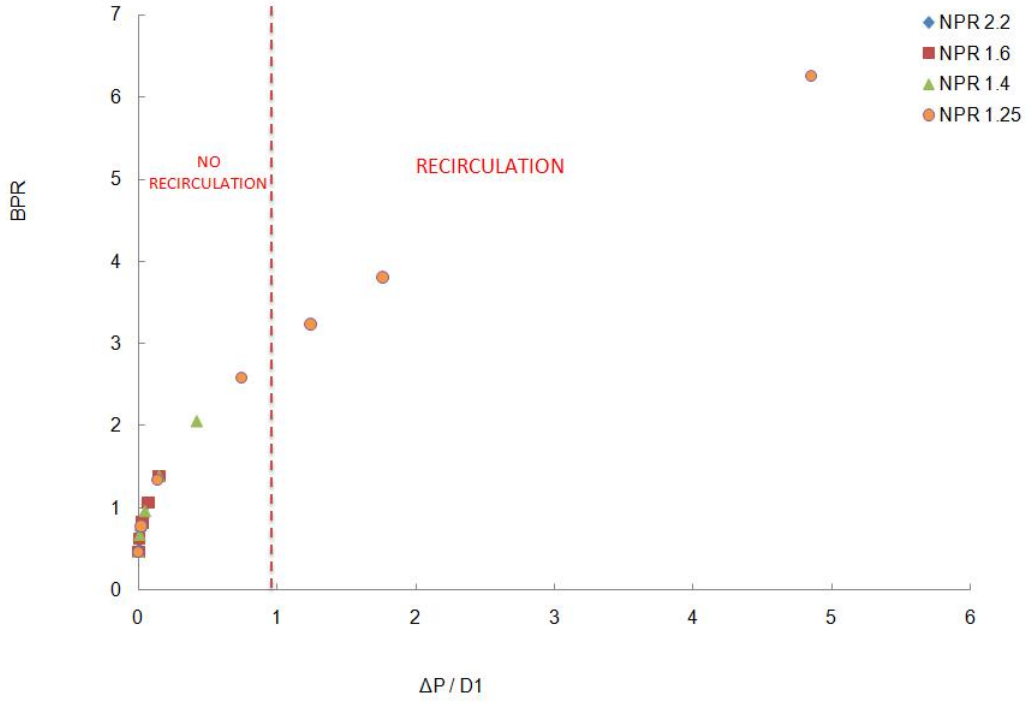

Figure 6.9: BPR as a function of the radial pressure jump upon the core dynamic head with recirculation regimes [103].

It can be easily, realised that all the results collapse one on top of the other. It

has already been proved that the BPR depends only upon the velocity ratio of the system upon which the ratio $\Delta P/D_1$ is, in turn, linearly related.

The recirculating flow pattern mentioned above can be also seen by tracking the radial velocity profiles at several stations downstream of the mixing plane, as predicted by the numerical simulation and illustrated in Figs. 6.10 to 6.12.

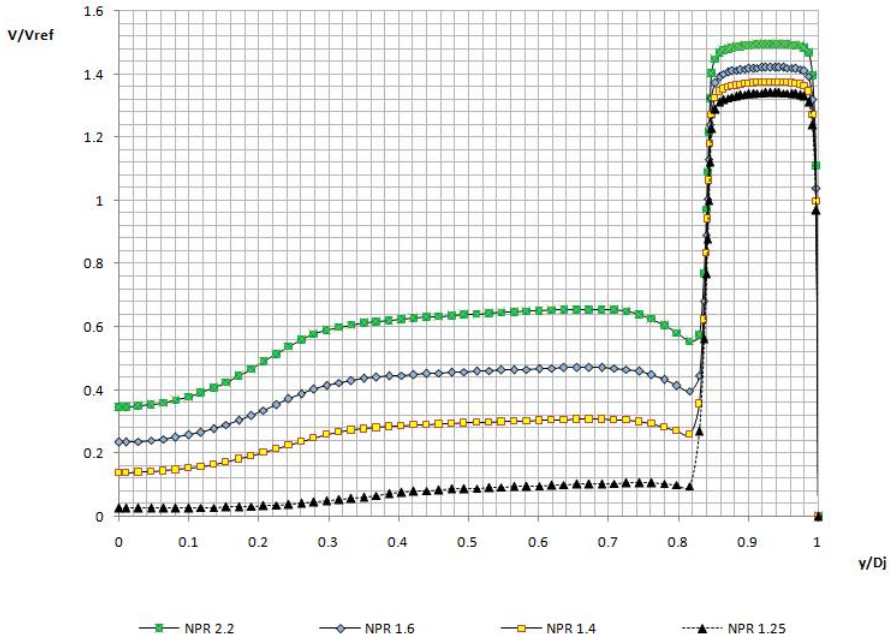

Figure 6.10: Radial velocity profiles for TMPR = 1.2 - plane 1 [103].

It should be pointed out that the last value of NPR, namely 1.25, corresponds to a recirculating bubble regime. The results are presented as radial velocity profiles, non dimensionalized with reference velocity V_{ref}, which is the mass-weighted average velocity in the bypass throat at full power conditions: NPR 2.2 and TMPR 1.

The plots correspond to three different planes; on the mixing plane, half distance between the latter and the nozzle throat and finally, at the nozzle throat. The most noticeable feature of these plots is that the core stream velocity is strongly dependent upon the nozzle pressure ratio, whereas the bypass stream is almost insensitive to variations in nozzle pressure ratio. As the NPR reduces, the percentage of bypass

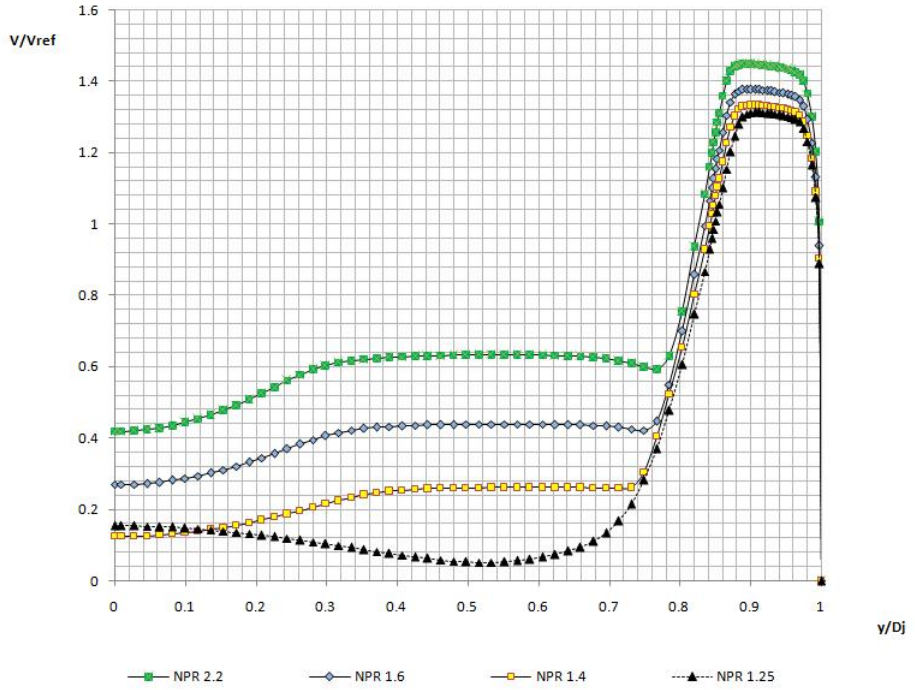

Figure 6.11: Radial velocity profiles for TMPR = 1.2 - plane 3 [103].

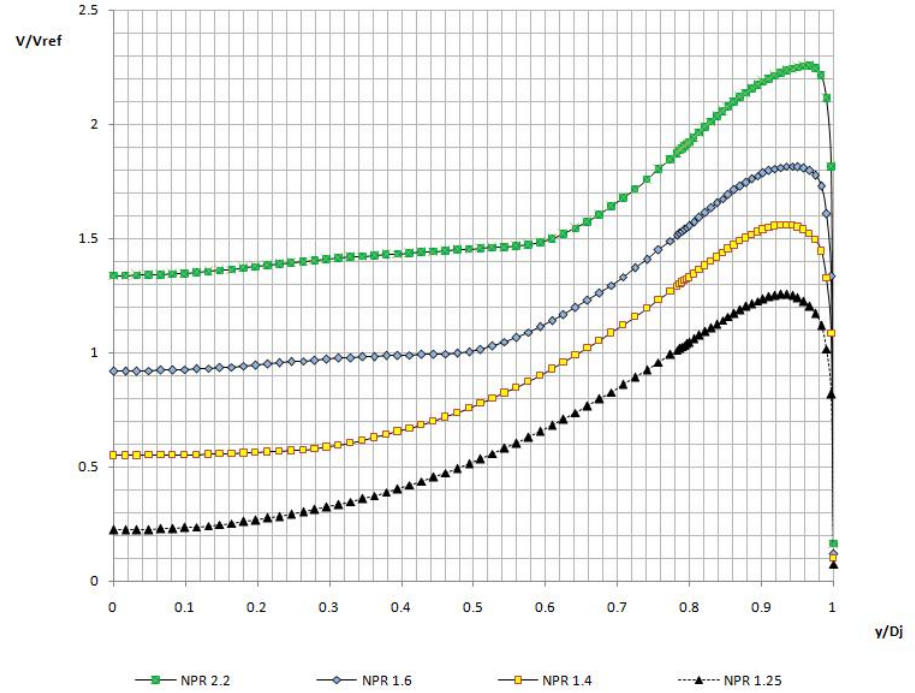

Figure 6.12: Radial velocity profiles for TMPR = 1.2 - plane 5 [103].

expansion to nozzle expansion tends to increase, up to the point in which, when the NPR is 1.25, the whole expansion happens in the bypass duct only. At a nozzle pressure ratio of 1.25 the velocity magnitude profile highlights quite a strong increase in velocity towards the centerline (Fig. 6.11). This is actually reverse flow and the velocity is negative in reality.

A second study was carried out fixing the NPR to 1.25 and varying the TMPR. The results are shown in Figs. 6.13 to 6.15. It is very interesting how both flows are highly influenced by a change in TMPR.

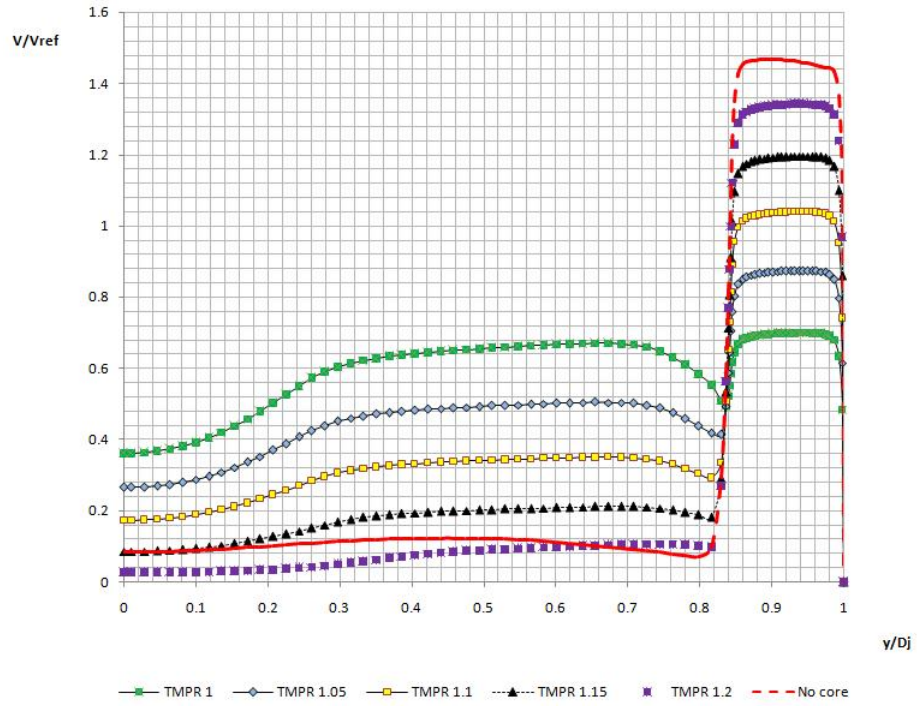

Figure 6.13: Velocity profiles for NPR = 1.25 - plane 1 [103].

The limiting case is represented by the "no core flow" condition. At these conditions the core stream has been canceled from the domain and a wall was built at the core mixing plane.

In overall, as shown by the previous study, it can be concluded:

- The effect of the NPR is to decrease the level of velocity in the core stream but the effect on the bypass stream is very little.

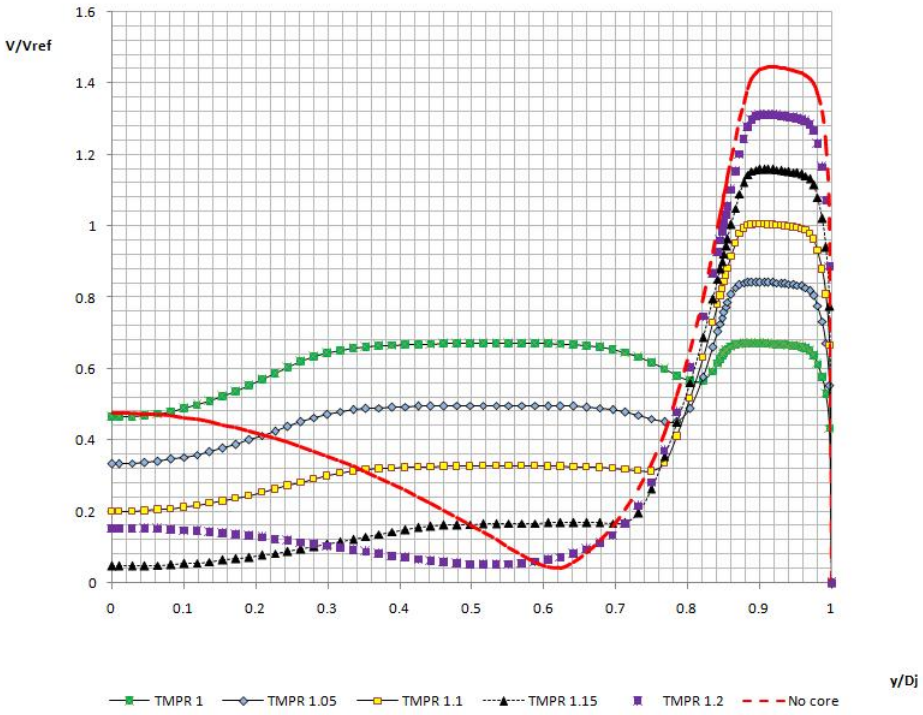

Figure 6.14: Velocity profiles for PR = 1.25 - plane 3 [103].

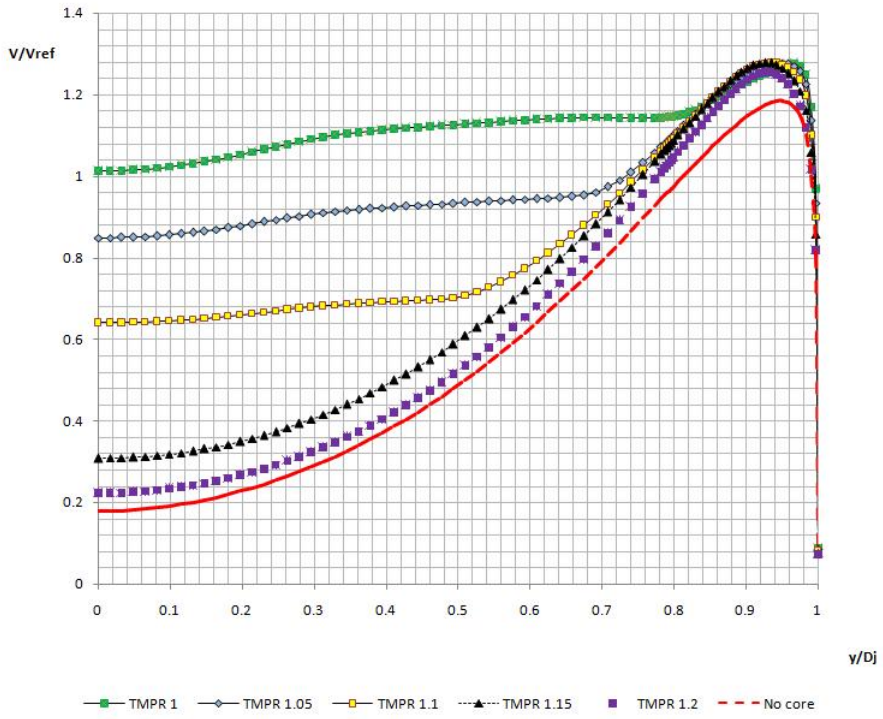

Figure 6.15: Velocity profiles for NPR = 1.25 - plane 5 [103].

- The effect of an increase in TMPR is to increase the bypass stream velocity and decrease the core stream velocity.
- High TMPR and low NPR lead to very high velocity ratios increasing significantly the overall BPR.

6.3.3.2 Parametric study and generic modelling approach

The present study has been carried out in order to quantitatively and qualitatively predict the effect of a change in engine geometry on mixer windmilling performance. The outcome of this study shall be an increase in the knowledge for the creation of a mixer map, which, like other component maps, can truly represent mixer performance at any level.

Three different mixer configurations have been studied; Engine A provided by the sponsor, engine B and engine C. It is reminded that the two latter cases can be found in the open domain [48]. The area ratio defined as the bypass geometrical flow area upon the core geometrical flow area results in diameter ratios of 0.87, 0.84 and 0.74 respectively.

As the diameter ratio changes the BPR is not any more the independent variable in the system (Fig. 6.16). Consequently, the parameter that the study needs to be done in respect to, is the velocity ratio of the two streams as defined earlier in the chapter (Fig. 6.17).

By a closer look at Fig. 6.17 it can be concluded that no matter what the design of the mixer is, the pressure jump defines the velocity ratio between the two streams which as shown is strongly related to the BPR. In other words, the pressure of both streams, is directly related with the engine's BPR and the exact conditions at the inlet of the mixer can be predicted. A feeling about the BPR at every time step affects also the fan map selection and has an impact on the accuracy of the modelling as well as on the convergence time of the solver.

No discussion is made regarding the prediction of the outlet conditions and if

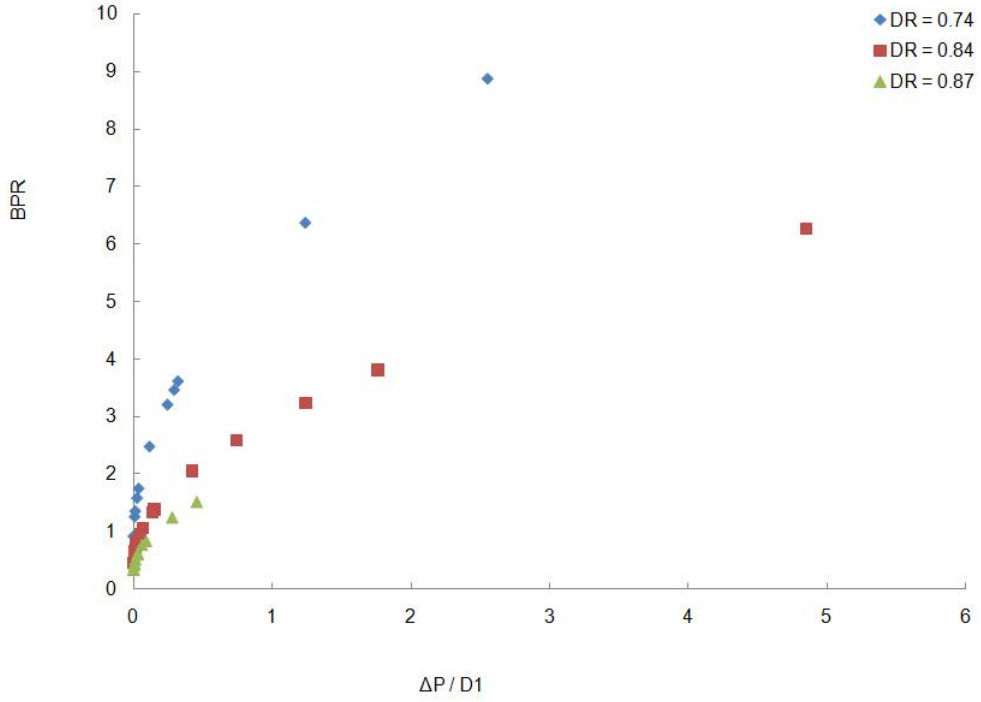

Figure 6.16: BPR as a function of radial pressure jump upon core dynamic head for different mixer diameter ratios [103].

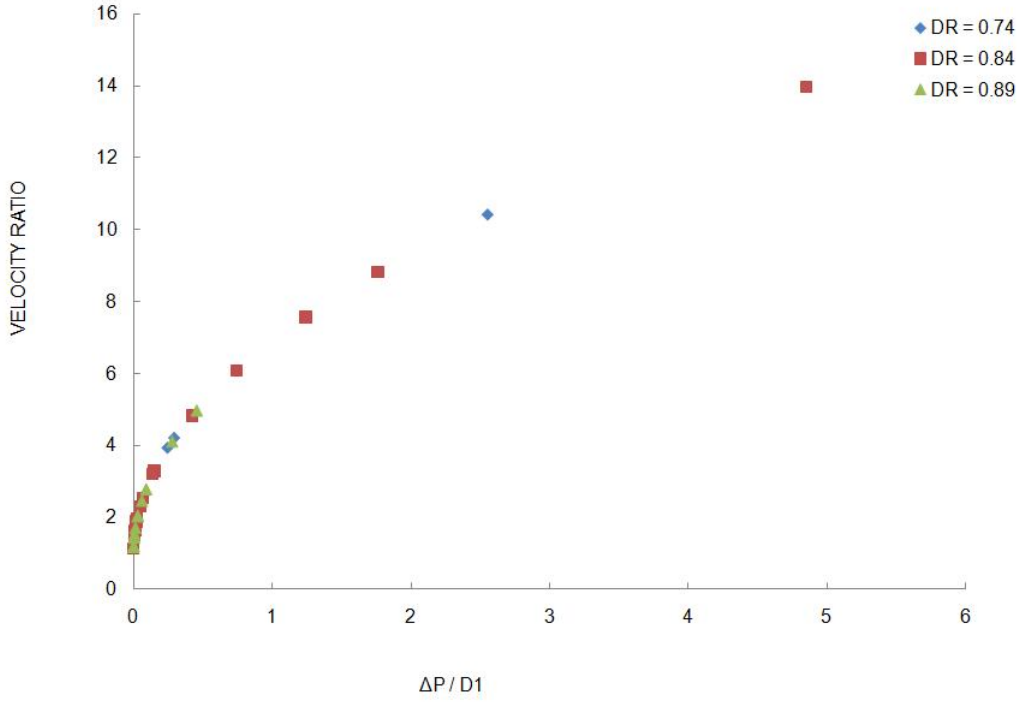

Figure 6.17: Velocity ratio as a function of radial pressure jump upon core dynamic head for different mixer diameter ratios [103].

any similar laws can be identified as there was no time for further analysis within the given timeframe.

6.4 General comments - concluding remarks

By the current analysis an insight into the low speed mixing phenomena is attempted. Mixing flows is an issue concerning a wide range of the scientific community as it is applicable in several different cases (rocket science, test bed and detuner design, gas turbines etc.), which results in studies from respectively many different scientific areas. However, it is a common sense that it is not an easy problem to cope with, as the flow structures are extremely complicated and affected by many factors.

From that respect, the research conducted within the current project and presented in this chapter attempted to give a better insight into the physical structure of the system by investigating rather fundamental phenomena from the point of view of gas turbine performance. By no means this research is completed, as no clear view of the most suitable modelling approach for such a component has been obtained. The material presented here, pushes forward the previous studies, which as mentioned above relied mostly on observations made out of engine data analysis, highlighting some of the basic mechanisms affecting the system and providing expressions that might be useful for future progress.

As a result, more work is required in order for a better understanding of the component performance to be obtained. This knowledge needs finally to be translated into a robust performance model to enhance the predictive capability of the overall engine performance as far as the exhaust mixer is concerned.

Chapter 7

Whole engine modelling

7.1 Introduction

As demonstrated in the earlier chapters of this thesis, the aim of the sub-idle research is to increase the predictive capability of the whole engine performance simulation solver by enhancing the physical background of the component performance prediction methods. The latter was achieved by extensive research on compressors, combustion / injection dynamics and mixer performance. The last objective is to assess the relight performance prediction capability after the integration of the newly developed methods. This study was carried out within the last phases of the doctoral course during the author's industrial placement in the performance department of Rolls-Royce in Derby.

Despite the limited time given for this task, a number of parametrical studies on engine starting and relighting was conducted using RRAP-BD19 solver [78]. The objective was to identify the robustness of the code by demonstrating the IP starting and offtake capability of a modern high bypass civil aero engine. Engine models and flight environments were provided by Rolls-Royce. However, as there was no code modification capability within the given timeframe, neither torque characteristics nor the new combustion model could be implemented. Therefore, the validation

of the tool was conducted using the conventional component representation for a number of typical windmilling relight and groundstarting cases.

The research presented within this chapter is based on the sub-idle performance engine reports [82] and [83] where the most important issues that require more work are clearly indicated. Additional work was done and reported by Howard in [50]. Recommended way forward regarding the whole engine modelling can be found in the concluding section of this chapter.

7.2 Steady windmilling power offtake capability

The first part of the modelling regards the prediction of the IP (and also the LP) power offtake capability when the engine is steadily windmilling. The availability of offtake power under this condition represents the capability of the engine to cover the power requirement in an emergency situation. Therefore a range of flight Mach numbers needs to be simulated representing several different points within the relight envelope of the engine. This kind of study can be considered as quite representative for the evaluation of the code's functionality. Bringing numerically the engine at a steady state windmilling situation (condition where a compressor can absorb or produce power depending on the operating point that stabilizes on) is quite challenging from the engine matching point of view and also not widely explored with the current version of BD19. Lighting up the model is just a matter of fuel scheduling and controlling, but as the energy levels of the engine start to increase, the transient simulation becomes more reliable.

A representative altitude of 15,000 ft has been selected for the current study. The latest version of BD19 demonstrated a good behavior on the above mentioned simulations. More specifically, the engine was brought to a steady state windmilling point by reducing the fuel flow rate to a minimum before gradually imposing any power offtake demand from the shafts.

A typical, gradually increasing power offtake demand from the IP shaft is shown in Fig. 7.1 for a flight Mach number case of 0.7. BD19 demonstrated a very good response on the imposed offtake requirement. The latter has an effect on the IP shaft rotational speed as represented in Fig. 7.2. In addition, the available power at the IP shaft is also increasing as shown in Fig. 7.3. It is worthy noting that the power value has a negative sign, meaning that the shaft works as a turbine, producing power, due to the ram pressure ratio imposed by the high flight Mach number at windmilling conditions.

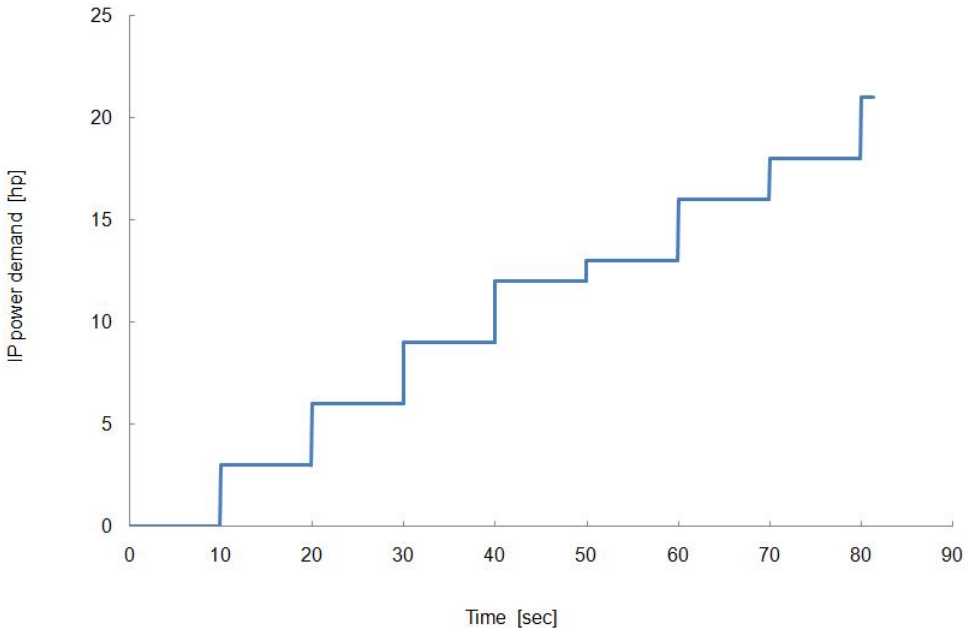

Figure 7.1: Gradually increasing IP power offtake demand for a steadily windmilling high bypass engine.

Similar studies have been carried out for a quite wide range of flight Mach numbers. The emergency (that is at steady state windmilling conditions) IP as well as LP power offtake capability of the engine is represented at the power offtake envelopes, as shown in Figs.7.4 and 7.5.

These plots demonstrate the engine's capability to provide emergency power at different flight conditions for an altitude of 15,000 ft. As shown by the figures, the

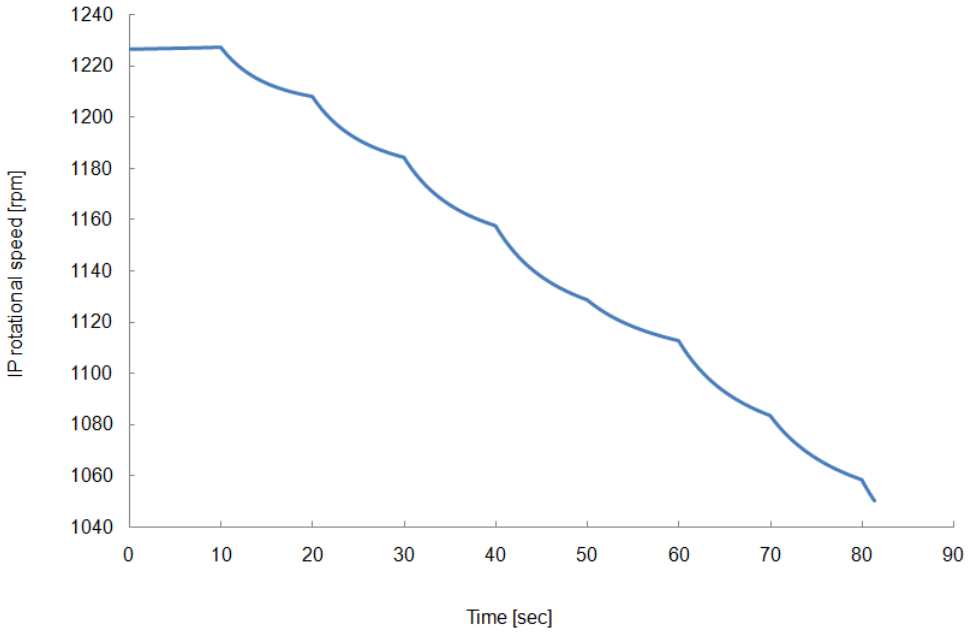

Figure 7.2: Effect of increasing power offtake demand on the IP shaft rotational speed of a steadily windmilling engine.

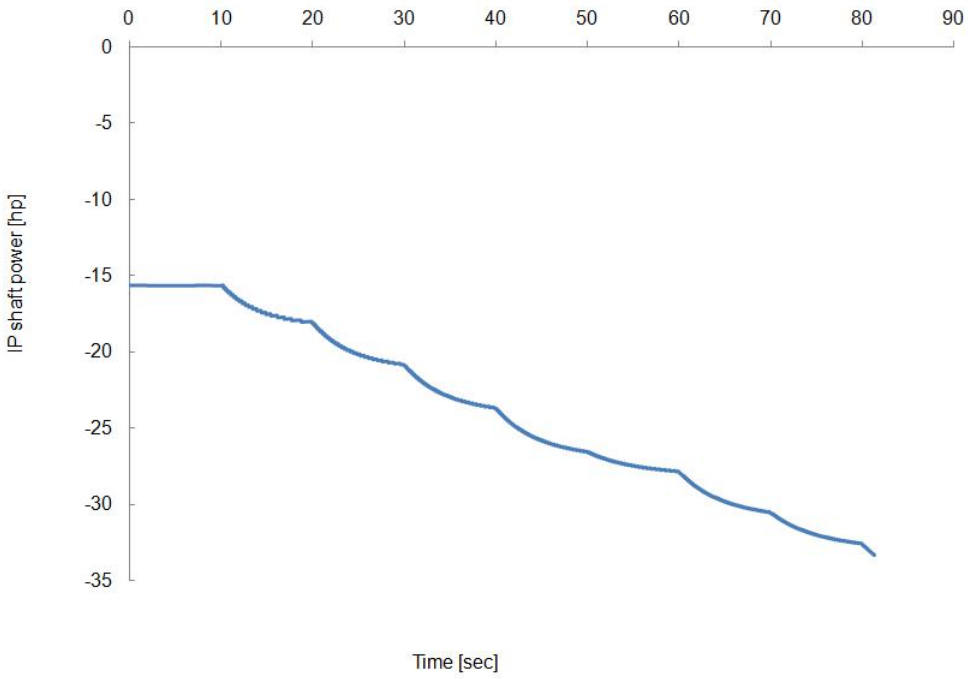

Figure 7.3: IP shaft power of a steadily windmilling engine.

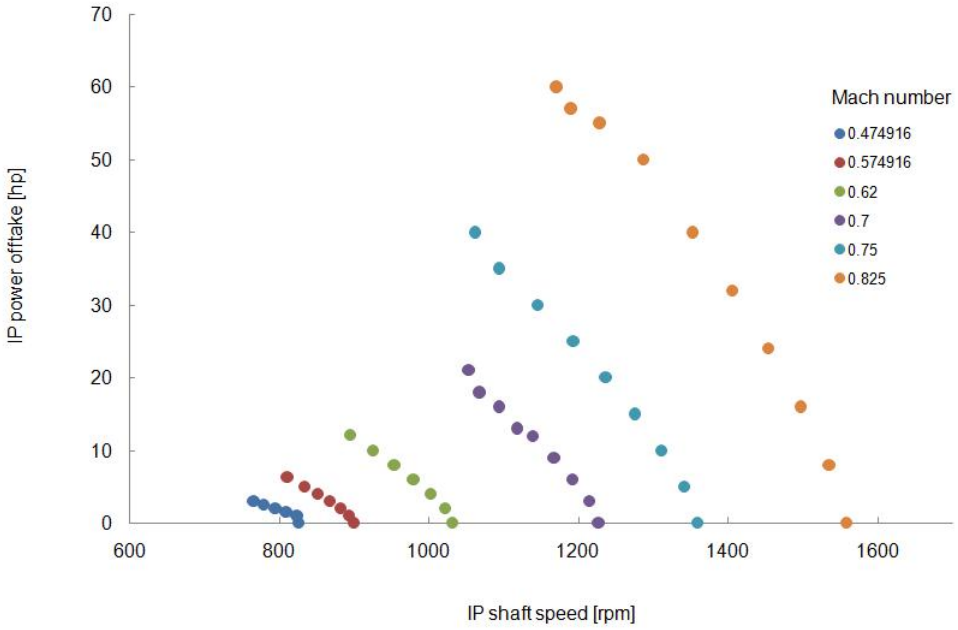

Figure 7.4: IP windmilling power offtake envelope.

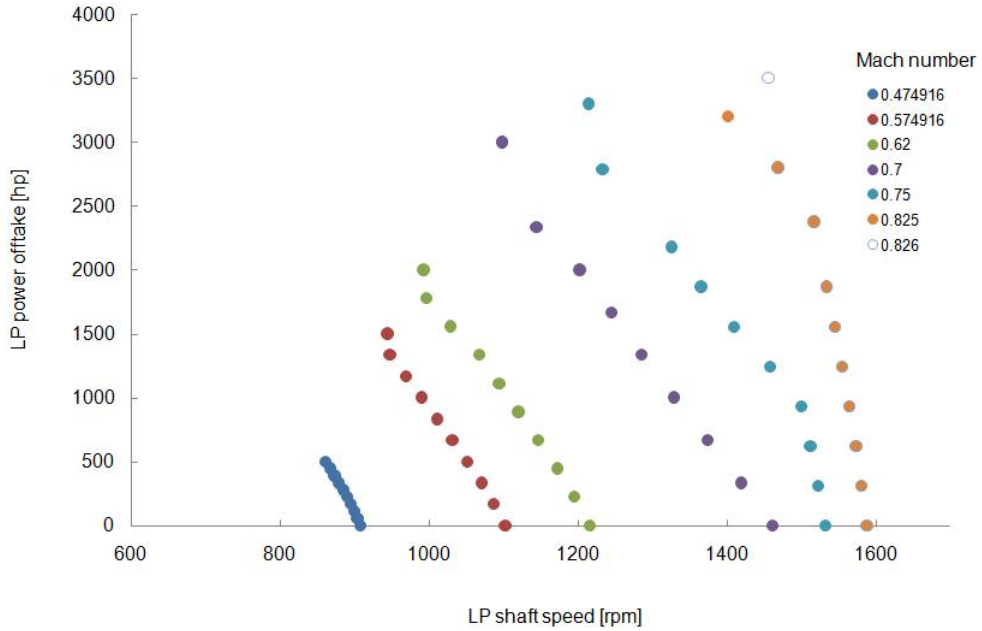

Figure 7.5: LP windmilling power offtake envelope.

LP capability is significantly higher than the IP one, which roughly exceeds the typical windmilling power requirement of 40 hp [35].

As underlined in [83] and also confirmed by the current simulations, the prediction of the LP shaft steady state windmilling speed is rather poor and for most cases a deviation between the simulation and the engine data of the order of 90-100% can be observed. Therefore the power offtake capability of the LP shaft is significantly over-predicted. The LP map is most likely to be the cause of this issue as it does not allow acurate steady state windmilling speed prediction. This issue rises from the map scaling parameters used for the modelling as there was no test rig fan map available. Nevertheless, such a problem is not faced for the IP shaft.

7.2.1 General comments

Even though the power offtake study is carried out in the sake of code robustness assessment, a few further thoughts are triggered by this.

As shown previously, the IP windmilling capability of such an engine is quite poor as the power levels that can be extracted from the shaft are low. On the other hand, the LP shaft looks quite more powerful when the offtake demand is taken by it. This issue increases the safety margin of the engine as it looks that the LP shaft can undertake all the power load in an emergency situation. The LP power offtake capability is also of vital importance when the engine is flying at extremely low flight Mach numbers as for example during landing. Typically the power demands under those conditions are covered by the Ram Air Turbine (RAT) but it seems that the LP shaft can easily replace the RAT system reducing the complexity of the engine. Finally, part of the LP available power can be beneficial in "*more electric*" engine configurations.

7.3 Turbofan groundstating using the IP shaft

The capability of BD19 to simulate a groundstarting process is assessed herein. Having a feeling of the starting time and the rotational speed of the shafts during this procedure is considered as a very significant piece of information during the design as well as the development phase of an engine. The fact that makes the current modelling more complicated is that the shaft cranked during the starting process is the IP one, instead of the HP, as typically happens. In addition, a Start Power Coupling (SPC) system which engages the IP with the HP shaft during the groundstarting process makes the simulation even more challenging.

7.3.1 Starting system description

Conventionally, aero engines are started up by one or more starter motors (the so called starting system) which are connected to the HP shaft. During the deadcranking phase of the starting manoeuvre the starting systems accelerates the shaft in order to create a flow stream and a slightly increased pressure at the inlet of the combustion chamber preparing the conditions before the fuel injection which at the end will lead to the ignition of the engine. BD19 groundstart modelling using the HP shaft has been extensively conducted for a wide range of engines as described in [51] and [50].

Additionally, there might be engine designs in which the starting system uses the IP shaft to accelerate the engine during the first phase of the starting process. This kind of design allows shorter starting time as the IP shaft allows more mass flow to pass through the cold part of the engine in a shorter period of time. Therefore the drycranking phase before the fuel injection is faster in comparison to an HP starting process.

The disadvantage of this configuration is that the IP compressor is forced to pass through a stalling condition for a specific amount of time while the mass flow

through the engine caused by its rotation is not enough to prevent stalling. A possible alternative configuration that improves the above described issue is the implementation of a Start Power Coupling (SPC) system. The IP is engaged to the HP shaft through a gearbox with a specific shaft speed ratio. This system allows the acceleration torque provided by the starting system during the groundstart process to be distributed between the two shafts, enabling also the HP to accelerate with a different, though, rate. As a result the mass flow through the engine increases protecting the IP shaft from operating under stalling conditions. Nevertheless, an SPC system increases significantly the weight of the engine adding also extra manufacturing and assembling complexity. Those parameters increase also the overall cost of the product but their impact is reflected on the development timescales as well. A better IP compressor design with a bigger surge margin might be extremely beneficial in this case. If the IP compressor operates unstalled there is no need for the SPC system and the engine could be started up using only the IP shaft, thus being at the same time as simple as possible in terms of system design.

The research approach is described in the following section along with groundstarting simulation results.

7.3.2 Groundstart simulation results

A parametric study using BD19 might reveal a better IP design initially by scaling the existing IP map. At a second stage the map could be further adjusted or re-generated to achieve an even better IP compressor design. The current modelling is carried out in the above described directions in order also for the BD19's groundstarting simulation capability to be assessed.

More specifically, starting from a baseline configuration in terms of coupling ratio (that is the fixed HP upon IP shaft speed ratio during the groundstart manoeuvre), its value is gradually reduced in order to increase the torque -thus the rotational speed- absorbed by the IP shaft decreasing at the same time the speed and torque

of the HP shaft. In other words the importance of the HP shaft during the ground-start is de-emphasised while more importance is given to the IP shaft. In this way the model is pushed towards an IP-only starting process while BD19's simulation capability is investigated.

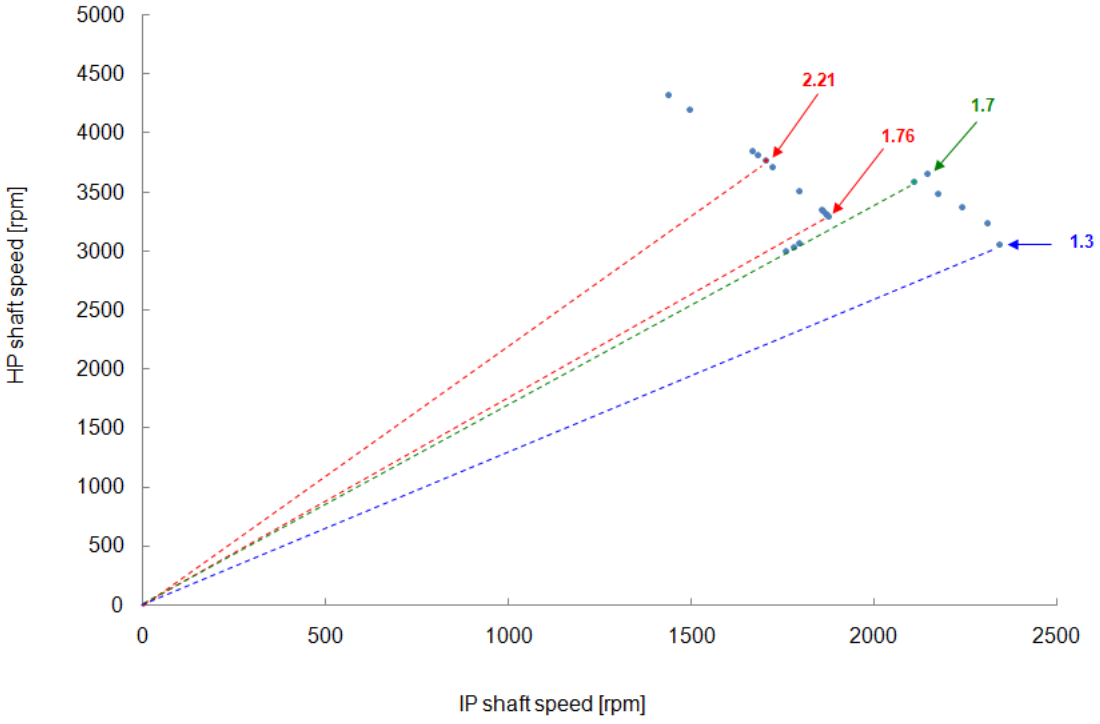

Figure 7.6: Successfully simulated groundstarts for different values of shaft coupling ratios.

As shown in Fig.7.6, the current model is able to successfully handle ground-starts up to a minimum coupling ratio value of 1.76 starting from the baseline case of coupling ratio 2.21. Greater values than the latter are not considered to be challenging since in that case the HP shaft is of higher importance (absorbs more torque and obtains higher acceleration). Such an HP based starting simulation capability already exists and has been validated in the past.

The solver is not able to match the engine components during groundstarts with a shaft coupling ratio less than 1.76. The reason is that the IP compressor stalls and the model fails as the boundaries of the map are abused. A map scaling process is

here required. Adjusting the IP map, successful simulations with even smaller shaft coupling ratio are achieved while at the same time a better IP compressor design is revealed by the new characteristics. As shown in Fig.7.6, the IP map has been scaled up and the minimum coupling ratio value that the solver was able to handle was 1.3. That brings the engine modelling significantly closer to the IP-only starting engine.

It needs to be underlined that BD19 has no full groundstart simulation capability. The simulation's starting point is always the steady state deadcrank speed. That means that there is no simulation capability during the acceleration phase of the engine before the lighting up. In addition, a limited amount of experimental data was available for the validation of the above presented groundstarting simulations. Therefore only the robustness of the code could be evaluated while its accuracy could only be partially assessed. The comparison of the simulation results against the only experimental case found showed that all shaft speeds match the test data quite well while also the fuel consumption is the same for the biggest time range of the acceleration manoeuvre.

In general, BD19 demonstrates a good groundstart simulation capability. Nevertheless more work is required in for order the whole acceleration phase to be simulated. This can be achieved only by implementing the torque maps as explained in an earlier chapter. In addition, more work is required regarding the modelling of cases in which the SPC system is not in use, that is a IP-only starting engine. The major issue regarding the latter is the modelling of the characteristics of compressors in stall.

7.4 Concluding remarks

The latest version of BD19 code in which the SPC as well as the IP offtake and starting capability were implemented was used for the derivation of the windmilling

power offtake capability of the engine as well as for IP shaft groundstarting simulations in order for the reliability and robustness of the tool to be assessed. The study was carried out according to the recommended strategy as described in [83] where a limited amount of groundstarting and windmilling relight simulations is presented. At the same time the modelling aspects that BD19 seems less capable to cope with are explained in great detail.

As far as the windmilling performance of the engine is concerned, it looks that BD19 is greatly capable to simulate a large amount of cases within the relight envelope, coping efficiently with power offtake demand taken either by the IP or the LP shaft. More work is required regarding the fan characteristics, as steady state windmilling speeds are over-predicted leading to an over-prediction of the LP shaft's power offtake capability as well. Potentially, a first principles modelling for the prediction of the LP steady state windmilling speed might increase the simulation's fidelity in this aspect. In addition, HP shaft speeds are slightly over-predicted too which implies that a re-adjustment of the characteristics is required as mentioned also in [83]. Apart from that, the windmilling performance simulation capability using BD19 is at a quite satisfactory level.

More issues to discuss regarding the groundstarting simulation capability exist. In spite of the good model response to the herein simulated cases, the implementation of torque maps is necessary for real groundstart simulation capability. In addition, more work is required for the modelling of the characteristics of compressors in stall in order to achieve a better simulation capability of the IP-only starting manoeuvre. Finally, the effect of the control system which defines the fuel schedule, thus the acceleration rate needs to be further examined as its influence is not well understood by the author.

Chapter 8

Technology transfer

8.1 Introduction

One of the major aims of the UTC in Performance engineering at Cranfield is the *knowledge* or the *technology* transfer of the methods developed at the university to Rolls-Royce and, if possible, their incorporation within the company methods suite. Consequently, every doctoral project is structured in such a way that its outcomes could be transfered to the company.

This doctoral project has offered a number of methods that enhance the physical background of the engine component performance prediction as well as highlighted the way forward regarding the sub-idle whole engine modelling. In order for the development of the methods to be completed, a number of additional actions has been required apart from the author's effort within the doctoral course; assistance of numerous MSC projects, regular technical reviews and meetings between the university project group and various Rolls-Royce groups, depending on the research topic under discussion and finally an industrial placement.

8.2 Project management

As realised from the very beginning the sub-idle research is an extremely wide topic, thus the areas where the current project had to focus on, cover a big range of gas turbine engine operation. This is obviously reflected by the project objective list which implies that this research is a quite multidisciplinary effort.

Consequently, it was decided to divide the whole project in two main parts; component performance and engine performance with the most emphasis to be given into the former as the sponsor had identified weaknesses in the physical background of its sub-idle performance component methods. At a later stage, integration of the generated methods within the sub-idle performance solver (BD19) took place. As the sub-idle phenomena are extremely complicated there was no specific timeframe regarding where the whole engine research would start. That was dependent on the technology readiness level of the component related research progress.

Regarding the component related research it was decided that three main components had to be investigated; compression systems, combustion systems and exhaust mixing systems with more emphasis to be given into the first one. In addition, it was also decided that the doctoral effort had to be assisted by a number of MSC projects closely supervised every year by the author of this thesis and Dr. V. Pachidis. It needs to be highlighted that all the proposed and accomplished MSC projects were of major importance for the progress of the project thus extra care and time was given. This effort was also assisted by the company, thanks to the frequent technical reviews and meetings with specialists for tracking the progress in each part individually.

8.3 The MSC students

As already mentioned a number of MSC students has been working on sub-idle research topics assisting the doctoral effort by undertaking vital parts of the whole

research.

Schematic 8.1 illustrates the interaction between the author of this thesis and the MSC students who undertook a sub-idle related research topic each year.

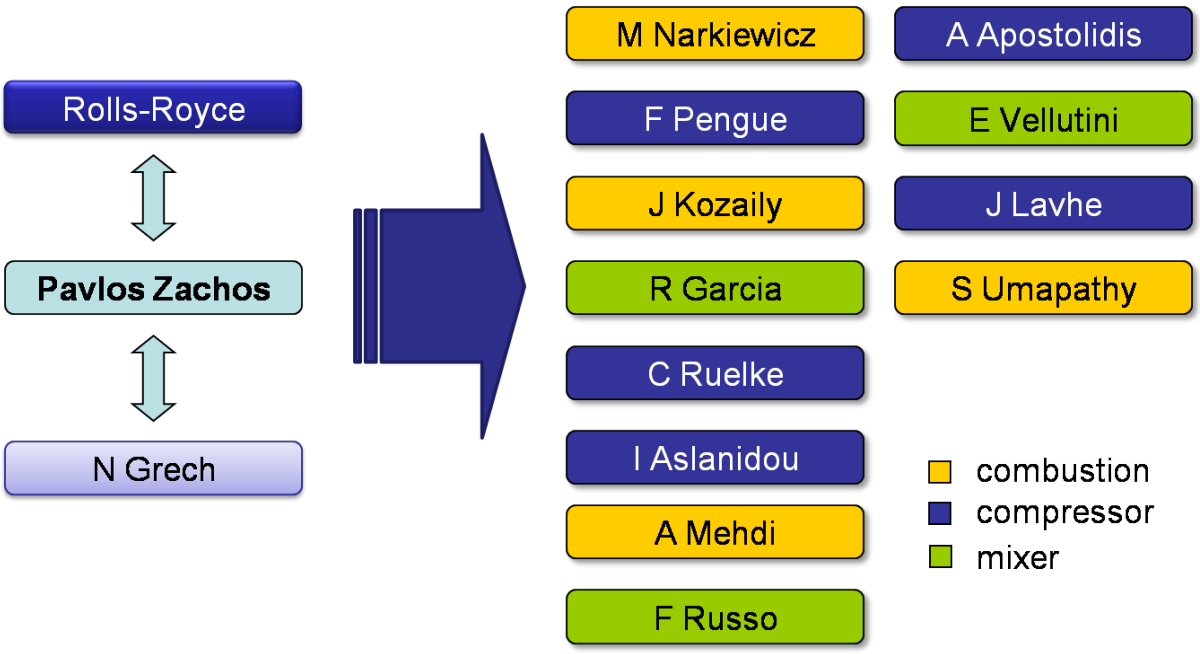

Figure 8.1: Project players interaction (schematic).

During the first year, which was in overlap with J Howard, the MSC student M Narkiewicz [84] undertook the combustion modelling required after Howard's and Prof. Pilidis' decision.

In the second year, it was decided to increase the number of the MSC projects to reflect the multi-discipline of the sub-idle research. Thus, in addition to the doctoral work which was mainly focused on the experimental testing of the compressor cascade, F. Pengue [91] was responsible for the numerical modelling of it while J. Kozaily [65] undertook the combustion related research. Mixed exhaust engine numerical modelling was carried out by R. Garcia [39].

During the third year, the compressor work was continued by C. Ruelke [102] while the sub-idle compressor map generation was carried out by I. Aslanidou [7]. In addition, combustion research was conducted by A. Mehdi [79] while F. Russo undertook the research on the exhaust mixer [103].

Finally, a last set of MSC projects was launched for the acad. year 2009-2010 aiming to be advised by the next doctoral student. In that context, A. Apostolidis is responsible to finilise the compressor related research, S. Umapathy the combustion studies, E. Vellutini the mixer issues while J. Lavhe will be generating an advanced pressure loss model for compressors at highly negative incidence based on previous research.

As it appears from the current thesis, the MSC contribution was quite valuable throughout the doctoral course. This implies the close supervision the students experienced both from the author and Dr. V. Pachidis throughout each academic year, in order to give and receive the most out of their MSC diploma thesis.

These activities involved of course the interaction with Rolls-Royce in the form of regular presentations as well as meetings, either at Cranfield, in Derby or Bristol, for more detailed conversations, where also company specialists could contribute.

Finally, during the concluding phase of this research, a knowledge transfer towards the next doctoral student, N. Grech was carried out.

8.4 Reporting and meetings

As already mentioned, the progress of the entire project was regularly and frequently tracked by Rolls-Royce. Technical reviews approximately every two months were held at Cranfield where all the latest progress done was presented to the industrial supervisors.

When necessary, additional meetings either at Cranfield, in Derby or Bristol were organised for in-depth discussions on a specific topic where also company specialists were present. Very often those meetings were extremely crucial for the progress of the work.

Finally, annual presentations were given to a much wider Rolls-Royce audience during the annual reviews of the university, in order for all the progress done within

the previous year to be widely demonstrated.

8.5 Industrial placements

During the latest stages of the course an industrial placement within the performance department of Rolls-Royce Derby was done by the author. The objective was to perform whole engine modelling using the latest version of BD19 code and also to prepare the ground for the future project tasks which will be focused on whole engine performance. The placement occurred between November 2009 and January 2010.

8.6 Knowledge transfer

The entire project's outcome is a number of methods regarding the sub-idle performance prediction of gas turbine components. As mentioned in the beginning of the chapter the policy of the UTC is to highlight ways in which the developed methods will have a benefit for the industrial sponsor if transfered.

More specifically, the compressor related research enhances the industrial capability. Locked rotor studies (experimental and numerical) provide a reliable platform for the validation of similar studies done in-house, while the sub-idle compressor characteristics generation capability has been enhanced by the new interpolation methods developed. The map generation module can be easily delivered to the company for future use as it features RRAP-BD19 compatibility and it will also be accompanied by a user's guide. In addition the highly negative incidence pressure loss modelling has an important contribution when such models are required (e.g. through-flow analysis solvers).

A very important aspect of the compressor related work is the fact that it was done in real modern blade designs, whereas the map generation methods were developed using real engine maps as well. Thus, the value of the generated knowledge has been directly translated into useful material for the company.

The zooming into the sub-atmospheric injection dynamics provides an insight into the mixed reaction-evaporation rate based modelling for the calculation of the combustion efficiency during the relight process. More work is required to define the most appropriate way to implement the model within the performance solver. However, the outcome of the research is really promising while the high fidelity numerical models of the atomiser and the combustion chamber will be of future use too.

In addition, the mixer related research has highlighted the approach should be adapted for the development of a robust mixed exhaust engine model able to capture and represent the physics of the problem. However, more work is required in this direction as the current research has not been able to provide with a concrete final model. Nevertheless, the high fidelity mixer models can always be used for future research.

Finally, all the outcomes of this research need to be implemented within BD19 solver. As shown previously, the component related research has always been performed bearing in mind that engine performance simulation is mostly benefited by simple component models able, though, to represent as much of the component physics as possible. The first steps towards this direction have been presented in the corresponding chapter where the first extensive assessments of the latest sub-idle performance solver were carried out.

Changes in the design process of a future engine, as far as its relight capability is concerned, are as mentioned by Howard in [51] and reproduced in Fig. 8.2.

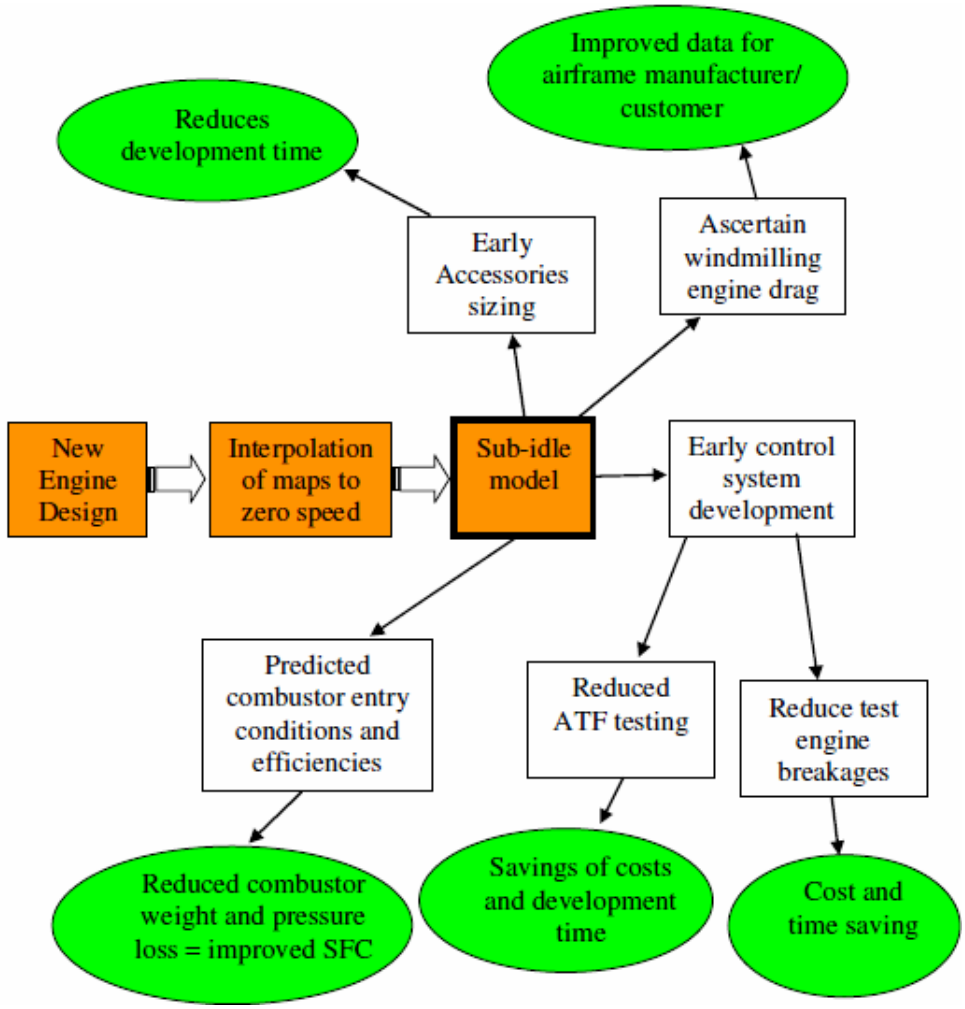

Figure 8.2: Design process change from introduction of sub-idle modelling and the possible benefits [51].

Chapter 9

Summary, contribution and future work

As explained in the first chapters, the current thesis attempts an insight into the physical phenomena occurring within a few major components of a gas turbine aero engine under very low speeds or sub-idle conditions. The aim is not only to increase the knowledge on sub-idle component behavior but also to achieve the most advantageous component performance representation from which a whole engine performance simulation solver can have the maximum benefit in terms of accuracy and robustness. Therefore, component performance research was the task which most effort was put on, before any whole engine performance modelling attempts. As described in Chapter 7, only a few preliminary tasks have been carried out regarding the whole engine modelling and consequently most of the future work is pointing toward this direction.

This chapter, summarises the major contribution done out of each research topic, while recommended tasks for the way forward of the project are also given hereafter.

9.1 Research topic summary and contribution

Each subsection herein, summarises the contribution done in each research topic separately according to the order in which the thesis is structured, starting with component performance and concluding with whole engine modelling issues.

9.1.1 Sub-idle compressor performance

Regarding the low-speed compressor performance, most of the work is dealing with the locked-rotor compressor performance which represents the most extreme off-design compressor operating mode. The accurate derivation of a compressor zero-speed line is of vital importance as the sub-idle map generation process is also significantly enhanced by that. This research focuses on investigating and modelling the phenomena occurring within compressor blade rows when operating at highly negative incidence angles, that is with fully separated flows at the pressure side of the blade. Numerical as well as experimental approaches have been applied while a generic method to predict compressor locked rotor performance has been put together based on the blade element theory whose validity has been proved before for far off-design blade operation.

The generic loss model, which provides predictive capability for the locked rotor performance of every compressor design, can be characterised as the major contribution out of this work. In addition, a set of experimental data from highly negative incidence blade testing, published in the open literature [123], can be considered as a platform that similar numerical or analytical studies can be validated against.

9.1.2 Sub-idle engine characteristics generation

This research topic is strongly related to the locked-rotor compressor performance work as the development of more advanced sub-idle map generation methodologies is based on the accurate definition of the zero-speed line. Having mentioned that,

the research regarding the sub-idle characteristics focuses on generating low-speed compressor characteristics using interpolation processes between the zero-speed and the above idle given speed lines. In that respect, the map generation obtains a more enhanced physical background as more low-speed physical phenomena are captured within the characteristic. Finally, a number of additional checks applied during the generation process enhance even more the physical background of the process.

All the above have been implemented within a numerical sub-idle map generator FORTRAN tool providing the capability for rapid, fully automated low-speed compressor characteristic generation with of course significantly enhanced physical background. The development of the new interpolation methodologies as well as the implementation of the tool are considered to be the major contributions out of this research topic which undoubtedly pushes forward the whole engine sub-idle performance predictions.

9.1.3 Sub-idle combustion performance

The research on low-speed combustion definition focuses on the definition of the factors affecting combustion efficiency under sub-idle conditions. Engine data analysis implies that fuel evaporation plays a significant role on this, therefore evaporation effects during the fuel injection phases have been studied within a wide range of operating conditions emphasizing on the effect of the sub-atmospheric pressure on the spray structure and more specifically on the Sauter Mean Diameter of the droplets. The latter has a direct impact on the combustion efficiency. It was found that for really low engine speeds and ambient pressures, an evaporation rate based combustion efficiency model is more appropriate to describe the process rather than an extrapolation toward the sub-idle regime of the reaction rate based model values. Extensive numerical studies to quantify the effect of low pressure on the performance of an airblast atomiser were carried out aiming at the generation of an evaporation rate based model for the calculation of the combustion efficiency.

A new expression for the calculation of the droplet SMD taking into account the sub-atmospheric pressure was derived, based on previous SMD calculation approaches found in the open literature. Consequently, an evaporation rate based model to calculate combustion efficiency was put together. In overall, the main contribution regarding the combustion related studies is the introduction of a mixed reaction-evaporation rate based combustion efficiency model suitable for sub-idle engine performance simulations.

9.1.4 Sub-idle exhaust mixer performance

The research on mixed exhaust engine performance focuses on investigating low-speed mixing flow phenomena aiming at introducing a mixer characteristic as engine data imply once again that the traditional modelling approach is not appropriate enough for sub-idle simulations. Numerical studies to identify the performance of an exhaust mixer within a range of operating conditions have been carried out. A better understanding of the phenomena occurring when flows with significantly different pressures and velocities come in contact has been obtained. However no specific mixer performance model has been proposed as there was not enough time within the given timeframe.

The generation of high-fidelity exhaust mixer numerical models as well as the definition of the factors that dominate the component's behavior under sub-idle conditions, on which a mixer characteristic can be later relied on are considered to be the major contributions out of this research.

9.1.5 Sub-idle engine performance

Since the biggest amount of project time was invested on improving the sub-idle component performance methods, little effort has been put on whole engine performance research. In reality, only preliminary whole engine modelling took place within the current doctoral project. However, a number of tasks aiming at validat-

ing the latest version of RRAP-BD19 code has been carried out. More specifically, code's ability to simulate engine windmill relights has been assessed by generating the emergency power offtake envelopes as shown in Chapter 7. In addition engine groundstarting by IP or both IP-HP spool cranking has been investigated in an effort to evaluate the groundstarting simulation capability of the same solver.

The above mentioned tasks offered a better understanding of the latest version of numerical tool highlighting where and how the component performance prediction methods developed can be incorporated within. Consequently, the major contribution out of the BD19 whole engine modelling shall be the identification of the ways forward or, in other words, from which perspective whole engine simulation can have the maximum out of the component related research findings. At the same time, a feeling of the windmilling and groundstarting performance parameters for a modern, high bypass ratio civil turbofan engine has been obtained.

9.2 Recommendations for future work

As it happens with every research course, all the questions cannot be answered by its end. Unavoidably here is the point that the way forward for the future researchers must be highlighted.

Sub-idle engine modelling seems to be a never-ending research topic. There is no question whose answer (if there is only one!) doesn't create further question marks, identifying the areas where more work is required. However, this is quite a healthy situation as it offers reasons to continue our investigations to create useful and important knowledge on a rather unexplored region of engine operation.

Most of the recommended future tasks have been reported within the concluding remarks section of each chapter. However, it is worthy to summarise everything in a separate section for reasons of completeness. Again, within the current section there is a subsection for the future work regarding every research topic, according

to the already followed structure of the thesis.

9.2.1 Sub-idle compressor performance

Regarding the sub-idle and low speed compressor aerodynamics, future work can be pointing toward the refinement of the generic, highly negative incidence pressure loss model for a locked rotor stage. Numerical simulations of a locked rotor stage and interpretation of the results in a similar, initially, to the one proposed herein way will lead to a more accurate pressure loss model. The mixing flow effects created by the wake interaction between the two blade rows which increase the total pressure loss through the stage will be captured. Consequently, the generation of the whole compressor characteristic using the stage stacking technique will also be significantly enhanced.

In addition, a more sophisticated model layout derived by a better representation-interpretation of the CFD results can provide a higher accuracy for pressure loss model based calculations. Such a layout can be based on Lieblein's approaches that can be found in the open literature whose effectiveness is already well proved by their implementation and use within compressor performance prediction solvers.

Finally, extension of the 2D blade database to cover an even wider range of stager and camber angles might increase the flexibility and applicability of such a model.

9.2.2 Sub-idle engine characteristics generation

The future work on the sub-idle characteristic generation must be focusing on improving the capability of the numerical tool.

It has already been mentioned that implementing more interpolation options (exponential or logarithmic apart from polynomial) is an approach to create more accurate maps. Additionally, performance simulations can contribute to the map quality as validation of simulation results against experimental data can reveal the required map readjustments for obtaining the most accurate results. Implementation

of a better map alignment capability against ATF data also needs to be carried out. Research on whole map prediction using rapid zooming techniques such as streamline curvature might be required to offer the highest fidelity characteristic. The definition of the steady state windmilling line is finally a very challenging task as far as the map generation is concerned.

9.2.3 Sub-idle combustion performance

Regarding the combustion related performance, more work is required on identifying the most effective implementation strategy of the generated model within a performance prediction solver. Thoughts in this direction have already been mentioned in a previous chapter.

In addition, the model can become generic by comparing the sub-atmospheric performance of several different atomisers and creating a refined expression to cover a wider range of injector types.

9.2.4 Sub-idle exhaust mixer performance

More work is required for the generation of a mixer performance model based on the conclusions done by the current numerical research. It has been shown that velocity and mixer diameter ratio are the two dominant factors that a mixer characteristic can be built on, as most of the flow phenomena can be explained on the basis of the two aforementioned parameters. What remains is to represent the performance of the component in a characteristic plot and find the most efficient approach to incorporate it within a performance solver.

9.2.5 Sub-idle engine performance

This is the area where most of the future effort must be put in, to get the maximum benefit out of the component related research.

The main aims shall be to increase the solver's predictive accuracy as far as the windmill relights are concerned as well as to push forward the groundstarting simulation capability.

The former can be achieved by a more careful fan modelling to allow for a better prediction of its steady state windmilling speed. Regarding the latter, a new version of BD19 with the capability to read and use torque maps is required. In such a way the simulation of the whole groundstarting process will be allowed and further research on the starting performance of an engine when its IP shaft is crancked will also be allowed. Needless to mention that validation of the new version against the older one will be necessary also as far as windmilling and starter assisted relights are concerned. Work on understanding the effect of the control system is also required.

The implementation of the new combustion model is also something that needs to be carried out in order for the modelling to become less dependent upon the combustion inefficiency factor which is currently employed. Finally, the new mixer model might also have a great benefit as far as the sub-idle simulation of mixed exhaust engines is concerned.

It is highly recommended not to conduct all the changes at once but gradually and step by step in order to track errors easier. The final stage will be to assess the functionality of BD19 solver after all the code changes and validation take place. Using such an approach sub-idle modelling will be pushed forward having increased the accuracy and the predictive capability of the performance simulation tool.

References & Bibliography

[1] *ANSYS CFX Manual*.

[2] R. B. Abernethy, R. P. Benedict, and R. B. Dowdell. Asme measurement uncertainty. *Journal of Fluids Engineering*, 107:161–164, 1985.

[3] AGARD. C.f.d. validation for propulsion system components. *AGARD Advisory report 355*, 1998.

[4] R. K. Agrawal and M. Yunis. A generalized mathematical model to estimate gas turbine starting characteristics. *ASME Journal of Engineering for Power*, 104:194–201, 1982.

[5] A. Alexiou, E. Baaldbergen, K. Mathioudakis, O. Kogenhop, and P. Arendsen. Advanced capabilities for gas turbine engine performance simulations. *ASME Turbo Expo, Montreal, Canada, 2007*.

[6] B. A. Anderson, D. Messih, and R. C. Plybon. Engine-out performance characteristics. *ISABE 97-7216*.

[7] I. Aslanidou. Physically enhanced compressor map generation for sub-idle performance studies. MSc thesis, Cranfield University School of Engineering, 2009.

[8] I. Aslanidou, P. K. Zachos, V. Pachidis, and R. Singh. A physically enhanced method for sub-idle compressor map generation and representation. *ASME Turbo Expo, Glasgow, Scotland, UK, 2010*.

[9] J. Beck, A. H. Lefebvre, and T. Koblish. Airblast atomisation at conditions of low air velocity. *27th AIAA, Aerospace sciences meeting, Reno, US*, 1989.

[10] J. Beer and N. Chigier. *Gas turbine aerodynamics*. Wiley - Interscience Publications, 1972.

[11] J. J. Bittan. Study of a compressor during windmilling using computational fluid dynamics. MSc thesis, Cranfield University School of Engineering, 2005.

[12] W. Braig, H. Schulte, and C. Riegler. Comparative analysis of the windmilling performance of turbojet and turbofan engines. *ASME Journal of Propulsion and Power*, 15(2):326–333, 1999.

[13] M. Breuer and N. Jovicic. Separated flow around a flat plate at high incidence: an l.e.s. investigation. *Journal of Turbulence*, 2, 2001.

[14] B. N. Caines, R. A. Hicks, and C. W. Wilson. Influence of sub-atmospheric conditions on the performance of an airblast tomiser. *37th AIAA/ASME/SAE/ASEE Joint propulsion conference and exhibit, Salt Lake City, US, 2001.*

[15] A. D. S. Carter. Low-speed performance of related aerofoils in cascade. *ARC*, 29, 1950.

[16] V. S. P. Chaluvadi, A. I. Kalfas, and H. P. Hodson. Vortex transport and blade interactions in high pressure turbines. *ASME Journal of Turbomachinery*, 126:395–405, 2004.

[17] V. S. P. Chaluvadi, A. I. Kalfas, H. P. Hodson, H. Ohyama, and E. Watanabe. Blade row interaction in a high pressure steam turbine. *ASME Journal of Turbomachinery*, 125:014–024, 2003.

[18] M. S. Choi, J. S. Lim, and Y. S. Hong. A practical method for predicting the windmilling characteristics of simple turbojet engines. *ASME Turbo Asia Conference, November 1996, Jakarta, Indonesia*.

[19] W. G. Cornell. The stall performance of cascades. *Proceedings of the 2nd U. S. National congress of applied mechanics, Michigan, 1954*, 1954.

[20] R.M. Cummings, J.R. Forsythe, S.A. Morton, and K.D. Squires. Computational challenges in high angle of attack flow prediction. *Progress in Aerospace Sciences*, 39:369–384, 2003.

[21] N. A. Cumpsty. *Compressor aerodynamics*. Longman Scientific and Technical, 1989.

[22] N. A. Cumpsty. Averaging nonuniform flow for a purpose. *Journal of Turbomachinery*, 128:120–129, 2006.

[23] I. J. Day. Stall inception in axial flow compressors. *ASME Journal of Turbomachinery*, 115:1–9, 1993.

[24] I. J. Day and C. Freeman. The unstable behavior of low and high-speed compressors. *ASME Journal of Turbomachinery*, 116:194–201, 1994.

[25] J. D. Denton. Loss mechanisms in turbomachines. *IGTI scholar lecture*, 1993.

[26] J. D. Denton and W. N. Dawes. Computational fluid dynamics for turbomachinery design. *Proceedings of I.Mech.E.*, 213, 1998.

[27] S. Deutsch and W.C. Zierke. The measurement of boundary layers on a compressor blade in cascade at high positive incidence angle. 1-experimental techniques and results. *NASA-CR-179491*, 1986.

[28] S. Deutsch and W.C. Zierke. The measurement of boundary layers on a compressor blade in cascade. part 1- a unique experimental facility. *ASME Journal of Turbomachinery*, 109:520–526, 1987.

[29] S. Deutsch and W.C. Zierke. The measurement of boundary layers on a compressor blade in cascade. part 2- suction surface boundary layers. *ASME Journal of Turbomachinery*, 110:138–145, 1988.

[30] S. Deutsch and W.C. Zierke. The measurement of boundary layers on a compressor blade in cascade. part 3- pressure surface boundary layers and the near wake. *ASME Journal of Turbomachinery*, 110:146–152, 1988.

[31] S. Deutsch and W.C. Zierke. The measurement of boundary layers on a compressor blade in cascade. part 4- flowfields for incidence angles of -1.5 and -8.5 degrees. *ASME Journal of Turbomachinery*, 112:241–255, 1990.

[32] S. L. Dixon. *Fluid mechanics and thermodynamics of turbomachinery*. Pergamon Press, 4th edition, 1998.

[33] R. P. Dring and D. A. Spear. The effects of wake mixing on compressor aerodynamics. *ASME Journal of Turbomachinery*, 113:600–607, 1991.

[34] J.A. Ekaterinaris and F.R. Menter. Computation of separated and unsteady flows with one and two-equation turbulence models. *AIAA 32nd Aerospace Sciences Meeting and Exhibit, Reno, Nevada*, 1994.

[35] P. Foster. *Personal communication, December 2009.*

[36] T. H. Frost. Practical bypass mixing systems for fan jet aero engines. *The Aeronautical Quarterly*, pages 141–160, 1966.

[37] S. J. Gallimore. Axial flow compressor design. *Proceedings of I.Mech.E.*, 213, 1998.

[38] S. J. Gallimore. Viscous throughflow modelling of axial compressor blade rows using a tangential blade force hypothesis. *Journal of Turbomachinery*, 120:662–670, 1998.

[39] R. Garcia. Sub-idle mixer performance modelling. MSc thesis, Cranfield University School of Engineering, 2008.

[40] S. R. Gaudet and J. E. D. Gauthier. A simple sub-idle component map extrapolation method. *ASME Turbo Expo, Montreal, Canada*, 2007.

[41] C. Georgakis. *Experimental studies on volute-impeller interactions of centrifugal compressors having vaned diffusers*. PhD thesis, Cranfield University, School of Engineering, 2003.

[42] R. A. Gore and C. T. Crowe. Observations on the flow in a confined coaxial jet. *AIAA, 88-3591-CP*, 1988.

[43] J. P. Gostelow. *Cascade aerodynamics*. Pergamon Press, 1984.

[44] E. M. Greitzer, C. S. Tan, and M. B. Graf. *Internal flow concepts and applications*. Cambridge University Press, 2004.

[45] N. G. Hatton. Windmilling performance of bypass engines. Technical report, PTR00736, Rolls-Royce internal report, 1984.

[46] W. R. Hawthorne. *Aerodynamics of turbines and compressors. High speed aerodynamics and jet propulsion*. Princeton University Press, 1964.

[47] G. J. Hendricks, L. P. Bonnaure, J. P. Longley, E. M. Greitzer, and A. H. Epstein. Analysis of rotating stall onset in high speed axial flow compressors. *AIAA 93-2233*, 1993.

[48] M. Holmes. An investigation into mixing between bypass air and turbine exhaust gates. *NGTE notes R-261/262/263/277*, 1964.

[49] J. H. Horlock. *Axial flow compressors. Fluid mechanics and thermodynamics*. Robert Krieger publishing company, New York, 1973.

[50] J. Howard. Adour 951 sub-idle 2-spool modelling; bd19 code; main report. Technical report, Cranfield University Rolls-Royce UTC report No. 121, 2007.

[51] J. Howard. Sub-idle modelling of gas turbines; altitude relight and windmilling. EngD. thesis, Cranfield University School of Engineering, 2007.

[52] A. R. Howell. The present basis of axial flow compressor design: Part i, cascade theory and performance. *ARC R and M*, 2095, 1942.

[53] A. R. Howell. Design of axial compressors. *Proceedings of IMechE*, 153, 1945.

[54] A. R. Howell and A. D. S. Carter. Fluid flow through cascades of aerofoils. *6th International congress on applied mechanics, Paris, 1946.*

[55] A. J. B. Jackson. Aero gas turbine windmilling, relighting and pull-away: A position paper. Rolls-Royce University Technology Centers in Performance and Combustion, AJCR2002, Rolls-Royce Proprietary Data, Cranfield University School of Engineering, 1998.

[56] A. K. Jasuja. Atomisation of crude and residual fuel oils. *Journal of Engineering for Power*, 101:250 – 258, 1979.

[57] A. K. Jasuja and A. H. Lefebvre. Influence of ambient pressure on drop size and velocity distributions in dense sprays. *International Symposium on Combustion*, 25:345 – 352, 1994.

[58] G. Jones. Performance modelling of windmilling gas turbines. EngD thesis, Cranfield University School of Engineering, 2002.

[59] G. Jones, P. Pilidis, and B. Curnock. Compressor characteristics in gas turbine performance modelling. *ASME Turbo Expo, New Orleans, Louisiana*, 2001.

[60] G. Jones, P. Pilidis, and B. Curnock. Extrapolation of compressor characteristics to the low-speed region for sub-idle performance modelling. *ASME Turbo Expo, Amsterdam, The Netherlands*, 2002.

[61] I.-S. Kang, M.-S. Choi, J.-S. Lim, and Y.-S. Kong. Analysis of windmilling characteristics for a twin-spool turbofan engine. *ASME Asia 1997 Congress and Exhibition, 1997, Singapore.*

[62] T. Kipouros, D. M. Jaeggi, W. Dawes, G. T. Parks, and M. Savill. Multi-objective aerodynamic design optimisation for axial compressors. *ERCOFTAC Bulletin*, 66:21–24.

[63] S. J. Kline and F. A. McClintock. Describing uncertainties in single sample experiments. *Mechanical Engineering*, 75:3–8, 1953.

[64] T. Korakianitis. On the propagation of viscous wakes and potential flow in axial-turbine cascades. *Journal of Turbomachinery*, 115:118–127, 1993.

[65] J. Kozaily. Altitude relight performance modelling; numerical analysis of an airblast atomiser under sub-atmospheric conditions and low air velocities. MSc thesis, Cranfield University School of Engineering, 2008.

[66] J. Kozaily, P. K. Zachos, V. Pachidis, and R. Singh. Gas turbine fuel atomisation dynamics under sub-atmospheric conditions. *ISABE 2009, Montreal, Canada.*

[67] J. Kurzke. How to get component maps for aircraft gs turbine performance simulations. *International Gas Turbine and Aeroengine Congress and Exhibition, Birmingham, UK, 1996.*

[68] A. H. Lefebvre. *Gas Turbine Combustion.* McGraw-Hill Series in Energy, 1983.

[69] A. H. Lefebvre. *Atomisation and Sprays.* Hemisphere Publishing corporation, Taylor and Francis, 1989.

[70] S. Lieblein. Loss and stall analysis of compressor cascades. *Transactions of ASME, Series D*, 81, 1959.

[71] S. Lieblein. Experimental flow in two-dimensional cascades. *NASA SP-36, Chapter VI*, 1965.

[72] S. Lieblein and W. Roudebush. Theoretical loss relation for low-speed 2d cascade flow. *NACA T.N. 3662*, 1956.

[73] J. P. Longley. A review of non-steady flow models for compressor stability. *ASME Turbo Expo, Cincinnati, Ohio, USA, 1993.*

[74] A. F. Massardo and M. Scialo. Thermoeconomic analysis of gas turbine based cycles. *ASME Journal of Engineering for Gas Turbines and Power*, 2000.

[75] B. S. Massey. *Mechanics of fluids.* Chapman and Hall, 4th edition.

[76] J. D. Mattingly. *Elements of Gas Turbine Propulsion.* McGraw-Hill International Editions, 1996.

[77] A. B. McKenzie. *Axial flow fans and compressors: aerodynamic design and performance.* Ashgate, 1997.

[78] R. Meads, D. Widdowson, D. G. Johnson, and C. A. W. K. Syed. Bd19 user's guide; 3 shaft turbofan starting synthesis program. Technical report, PTR90900, Rolls-Royce internal report, 2006.

[79] A. Mehdi. Altitude relight sub-idle combustion modelling. MSc thesis, Cranfield University School of Engineering, 2009.

[80] F.R. Menter. Zonal two equation k-ω turbulence models for aerodynamic flows. *AIAA 24th Fluid Dynamics Conference, Orlando, Florida*, 1993.

[81] F.R. Menter. Two-equation eddy-viscosity turbulence models for engineering applications. *AIAA Journal*, 32, 1994.

[82] M. Monticelli. Txxx bd19 sub-idle model. Technical report, PTR23159, Rolls-Royce internal report, 2003.

[83] A. Moxon. Txxx bd19 sub-idle model with start power coupling. Technical report, PTR109212, Rolls-Royce internal report, 2007.

[84] M. Narkiewicz. Engine relight performance; a combustion analysis. MSc thesis, Cranfield University School of Engineering, 2007.

[85] C. G. Van Niekerk. Ducted fan design theory. *Journal of applied mechanics*, 25, 1958.

[86] V. Pachidis. Gas turbine advanced performance simulation. PhD thesis, Cranfield University School of Engineering, 2006.

[87] V. Pachidis, P. Pilidis, F. Talhouarn, A. Kalfas, and I. Templalexis. A fully integrated approach to component zooming using computational fluid dynamics. *ASME Journal of Engineering for Gas Turbines and Power*, 128, 2006.

[88] D. E. Paxson. A comparison between numerically modelled and experimentally measured loss mechanisms in wave rotors. *AIAA Journal of Propulsion and Power*, 11, 1985.

[89] D. E. Paxson. An incidence loss model for wave rotors with axially aligned passages. *NASA / TM-1998-207923*, 1998.

[90] H. Pearson. Mixing of exhaust and bypass flow in a bypass engine. *Journal of the Royal Aeronautical Society*, pages 528–531, 1962.

[91] F. Pengue. Numerical and experimental analysis of an h.p. compressor cascade. MSc thesis, Cranfield University School of Engineering, 2008.

[92] D. Pollard and J. P. Gostelow. Some experiments at low speed on compressor cascades. *Journal of Engineering for Power*, 89(3):427–436, 1967.

[93] L. Porreca, T. Behr, J. Schlienger, A. I. Kalfas, R. S. Abhari, J. Ehrhard, and E. Janke. Fluid dynamics and performance of partially and fully shrouded axial turbines. *ASME Journal of Turbomachinery*, 127:668–678, 2005.

[94] L. Porreca, M. Hollenstein, A. I. Kalfas, and R. S. Abhari. Turbulence measurements and analysis in a multistage axial turbine. *ASME Journal of Propulsion and Power*, 23:227–234, 2007.

[95] A. Prasad. Calculation of the mixed-out state in turbomachine flows. *Journal of Turbomachinery*, 127:564–572, 2005.

[96] H. Rehab and E. Villermaux. Flow regimes of large velocity ratio coaxial jets. *Journal of Fluid Mechanics*, 345, 1997.

[97] C. Riegler, M. Bauer, and J. Kurzke. Some aspects of modeling compressor behavior in gas turbine performance calculations. *ASME Turbo Expo, Munich, Germany, 2000*.

[98] W. H. Robbins, R. J. Jackson, and S. Lieblein. Blade element flow in annular cascades. *NASA SP-36, Chapter VII*, 1965.

[99] C. Rodgers. Starting of torque characteristics of small aircraft gas turbines and apu's. *ASME Journal of Engineering Power*, 102:231–238, 1980.

[100] R. J. Roelke. *Miscellaneous losses*. Chapter 8 of turbine design and applications, NASA SP-290, A. J. Glassman, 1994.

[101] A. L. Rowe. *Personal communication, September 2007*.

[102] C. Ruelke. Numerical and experimental analysis of an hp compressor cascade. MSc thesis, Cranfield University School of Engineering, 2009.

[103] F. Russo. Aero engine sub-idle mixer performance modelling. MSc thesis, Cranfield University School of Engineering, 2009.

[104] N. L. Sanger. The use of optimisation techniques to design controlled diffusion compressor blading. *ASME Journal of Engineering for Power*, 105:256–264, 1983.

[105] H. Saravanammuttoo, G. F. C. Rogers, and H. Cohen. *Gas turbine theory*. Prentice Hall, 5th edition.

[106] W. M. Schulze, J. R. Erwin, and G. C. Ashby. Naca-65 compressor rotor performance with varying annulus-area ratio, solidity, blade angle and reynolds number and comparison with cascade result. *NACA TN-4130*.

[107] Z. Q. Shou. Calculation of windmilling characteristics of turbojet engines. *ASME Journal of Engineering for Power*, 103(1):1–12, 1981.

[108] R. P. Shreeve, Y. Elazar, J. W. Dreon, and A. Baydar. Wake measurements and loss evaluation in a controlled diffusion compressor cascade. *ASME Journal of Turbomachinery*, 113:591–599, 1991.

[109] R. P. Shreeve, Y. Elazar, J. W. Dreon, and A. Baydar. Wake measurements and loss evaluation in a controlled diffusion compressor cascade. *Journal of Turbomachinery*, 113:591–607, 1991.

[110] C. H. Sieverding. Pressure probe measurements in cascades. *Modern methods of testing rotating components of turbomachines, AGARDOgraph*, 207, 1975.

[111] C. H. Sieverding. Aerodynamic development of axial turbomachinery blading. *Thermodynamics and fluid mechanics of turbomachinery*, 1:513–565, 1985.

[112] Q. Sun and I. D. Boyd. Flat plate aerodynamics at very low reynolds number. *Journal of Fluid Mechanics*, 502, 2004.

[113] K. Taira, W. B. Dickson, T. Colonius, and M. H. Dickinson. Unsteadiness in flow over a flat plate at angle of attack at low reynolds numbers. *Journal of AIAA*.

[114] S. Tavoularis. *Measurement in fluid mechanics*. Cambridge University Press, 2005.

[115] W.P.J. Visser. Gas turbine engine simulation at n.l.r.

[116] R. A. Wallis. *Axial flow fans and ducts*. John Wiley & Sons, 1983.

[117] P. P. Walsh and P. Fletcher. *Gas Turbine Performance*. Blackwell Publishing, second edition, 1996.

[118] C. W. Wenger, W. J. Devenport, K. S. Wittmer, and C. Muthanna. Two-point measurements in the wake of a compressor cascade. *29th AIAA Fluid Dynamics Conference*, 1950.

[119] D.C. Wilcox. Reassessment of the scale-determining equation for advance turbulence models. *AIAA Journal*, 26, 1988.

[120] A. G. Wilson and C. Freeman. Stall inception and development in an axial flow aeroengine. *ASME Journal of Turbomachinery*, 116, 1994.

[121] A. M. Yocum. Separated flow in a low-speed two-dimensional cascade - part 2: Cascade performance. *Journal of Turbomachinery*, 115, 1993.

[122] A. M. Yocum and W. F. O' Brien. Separated flow in a low-speed two-dimensional cascade - part 1: Flow visualisation and time-mean velocity measurements. *Journal of Turbomachinery*, 115, 1993.

[123] P. K. Zachos, V. Pachidis, B. Charnley, and Pericles Pilidis. Flowfield investigation of a compressor cascade at high incidence-part i: Pneumatic probe measurements. *ASME Turbo Expo, Orlando, Florida, 2009*.

[124] P. K. Zachos, F. Pengue, V. Pachidis, and Pericles Pilidis. Flowfield investigation of a compressor cascade at high incidence-part ii: Numerical analysis. *ASME Turbo Expo, Orlando, Florida, 2009*.